Universitat Autònoma de Barcelona

MULTI-APPROACH INVESTIGATION OF THE DYNAMICS OF RAINFALL PARTITIONING FLUXES AND THEIR IMPLICATIONS IN A MEDITERRANEAN ENVIRONMENT

Juan Andrés Pinos Flores

MULTI-APPROACH INVESTIGATION OF THE DYNAMICS OF RAINFALL PARTITIONING FLUXES AND THEIR IMPLICATIONS IN A MEDITERRANEAN ENVIRONMENT

Doctoral Thesis

Juan Andrés Pinos Flores

To be eligible for the Doctor degree

Supervised by:

Dra. Pilar Llorens and **Dr. Jérôme Latron**

Tutor:

Dr. Rafael Poyatos

Institute of Environmental Assessment and Water Research (IDAEA)
Spanish National Research Council (CSIC)

Autonomous University of Barcelona (UAB)
PhD program in Terrestrial Ecology

Barcelona, January 2023

MULTI-APPROACH INVESTIGATION OF THE DYNAMICS OF RAINFALL PARTITIONING FLUXES AND THEIR IMPLICATIONS IN A MEDITERRANEAN ENVIRONMENT

Doctoral Thesis

Juan Andrés Pinos Flores

To be eligible for the Doctor degree

With the approval of the supervisors:

Dra. Pilar Llorens **Dr. Jérôme Latron**

Institute of Environmental Assessment and Water Research (IDAEA)
Spanish National Research Council (CSIC)

Autonomous University of Barcelona (UAB)
PhD program in Terrestrial Ecology

Barcelona, January 2023

AGRADECIMIENTOS

Finalmente cierro este capítulo de mi vida, estos años realizando mis estudios doctorales han sido un largo viaje lleno de experiencias y emociones de los cuales he aprendido a ser un mejor científico, pero sobre todo una mejor persona. Esta tesis refleja todo el esfuerzo que he puesto durante este tiempo. Sin embargo, no lo he hecho solo, por eso quiero agradecer a todas las personas que directa o indirectamente han formado parte de este viaje.

En primer lugar, me gustaría agradecer a mis directores Pilar Llorens y Jérôme Latron por haberme dado la oportunidad de incorporarme al IDAEA y adentrarme en la hidrología forestal. Gracias por la experiencia de campo en Vallcebre, los congresos y cursos internacionales, y por todas las revisiones y correcciones que han hecho que mi trabajo de tesis sea de calidad, del cual estoy muy orgulloso.

En segundo lugar, quiero extender mis agradecimientos a los colegas del grupo de investigación del IDAEA, que han sido parte importante en los consejos y discusiones científicas y sociales que me han ayudado a seguir día a día con entusiasmo. Gracias a todos ustedes: Francesc Gallart, Carles Cayuela, Mariano Moreno, Elisenda Sanchéz, Gisel Bertran; y de igual manera a las incorporaciones más recientes Pauline y Loujain. Muchas gracias también a Anna Ávila por su seguimiento del desarrollo de la tesis, y a Rafael Poyatos por ser tutor de la tesis y dar sus observaciones.

En tercer lugar, me gustaría agradecer a Markus Flury y Beate Michalzik, que han sido mis supervisores durante mis estancias de investigación en la Universidad Estatal de Washington (EE. UU.) y la Universidad de Jena (Alemania), respectivamente. Gracias por todos los consejos y hospitalidad, y expandir mi conocimiento y visión del mundo científico. También quiero agradecer a mis colaboradores Delphis Levia y Kazuki Nanko, ha sido un placer trabajar conjuntamente como equipo. De igual manera quiero agradecer a Carlos Gracia y Jan Feyen, mis mentores “no oficiales”, que han sido parte importante de esta travesía.

Finalmente me gustaría agradecer infinitamente a toda mi familia que me mostró su apoyo incondicional y el ánimo necesario durante todo el proceso de escribir mi tesis. Gracias a Ophelia por impulsarme a ser mejor cada día y llenar de color y alegría mi vida. De igual manera, este viaje académico no habría sido tan agradable sin mis amigos pues su motivación y actitud positiva me han ayudado mucho durante estos años.

Espero que esta tesis pueda aportar a mejorar la compresión de la dinámica de los distintos procesos de interceptación de lluvia y consecuentemente sobre el rol de los bosques en el ciclo hidrológico de las cuencas Mediterráneas.

He tenido el soporte económico de una beca FPI del Ministerio de Ciencia e Innovación (BES-2017-082234). Esta investigación ha sido financiada por los proyectos TransHyMed (CGL2016-75957-R AEI/FEDER UE) y Rhysotto (PID2019-106583RB-I00) del Ministerio de Ciencia e Innovación, así como por la Agencia de Gestión de Ayudas Universitarias y de Investigación (AGAUR) (Subvención 2017SGR1643).

ABSTRACT

Rainfall interception by forest canopies prevents rainfall from immediately reaching the soil, redistributing it in the form of throughfall and stemflow. The aim of the present research was to investigate the role of forest cover on the spatial and temporal distribution of both flows in a Mediterranean forest. The dissertation aimed to fill some knowledge gaps by using novel ecohydrological approaches in a Scots pine forest in the Vallcebre research catchments, a representative area of Mediterranean middle mountain environments. High temporal resolution monitoring of rainfall, throughfall, stemflow, meteorological variables, and soil water content, as well as water sampling of the different fluxes for the determination of the stable water isotopes signatures in the period 2018-2020, were used to improve the mechanistic understanding of forest-water interactions.

With this information, we investigated the throughfall partitioning into splash throughfall, free throughfall, and canopy drip by means of rainfall and throughfall drop size distributions, and their relationships with the observed shift in their isotopic composition. Throughfall types were characterized according to different rainfall classes based on duration and intensity. We found that during rainfall events, splash throughfall was greater at the beginning of the events, as well as the vapour pressure deficit. This initial stage coincided also with the greater throughfall isotopic enrichment with respect to rainfall isotopic signal. Higher splash throughfall and vapour pressure deficit indicated that the isotopic enrichment was caused by splash droplet evaporation. Moreover, isotopic differences among rainfall, throughfall, and stemflow were analysed. Throughfall was more enriched than rainfall and stemflow more than throughfall. Seasonal differences in isotopic shift were also observed, with throughfall being more depleted during the growing season whereas stemflow was more enriched. Meteorological variables did not show a relationship with either throughfall or stemflow isotopic shifts. Isotopic fractionation was caused by a combination of factors occurring throughout the event, with evaporation being more relevant during the initial stage of the events, whereas canopy selection processes (i.e., the possibility of intercepted rainfall to be retained and transmitted asynchronously) dominated towards the end of the events. Nevertheless, intra-event mixing of waters could occur during the same event.

Stemflow is a spatially-concentrated and chemically-enriched water flux input, altering soil moisture and chemistry in near-stem areas when infiltrating in the vicinity of tree trunks. While many studies have

examined stemflow production among tree species, no known research examined the stemflow distribution around the trunk before reaching the ground. Moreover, only a few studies explored its infiltration dynamics (the double funnelling effect). The results of our study clearly show a non-uniform distribution of stemflow down in the trunk surface, meaning that stemflow distribution shows preferential flow paths. These flow paths are related to biotic factors (trunk lean, bark morphology, and tree neighbourhood), and to a lesser extent to abiotic factors (rainfall intensity peaks). By conducting a field experiment simulating stemflow, labelled with a dual-tracer approach, we were able to determine the influence of stemflow in the soil moisture response at the base of the tree. We observed that stemflow primarily infiltrated along the surface of coarse roots and through macropores, and demonstrate, by a set of metrics, the prevalence of preferential flow. Knowledge of above- and below-ground stemflow distribution and its implications is therefore emphasized.

The insights and findings presented in this dissertation will enable forest hydrologists to better characterize the hydrological processes in Mediterranean forest landscapes. In addition, future research lines that could extend and complement our results are also discussed.

RESUMEN

La interceptación de la precipitación por el dosel arbóreo impide que la lluvia llegue inmediatamente al suelo, redistribuyéndola en forma de trascolación y escorrentía cortical. El objetivo de la presente investigación es investigar el papel de la cubierta forestal en la distribución espacial y temporal de los flujos de trascolación y escorrentía cortical en un bosque Mediterráneo. La tesis pretende llenar vacíos de conocimiento utilizando enfoques ecohidrológicos novedosos en un bosque de pino silvestre en las cuencas de investigación de Vallcebre, un área representativa de los ambientes Mediterráneos de montaña media. Con la finalidad de mejorar la comprensión de las interacciones bosque-agua, durante el período 2018-2020 se ha monitorizado, con alta resolución temporal, la precipitación, la trascolación, la escorrentía cortical, las variables meteorológicas y la humedad del suelo, y se ha muestreado el agua de los diferentes flujos para la determinación de su señal isotópica (^{18}O y ^{2}H).

Con esta información, y determinando las distribuciones de tamaño de gotas de lluvia y de trascolación, hemos investigado la partición de la trascolación en: trascolación por salpicadura ('splash throughfall'), trascolación libre ('free throughfall') y goteo del dosel ('canopy drip'), y sus relaciones con los cambios observados en composición isotópica. Los resultados indican que, durante los eventos, la trascolación por salpicadura es mayor al principio de los eventos, así como lo es el déficit de presión de vapor. Esta etapa inicial coincide con un enriquecimiento isotópico de la trascolación respecto a la señal isotópica de la lluvia. Una mayor trascolación por salpicadura y un mayor déficit de presión de vapor indican que el enriquecimiento isotópico fue causado por la evaporación de las gotas de pequeño tamaño que forman las salpicaduras. Paralelamente, se analizaron las diferencias isotópicas entre la lluvia, la trascolación y la escorrentía cortical. Los resultados indican que la trascolación es más enriquecida que la lluvia, y que la escorrentía cortical es más enriquecida que la trascolación. También se observaron diferencias estacionales, la trascolación estaba más empobrecida durante el periodo vegetativo, mientras que la escorrentía cortical estaba más enriquecida. Las variables meteorológicas no mostraron una relación con las diferencias isotópicas entre la trascolación o escorrentía cortical y la lluvia. El fraccionamiento isotópico fue causado por una combinación de factores a lo largo del evento, siendo la evaporación más relevante durante la etapa inicial de los eventos, mientras que los procesos de selección (es decir, la posibilidad de que la lluvia interceptada sea retenida por el dosel y transferida asincrónicamente) dominaron hacia el final de los eventos. No obstante, durante un mismo evento podía también ocurrir la mezcla de aguas.

La escorrentía cortical es un flujo de entrada de agua espacialmente concentrada y químicamente enriquecida, que al infiltrarse altera la humedad y la química del suelo en las zonas cercanas a los troncos de los árboles. Mientras que muchos estudios han examinado la producción de la escorrentía cortical en diferentes especies de árboles, no se conoce ningún trabajo que haya examinado la distribución de la escorrentía cortical alrededor del tronco de los árboles antes de llegar al suelo. Además, sólo pocos estudios han explorado la dinámica de infiltración de la escorrentía cortical (el efecto de doble embudo). Los resultados de nuestro estudio muestran una distribución no uniforme de la escorrentía cortical por el tronco, lo que significa que la distribución de la escorrentía cortical muestra vías de flujo preferenciales. Estas vías de flujo pueden relacionarse con factores bióticos (inclinación del tronco, morfología de la corteza y vecindad del árbol) y, en menor medida, con factores abióticos (intensidad de lluvia). Mediante la realización de un experimento en campo de simulación de la escorrentía cortical, con agua marcada con dos trazadores, pudimos determinar la influencia de la escorrentía cortical en la dinámica de la humedad del suelo en la base de un árbol. Observamos que la escorrentía cortical se infiltraba principalmente a lo largo de la superficie de las raíces gruesas y a través de los macroporos, y demostramos, con un conjunto de métricas, la prevalencia del flujo preferencial. Nuestros resultados aportan información valiosa sobre la distribución de la escorrentía cortical tanto en el tronco como en el suelo y sus implicaciones.

Los resultados presentados en esta tesis permitirán a los hidrólogos forestales caracterizar mejor los procesos hidrológicos en paisajes forestales Mediterráneos. Finalmente, se discuten futuras líneas de investigación que podrían ampliar y complementar nuestros resultados.

CONTENTS

CHAPTER 1

GENERAL INTRODUCTION

1.1 Introduction to forest hydrology

The emergence of forest hydrology as a sub-discipline of hydrology had its beginning in the 2nd half of the 19th century with few seminal works that helped the field of forest hydrology and watershed science to develop, whereby the role of forests in catchment functioning began to be recognized and draw the attention of scientists around the world (Andréassian, 2004; McGuire and Likens, 2011; Bren, 2016; Van Stan and Friesen, 2020). Forest hydrology can be described as the discipline that study the structure, function and dynamics of forested watersheds and their influence on the transport, storage, and fate of water. It is a process-based discipline supported by the conservation of mass and energy, but in practice due to the spatial variations of the inputs (e.g., rainfall) and materials (e.g., soils) that make up the catchment, processes become more complex (Bren, 2016).

Today, the development of forestry and hydrology fields associated with the growing boom of scientific research around the world and the advent of sophisticated and reliable instruments to measure different physical compartments of the watersheds (e.g., rainfall, water level, air temperature, solar radiation, transpiration, stemflow, xylem, soil water, etc.) has made the discipline of forest hydrology highly developed compared to previous decades. Therefore, forest hydrology research has helped and will help to better understand various interactions and pressures, including that of land use and climate change, on the atmosphere–plant–soil continuum (and vice versa, Goldsmith, 2013) in order to improve forest and watershed management (Amatya et al., 2011). However, despite all the research done on forest hydrology, and the great advances in the understanding of forest–water interactions, the role of the forest in relation to the sustainable management of water resources, in a global change context, remains a key issue in many parts of the world.

1.2 Canopy interception and the use of hydrometric data and stable isotope tracers

Canopy interception is the first hydrologic process that acts to redistribute incident rainfall (before possibly reaching the forest floor) by means of three processes: interception loss, throughfall and stemflow (Horton, 1919). Interception loss is the portion of the precipitation that is returned to the atmosphere through evaporation from plant surfaces or is absorbed by the plant. Throughfall is the rainwater that may or may not have contact with vegetative surfaces and falls or drips to the forest ground, whereas stemflow is the

proportion of rainwater that is channeled to the stem, which eventually flows downward and reaches the forest floor around the stem base (Hamilton and Rowe, 1949). Net precipitation defined as the sum of throughfall and stemflow constitute the majority of the incident rainfall (between 70 and 90%) and play a critical role in the hydrology and biogeochemistry of forested catchments. Due to the different flowpaths and residence times along vegetative surfaces between throughfall and stemflow, notable distinctions in chemical, geological, and biological materials can be observed in these fluxes (Levia et al., 2011a; Van Stan et al., 2021).

An extensive synthesis showed that most of the throughfall and stemflow observations were made in forest ecosystems (n = 718 and n = 816, respectively), and to a lesser extent in shrubs (n = 43 and n = 63, respectively) (Yue et al., 2021). The concentrated fluxes vary widely between vegetation types and climatic regions, and they are controlled by a range of biotic and abiotic factors, such as meteorological conditions and tree features (Llorens and Domingo, 2007; Yue et al., 2021). A large body of literature has been published in the last decades summarizing the research conducted on throughfall and stemflow. Despite its ecohydrological importance as an input of water and nutrients in forested and agricultural ecosystems, which has been recognized by the scientific community, many aspects remain underexposed or unexplored (Levia et al., 2011b). The lack of a detailed understanding of interception processes has led to omitting or simplifying these processes in hydrological models. Oversimplification of interception processes can significantly affect the evaluation of other individual components of the hydrological balance and consequently the accuracy of hydrological models (Stockinger et al., 2017; Kofroňová et al., 2021).

To study the rainfall partitioning process, the classical hydrometric approach of measuring rainfall partitioning has been recently complemented and expanded by natural tracing with water stable isotopes (^{18}O and ^{2}H) (Dawson and Simonin, 2011; Allen et al., 2017). To characterize temporally and spatially the rainfall, throughfall and stemflow a set of reliable and affordable sensor as well as better data logging and storage technologies has been developed and implemented during the last decades (e.g., rainfall tipping buckets, disdrometers, dataloggers, automatic water samples, etc.). On the other hand, stable isotopes provide new and important insights for tracing the origin and movement of water (e.g., transit and travel time) in the atmosphere–plant–soil continuum (Sprenger et al., 2016). The isotopic composition of water transmitted as throughfall or stemflow may therefore be used as a way to characterize a suite of processes occurring in the canopy (Allen et al., 2017).

1.3 Forest stand scale

In nature, scales are not arbitrary but arise sequentially as a function of their basic units, for example, Leaf scale < Forest stand scale < Hillslope scale < Catchment scale < Regional scale < Continental scale, and < Global scale (Moore et al., 2015). Given that forest hydrology is a science, then the concepts should be able to be quantified and hypotheses should be testable by experiments. In forest hydrology, the use of the paired–catchment approach, which is a larger scale than the forest stand scale, has served to understand forest–water interactions in terms of water yield, water quality, and timing of streamflow from forested catchments after forest cover reduction or thinning (Andréassian, 2004; Amatya et al., 2011). In contrast, the forest stand scale uses experimental forest plots to better understand forest ecohydrological processes (e.g., transpiration and photosynthesis, interception and redistribution of precipitation, drainage in the soil, etc.) through planned experiments (Moore et al., 2015). The advantages of small–scale units are that (1) it represents homogeneous systems; (2) they can be spatially delimited to convenience as it is not dependent on any topographical limits, and (3) cost wise they can more easily be instrumented, maintained, and monitored in the short, medium, or long term. Data generated at the forest stand scale helps to observe temporal trends, and changes associated with landscape disturbances, and to calibrate and validate ecohydrological models. In sum, the experimental forest plots may constitute a permanent field laboratory where it is possible to observe hydrological processes and their relation to/dependency on forest cover modification.

There is also currently a new trend in hydrology to develop investigations using satellite imagery products, which are cheaper and cover larger scales than field work, which has led to a decrease in field studies and left complex hydrological issues unresolved (Burt and McDonnell, 2015). Therefore nowadays, the generation of field data is still very important and sorely needed to yield insights on water pathways and their alterations by natural or anthropogenic disturbances in forest landscapes.

1.4 The hydrology of Mediterranean catchments

Water is an essential resource to life, the environment, and human development. Earth is called the ‘Blue Planet’ because more than 70% of the Earth’s surface is cover by water. However, only 3% is fresh water,

and 70% of that 3% is in the polar icecaps and mountains glaciers, thus unavailable for ordinary anthropogenic uses (Robinson and Ward, 2017).

In Mediterranean catchments, hydrological processes such as soil water content, water table depth, and runoff generation are widely variable in time and space due to the high variability of precipitation and evapotranspiration (Latron et al., 2009). Moreover, the uneven spatial and temporal distribution of precipitation leads to disproportional water availability across Mediterranean territories, making these areas vulnerable in terms of water security (Correia, 1999). Mediterranean regions depend on runoff generated in mountain headwaters for water supply (Latron et al., 2009). However, annual rainfall is variable between years, and climate change together with the increasing demands on water by various socioeconomic sectors generates several water challenges across the Mediterranean (Latron et al., 2009; García-Ruiz et al., 2011; Allam et al., 2020).

In addition to climate change is the hydrology of Mediterranean mountain areas susceptible to environmental changes by anthropogenic activities such as land-use change, either through abandonment or intensification (Latron et al., 2009). In low-productive mountain areas, leads the abandonment of farmland and pastures to a natural expansion of shrub and forest cover reducing runoff generation and deep-water percolation. On the contrary, in the lowlands, urbanization and agriculture intensification are occurring and are accompanied by an increase in water demand, which may also lead to a decline in river discharges and aquifer overexploitation (Lana-Renault et al., 2020).

Therefore, the study of hydrology in Mediterranean regions and the effect of the vegetation in the catchments water cycle is particularly important to properly and timely develop and implement measures and policies to improve forest and water resources management in these vulnerable regions, in order to anticipate negative hydrologic consequences (e.g., water scarcity) derived from global change scenarios.

1.5 Vallcebre research catchments

This research was conducted in the headwaters of the Llobregat river in the Vallcebre research catchments (Figure 1a). This research area is located at 90 km North from the city of Barcelona (Northeastern Spain), at the Southern margin of the Pyrenees (42°12′ N, 1°49′ E). The catchments are divided in two clusters of

five catchments. The first cluster, the Cal Rodó catchment (4.17 km^2) has two sub-catchments: Can Vila (0.56 km^2) and Ca l´Isard (1.32 km^2). The second cluster, Cal Parisa (0.32 km^2) is formed by two contiguous catchments of similar size. The climate is sub-Mediterranean with a mean annual precipitation, reference evapotranspiration and air temperature of 867 ± 223 mm, 856 ± 69 mm and 9.2ºC respectively (mean for the period 1999 to 2018; Llorens et al., 2018).

Figure 1. (a) General view of the landscapes of the Vallcebre research catchments; (b) dominance of pine forest cover in the landscape of the study area; (c) Cal Rotes experimental forest plot.

These catchments have been monitored for more than 30 years for hydrological, geomorphological and ecohydrological purposes by the Surface and Hydrology and Erosion Group IDAEA-CSIC (Llorens et al., 2018). Therefore, research derived from this study area has served as a referent to improve understanding of hydrological processes at different spatial and temporal scales in Mediterranean ecosystems (e.g., rainfall, soil water, groundwater, erosion and sediment transport, runoff generation, rainfall interception processes, isotope-based studies, hydrological modelling, etc.) and to generate long-term data sets of several variables (e.g., rainfall, throughfall, transpiration, water levels, dissolved organ carbon, turbidity, etc.). The extensive knowledge generated over the past three decades of research in these catchments has provided information on the effect of land use change and global change on water resources; however, work continues today to unravel the remaining gaps and new questions that have emerged with scientific progress.

The experimental research of the present study was carried out in the Can Vila catchment, which had an altitude that ranges between 1,108 and 1,462 m a.s.l. Can Vila catchment drain to the river Llobregat, which is the main supply of surface water to the city of Barcelona. The catchment is mainly covered by forest (60%) and meadows on old agricultural fields is the second most common land cover (35%). Scots pine

forests (*Pinus sylvestris L.*) is the dominant forest vegetation which arose through natural afforestation on old agricultural terraces (Figure 1b), followed by small original fragmented oak forests (*Quercus pubescens Willd.*) (Poyatos et al., 2003). The hydrological functioning of Can Vila is dominated by antecedent wetness conditions (Gallart et al., 2002). Soils have a silt-loam texture and are characterized by the rapid decrease of their hydraulic conductivity with depth (Rubio et al., 2008). Stream length is 1.1 km, with a mean hillslope gradient of 25%. Streamflow is highly seasonal, being less reactive to precipitation during dry periods and vice versa during wet periods (Latron et al., 2008).

Within the Can Vila catchment an experimental forest stand named Cal Rotes has been delineated to study rainfall interception processes and soil water dynamics (Figure 1c). The stand has an area of 900 m^2 and is located at an elevation of 1200 m with a northeastern aspect. The stand has a mean diameter at breast height (DBH, 1.3 m) of 19.9 ± 9.2 cm, a stand density of 1189 trees ha^{-1}, a stand basal area of 45.1 m^2 ha^{-1}, a mean tree height of 17.0 ± 4.4 m and a mean canopy cover of 69.3 ± 17.7%. The forest plot has been instrumented to monitor and sampling at high spatial and temporal resolution the throughfall, stemflow, and soil water. For the development of this thesis, forest hydrological monitoring was conducted (2018-2021) in four representative trees which were selected based on the experience of several years of monitoring and sampling throughfall and stemflow within the forest plot (see Cayuela et al., 2018; Llorens et al., 2018). The forest plot was equipped with two tipping bucket rain gauges (model AW-P, Institut Analític, Barcelona, Spain) to measure throughfall at two different distances from the trunk of a representative tree. Sequential throughfall samples were collected by an automatic water sampler (ISCO 3700 with 500 ml bottles, Teledyne ISCO Inc., Lincoln, NE, USA) at 5 mm rainfall intervals. Stemflow was measured in three representative trees that were monitored since 2015. A common stemflow collar, constructed from a plastic longitudinal funnel cut, was adjusted, and placed around the stem at breast height, and the edges were sealed with silicone. Two collars were divided into four sections and connected to tipping bucket rain gauges (Davis Rain Collector II, Davis Instruments, Hayward, CA, USA) to monitor high temporal resolution stemflow. The third collar was also connected to a tipping bucket rain gauge (model AW-P, Institut Analític, Barcelona, Spain) and sequential stemflow samples were collected by means of an automatic water sampler sampler (ISCO 2700 with 1000 ml bottles, Teledyne ISCO Inc., Lincoln, NE, USA) at 2-L stemflow intervals.

Rainfall was measured from 2015 onwards on a fallow piece of land located approximately 100 m from the forest plot by a tipping bucket rain gauge (model AW-P, Institut Analític, Barcelona, Spain) and collected at 5 mm rainfall intervals by means of an automatic sampler (ISCO 3700 with 500 ml bottles, Teledyne ISCO Inc., Lincoln, NE, USA). Meteorological data were obtained from 2012 onwards from an automatic weather station located 2 m above the canopy of the forest stand. The station is equipped with the following sensors: an air temperature and relative humidity probe (HMP45C, Vaisala, Vantaa, Finland), an anemometer and wind vane (A100R, Vector Instruments, Rhyl, North Wales, UK), and a net radiometer (NR Lite, Kipp & Zonen, Delft, The Netherlands). All the above-mentioned data are recorded at 5 min intervals by dataloggers (Data Taker DT85, Thermo Fisher Scientific Inc., Sunbury, Victoria, Australia).

Rainfall and throughfall drop sizes distributions were also measured (2018-2019) by means of laser disdrometers, built using a laser transmitter and a receiver (IB-30, KEYENCE Corporation, Osaka, Japan) with an amplifier (IB-1000, KEYENCE Corporation, Osaka, Japan) covered by two protection screens, following the design by Nanko et al. (2006), and recorded by an Arduino datalogging system. Soil moisture was measured (2019-2021) using 32 TDR probes (16 CS605 probes and 16 CS615 probes, Campbell Scientific, Logan, UT, USA) located in depth profiles and spatially distributed around an experimental tree.

1.6 Objectives and thesis structure

The evaluation of the effect of rainfall partitioning fluxes on soil moisture heterogeneity and/or groundwater recharge can provide a better understanding and conceptualization of subsurface water fluxes in forest soils, allowing to improve our perceptual model of hydrological functioning at the catchment scale. This thesis aims therefore to improve the knowledge of hydrological processes in Mediterranean environments by focusing on the role of forest cover.

From this general objective, the following research questions of the doctoral thesis are derived:
(a) How is the throughfall drop size distribution related to its isotopic fractionation as it passes through the canopy?
b) What isotopic fractionation processes control throughfall and stemflow isotopic shift?
c) Does stemflow flow downward with a uniform or non-uniform distribution?
d) How does stemflow infiltrate into the soil?

The present thesis is divided in six chapters and built as a compendium of four publications: Chapter 1 includes the general introduction which presents the state of art of the general topics addressed in this thesis as well as the research questions. The following four chapters (Chapter 2 to Chapter 5) constitute the core of the thesis, including 3 published and 1 submitted papers, which answers the general research questions. Finally, Chapter 6 includes the general discussion and conclusions and a short description of future research lines that could complement the research done in the present thesis.

Chapter 2 analyses the relationship between drop characteristics and isotopic composition of throughfall and rainfall. This study uses rainfall and throughfall data collected with tipping buckets and disdrometers as well as water samples for isotopic composition with the following aims: (a) the quantification and analysis of isotopic composition and drop sizes of both rainfall and throughfall at the intra-event scale; (b) the calculation of the proportion of each throughfall type (free throughfall, splash and drip); and (c) the analysis of the interrelationships of the observed isotopic shift and drop size between open rainfall and throughfall.

Chapter 3 focuses on assess the shift in the isotopic composition of stemflow in relation to rainfall and throughfall, and storm characteristics. The intra-storm variation of stemflow isotopic composition and its dynamics has been poorly studied, with no concluding remarks. Therefore, this study was designed (a) to develop an approach to measure and sample stemflow at high temporal resolution, (b) to analyze the seasonal, inter-storm and intra-storm temporal dynamics of the isotopic compositions of throughfall and stemflow and (c) to compare these with that of rainfall. The aims were to shed light on the causes of isotopic fractionation between these fluxes and the influence of throughfall and stemflow on soil water and groundwater isotopic dynamics.

Chapter 4 evaluate the distribution of stemflow around the trunk. Stemflow distribution has always been measured assuming that it has a uniform distribution around the trunk, however, rainfall characteristics and tree architecture could be factors that generate non-uniform stemflow. The determination of these dynamics plays an important role in the design of infiltration models. Here, this study uses a novel stemflow collar approach with the aim (a) to quantify the circumferential variability of stemflow around tree stems and (b) to assess how some biotic and abiotic factors might affect this stemflow variability. This is the first study that directly quantifies the stemflow distribution around tree stems at fine (5-min) temporal scale.

Chapter 5 evaluate the role of stemflow infiltration in the formation of preferential flows and its effect on recharge from an experiment under controlled conditions. To date, there are very few experimental studies on the subject. The experiment in this study uses a novel dual labelling approach with artificial tracers together with a high spatial and temporal monitoring of soil moisture around an experimental tree. The main goal of this study was to quantitively assess stemflow infiltration by using dye concentrations, isotopic compositions, and hydrometric data (soil water content), and to visualize the spatial distribution of preferential flow pathways by using dye staining.

CHAPTER 2

Throughfall isotopic composition in relation to drop size at the intra-event scale in a Mediterranean Scots pine stand

Throughfall isotopic composition in relation to drop size at the intra-event scale in a Mediterranean Scots pine stand

The major fraction of water reaching the forest floor is throughfall, which consists of free throughfall, splash throughfall and canopy drip. Research has shown that forest canopies modify the isotopic composition of throughfall by means of evaporation, isotopic exchange, canopy selection and mixing of rainfall waters. However, the effects of these factors in relation to throughfall isotopic composition and the throughfall drop size reaching the soil surface are unclear. Based on research in a mountainous Scots pine stand in northeastern Spain, this study sought to fill this knowledge gap by examining the isotopic composition of throughfall in relation to throughfall drop size. In the experimental stand, throughfall consisted on average of 65 % canopy drip, 19 % free throughfall and 16 % splash throughfall. The dynamics of the isotopic composition of throughfall and rainfall showed complex behaviour throughout events. The isotopic shift showed no direct relationship with meteorological variables, number of drops, drop velocities, throughfall and rainfall amount, or raindrop kinetic energy. However, the experiment did reveal that the isotopic shift was higher at the beginning of an event, decreasing as cumulative rainfall increased, and that it also increased when the median volume drop size of throughfall (D_{50_TF}) approached or was lower than the median volume drop size of rainfall (D_{50_RF}). This finding indicates that the major contribution of splash throughfall at the initial phase of rain events matched the highest vapour pressure deficit (VPD) and, at the same time, corresponded to higher isotopic enrichment, which implies that splash droplet evaporation occurred. Future applications of our approach will improve understanding of how throughfall isotopic composition may vary with drop type and size during rainfall events across a range of forest types.

Original work: Pinos, J., Latron, J., Nanko, K., Levia, D. F., & Llorens, P. (2020). Throughfall isotopic composition in relation to drop size at the intra-event scale in a Mediterranean Scots pine stand. Hydrology and Earth System Sciences, 24(9), 4675-4690. https://doi.org/10.5194/hess-24-4675-2020

2.1 Introduction

Forests play an important role in the water balance of catchments by redistributing rainfall in throughfall, stemflow and interception loss. To study the rainfall partitioning process, the classical hydrometric approach of measuring rainfall partitioning has been recently complemented and expanded by natural tracing with water stable isotopes ($\delta^{18}O$ and $\delta^{2}H$). It has been shown that the forest canopy modifies the isotopic composition of throughfall and stemflow in relation to open rainfall (Allen et al., 2017; Cayuela et al., 2018a). Isotopic fractionation can occur in both directions (enrichment and depletion), with enrichment being more frequent (Saxena, 1986). Throughfall isotopic shifts are mainly caused by four factors: evaporation, isotopic exchange, canopy selection and mixing of waters (Allen et al., 2017), although subcanopy water recycling i.e. evapotranspiration and re-condensation (Green et al., 2015), may also exert an influence. However, it is important to note that the effect of each factor and the magnitude of the isotopic shift remain unclear. Isotopic fractionation by evaporation occurs when rain water molecules achieve enough energy to change from liquid to the gas phase, resulting in an enrichment of heavy isotopes. Isotopic exchange is the exchange between liquid and environmental vapor when these pools are not at an isotopic steady state. Canopy selection is the result of selective water retention in the canopy of different lapses within rainfall events that temporally vary its isotopic composition. Mixing of water relates to the storage of the residual water of previous rainfall in the canopy that is eventually mixed with new rain water. Exchange, canopy selection and mixing of water can cause either isotopic enrichment or depletion.

Because throughfall represents the main water input to the soil (Levia and Frost, 2006), understanding the spatiotemporal variability of throughfall isotopic composition is of paramount importance to use it as an input value in isotope-based hydrological studies. Spatial variability of the throughfall isotopic composition between collectors seems to be related to canopy cover (Cayuela et al., 2018a) but not to throughfall amount (Allen et al., 2015). However, all isotopic fractionation factors could very well occur during the same rainfall event, which complicates the understanding of the mechanisms that influence the intra-event isotopic differences between rainfall and throughfall. Although a small number of studies have focused on understanding the spatiotemporal variability of throughfall isotopic composition at the intra-event scale (e.g., Kubota and Tsuboyama, 2003; Ikawa et al., 2011; Cayuela et al., 2018a), the factors controlling this variability remain largely unclear.

Laboratory experiments demonstrated that falling water droplets experience isotopic fractionation due to evaporation and isotopic exchange with the environment and that the degree of evaporation is related to drop characteristics (size, velocity, number, temperature), air conditions, and exposure time or falling distance (Friedman et al., 1962; Stewart, 1975). More recently, Murakami (2006) and Dunkerley (2009) analysed the concept of splash droplet evaporation, showing that numerous small droplets are produced when a raindrop hits the canopy, enhancing the evaporation of the droplets. However, the influence that splash generation and subsequent evaporation or ionic exchange exerts on the isotopic composition of throughfall remains unexplored (Allen et al., 2017).

An increasing number of studies of throughfall drop characteristics, such as drop size, velocity and kinetic energy, have shed light on the partitioning of throughfall by trees. Some recent studies have shown that the way in which water reaches the forest floor is affected by throughfall drop characteristics and, therefore, affects soil erosion and probably soil moisture (Levia et al., 2017; Nanko et al., 2020). Moreover, several studies have shown that biotic and abiotic factors affect throughfall drop characteristics. These diverse factors have been related to whether trees are coniferous or broadleaved deciduous (Levia et al., 2019), the presence or absence of foliage (Nanko et al., 2016), canopy species and meteorological factors (wind and rainfall intensity) (Nanko et al., 2006; Lüpke et al., 2019), physical leaf characteristics (Nanko et al., 2013), the thickness and saturation of the canopy (Nanko et al., 2008a) and the spatial variation between crown positions under a single tree (Nanko et al., 2011) or within tree stands (Nanko et al., 2020).

For a given rainfall event with simultaneous measurements of drop size distributions (DSDs) measured both inside and outside the forest, throughfall can be divided into three types: (1) free throughfall (FR), which is the proportion of throughfall that does not contact the canopy surface and, thus, maintains the same DSD as open rainfall; (2) splash throughfall (SP), corresponding to the drops that hit the canopy and split into smaller drops; and (3) canopy drip (DR), which is the proportion of throughfall that is initially retained and routed by vegetative surfaces but eventually detaches from the vegetation (Levia et al., 2017; 2019). Canopy drip has the largest drop diameter and splash throughfall has the smallest (Levia et al., 2017).

Despite the important progress made in investigating throughfall dynamics using drop size data from disdrometers, the interrelationships between throughfall isotopic composition and throughfall drop size need to be investigated at the intra-event scale to yield insights into evaporative demand (Allen et al., 2017;

Cayuela et al., 2018a; Levia et al., 2011, 2017). To our knowledge, no existing studies have analysed the details of the interplay between fine-scale rainfall and throughfall drop characteristics in terms of isotopic composition. Accordingly, the specific objectives of this study were as follows: (i) the quantification and analysis of isotopic composition and drop sizes of both rainfall and throughfall at the intra-event scale; (ii) the calculation of the proportion of each throughfall type (free throughfall, splash and drip); and (iii) the analysis of the interrelationships of the observed isotopic shift and drop size between open rainfall and throughfall.

2.2 Material and methods

2.2.1 Site description

The study was conducted in the Can Vila catchment (Fig. 1), one of the Vallcebre research catchments (northeastern Spain; 42° 12′N, 1° 49′E) in the eastern Pyrenees. These catchments have been monitored for 30 years for hydrological and ecohydrological purposes (see Latron et al., 2009; Llorens et al., 2018). Nowadays, most of the catchment is covered by Scots pine forests (*Pinus sylvestris L.*), which arose through afforestation of old agricultural terraces and small original fragmented oak forests (*Quercus pubescens Willd.*) (Poyatos et al., 2003). The climate is sub-Mediterranean with a mean annual precipitation, reference evapotranspiration and air temperature of 867 ± 223 mm, 856 ± 69 mm and 9.2ºC respectively (mean for the period 1999 to 2018; Llorens et al., 2018). Precipitation is seasonal throughout the year, with spring and autumn being the wettest seasons and summer and winter being the driest. Evapotranspiration shows a seasonal pattern with maximum values in summer of up to 6.9 mm d^{-1}. Our study is based on data obtained within the Scots pine stand of Cal Rotes, located in the central part of the Can Vila catchment. The stand has an area of 900 m^2 and is located at an elevation of 1200 m with a northeastern aspect. The stand has a mean diameter at breast height (DBH, 1.3 m) of 19.9 ± 9.2 cm, a stand density of 1189 trees ha^{-1}, a stand basal area of 45.1 m^2 ha^{-1}, a mean tree height of 17.0 ± 4.4 m and a mean canopy cover of 69.3 ± 17.7% (Molina et al., 2019).

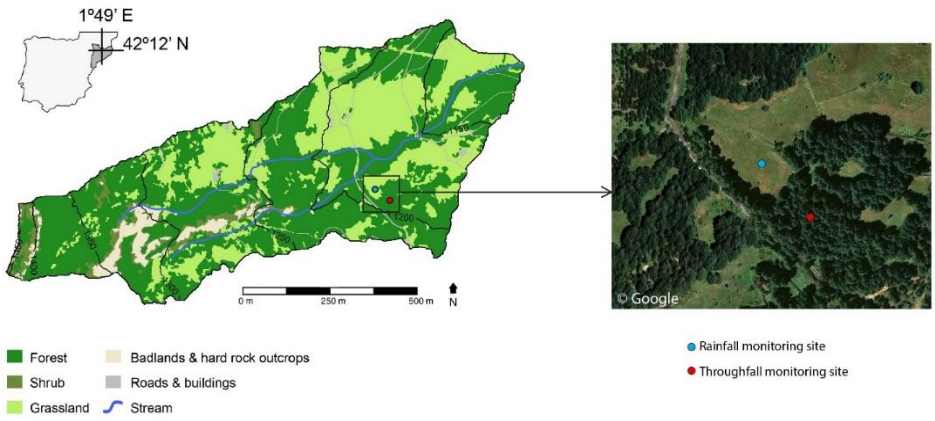

Figure 1. Location of the monitoring sites within the Can Vila catchment, Spain.

2.2.2 Monitoring design and data collection

The experimental work involved the continuous measurement, characterisation and sampling of open rainfall and throughfall. The rainfall monitoring site was located in an open area approximately 100 m from the Scots pine stand where throughfall was monitored (Fig. 1). The study tree is representative of the forest plot and has a canopy projected area large enough to locate the throughfall instruments. Throughfall was monitored at two randomly selected distances (0.8 and 1.2 m) from the bole of the study tree (Table 1). Other nearby trees that might have affected the throughfall monitoring location were located at an average distance of 4.4 ± 1.1 m.

Table 1. Biometric characteristics of the monitored tree (adapted from Cayuela et al., 2018b).

Diameter at breast height (cm)	35.2	Crown volume (m^3)	228
Basal area (cm^2)	973.1	Mean branch angle (°)	19.2
Height (m)	22.3	Mean branch diameter (cm)	4.4
Canopy cover (%)†	85.2	Tree lean (°)	7.9
Crown area (m^2)	17.3	Distance to first live branch (m)	12.4

† Canopy cover was measured over the throughfall tipping-bucket collection area.

The monitoring design used ground-based laser disdrometers developed by Nanko et al. (2006; 2008b) (see *Laser disdrometer characteristics* section), one for open rainfall and two for throughfall, each placed just above a tipping-bucket rain gauge (model AW-P, Institut Analític, Barcelona, Spain) with a 0.2 mm resolution. Cumulative rainfall and throughfall amounts measured by the tipping buckets were recorded every 5 minutes with a datalogger (Data Taker DT85, Thermo Fisher Scientific Inc., Sunbury, Victoria, Australia). According to Iida et al. (2020), dynamic calibration of the tipping buckets was performed to ensure the quality of data. The rainfall and throughfall passing through the laser disdrometers and the tipping buckets were sequentially collected at 5 mm rainfall intervals (i.e. both samplers switched to the next bottle simultaneously) by means of automatic samplers (ISCO 3700, Teledyne ISCO Inc., Lincoln, NE, USA) buried in the ground to prevent evaporation from the water samples (Fig. 2). All samples were collected a maximum of 1 week after each storm. Unfortunately, the disdrometer located furthest from the tree lost a substantial amount of throughfall data due to technical problems and was therefore discarded from the analysis.

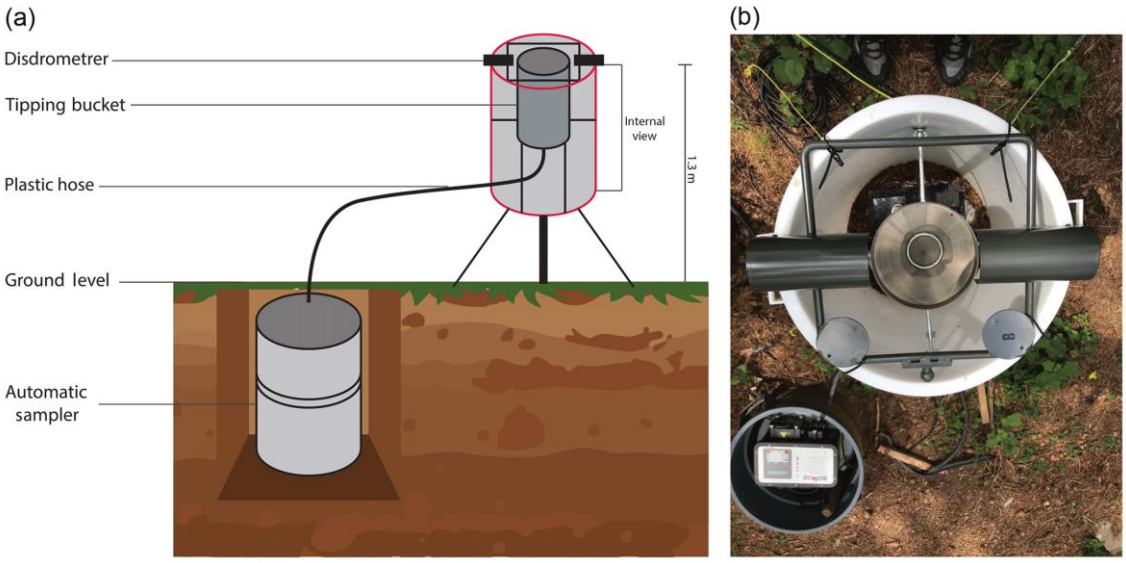

Figure 2. Set-up for continuous measurement and sampling of open rainfall and throughfall. Diagram of the experimental equipment (a) and top view of the equipment installed in the forest stand (b).

2.2.2.1 Laser disdrometer characteristics

The laser disdrometers continuously measured the number of drops, as well as individual drop size and velocity. The instruments were built using a laser transmitter and a receiver (IB-30, KEYENCE Corporation, Osaka, Japan) with an amplifier (IB-1000, KEYENCE Corporation, Osaka, Japan) covered by two protection screens, following the design by Nanko et al. (2006). The sensors were attached to an iron frame. The light source of the laser sensor was a visible semiconductor 660 nm laser. Drops were measured within a 4500 mm^2 sampling area (30 mm wide and 150 mm long) of 1 mm thickness. When a drop passed through the laser beam, the receiving laser beam decreased and the output voltage from the amplifier fell in proportion to the intercepted area of the laser beam. The output voltage was collected by an Arduino UNO every 50 μs (equivalent to 20kHz). The output voltage data were converted into drop diameter and velocity data. The detailed calculation protocol is shown in Nanko et al. (2020). The shape of raindrops was assumed to be an oblate spheroid, whose axis ratio was determined by Andsager et al. (1999). The recorded drop data were collected weekly (emptying the Arduino SD memory card) and later post-processed at 5 min intervals, arranged into 0.1 mm drop size classes, and their respective numbers of drops and drop velocities were computed. The Arduino datalogging system used in this study had some limitations, as it could not record all the drops passing simultaneously through the laser beam (see Appendix A for further details).

2.2.2.2 Meteorological data

Meteorological data were obtained from an automatic weather station located 2 m above the canopy of the forest stand. The station was equipped with the following sensors: an air temperature and relative humidity probe (HMP45C, Vaisala, Vantaa, Finland), an anemometer and wind vane (A100R, Vector Instruments, Rhyl, North Wales, UK) and a net radiometer (NR Lite, Kipp & Zonen, Delft, The Netherlands). Data were measured every 30 s and averaged at 5 min intervals by the datalogger (Data Taker DT85, Thermo Fisher Scientific Inc., Sunbury, Victoria, Australia).

2.2.2.3 Event classification

This study was carried out on an event basis. A rain-free period of 6 h (day) and 12 h (night), allowing for the drying of the canopy, was considered necessary to define separate events (Llorens et al., 2014). All

event data were evaluated (i.e. quality controlled) for potential errors, and events with missing or erratic data were discarded. The definition of rainfall event classes was based on the duration and intensity of the event according to the following criteria: (a) a rainfall duration of 7 h was used to distinguish between short and long rainfall events; and (b) a maximum 30 min rainfall intensity threshold of 10 mm h^{-1} was used to separate low- and high-intensity events. By using both thresholds, rainfall was classified as: (1) short duration–low intensity (S–L) (≤ 7 h and ≤ 10 mm h^{-1}); (2) short duration–high intensity (S–H) (≤ 7 h and > 10 mm h^{-1}); (3) long duration–low intensity (L–L) (> 7 h and ≤ 10 mm h^{-1}); and (4) long duration–high intensity (L–H) (> 7 h and > 10 mm h^{-1}).

2.2.3 Estimation of throughfall types

The simultaneous measured open rainfall and throughfall DSD data were used for the separation of throughfall types by applying the protocol described by Levia et al. (2019). The separation, based on the DSD of throughfall and rainfall, consists of the calculation of the accumulated volume for each 0.1 mm drop diameter class. For each class *i* the volume of throughfall (TF_i) is partitioned in the corresponding class *i* of free throughfall (FR_i), splash throughfall (SP_i) and canopy drip (DR_i).

$$\Sigma TF_i = \Sigma(FR_i + SP_i + DR_i) \quad (1)$$

FR_i is calculated as

$$FR_i = p\, OP_i \quad (2)$$

where OP_i is the class *i* of open rainfall, and *p* is the free throughfall fraction (dimensionless, from 0 to 1), which is related to canopy openness. Raindrop impact on the canopy and/or wind and turbulence can cause the canopy to sway during rainfall events, triggering dynamic variation in the degree of canopy openness. Because it is difficult (or impossible) to determine actual *p*, an approximation of *p* was assigned as the maximum value under the condition (FR_i - $p\, OP_i$) > 0, utilising the same protocol as Nakaya et al. (2011); this protocol might overestimate *p*.

Splash throughfall is smaller than canopy drip. We set the maximum splash throughfall diameter (D_{MAX_SP}) at 2.0 mm and the minimum canopy drip diameter at 1.0 mm, respectively. This indicated that throughfall

drops with diameter (d_i) from 1.0 to 2.0 mm were generated from the mixture of FR, SP, and DR. The drop size distribution of SP_i was determined by a Weibull cumulative distribution function (Eq. 3). In this study, the minimum splash drop diameter was set at 0.5 mm (rather than the 0.4 mm used by Levia et al., 2019), as the datalogging systems were different: Arduino in this study and laptop in Levia et al. (2019). Therefore, in the Weibull function this value was set at 0.5 instead of 0.4.

$$F(d_i) = 1 - exp\left\{-\left(\frac{d_i - 0.5}{b}\right)^c\right\} \quad (3)$$

Equation (4) was used for the calculation of the estimated splash throughfall distribution (SP^*_i).

$$SP^*_i = \{\Sigma(TF_i - FR_i)\}\{F(d_i) - F(d_{i-1})\} \quad (4)$$

SP_i is determined by the minimum value between SP^*_i and ($TF_i - FR_i$). Finally, DR_i was calculated using Eq. (5) when $d_i > D_{MAX\_SP}$ or by Eq. 6 when splash was present.

$$DR_i = TF_i - FR_i \quad (5)$$

$$DR_i = TF_i - FR_i - SP_i \quad (6)$$

For a detailed explanation of the formulas, calculations and assumptions employed, the reader is referred to Levia et al. (2017, 2019).

2.2.4 Isotopic analysis

Rainfall and throughfall samples collected by the automatic samplers every 5 mm rainfall were analysed for water stable isotopes ($\delta^{18}O$ and $\delta^{2}H$) by the Scientific and Technical Services of the University of Lleida using the cavity ring-down spectroscopy technique with a Picarro L2120-i analyzer (Picarro Inc., Santa Clara, CA, USA). The equipment had an accuracy of < 0.1‰ for $\delta^{18}O$ and < 0.4‰ for $\delta^{2}H$, based on the repetition of four reference samples provided by the International Atomic Energy Agency (IAEA).
All isotopic data were expressed in terms of δ values and calculated as follows:

$$\delta = \left(\frac{R_{sample}}{R_{VSMOW}} - 1\right) \cdot 1000‰ \quad (7)$$

where *VSMOW* is the Vienna Standard Mean Ocean Water and *R* is the isotope ratio ($^{18}O/^{16}O$ or $^{2}H/^{1}H$). The isotopic shift between throughfall and open rainfall ($\Delta\delta^{18}O_{TF\text{-}RF}$) corresponds to the direct difference between the values of $\delta^{18}O$ throughfall and $\delta^{18}O$ open rainfall:

$$\Delta\delta^{18}O_{TF-RF} = \delta^{18}O_{TF} - \delta^{18}O_{RF} \quad (8)$$

Deuterium excess (*d*-excess) was later determined to describe the deviation from the global meteoric water line (GMWL) and to indicate kinetic fractionation effects caused by evaporation, as in Gat (1996):

$$d\text{-}excess = \delta^{2}H - 8 \cdot \delta^{18}O \quad (9)$$

2.2.5 Statistical analysis

IBM SPSS Statistics 25 software (IBM Corporation, Armonk, NY, USA) was employed for the statistical analyses. As the correlation between variables of our dataset was not necessarily linear, the Spearman's rank correlation coefficient (R_s) was computed. Data not normally distributed were analysed by the nonparametric rank-based Kruskall–Wallis *H* test, which examines the significance of the differences among throughfall type percentages or drop diameters with respect to the grouping of the four rainfall classes (based on duration and intensity). Statistical significance was set at $p < 0.05$. If the *H*-value from the Kruskal–Wallis test was significant, the Mann–Whitney–Wilcoxon test was applied as a *post hoc* evaluation for the pairwise comparisons to determine which groups were significantly different.

2.3 Results and discussion

2.3.1 Open rainfall, throughfall and drop characteristics

A total of 21 rainfall events were selected for analysis during the observation period (May 2018 to July 2019; Table S1), amounting to a total rainfall of 482 mm. The rainfall depth per event ranged from 6.0 to 52.5 mm, and the maximum 30 min intensities varied between 2.7 and 38.2 mm h^{-1}. The total amount of throughfall for the selected events was 428 mm (equivalent to 89% of total incident rainfall), and the maximum throughfall was 48.3 mm (equivalent to 92% of event incident rainfall). The total amount of rainfall–throughfall collected during the 21 events was distributed in 98 pairs of samples collected at 5 mm

rainfall intervals. For 33 of the 98 pairs of samples, throughfall was higher than rainfall; one-third of these samples corresponded to the end of the rainfall event, after rainfall stopped, whereas the remaining two-thirds were distributed without any specific pattern at different time intervals during the rainfall events.

The total number of drops in the dataset (i.e. the 98 samples) was 529750 for open rainfall and 271963 for throughfall, which means that the number of throughfall drops was 48% lower than that of rainfall. Altogether, 88% of the samples had fewer throughfall drops than rainfall (Fig. S1a). The median volume drop diameter (D_{50}), calculated for the 98 pairs of samples, ranged between 1.20 and 4.44 mm for open rainfall and between 1.47 and 4.17 mm for throughfall. The maximum diameter (D_{MAX}) ranged between 2.51 and 7.87 mm for open rainfall and between 3.25 and 7.92 mm for throughfall. At the event scale, the median volume drop diameter (D_{50}) ranged between 1.36 and 3.24 mm for open rainfall and between 2.83 and 3.90 mm for throughfall. Overall, the mean throughfall D_{50} found in this study (3.36 mm) was larger than values reported in other DSD studies. For example, Nanko et al. (2006) found that the throughfall D_{50} ranged from 1.77 to 2.93 mm for two coniferous species (Japanese cypress and Japanese cedar) under different meteorological conditions; moreover, Lüpke et al. (2019) reported throughfall D_{50} values of 2.7 and 0.80 for a European beech and Norway spruce tree respectively. The throughfall D_{50} was on average 1.3 mm larger than the rainfall D_{50}. However, in moments with very large rainfall drops, generally during the first two rainfall intervals (i.e. ≤ 10 mm), rainfall (8% of the total samples) had on average a diameter 0.37 mm larger than that of throughfall (Fig. S1b). The mean drop velocity was 4.34 ± 0.62 m s^{-1} for rainfall and 3.97 ± 0.29 m s^{-1} for throughfall. As expected, the mean velocity of throughfall drops was on average slower (0.4 m s^{-1}) than rainfall (Fig. S1c), due to the differences in drop falling distance caused by the canopy.

2.3.2 Partitioning throughfall types

Canopy drip, free throughfall and splash throughfall represented respectively 65 %, 19 % and 16 % of the total throughfall volume collected respectively (Fig. 3). In comparison with our results, Levia et al. (2019) found less canopy drip (51 %), but higher free throughfall (31 %) and a similar splash percentage (18 %) for other types of coniferous species. Tree height and canopy architecture differences between the coniferous species investigated by Levia et al. (2019) and the trees in our study may explain the differences in throughfall type percentages. In our study plot, higher tree canopy density and more woody surfaces

(branches that may be dying or shed) from the lower part of the crown towards the stem base probably reduced the contribution of free throughfall but raised canopy drip, in comparison with the shorter coniferous trees considered by Levia et al. (2019).

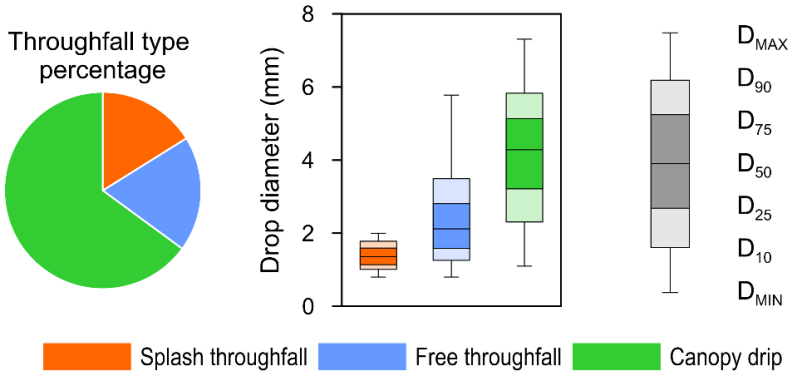

Figure 3. Throughfall type percentages (pie chart) and drop diameters for the three throughfall types (boxplots) for the 21 events studied. The drop diameters are based on the mean of examined events.

When separating events by rainfall classes (depending on rainfall duration and intensity), the Kruskal–Wallis test indicated that the percentages of splash throughfall were not significantly different between classes ($H = 3.34$, $p = 0.342$). In contrast, the percentages between classes for free throughfall ($H = 12.22$, $p = 0.007$) and canopy drip ($H = 15.16$, $p = 0.002$) were significantly different. The Mann–Whitney–Wilcoxon *post hoc* pairwise comparisons indicated that long-duration–low-intensity rainfall events had a significantly lower percentage of free throughfall and a higher percentage of canopy drip than long-duration–high-intensity events ($p = 0.009$ for both) and short-duration–high-intensity events ($p = 0.004$ and 0.002 respectively). Furthermore, short-duration–low-intensity events had a significantly higher percentage of canopy drip than short-duration–high-intensity events ($p = 0.004$). The percentages of throughfall types per rainfall classes are shown in Table S2.

The median volume drop diameters of the canopy drip, free throughfall and splash throughfall averaged for the 21 studied events were 4.28, 2.12 and 1.36 mm respectively (Fig. 3). When analysing drop diameters in cumulative drop volume percentiles, the Kruskal–Wallis test showed that drop diameters in the four rainfall classes were not significantly different for splash throughfall (H ranging from 1.12 to 2.44 and p

ranging from 0.478 to 0.772) and canopy drip (*H* ranging from 1.12 to 7.46 and *p* ranging from 0.059 to 0.773), with the exception of the 75th percentile which was significantly different for canopy drip ($H = 9.36$, $p = 0.025$). The Mann–Whitney–Wilcoxon *post hoc* pairwise comparisons indicated that short-duration–low-intensity rainfall events had significantly smaller canopy drip than short-duration–high-intensity events ($p = 0.017$). As expected, the Kruskal–Wallis test revealed that the free throughfall diameter was significantly different in the four rainfall classes (*H* ranging from 13.22 to 14.52 and *p* ranging from 0.002 to 0.004).

In summary, throughfall during low-intensity events gave higher canopy drip percentages (69% and 72%, for S–L and L–L events respectively) and lower free throughfall (16% and 13% respectively) than events with high intensities (56% and 62% of canopy drip and 25% and 21% of free throughfall for S–H and L–H respectively). Short-duration–low-intensity events generated smaller canopy drip diameters (D_{50_DR} = 4.03 mm), and long-duration–low-intensity events generated smaller free throughfall drop diameters (D_{50_FR} = 1.52 mm). Based on volume, our results show that low rainfall intensities increased canopy drip in both short and long events. On the other hand, rainfall duration increased canopy drip for both low- and high-intensity events. Therefore, long rainfall events with low rainfall intensity yielded the highest percentage of drip, whereas short rainfall events with high rainfall intensities yielded the lowest (difference of 16%).

2.3.3 Isotopic composition of open rainfall and throughfall

The $\delta^{18}O$ isotopic composition of the 98 pair samples (21 studied events) ranged from −13.72 ‰ to −2.18 ‰ for open rainfall and from −13.65 ‰ to −2.20 ‰ for throughfall. For $\delta^{2}H$, values ranged from −101.25 ‰ to −4.84 ‰ for open rainfall and from −98.54 ‰ to −3.61 ‰ for throughfall. As shown in Fig. 4a, open rainfall and throughfall samples fell on the local meteoric water line (LMWL) defined for the Vallcebre catchments ($\delta^{2}H = 7.9\ \delta^{18}O + 12.9$) (Casellas et al., 2019). Most of the throughfall samples (83 %) were more enriched ($\delta^{18}O$ and $\delta^{2}H$) than the open rainfall samples, showing predominant enrichment rather than depletion, which corroborates the results of several previous studies (Saxena, 1986; Dewalle and Swistock, 1994; Kubota and Tsuboyama, 2003; Cayuela et al., 2018a). The isotopic shift between throughfall and open rainfall ($\Delta\delta^{18}O_{TF\text{-}RF}$) ranged from −1.48 ‰ to 2.17 ‰. These differences are slightly higher than those reported by Cayuela et al. (2018a) for the same stand, probably due to the difference in the number of throughfall collectors in the two studies (10 *vs.* 1 in our study). Our results indicated preferential throughfall

enrichment at the event scale, based on the volume-weighted mean of $\delta^{18}O$ (Table S1), this is contrary to the results of Xu et al. (2014), who reported preferential throughfall depletion for a *Pinus radiata* forest in a Mediterranean climate. However, the values reported by these authors were bulked over multiple events. This highlights the paramount importance of using finer-scale sampling resolutions. Figure 4b indicates the presence of nonequilibrium fractionation processes, as not all of the enriched samples corresponded to a decrease in d-excess, and not all of the depleted samples corresponded to an increase. In fact, 50 % of the $\delta^{18}O$-enriched samples of throughfall had negative d-excess difference. Similarly, Herbstritt et al. (2019) observed that enrichment does not always lead to negative d-excess values and argued that such a phenomenon is usually attributed to mixing processes. For the case of pre-event water mixing (Allen et al., 2014), we ensured that all measured events started with an initially dry canopy, preventing the mixing of event water with water previously stored in the canopy. Consequently, the extent to which the differences in isotopic composition between rainfall and throughfall can be attributed to mixing processes remains unclear.

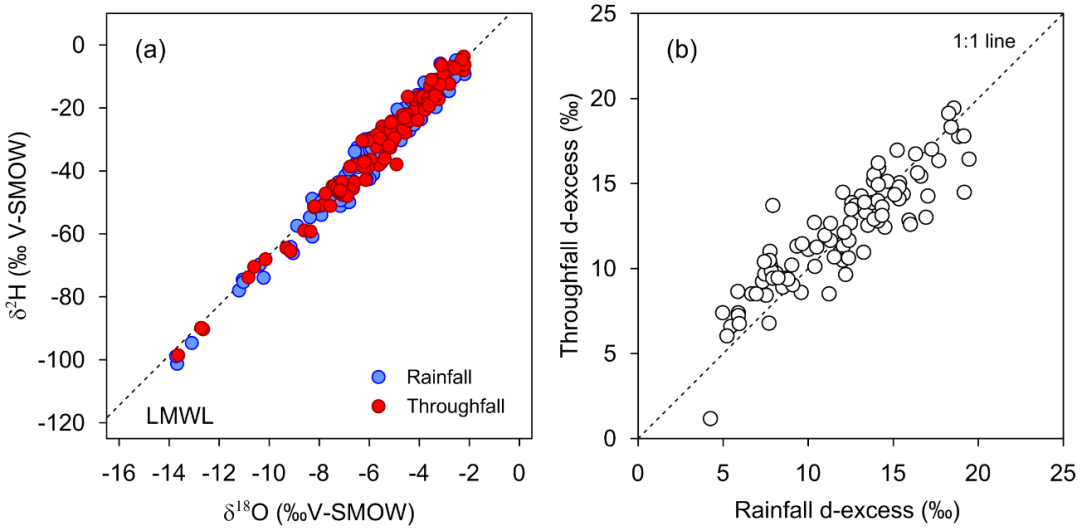

Figure 4. (a) $\delta^{18}O$ and $\delta^{2}H$ values of open rainfall and throughfall. The dashed line shows the local meteoric water line (LMWL). (b) The relationship between the deuterium excess (d-excess) of open rainfall and throughfall.

2.3.4 Drop sizes, throughfall types, and isotopic composition in rainfall events of different durations and intensities

To improve understanding of the temporal dynamics of throughfall types, the drop diameter of canopy drip and the isotopic composition of rainfall and throughfall, four events representative of each rainfall class were investigated in detail (i.e. at 5 min intervals, Fig. 5). The main characteristics of these events, which occurred in spring 2018 and 2019, are shown in Table 2. Rainfall classes grouped by intensities showed similar intensity values (i.e. S–L with L–L and S–H with L–H), whereas when grouped by duration the time values were almost double (i.e. S–L with S–H and L–L with L–H). The throughfall amount was lower than the incident rainfall except for the event on 11 June 2019 (Fig. 5c), in which it was slightly higher.

Table 2. Measured variables for the four selected events: S–L denotes short duration–low intensity, S–H denotes short duration–high intensity, L–L denotes long duration–low intensity and L–H denotes long duration–high intensity. RF is rainfall, TF is throughfall, D is rainfall duration, I_{Max} is the maximum 30 min rainfall intensity, N is the number of drops, D_{50} is the median volume drop diameter, SP is splash throughfall, FR is free throughfall and DR is canopy drip.

Date	RF class	RF (mm)	TF (mm)	D (h)	I_{Max} (mm h^{-1})	N_{RF}	N_{TF}	D_{50_RF}	D_{50_TF}	SP (%)	FR (%)	DR (%)
10 June 2018	S–L	7.8	5.4	3.0	5.9	9367	4230	1.9	3.4	17	16	67
06 June 2018	S–H	26.9	25.7	5.8	18.3	31472	19922	2.1	3.5	14	24	62
11 June 2019	L–L	32.6	33.0	16.2	5.9	58073	12753	1.4	3.9	9	11	80
12 May 2018	L–H	52.5	48.3	9.8	19.9	60559	32893	2.2	3.3	17	23	60

For the short-duration–low-intensity event (S–L, Fig. 5a), throughfall was mainly composed of free throughfall and splash throughfall during the first 30 min (< 0.6 mm of rain), and the canopy drip diameter (D_{50_DR}) was almost constant with a mean of 1.54 mm. After 30 min, the percentage of canopy drip gradually increased for 2 h, as did the drop diameter that reached an average D_{50_DR} of 3.65 mm, with a maximum canopy drip diameter (D_{MAX_DR}) of 4.70 mm. Canopy drip is clearly the main throughfall type during the last 30 min of the event, but the average D_{50_DR} decreased to 3.17 mm. Levia et al. (2019) observed a similar trend for the proportionate contribution of throughfall types for coniferous trees in a simulated steady short-duration event. As the water corresponding to the first ~1.9 mm of rainfall (1 h from the beginning of the event) was mixed with pre-event water in the sampling bottle, it was discarded from

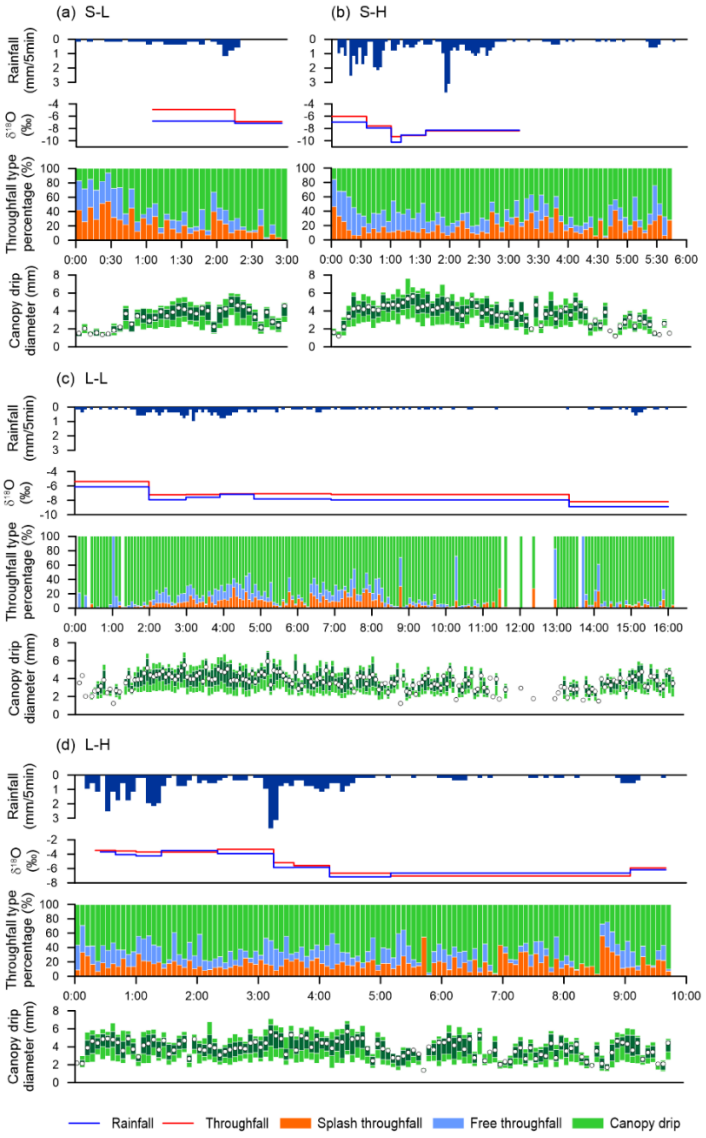

Figure 5. Temporal evolution (time since the start of the even) of rainfall dynamics (5 min time step), δ18O in rainfall and in throughfall (collected by the sequential samplers every 5 mm of rainfall), the throughfall type percentages based on volume, and the drop diameter of canopy drip (5 min time step). (a) Short-duration–low-intensity event (S–L), (b) short-duration–high-intensity event (S–H), (c) long-duration–low-intensity event (L–L) and (d) long-duration–high-intensity event (L–H). The drop diameter is shown in the boxplots with the respective cumulative drop volume percentiles (light green denotes 10% and 90%, dark green denotes 25% and 75%, and the white dot denotes 50%).

the analysis. The throughfall isotopic composition of the first sample (t = 1:00 to 2:15 h) was enriched (1.89 ‰) compared with open rainfall when splash throughfall reached 16.6%, which may be related to increased evaporation. For the second sample (t = 2:15 h to the end of the event), with a high contribution of canopy drip (75.8 %), the isotopic shift was almost zero, indicating a strong reduction of evaporation fractionation.

During the first 30 min (< 3.2 mm of rain) of the short-duration–high-intensity event (S–H, Fig. 5b) there was a gradual decrease in splash throughfall, balanced by an increase in canopy drip, whereas free throughfall remained relatively stable. During this time interval the D_{50_DR} increased from 1.60 to 4.33 mm. After 30 min, the contribution of various throughfall types was highly variable between successive time steps. Overall, canopy drip remained the main throughfall type during the event, but free throughfall tended to increase with rainfall intensity (from t = 1:00 to 1:30 h), whereas splash throughfall increased from 13 % (t = 0:30 to 2:40 h) to 21 % (t = 2:40 h to the end of the event) as rainfall intensity decreased. During the central part of the event (t = 0:30 to 4:30 h), the mean D_{50_DR} and D_{MAX} were 4.04 and 5.48 mm respectively; when rainfall almost stopped (t = 4:30 h), D_{50_DR} decreased to 2.33 mm. Similar to the previous event, the isotopic composition of the first throughfall sample was more enriched (0.93 ‰) than open rainfall, with a splash contribution of around 11.8 %. The throughfall isotopic composition of the second sample was slightly enriched (0.35 ‰), which was probably as a consequence of the canopy drip increase (from 56 % to 65 %), even if splash throughfall type also increased to 14.5 %. Enrichment of the third sample was similar to that of the first sample (0.92 ‰), with a splash contribution of 12.6 % and a canopy drip contribution of 55 %. The isotopic shift for the last two samples was almost zero. For these two samples, higher rainfall intensities may have reduced the lag time between throughfall and rainfall. Therefore, the evaporation impact may have led to periods of null or minimum isotopic shift, as suggested by Ikawa et al. (2011).

For the long-duration–low-intensity event (L–L, Fig. 5c), canopy drip was clearly the main throughfall type during the entire event with an average contribution of 80 % (Table 2). For this very light rain during a long time period, the canopy probably intercepted almost all the raindrops, triggering canopy drip after the water storage capacity of the vegetative surfaces was exceeded. Data showed that the drop diameter broadly stabilized after 80 min with an average D_{50_DR} of 3.87 mm and D_{MAX_DR} of 5.10 mm until rainfall stopped for the first time (t = 11:30 h). This intra-storm gap without rain was probably too short (< 90 min) to document any drying effect of the canopy on DSD, but a reduction in the canopy drop diameter at the

beginning of the second burst of rainfall (t = 13:00 h) was observed (D_{50_DR} of 2.58 mm). The throughfall isotopic composition was enriched for all of the samples from the event. As the splash throughfall type was small, splash droplet evaporation did not exert any significant influence. As mentioned, most of the rainwater was intercepted by the canopy and was retained on the vegetative surfaces for large periods of time (between ~1 and ~6.5 h). Partial evaporation probably took place during these periods, which explains the isotopic enrichment of the throughfall samples (Xu et al., 2014).

Finally, intermittent rain showers in the long-duration–high-intensity event (L–H, Fig. 5d) produced a heterogeneous contribution of throughfall types during the entire rainfall event. Canopy drip was evidently the main type, the free throughfall percentage increased with rainfall intensity and splash increased during low-intensity intervals. During a 20 min long period (t = 8:10 to 8:35 h) without rainfall, throughfall was formed by canopy drip and splash throughfall alone. This suggests that, in the absence of rainfall, dripping from the upper canopy may have impacted the lower canopy layers, which subsequently produced splash droplets, as also observed by Nanko et al. (2011). During this event, canopy drip increased after 10 min of rainfall, with mean D_{50_DR} rising from 2.16 mm to 4.28 mm and D_{MAX_DR} rising from 2.79 mm to 5.83 mm, until the end of the period with more intense rainfall (~ t = 5 h). Subsequently, the average D_{50_DR} decreased to 3.39 mm and D_{MAX_DR} decreased to 4.38 mm. An unclear pattern in the isotopic shift between rainfall and throughfall was observed throughout the event, even if the throughfall isotopic composition was only slightly enriched for most of the samples. This heterogeneous distribution of throughfall types and the absence of a clear pattern of isotopic shift suggest that, during this type of large event, a combination of evaporation, isotopic exchange and canopy selection processes probably occurred, which was similar to the findings of Cayuela et al. (2018a).

In general terms, the dynamics of throughfall partitioning were different for each rainfall type, which caused changes in the proportions of throughfall type (data at 5 min intervals) as well as in the isotopic composition (samples at 5 mm intervals) at the finer scale within individual rain events. It seems that the increase or decrease in canopy drip diameter was related to rainfall event evolution and was lower at the beginning and the end of all events. Similar to Lüpke et al. (2019), splash throughfall for a coniferous species was important at the beginning of the analysed events.

2.3.5 Relationship between isotopic shift and rainfall–throughfall characteristics

For the complete sample dataset (98 pairs of rainfall–throughfall samples), Spearman's rank-order correlation revealed no direct relationship between the $\delta^{18}O$ isotopic shift ($\Delta\delta^{18}O_{TF\text{-}RF}$) and meteorological variables such as the vapour pressure deficit (VPD; $R_s = -0.075$, $p = 0.464$) or wind velocity ($R_s = -0.027$, $p = 0.795$) (Fig. S2a and b). This confirms the results of Herbstritt et al. (2019), who found that meteorological variables did not provide consistent evidence to explain the observed isotopic shift. The most likely scenario is that a combination of rainfall characteristics, meteorological variables and isotopic fractionation factors exerted influence on the isotopic fractionation observed in the canopy. Moreover, Spearman's test showed no relationship between $\Delta\delta^{18}O_{TF\text{-}RF}$ and the difference in the number of drops between rainfall and throughfall ($R_s = -0.048$, $p = 0.642$), in drop velocities ($R_s = 0.114$, $p = 0.262$), or in amounts per sample ($R_s = -0.193$, $p = 0.057$) (Figs. S2c, d and e). However, some trends were observed. The isotopic shift ($\delta^{18}O$) between throughfall and rainfall increased when the D_{50_TF} got closer to or lower than the D_{50_RF} (i.e. with smaller throughfall drops; Fig. 6a). The isotopic shift also slightly decreased and become less variable with increasing cumulative rainfall (average values shifted from 0.44 ‰ to 0.14 ‰ for rainfall between 5 and more than 40 mm; Fig. 6b). This pattern is consistent with results found by Allen et al. (2017) in their meta-analysis, which showed larger isotopic shift differences for events with lower rainfall amounts. On the contrary, no relationship was found between the isotopic shift and the sampling time, the time each 5 mm sample took to be filled (Fig. 6c), as shown by the relatively stable isotopic shift (on average 0.40 ‰) observed for sampling times ranging from fewer than 30 min to more than 8 h. Finally, no clear relationship was found between the $\delta^{18}O$ isotopic shift and the kinetic energy of the rainfall drops (Fig. 6d). Similar results were obtained for the $\delta^{2}H$ isotopic shift (data not shown). The variability observed in the isotopic shift was found to decrease with increasing cumulative rainfall and sampling times (Fig. S3a and b).

The intra-event dynamics of the isotopic shift between rainfall and throughfall were analysed for events with a rainfall depth larger than 10 mm (i.e. for events giving more than two water samples). A total of 88 water samples corresponding to 16 events, with a rainfall depth ranging from 12.5 to 52.5 mm, were selected. Following Cayuela et al. (2018a), the selected events were split according to initial, middle and final stages. The initial stage corresponded to the first 5 mm of the event, the middle stage consisted of all

samples between the first and the last sample, and the final stage coincided with the sample collected during the last 5 mm of the event.

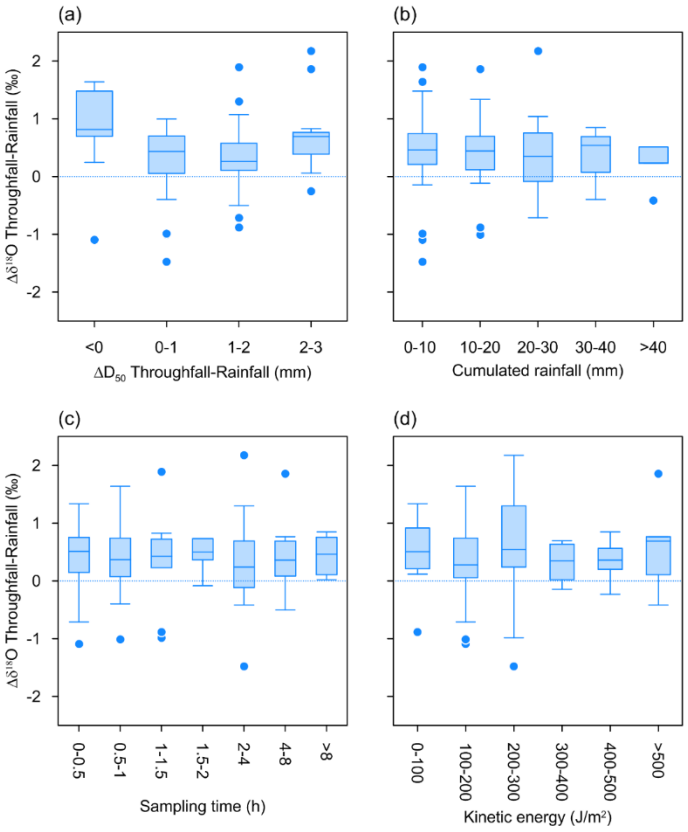

Figure 6. Boxplot of the isotopic shift ($\delta^{18}O_{TF\text{-}RF}$) *versus* classes of (a) differences in median volume drop diameter ($D_{50\ TF\text{-}RF}$), (b) cumulative rainfall throughout the rainfall event, (c) sampling time (i.e. time each 5 mm sample took to be filled) and (d) rainfall kinetic energy per sample. The light blue dots represent outliers.

The higher shift ($\Delta\delta^{18}O_{TF\text{-}RF}$) between throughfall and rainfall coincided with a higher VPD at the initial phase, and the lower $\Delta\delta^{18}O_{TF\text{-}RF}$ coincided with a lower VPD during the final phase of the events (Fig. 7). The first samples presented a median difference of 0.49 ‰ and, except for one outlier, all samples had positive $\Delta\delta^{18}O_{TF\text{-}RF}$, indicating throughfall enrichment. This isotopic enrichment at the beginning of the events was congruent with the higher VPD observed, with a mean value of 0.12 kPa, indicating higher atmospheric demand, which could increase evaporation in the canopy. Ikawa et al. (2011) and Cayuela et al. (2018a) observed the same fractionation pattern and suggested a greater impact of evaporation at the beginning of the event. Congruent with the isotopic shift and VPD dynamics during the events, the higher contribution of splash throughfall (17 %) also corresponded to the initial phase of events, and the lower

splash contribution (14 %) corresponded to the final phase of events (Fig. 7). Although the difference between the initial and final phases seems small (3 %), calculated percentages are based on volume: to achieve this difference, a huge amount of splash droplets is required. Because splash droplets are prone to a high degree of evaporation during their fall towards the ground (Dunin et al., 1988; Murakami, 2006; Xie et al., 2007), it is inferred that the net contribution of splash throughfall based on volume is linked to the splash evaporation mechanism that exerts influence at the initial stage of events, leading to greater isotopic enrichment of throughfall than of open rainfall.

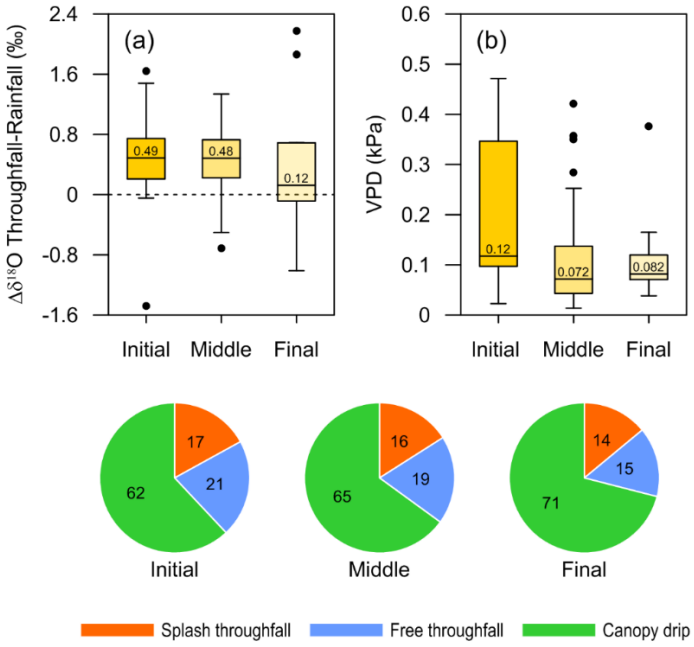

Figure 7. Boxplot of the intra-event dynamic observed in the initial, middle and final stages of 16 rainfall events (> 10 mm) for (a) isotopic shift differences ($\delta^{18}O_{TF\text{-}RF}$) and (b) VPD. Black dots represent outliers. Pie charts shows the proportion of throughfall types (%) for the different stages of rainfall events.

On the other hand, the lower contribution of canopy drip (62 %) corresponded to the initial phase of events, and higher drip contribution (71 %) corresponded to the final phase of events. As larger drop sizes reduce droplet evaporation rates, as demonstrated several decades ago (e.g. Best, 1952; Brain and Butler, 1985), an increase in the canopy drip contribution should reduce the isotopic shift due to fractionation by evaporation. However, canopy drip may also be the result of water accumulation originating from different flow paths (e.g. branchflow diverted from stemflow or drip recapture by lower canopy layers), representing a mixing process over canopy surfaces (e.g. vertical redistribution of water can trigger the mixing of water

from various small reservoirs formed by bark microrelief or cones in pine species), which may cause ambiguity in the isotopic shift between throughfall and open rainfall. In addition, as mentioned by Herbstritt et al. (2019), the mechanistic understanding of the variability of mixing between leaves (i.e. the water drip from leaf to leaf being able or not to cause subsequent splashing) could also be a key element in water mixing and evaporation in the rainfall interception processes.

2.4 Conclusions

This study sought to measure the isotopic compositions and drop characteristics of both rainfall and throughfall at the intra-event scale and to examine if there is any correspondence between the rainfall–throughfall isotopic shift and their drop size distribution differences. Results indicated that throughfall showed a lower number of drops, slower drop velocity and larger drop diameter than open rainfall did. Canopy drip accounts for most throughfall based on volume and corresponds to the largest drop diameter (average D_{50_DR} of 4.28 mm). Furthermore, our results showed that rainfall characteristics are an important abiotic factor that affects the throughfall DSD and, consequently, the proportion of throughfall types. Throughfall samples were almost always more enriched (δ^2H and $\delta^{18}O$) than rainfall. No correlation was found for the isotopic shift ($\Delta\delta^{18}O_{TF\text{-}RF}$ and $\Delta\delta^2H_{TF\text{-}RF}$) between throughfall and open rainfall in relation to meteorological variables, number of drops, drop velocities, throughfall and rainfall amount, or raindrop kinetic energy. However, the experiment's findings suggest that the isotopic shift decreased during the progression of discrete rainfall events and increased with a larger proportion of splash droplets. Our key finding indicates that higher contribution of splash throughfall and higher VPD at the initial stage of the rainfall events correspond to a greater isotopic shift ($\Delta\delta^{18}O_{TF\text{-}RF}$). This provides evidence for the net contribution of splash droplets to isotopic enrichment by means of the greater evaporation of throughfall than of open rainfall.

Future research should aim to assess the intra-canopy mixing of waters during intra-event wetting–drying cycles of a rainfall event in order to distinguish the isotopic fractionation factors. Additionally, using more throughfall tipping buckets with disdrometers in different locations below the canopy would help to further evaluate the spatial variability of DSD and its relationship with isotopic composition. Thus, future research should focus on the use of the fine spatiotemporal resolution of the isotopic composition of open rainfall and throughfall, in combination with meteorological variables and the various proportions of the different

types of throughfall, to enable better understanding of the physical processes controlling differences in the isotopic shift in different tree species. Such an improvement in our understanding of the fine-scale mechanism of the isotopic composition of throughfall in relation to throughfall drop size would permit strengthen assumptions of forest–water interactions.

Appendix A: Constraints with Arduino datalogging systems

Unlike the logging system using a laptop with A/D convertor (Nanko et al., 2006; Levia et al., 2019), the Arduino system could not record all of the temporal variations in output voltage due to the time required to record the data onto the SD card and an insufficient memory (compared with the random access memory, RAM, used in common devices). When a drop passes through the laser beam, output voltage was collected as shown in Fig. A1. When more than three continuous data values of output voltage were less than the threshold voltage (which was equal to the base voltage × 0.98, here), the Arduino system recorded five values, i.e. the base voltage, the minimum output voltage, the first output voltage, the last output voltage, and the number of data between the first and last output voltage, using a signal of drop data and a time stamp.

The Arduino threshold voltage setting means that drops with diameter < 0.8 mm could not be measured by this system. The Arduino system also has the disadvantage of failing to account for all drops when rainfall or throughfall continuously passes through the laser beam, due to its limited sampling speed. Finally, when several drops simultaneously pass in parallel in the same direction with respect to the laser beam, only the nearest drop to the transmitter is recorded. Consequently, due to the limitations of the Arduino datalogging system, on average 39% less incident rainfall and 45% less throughfall were observed between the tipping bucket and the disdrometer. Fortunately, these differences followed a consistent linear fit. Two assumptions were made for throughfall drop calculations to remedy the deficiencies of the Arduino system: (1) the percentage of throughfall drops < 0.8 mm is a marginal volume, and (2) the throughfall drops not measured by the disdrometers due to the other constraints of the Arduino system were distributed equally among the throughfall types.

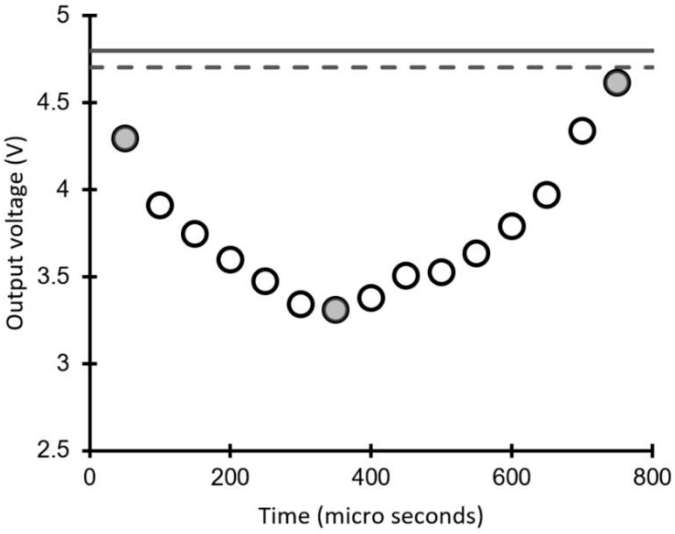

Figure A1. An example of temporal variation of output voltage due to a drop that passed through the laser beam. The solid line denotes the base voltage, the dashed line denotes the threshold voltage, the open circle denotes the output voltage every 50 μs and the closed circle denotes the data recording onto the Arduino.

2.5 References

Allen, S. T., Brooks, J. R., Keim, R. F., Bond, B. J., and McDonnell, J. J.: The role of pre-event canopy storage in throughfall and stemflow by using isotopic tracers, Ecohydrology, 7, 858-868, https://doi.org/10.1002/eco.1408, 2014.

Allen, S. T., Keim, R. F., and McDonnell, J. J.: Spatial patterns of throughfall isotopic composition at the event and seasonal timescales, J. Hydrol., 522, 58-66, https://doi.org/10.1016/j.jhydrol.2014.12.029, 2015.

Allen, S. T., Keim, R. F., Barnard, H. R., McDonnell, J. J., and Renée Brooks, J.: The role of stable isotopes in understanding rainfall interception processes: a review, WIREs Water, 4, e1187, https://doi.org/10.1002/wat2.1187, 2017.

Andsager, K., Beard, K. V., and Laird, N. F.: Laboratory measurements of axis ratios for large raindrops, J. Atmos. Sci., 56, 2673-2683, https://doi.org/10.1175/1520-0469(1999)056<2673:LMOARF>2.0.CO;2, 1999.

Best, A. C.: The evaporation of raindrops, Q. J. R. Meteorol. Soc., 78, 200-225, https://doi.org/10.1002/qj.49707833608, 1952.

Brain, P., and Butler, D. R.: A model of drop size distribution for a system with evaporation, Plant Cell Environ., 8, 247-252, https://doi.org/10.1111/1365-3040.ep11604646, 1985.

Casellas, E., Latron, J., Cayuela, C., Bech, J., Udina, M., Sola, Y., Lee, K.-O., and Llorens, P.: Moisture origin and characteristics of the isotopic signature of rainfall in a Mediterranean mountain catchment

(Vallcebre, eastern Pyrenees), J. Hydrol., 575, 767-779, https://doi.org/10.1016/j.jhydrol.2019.05.060, 2019.

Cayuela, C., Llorens, P., Sánchez-Costa, E., and Latron, J.: Modification of the isotopic composition of rainfall by throughfall and stemflow: the case of Scots pine and Downy oak forests under Mediterranean conditions, Ecohydrology, 11, e2025, https://doi.org/10.1002/eco.2025, 2018a.

Cayuela, C., Llorens, P., Sánchez-Costa, E., Levia, D. F., and Latron, J.: Effect of biotic and abiotic factors on inter-and intra-event variability in stemflow rates in oak and pine stands in a Mediterranean mountain area, J. Hydrol., 560, 396-406, https://doi.org/10.1016/j.jhydrol.2018.03.050, 2018b.

Dewalle, D. R., and Swistock, B. R.: Differences in oxygen-18 content of throughfall and rainfall in hardwood and coniferous forests, Hydrol. Process., 8, 75-82, https://doi.org/10.1002/hyp.3360080106, 1994.

Dunin, F. X., O'loughlin, E. M., and Reyenga, W.: Interception loss from eucalypt forest: lysimeter determination of hourly rates for long term evaluation, Hydrol. Process., 2, 315-329, https://doi.org/10.1002/hyp.3360020403, 1988.

Dunkerley, D. L.: Evaporation of impact water droplets in interception processes: historical precedence of the hypothesis and a brief literature overview, J. Hydrol., 376, 599-604, https://doi.org/10.1016/j.jhydrol.2009.08.004, 2009.

Friedman, I., Machta, L., and Soller, R.: Water-vapor exchange between a water droplet and its environment, J. Geophys. Res., 67, 2761-2766, https://doi.org/10.1029/JZ067i007p02761, 1962.

Gat, J. R.: Oxygen and hydrogen isotopes in the hydrologic cycle, Annu. Rev. Earth Planet. Sci., 24, 225-262, https://doi.org/10.1146/annurev.earth.24.1.225, 1996.

Green, M. B., Laursen, B. K., Campbell, J. L., McGuire, K. J., and Kelsey, E. P.: Stable water isotopes suggest sub-canopy water recycling in a northern forested catchment, Hydrol. Process., 29, 5193-5202, https://doi.org/10.1002/hyp.10706, 2015.

Herbstritt, B., Gralher, B., and Weiler, M.: Continuous, near-real-time observations of water stable isotope ratios during rainfall and throughfall events, Hydrol. Earth Syst. Sci., 23, 3007-3019, https://doi.org/10.5194/hess-23-3007-2019, 2019.

Iida, S., Shimizu, T., Shinohara, Y., Takeuchi, S. and Kumagai, T.: The Necessity of Sensor Calibration for the Precise Measurement of Water Fluxes in Forest Ecosystems, in: Forest-Water Interactions, edited by: Levia, D. F., Carlyle-Moses, D. E., Iida, S., Michalzik, B., Nanko, K. and Tischer, A., Springer, Cham, Switzerland, 29-54, https://doi.org/10.1007/978-3-030-26086-6_2, 2020

Ikawa, R., Yamamoto, T., Shimada, J., and Shimizu, T.: Temporal variations of isotopic compositions in gross rainfall, throughfall, and stemflow under a Japanese cedar forest during a typhoon event, Hydrol. Res. Lett., 5, 32-36, https://doi.org/10.3178/hrl.5.32, 2011.

Kubota, T., and Tsuboyama, Y.: Intra-and inter-storm oxygen-18 and deuterium variations of rain, throughfall, and stemflow, and two-component hydrograph separation in a small forested catchment in Japan, J. For. Res., 8, 179-190, https://doi.org/10.1007/s10310-002-0024-9, 2003.

Latron, J., Llorens, P., and Gallart, F.: The hydrology of Mediterranean mountain areas, Geography Compass, 3, 2045-2064, https://doi.org/10.1111/j.1749-8198.2009.00287.x, 2009.

Levia, D. F., Hudson, S. A., Llorens, P., and Nanko, K.: Throughfall drop size distributions: a review and prospectus for future research, WIREs Water, 4, e1225, https://doi.org/10.1002/wat2.1225, 2017.

Levia, D. F., Keim, R. F., Carlyle-Moses, D. E., and Frost, E. E.: Throughfall and stemflow in wooded ecosystems, in: Forest Hydrology and Biogeochemistry, edited by: Levia, D. F., Carlyle-Moses, D., and Tanaka, T., Springer, Dordrecht, Netherlands, 425-443, https://doi.org/10.1007/978-94-007-1363-5_21, 2011.

Levia, D. F., Nanko, K., Amasaki, H., Giambelluca, T. W., Hotta, N., Iida, S., Mudd, R. G., Sakai, N., Shinohara, Y., Sun, X., Suzuki, M., Tanaka, N., Tantasirin, C., and Yamada, K.: Throughfall partitioning by trees, Hydrol. Process., 33, 1698-1708, https://doi.org/10.1002/hyp.13432, 2019.

Levia, D. F., and Frost, E. E.: Variability of throughfall volume and solute inputs in wooded ecosystems, Prog. Phys. Geog., 30, 605-632, https://doi.org/10.1177/0309133306071145, 2006.

Llorens, P., Domingo, F., Garcia-Estringana, P., Muzylo, A., and Gallart, F.: Canopy wetness patterns in a Mediterranean deciduous stand, J. Hydrol., 512, 254-262, https://doi.org/10.1016/j.jhydrol.2014.03.007, 2014.

Llorens, P., Gallart, F., Cayuela, C., Roig-Planasdemunt, M., Casellas, E., Molina, A. J., Moreno-de las Heras, M., Bertran, G., Sánchez-Costa, E., and Latron, J.: What have we learnt about Mediterranean catchment hydrology? 30 years observing hydrological processes in the Vallcebre research catchments, Geogr. Res. Lett., 44, 475-501, https://doi.org/10.18172/cig.3432, 2018.

Lüpke, M., Leuchner, M., Levia, D., Nanko, K., Iida, S. I., and Menzel, A.: Characterization of differential throughfall drop size distributions beneath European beech and Norway spruce, Hydrol. Process., 33, 3391-3406, https://doi.org/10.1002/hyp.13565, 2019.

Molina, A. J., Llorens, P., Garcia-Estringana, P., de las Heras, M. M., Cayuela, C., Gallart, F., and Latron, J.: Contributions of throughfall, forest and soil characteristics to near-surface soil water-content variability at the plot scale in a mountainous Mediterranean area, Sci. Total Environ., 647, 1421-1432, https://doi.org/10.1016/j.scitotenv.2018.08.020, 2019.

Murakami, S.: A proposal for a new forest canopy interception mechanism: Splash droplet evaporation, J. Hydrol., 319, 72-82, https://doi.org/10.1016/j.jhydrol.2005.07.002, 2006.

Nakaya, K., Wakamatsu, T., Ikeda, H., Abe, S., and Toyoda, Y.: Development of raindrop kinetic energy model under canopy for the estimation of soil erosion in forest, CRIEPI Res. Rep. V11001, Central Research Institute of Electric Power Industry – CRIEPI, Japan, 2011.

Nanko, K., Hotta, N., and Suzuki, M.: Evaluating the influence of canopy species and meteorological factors on throughfall drop size distribution, J. Hydrol., 329, 422-431, https://doi.org/10.1016/j.jhydrol.2006.02.036, 2006.

Nanko, K., Hudson, S. A., and Levia, D. F.: Differences in throughfall drop size distributions in the presence and absence of foliage, Hydrol. Sci. J., 61, 620-627, https://doi.org/10.1080/02626667.2015.1052454, 2016.

Nanko, K., Mizugaki, S. and Onda, Y.: Estimation of soil splash detachment rates on the forest floor of an unmanaged Japanese cypress plantation based on field measurements of throughfall drop sizes and velocities, Catena, 72, 348-361, https://doi.org/10.1016/j.catena.2007.07.002, 2008b.

Nanko, K., Onda, Y., Ito, A., and Moriwaki, H.: Effect of canopy thickness and canopy saturation on the amount and kinetic energy of throughfall: An experimental approach, Geophys. Res. Lett., 35, L05401, https://doi.org/10.1029/2007GL033010, 2008a.

Nanko, K., Onda, Y., Ito, A., and Moriwaki, H.: Spatial variability of throughfall under a single tree: Experimental study of rainfall amount, raindrops, and kinetic energy, Agr. Forest Meteorol., 151, 1173-1182, https://doi.org/10.1016/j.agrformet.2011.04.006, 2011.

Nanko, K., Tanaka, N., Leuchner, M. and Levia, D. F.: Throughfall erosivity in relation to drop size and crown position: a case study from a teak plantation in Thailand, in: Forest-Water Interactions, edited by: Levia, D. F., Carlyle-Moses, D. E., Iida, S., Michalzik, B., Nanko, K. and Tischer, A., Springer, Cham, Switzerland, 279-298, https://doi.org/10.1007/978-3-030-26086-6_12, 2020

Nanko, K., Watanabe, A., Hotta, N., and Suzuki, M.: Physical interpretation of the difference in drop size distributions of leaf drips among tree species, Agr. Forest Meteorol., 169, 74-84. https://doi.org/10.1016/j.agrformet.2012.09.018, 2013.

Poyatos, R., Latron, J., and Llorens, P.: Land use and land cover change after agricultural abandonment, Mt. Res. Dev., 23, 362-369, https://doi.org/10.1659/0276-4741(2003)023[0362:LUALCC]2.0.CO;2, 2003.

Saxena, R. K.: Estimation of canopy reservoir capacity and oxygen-18 fractionation in throughfall in a pine forest, Hydrol. Res., 17, 251-260, https://doi.org/10.2166/nh.1986.0017, 1986.

Stewart, M. K.: Stable isotope fractionation due to evaporation and isotopic exchange of falling waterdrops: Applications to atmospheric processes and evaporation of lakes, J. Geophys. Res., 80, 1133-1146, https://doi.org/10.1029/JC080i009p01133, 1975.

Xie, X., Li, Y., Chwang, A. T., Ho, P. L., and Seto, W. H.: How far droplets can move in indoor environments - revisiting the Wells evaporation-falling curve, Indoor Air, 17, 211-225, https://doi.org/10.1111/j.1600-0668.2007.00469.x, 2007.

Xu, X., Guan, H., and Deng, Z.: Isotopic composition of throughfall in pine plantation and native eucalyptus forest in South Australia, J. Hydrol., 514, 150-157, https://doi.org/10.1016/j.jhydrol.2014.03.068, 2014.

CHAPTER 3

High-resolution temporal dynamics of intra-storm isotopic composition of stemflow and throughfall in a Mediterranean Scots pine forest

High-resolution temporal dynamics of intra-storm isotopic composition of stemflow and throughfall in a Mediterranean Scots pine forest

Vegetation plays a significant role in the isotopic fractionation of rainwater during rainfall partitioning through the canopy into throughfall and stemflow. Most studies focus on the isotopic composition of throughfall, whereas that of stemflow has been studied much less frequently. Moreover, only three studies to date have investigated stemflow isotopic composition at the intra-storm scale. Therefore, knowledge of the isotopic shift between rainfall and throughfall/stemflow at fine resolutions is sorely needed in order to better understand water input to forest soils. In this study, intra-event rainfall, throughfall and stemflow in a Scots pine forest under Mediterranean conditions were monitored (5-min time step) over a 20-month period (May 2018 to December 2019) and water samples of each component were collected sequentially by means of automatic samplers for isotopic analysis (^{18}O and ^{2}H). Results obtained for 21 rainfall events show that throughfall was usually more enriched than rainfall and stemflow was more enriched than throughfall. Isotopic differences between rainfall and throughfall/stemflow indicated that throughfall was more depleted during the higher air temperature season whereas stemflow was more enriched. The isotopic shift did not show any direct relationship with either meteorological variables or the amount effect. At the intra-storm scale, stemflow was more enriched than rainfall and throughfall at the start of the rainfall event and tended to decrease toward the end. Our results suggest that evaporation led to stemflow enrichment due to stemflow residing longer on the vegetative surfaces than throughfall. However, most fractionation factors can occur during the same event. Our study will improve understanding of the physical processes that control stemflow isotopic composition in coniferous trees before reaching the ground, as a step towards improving isotope-based models for forest-water interactions.

Original work: Pinos, J., Llorens, P., & Latron, J. (2022). High-resolution temporal dynamics of intra-storm isotopic composition of stemflow and throughfall in a Mediterranean Scots pine forest. Hydrological Processes, 36(8), e14641. https://doi.org/10.1002/hyp.14641

3.1 Introduction

In forested catchments, rainfall interception by forest canopies and its redistribution as throughfall and stemflow alter the volume of water that reaches soils, the spatiotemporal dynamics of water inputs and the initial characteristics of net precipitation, such as nutrient and particle concentrations and isotopic composition. Throughfall refers to the rainwater that may or may not have contact with vegetative surfaces and falls or drips to the forest ground, whereas stemflow is the proportion of rainwater than is captured by vegetative surfaces, is channeled to the bole and then flows towards the base of the tree (Levia et al., 2011).

Fractionation of stable water isotopes ($\delta^{18}O$ and $\delta^{2}H$) can lead to the enrichment or depletion of intercepted water by means of evaporation, isotopic exchange, canopy selection processes, mixing of waters and sub-canopy water recycling. Evaporation refers to the change from liquid to the gas phase; isotopic exchange may result from the interaction between liquid and environmental vapour when these pools are not in equilibrium; canopy selection refers to the possibility that intercepted rainfall is retained or transmitted depending on which rainfall event interval it falls; mixing of water refers to the mixing of waters of different isotopic composition in the canopy. This study defines inter-event mixing as when residual water of previous rainfall stored in the canopy is mixed with new rainwater; whereas the term intra-event mixing is used when this process occurs within the same event suggesting that flow paths vary across the event. Finally, sub-canopy water recycling refers to the water recondensation of evapotranspiration, which may be re-incorporated to the interception cycle (Green et al., 2015; Allen et al., 2017). Evaporation causes isotopic enrichment whereas exchange, canopy selection, mixing of waters and sub-canopy recycling cause either isotopic enrichment or depletion. Isotopic modification of throughfall can occur in both directions (enrichment and depletion) (e.g., Saxena, 1986; Pinos et al., 2020), whereas for stemflow, enrichment usually prevails, unlike both rainfall and throughfall isotopic compositions (e.g., Allen et al., 2014; Cayuela et al., 2018a). Therefore, in isotope-based hydrology studies, it is preferable to use the isotopic composition of throughfall and stemflow instead of that of rainfall as the water input signal into a catchment with ample forest cover (Klaus and McDonnell, 2013; Stockinger et al., 2017).

Greater academic attention has been paid to the isotopic composition of throughfall, because more water reaches the forest soil due to it than to stemflow. Nonetheless, despite stemflow usually accounting for only ~2% of gross rainfall, it provides a highly concentrated flux of water at the base of the trees. Consequently,

near-stem soils may receive water and nutrient inputs that greatly exceed those received by far-stem soils via throughfall (Carlyle-Moses et al., 2018). Moreover, stemflow can affect both the volume and isotopic signature of soil water (Snelgrove et al., 2020) and even of stream water (Crabtree and Trudgill, 1985) and groundwater (Tanaka et al., 1996). In contrast with throughfall, only a relatively limited number of studies have focused on stemflow isotopic composition, generally at coarse temporal resolution (i.e. event, daily or weekly scale) in forest/shrub ecosystems. To our knowledge, only three studies have looked at the isotopic composition of intra-storm stemflow (see Table A1), which means that the temporal dynamics of the intra-storm isotopic composition of stemflow remains poorly understood. Therefore, as Allen et al. (2017; 2020) argue, analysis of the intra-storm isotopic composition variability of throughfall and stemflow is sorely needed to improve the mechanistic understanding of the physics of rainfall interception processes controlling isotopic fractionation. This kind of analysis which will shed light on key forest hydrology processes, such as interception loss, canopy storage capacity and tree water routing.

Because of the much greater heterogeneity of stemflow response (in terms of volumes, intensities and lag times) than of rainfall and throughfall, the measurement and sampling of stemflow at fine time intervals within a storm event is challenging and no 'standard methodology' has been determined yet. Kubota and Tsuboyama (2003) were the first to sample rainfall, throughfall and stemflow at the intra-storm scale, using an autonomous homemade sequential water sampler (a modified version of Kennedy et al.'s (1979) rainfall sampler), which consists of 12 bottles and one storage tank. With this set-up, samples were obtained at every 3.5 mm increment of rainfall and throughfall, and 0.038 mm of stemflow. For each component, the water that exceeded the capacity of the last bottle was directed to the storage tank. The main constraints of this sampling design were basically the low number of samples before the tank filled and the lack of synchronization between rainfall, throughfall and stemflow sampling (i.e. sampling of each component depended on volume and not on time). The second study of intra-storm isotopic composition of rainfall, throughfall and stemflow, was carried out by Ikawa et al. (2011) for a single typhoon event, using an automatic water sampler designed by Ikawa et al. (2009). Collected water was first stored in plastic buckets with capacities of 40 L for rainfall and throughfall and 60 L for stemflow. Subsequently, an automatic water sampler (SIGMA900, HACH, 24 samples) took individual samples from each bucket at 1-h intervals, just before the remaining water in the buckets was automatically drained by an electro-magnetic valve. In this case, the main constraint of the sampling design was the need to collect samples every 24 h, which is suitable for sampling particularly large storm events such as typhoons but not for continuous monitoring of

rainfall events in more remote areas. In addition, the synchronized and continuous 1 h sampling time interval may not always be well suited to capturing all the rainfall, throughfall and especially stemflow isotopic composition variability throughout the event, as stemflow production is often concentrated within a short period during the rainfall event, once a gross rainfall threshold has been exceeded (Cayuela et al., 2018b; Pinos et al., 2021). The third and, we believe, most recent study of the intra-storm isotopic composition of rainfall, throughfall and stemflow was carried out by Tao et al. (2017) for two rainfall events. Rainfall, throughfall and stemflow water was manually collected at two different time intervals (every 15-30 min when rainfall intensity was high and 30-60 min when it was lower). The snag here is that manual sampling may be suitable for sampling one or two individual events, but not for long-term continuous monitoring.

Kubota and Tsuboyama (2003) found, for a coniferous forest plantation (Japanese cypress and Japanese cedar), that isotopic stemflow was in general more enriched than rainfall and throughfall. However, isotopic depletion was also observed during some intra-storm intervals in different events (see Figure 7 in Kubota and Tsuboyama, 2003). With the information available, the authors were not able to explain the differences in the intra-storm isotopic compositions of the different fluxes. Similarly, Ikawa et al. (2011), for a Japanese cedar forest, found that at the intra-storm scale, stemflow was more enriched than rainfall and throughfall, but some time intervals of isotopic depletion were also found (see Figure 1 in Ikawa et al., 2011). The authors attribute this pattern to the intra-event mixing of waters. Finally, Tao et al. (2017), for a Chinese jujube forest plantation, found a predominant isotopic enrichment of stemflow, in comparison to rainfall and throughfall (see Figure 4 in Tao et al., 2017). In this study, enrichment in stemflow is attributed to higher evaporation, due to the longer residence times than in throughfall, to canopy selection processes and to the intra-event mixing of waters.

To overcome the absence of a method suitable for measuring and sampling the intra-storm variability of stemflow and the lack of available knowledge about stemflow isotopic composition, the main objectives of this study were (i) to develop an approach to measure and sample stemflow at high temporal resolution, (ii) to analyze the seasonal, inter-storm and intra-storm temporal dynamics of the isotopic compositions of throughfall and stemflow and (iii) to compare these with that of rainfall. The aims were to shed light on the causes of isotopic fractionation between these fluxes and the influence of throughfall and stemflow on soil water and groundwater isotopic dynamics.

3.2 Data and methods

3.2.1 Study area and forest stand characteristics

The study was undertaken in the Can Vila catchment (0.56 Km^2) (Figure 1a), one of the Vallcebre research catchments (eastern Pyrenees, northeastern Spain 42°12′ N, 1°49′ E), managed by the Surface Hydrology and Erosion group (IDAEA-CSIC). Forest, covering around 60% of the catchment, is mostly Scots pine (*Pinus sylvestris L.*), but small original fragmented oak forests (*Quercus pubescens Willd.*) are still present. Mean annual precipitation (867 ± SD of 223 mm) is seasonal throughout the year, with spring and autumn being the wettest seasons and summer and winter being the driest (Llorens et al., 2018). Mean reference evapotranspiration (856 ± 69 mm) shows a seasonal pattern, with maximum values in summer of up to 6.9 mm d^{-1}. Mean air temperature is around 9.2°C (period 1999–2018).

The study was carried out in an experimental Scots pine forest plot (900 m^2), named Cal Rotes, in the central part of the Can Vila catchment at an elevation of 1200 m. In the forest plot, tree density averages 1189 trees ha^{-1}, mean diameter at breast height (DBH) 19.9 ± 9.2 cm, forest basal area 45.1 m^2 ha^{-1}, mean tree height 17.0 ± 4.4 m and mean canopy cover 69.3 ± 17.7%. Since 2012, a meteorological station has been situated 2 m above the canopy of the forest plot. The station is equipped with the following sensors: an air temperature and relative humidity probe (HMP45C, Vaisala, Vantaa, Finland), an anemometer and wind vane (A100R, Vector Instruments, Rhyl, North Wales, UK) and a net radiometer (NR Lite, Kipp & Zonen, Delft, the Netherlands). Data are measured every 30 s and averaged at 5 min intervals by the datalogger (Data Taker DT85, Thermo Fisher Scientific Inc., Sunbury, Victoria, Australia).

3.2.2 Rainfall, throughfall and stemflow measurement and sampling

This research is based on the continuous measurement and sampling of rainfall, throughfall and stemflow. The rainfall monitoring site was located in an open area approximately 100 m from the Scots pine plot where throughfall and stemflow were monitored (Figure 1a). Throughfall and stemflow were monitored and sampled at a single location within the forest plot. The choice of these two locations was based on the experience of several years monitoring and sampling throughfall and stemflow within the forest plot. During these years, throughfall was measured with 20 tipping bucket rain gauges and sampled with 10 collectors, located according to the canopy cover distribution. Stemflow was monitored with rings

connected to tipping buckets on 7 trees and sampled with rings draining to buckets on 4 trees, representative of the plot's DBH distribution (see Cayuela et al., 2018a; 2018b for details).

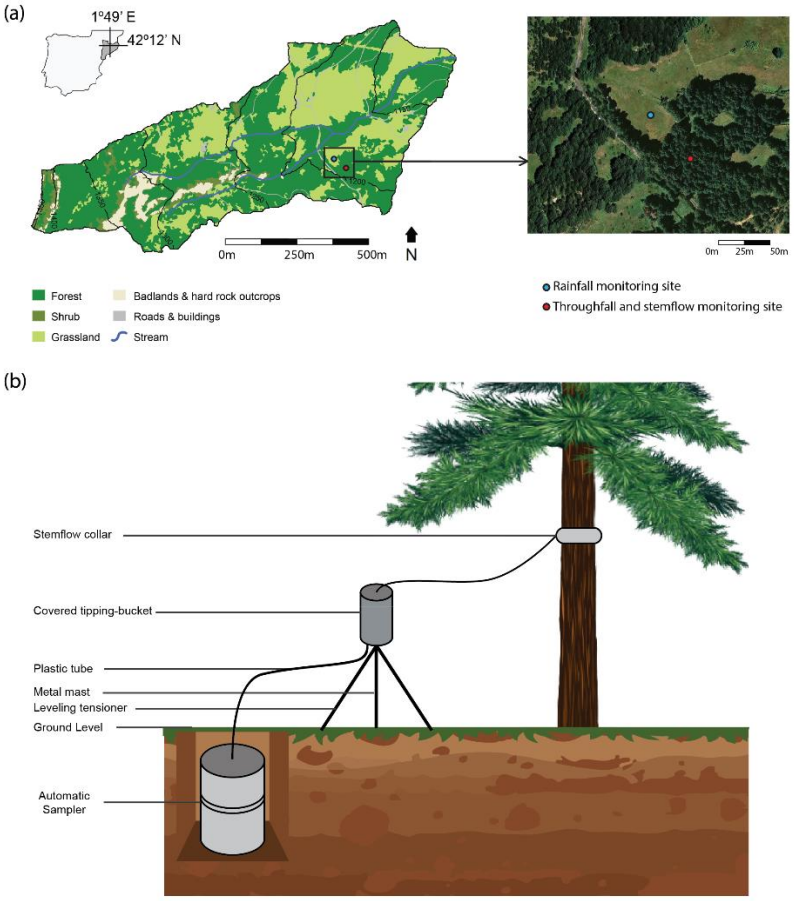

Figure 1. Location of the study area: (a) Can Vila catchment and the experimental Cal Rotes forest stand, and (b) diagram of the set-up for continuous measurement and sampling of stemflow.

In our study, throughfall was monitored and sampled under a tree that has a canopy large enough (17.3 m^2) to allow the positioning of the throughfall instruments (Pinos et al., 2020). Stemflow was monitored and sampled at a tree representative of the plot's DBH distribution with a high funneling ratio (tree P1 in Cayuela et al., 2018b) to ensure enough runoff volume for suitable intra-event sampling. The main biometric characteristics of the monitored trees are given in Table 1.

Table 1. Biometric characteristics of the monitored trees for throughfall and stemflow (adapted from Cayuela et al., 2018b). DBH indicates the diameter at breast height.

Throughfall			Stemflow	
DBH (cm)	35.2		DBH (cm)	18
Basal area (cm^2)	973.1		Basal area (cm^2)	254.5
Height (m)	22.3		Height (m)	17.5
Canopy projected area (m^2)	17.3		Canopy projected area (m^2)	7.5
Crown volume (m^3)	228		Crown volume (m^3)	59.7
Mean branch angle (º)	19.2		Mean branch angle (º)	29.5
Mean branch diameter (cm)	4.4		Mean branch diameter (cm)	3.1
Bark depth (cm)	3.3		Bark depth (cm)	1.5
Canopy cover (%)†	85.2		Stem bark surface (m^2)	6.3
Distance to first live branch (m)	12.4		Bark storage capacity (mm)	0.40
Tree lean (º)	7.9		Tree lean (º)	4.6

† Canopy cover was measured over the throughfall tipping-bucket collection area.

Five minute-interval rainfall and throughfall data were measured by tipping buckets (model AW-P, Institut Analític, Barcelona, Spain), with 0.2 mm resolution, connected to the datalogger. The tipping buckets were connected to automatic samplers (ISCO 3700 with 500 ml bottles, Teledyne ISCO Inc., Lincoln, NE, USA) by looped tubing, which sequentially collected rainfall and throughfall samples at 5 mm rainfall intervals (i.e. both samplers switched to the next bottle simultaneously after each 5 mm of rainfall).

To collect stemflow, a plastic ring was placed around the trunk at breast height of the selected tree and gaps were sealed with silicone to avoid leaking. The ring was connected by a plastic hose to a covered tipping bucket (model AW-P, Institut Analític, Barcelona, Spain) dynamically calibrated to measure stemflow volume (Equation 1). Stemflow data was recorded at 5 min-interval by the datalogger.

$$if\ n\ =\ 0;\ SF = 0$$

$$if\ n \geq 1;\ SF\ = -0.0040 + 0.0071 \cdot n\ + 0.00003215 \cdot n^2 - 0.0000001069 \cdot n^3 + 9.50686\ \times 10^{-11} \cdot n^4 \quad (1)$$

where *SF* represents the stemflow in litres, and *n* the number of tips recorded by the tipping bucket.

One of the two drainage openings for the tipping bucket was connected to an automatic sampler (ISCO 2700 with 1000 ml bottles, Teledyne ISCO Inc., Lincoln, NE, USA) by looped tubing, as depicted in Figure 1b. This means that the collected volume of stemflow corresponds to half the volume recorded by the tipping bucket. With this set-up, the maximum sequential sampling capacity of stemflow corresponded to 48 L of measured stemflow (24 1-L bottles). The water that exceeded the automatic sampler's capacity was stored in the container in which the sampler was placed. With our set-up, stemflow sampling had to be dependent on the volume of stemflow likely to be generated during an interval of 5 mins (which had to be less than 2 L so as to be [half] sampled correctly with 1000 ml bottles). For this reason, stemflow sampling intervals could not be matched with those of rainfall and throughfall (at 5 mm rainfall intervals).

All tipping buckets were calibrated dynamically to ensure the quality of data (Iida et al., 2020). To minimize evaporation, all automatic samplers were placed in containers buried in the ground and all samples were collected soon after each storm (1 week maximum). Three events with presence of snow that occurred during the study period were not included in the study. Some limitations of the sampling methodology used in the study are shown in Appendix B.

3.2.3 Isotopic analysis

Rainfall, throughfall and stemflow water samples were analysed for $\delta^{18}O$ and $\delta^{2}H$ by means of the cavity ring-down spectroscopy technique using a Picarro L2120-i analyzer (Picarro Inc., Santa Clara, CA, USA) by the Scientific and Technical Services of the University of Lleida. The L2120-i was coupled to an A0211 high-precision vaporizer module. The estimated precision for the L2120-i, based on the repeated analysis of four reference water samples, was <0.10 ‰ for $\delta^{18}O$ and <0.40 ‰ for $\delta^{2}H$.

Delta notation (δ) is used to express the isotopic composition ratios of hydrogen and oxygen in rainfall, throughfall and stemflow samples.

$$\delta = \left(\frac{R_{sample}}{R_{VSMOW}} - 1\right) \cdot 1000\ ‰ \quad (2)$$

where R represents the $^{18}O/^{16}O$ or $^{2}H/^{1}H$ isotopic abundance ratio, and VSMOW refers to Vienna Standard Mean Ocean Water.

Deuterium excess (d-excess = $\delta^2H - 8\delta^{18}O$) was calculated for all water samples as deviation from the global meteoric water line (GMWL) and indicates potential fractionation effects on the isotope samples (Gat, 1996).

3.2.4 Data analysis

Due to our set-up, stemflow sampling intervals could not match those of rainfall and throughfall (see Section 3.2.2). To compare the isotopic composition of the different fluxes, we paired rainfall and throughfall samples with stemflow ones. To do this, for each stemflow sampling subinterval, volume-weighted mean isotopic composition was calculated for rainfall and throughfall as

$$\bar{\delta} = \frac{\sum_{i=1}^{n} \delta_i P_i}{\sum_{i=1}^{n} P_i} \quad (3)$$

where δ_i and P_i are the isotopic composition of (rainfall or throughfall) samples and the (rainfall or throughfall) water amount, respectively, observed during each stemflow sampling time subinterval (i). An example of the result of applying this procedure for a single rainfall event is shown in Figure S1.

The isotopic shift ($\Delta\delta^{18}O_{TF–RF}$, $\Delta\delta^{18}O_{SF–RF}$ and $\Delta\delta^{18}O_{SF–TF}$) was then calculated for every sample as the direct differences between $\delta^{18}O$ of throughfall (TF) and rainfall (RF), $\delta^{18}O$ of stemflow (SF) and rainfall, and $\delta^{18}O$ of stemflow and throughfall. A similar procedure was followed for the δ^2H isotope and for determining the shift in d-excess (Δd-excess$_{TF–RF}$, Δd-excess$_{SF–RF}$ and Δd-excess$_{SF–TF}$).

The intra-storm dynamics of the isotopic shift ($\Delta\delta^{18}O_{TF–RF}$, $\Delta\delta^{18}O_{SF–RF}$ and $\Delta\delta^{18}O_{SF–TF}$) were analysed at three storm stages. The initial stage corresponded to the time interval from the onset of the storm to the end

of the first stemflow sample, the middle stage corresponded to the time interval of all samples between the first and last stemflow sample, and the final stage corresponded to the time interval of the last stemflow sample. In events where stemflow continued after rainfall ended (see Figure S1), the final stage corresponded to the volume-weighted mean isotopic composition of all stemflow samples after rainfall ceased. Events with only two stemflow samples and events where the 48-L capacity was exceeded (> 24 stemflow samples) were discarded for the stage analysis. The same criteria were used to investigate the relationship between the isotopic shift and the amount effect.

3.2.5 Statistical analysis

Throughfall and stemflow data were not normally distributed. Then, the non-parametric rank-based Kruskal-Wallis H test (XLSTAT 2021.3.1 software, Addinsoft Inc, NY, USA) was used to examine the isotopic differences between seasons and between event stages. Statistical significance was set at $p < 0.05$.

3.3 Results

3.3.1 Event scale rainfall, throughfall, stemflow amounts and their isotopic composition

A total of 21 events were selected for analysis during the observation period (May 2018 to December 2019; Table S1 in supplementary material). Rainfall amount of the 21 analysed events ranged from 8.8 to 83.7 mm (mean 30.2 mm; median 26.9 mm), and throughfall amount ranged from 7.1 to 82.3 mm (mean 27.7 mm; median 20.7 mm). Stemflow volume ranged from 1 to 81 L (mean 17.7 L; median 11.3 L). Throughfall showed a positive linear relationship with rainfall amount, whereas stemflow had a polynomial fit with rainfall amount (Figure S2). The rainfall thresholds needed to generate throughfall and stemflow were 2.7 and 9.1 mm, respectively, according to the fitted equations. Mean rainfall intensities ranged from 0.6 to 17.7 mm h^{-1}, with 76% of the events having mean intensities below 5 mm h^{-1}. Event duration varied between 1.2 and 43.3 hours, with 24% of the events classified as short-duration events (≤ 7 h; following Pinos et al., 2020).

At the event scale (21 events studied), the volume-weighted mean $\delta^{18}O$ values ranged from −13.10‰ to −3.67‰ for open rainfall, from −12.91‰ to −3.51‰ for throughfall and from −12.76‰ to −2.89‰ for

stemflow. For δ^2H, mean values ranged from −82.89‰ to −14.71‰ for open rainfall, from −82.43‰ to −13.48‰ for throughfall and from −82.25‰ to −10.58‰ for stemflow (Table S1). The isotopic seasonal pattern indicated that rainfall with heavier $\delta^{18}O$ values occurred during the growing season (May 15 to October 15) when air temperature was higher (Figure 2). At the event scale, the isotopic shift ($\Delta\delta^{18}O$) between open rainfall and throughfall ($\Delta\delta^{18}O_{TF-RF}$) ranged from −0.20‰ to 1.03‰, whereas $\Delta\delta^{18}O$ between open rainfall and stemflow ($\Delta\delta^{18}O_{SF-RF}$) ranged from 0.19‰ to 2.92‰ and $\Delta\delta^{18}O$ between throughfall and stemflow ($\Delta\delta^{18}O_{SF-TF}$) ranged from −0.56‰ to 2.65‰. For all 21 events, stemflow enrichment was observed at the event scale.

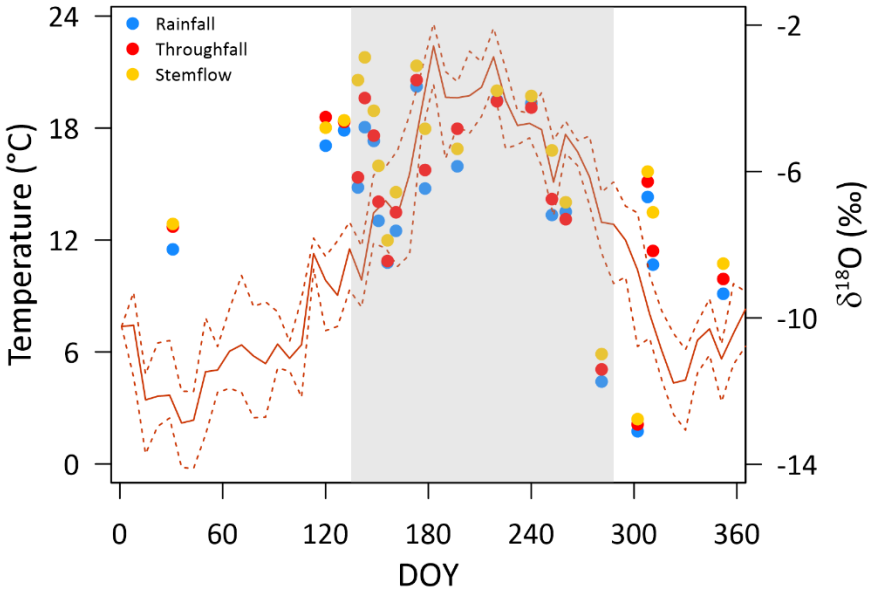

Figure 2. Time series of daily air temperature (min, mean and max) and mean event scale $\delta^{18}O$ values measured in rainfall, throughfall and stemflow in the Scots pine stand (period 2018–2019). Greyed area corresponds to the growing season.

3.3.2 Dual isotope plot and d-excess at the sample scale

The LMWL at Vallcebre research catchments, determined by Casellas et al. (2019), is $\delta^2H = 7.9\ \delta^{18}O + 12.9$. Most of the throughfall and stemflow samples fell on the LMWL (Figure 3), but the slopes and

intercepts of the relationships for throughfall and stemflow samples were lower than those of the LMWL, indicating that these fluxes experienced non-equilibrium fractionation processes.

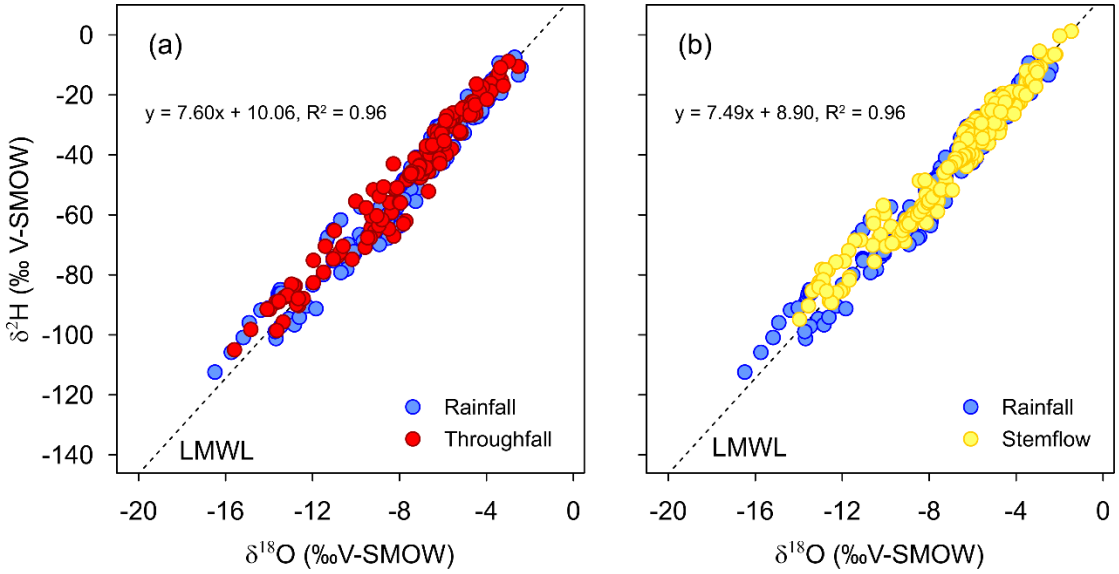

Figure 3. Dual-isotope plot of open rainfall, (a) throughfall, and (b) stemflow samples collected during the study period. The dashed line indicates the local meteoric water line (LMWL: $\delta^2H = 7.9\ \delta^{18}O + 12.9$), while the equation shown in the figure refers to the relation of throughfall (a) and stemflow (b) samples.

Considering all 178 triplets of samples (i.e. rainfall, throughfall and stemflow samples for the same established time interval), the $\delta^{18}O$ values ranged from −16.49‰ to −2.40‰ for open rainfall, from −15.59‰ to −2.54‰ for throughfall and from −13.96‰ to −1.47‰ for stemflow. For δ^2H, values ranged from −112.43‰ to −7.43‰ for open rainfall, from −104.96‰ to −8.83‰ for throughfall and from −94.84‰ to 1.20‰ for stemflow.

In general, for both isotopes throughfall and stemflow were more enriched than rainfall, but stemflow samples were more often more enriched than throughfall ones (Figure 4a and b). For $\delta^{18}O$, 78% and 90% of throughfall and stemflow samples, respectively, were more enriched than rainfall. Similar values were observed for δ^2H (81% in TF and 90% in SF). Consequently, depleted samples were most frequent in throughfall, almost twice that in stemflow in both isotopes. Stemflow was also usually more enriched than

throughfall. For $\delta^{18}O$, 92% of stemflow samples were more enriched than throughfall samples (88% for $\delta^{2}H$). Figure 4c and d shows the deuterium excess (d-excess) in open rainfall over that in throughfall and stemflow. This comparison indicates the presence of non-equilibrium fractionation processes (i.e. not only evaporation), since not all the enriched (throughfall or stemflow) samples corresponded to a decrease in deuterium excess (from that of rainfall); and not all the depleted samples, to an increase. Indeed, 37% and 44% of the $\delta^{18}O$ enriched samples of throughfall and stemflow showed negative deuterium excess.

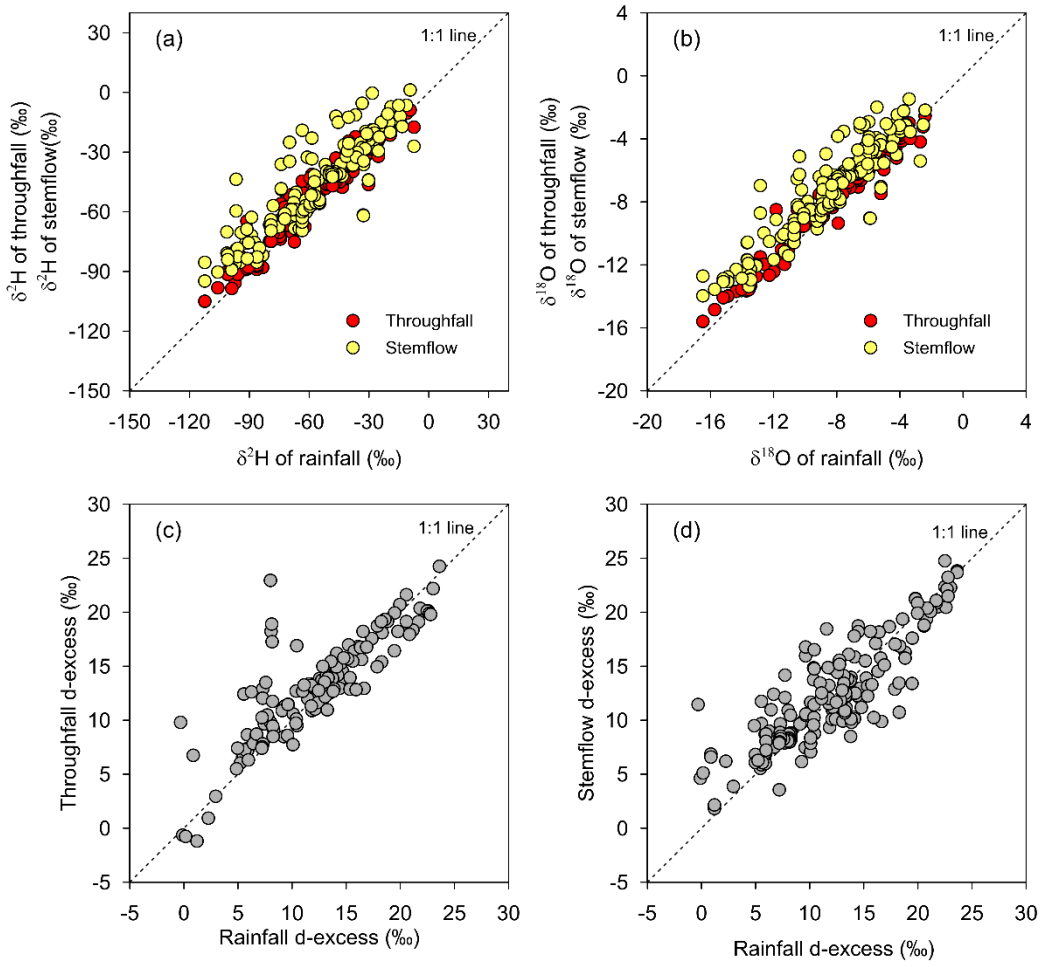

Figure 4. Isotopic composition in throughfall and stemflow relative to that of rainfall (a) for $\delta^{18}O$ and (b) for $\delta^{2}H$ and the relationship between the deuterium excess (d-excess) in open rainfall and (c) throughfall and (d) stemflow.

The isotopic shift ranged from −2.27‰ to 3.34‰ between open rainfall and throughfall ($\Delta\delta^{18}O_{TF\text{-}RF}$), from −3.16‰ to 5.88‰ between open rainfall and stemflow ($\Delta\delta^{18}O_{SF\text{-}RF}$), and from −3.98‰ to 4.54‰ between throughfall and stemflow ($\Delta\delta^{18}O_{SF\text{-}TF}$). The comparison of the isotopic shift of throughfall and stemflow in relation to open rainfall ($\Delta\delta^{18}O_{SF\text{-}RF}$ vs $\Delta\delta^{18}O_{TF\text{-}RF}$, Figure 5) clearly showed that stemflow samples were more enriched than throughfall ones. $\Delta\delta^{18}O_{TF\text{-}RF}$ correlated positively with $\Delta\delta^{18}O_{SF\text{-}RF}$ ($R^2 = 0.51$, n = 178, p = < 0.0001), indicating that the isotopic shift of both fluxes respect to rainfall increase together.

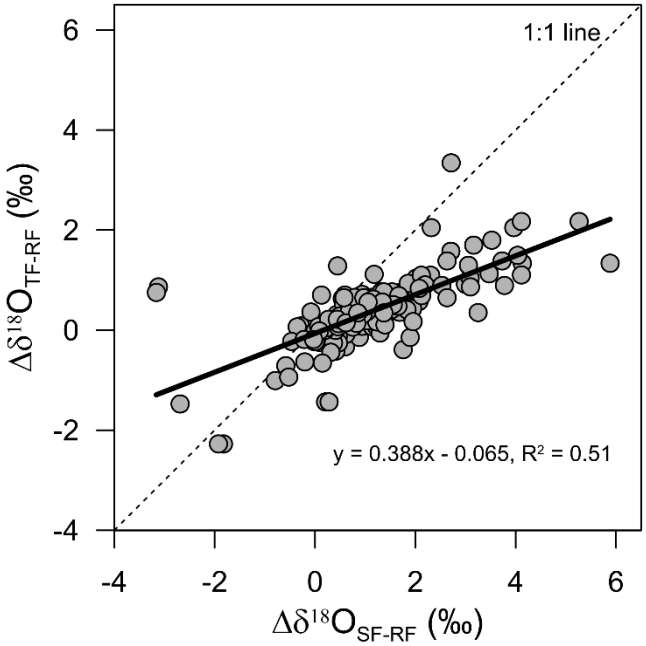

Figure 5. Relationship between the isotopic shift of stemflow ($\Delta\delta^{18}O_{SF\text{-}RF}$) and throughfall ($\Delta\delta^{18}O_{TF\text{-}RF}$) in relation to open rainfall for the 178 triplets of samples (i.e., open rainfall, throughfall and stemflow samples for the same time interval) obtained for the 21 events. The relationship ($\Delta\delta^{18}O_{SF\text{-}RF}$ vs $\Delta\delta^{18}O_{TF\text{-}RF}$) is significant at $p < 0.05$.

3.3.3 Influence of seasonal and meteorological characteristics

Differences in isotopic shift between open rainfall and throughfall/stemflow for the growing and dormant seasons were not statistically significant (as indicated by the *p*-values in Figure 6a and b). However, at both

temporal scales (event and sample scale), throughfall was less enriched during the growing season, which is the period of higher temperature, than during the dormant season (Figure 6a). On the contrary, also at both temporal scales, stemflow was slightly more enriched during the growing season than during the dormant season (Figure 6b). Finally, statistically significant differences in isotopic shift between throughfall and stemflow for the growing and dormant seasons were found, showing that stemflow was consistently more enriched than throughfall, especially in the growing season (Figure 6c).

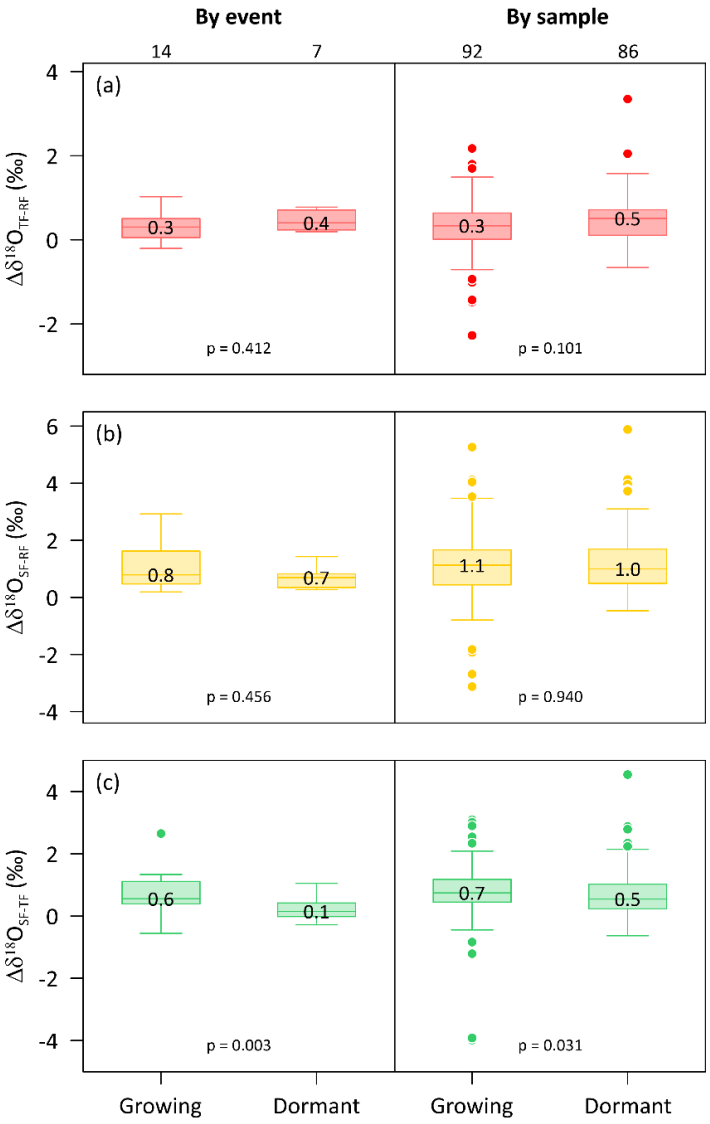

Figure 6. Isotopic shift between throughfall and open rainfall ($\Delta\delta^{18}O_{TF-RF}$) (a), stemflow and open rainfall ($\Delta\delta^{18}O_{SF-RF}$) (b), and stemflow and throughfall ($\Delta\delta^{18}O_{SF-TF}$) (c) for the growing and dormant seasons at the event (left column) and sample (right column) time scale. The number at the top of the graphs refers to the number of observations per season. Dots represent outliers. Kruskal-Wallis test results are shown within each graph.

No statistically significant relationships were found in the isotopic shift between open rainfall and throughfall/stemflow and maximum 5-min rainfall intensity (Figure 7a), maximum 5-min throughfall and stemflow intensities (Figure 7b), mean wind speed (Figure 7c) and mean vapour pressure deficit (Figure 7d). However, it is conjectured that $\Delta\delta^{18}O_{TF\text{-}RF}$ variability seemed to decrease when the maximum 5-min rainfall or throughfall intensities increased. Similarly, $\Delta\delta^{18}O_{SF\text{-}RF}$ variability decreased when the maximum 5-min rainfall intensity increased, whereas no clear pattern was found when maximum 5-min stemflow intensity increased (which correlated weakly with maximum 5-min rainfall intensity). These last results should be viewed with caution because of the small sample size of the highest rainfall intensity intervals. In addition, no relationship between the isotopic shift between open rainfall and throughfall/stemflow versus mean rainfall intensity, intra-event rainfall intermittency (Dunkerley, 2015) and sampling duration (i.e. time each 1-L stemflow sample took to be filled) was found (data not shown).

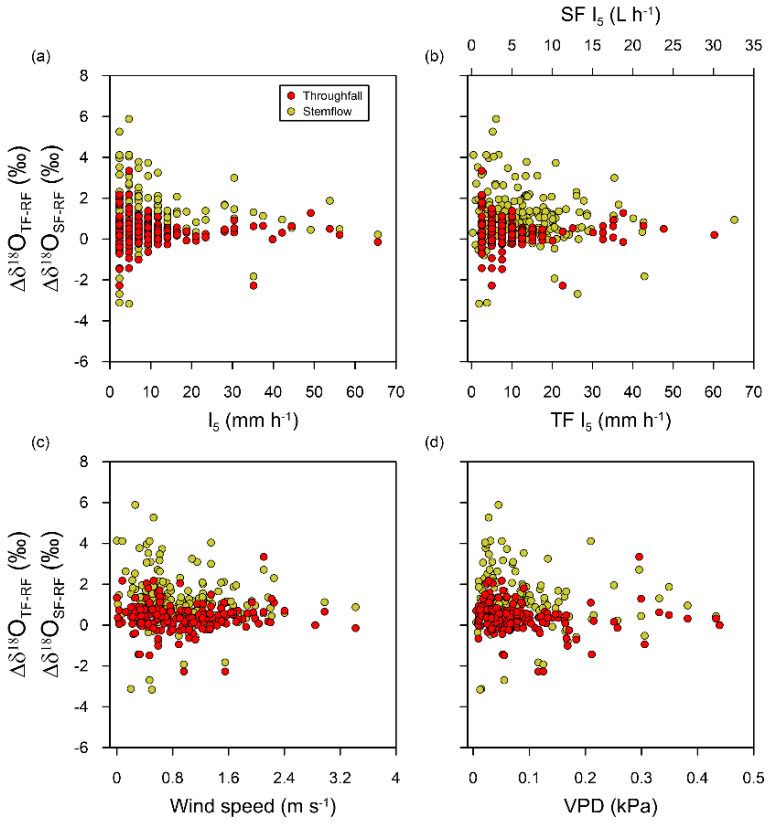

Figure 7. Isotopic shift between throughfall and open rainfall ($\Delta\delta^{18}O_{TF\text{-}RF}$) and stemflow and open rainfall ($\Delta\delta^{18}O_{SF\text{-}RF}$) versus maximum 5-min rainfall intensity (a), maximum 5-min throughfall/stemflow intensity (b), mean wind speed (c) and mean vapour pressure deficit during the event (d).

3.3.4 Intra-storm differences and amount effect

The intra-storm dynamics of the isotopic shift between open rainfall and throughfall/stemflow were analysed for events with at least 3 stemflow samples but no more than 24 samples (sampler capacity limit). A total of 122 triplets of samples, corresponding to 15 events, were selected for the analysis. The events were split according to initial, middle and final stages (see Section 3.2.4), and no statistically significant differences were found between consecutive stages (Figure 8). Although there was no statistical significance, some patterns could be observed. The isotopic shift between open rainfall and throughfall ($\Delta\delta^{18}O_{TF-RF}$) and between open rainfall and stemflow ($\Delta\delta^{18}O_{SF-RF}$) was higher at the beginning of the rainfall event and decreased towards the end of the event (difference between the medians from 0.41‰ to 0.19‰ and from 1.04‰ to 0.83‰, respectively, Figure 8a and c). A similar but smoother decreasing pattern was found for the isotopic shift between throughfall and stemflow ($\Delta\delta^{18}O_{SF-TF}$) (median difference from 0.69‰ to 0.58‰, Figure 8e). Shift in d-excess showed that Δd-excess$_{TF-RF}$ and Δd-excess$_{SF-RF}$ tended to increase during the event (difference between the medians from 0.53‰ to 1.84‰ and from -0.23‰ to 0.86‰, respectively, Figure 8b and d); whereas, on the contrary, a decreasing pattern was found for Δd-excess$_{SF-TF}$ (difference between the medians from -0.77‰ to -1.20‰, Figure 8f). Generally, a greater variability of the isotopic shift values was observed at the final stage of the events.

As throughfall and stemflow samples, for a given sampling interval, may be composed of water stored in the canopy and trunk, we investigated the correlation between stemflow and throughfall $\delta^{18}O$ with that of rainfall that fell in the previous interval. Results indicated that the isotopic shift was lessened, suggesting the effect of canopy selection processes (Figure S3). However, these results should be taken with caution since the duration of the intervals is not constant during the events (i.e. interval duration for the triplet samples corresponds to the period of time required to reach 2 litres of stemflow and ranged from 10 to 840 min).

No clear relationship was found of the isotopic shift between rainfall and throughfall ($\Delta\delta^{18}O_{TF-RF}$) with either cumulative rainfall or throughfall (Figure 9a), and of the isotopic shift between rainfall and stemflow ($\Delta\delta^{18}O_{SF-RF}$) with either cumulative rainfall or stemflow (Figure 9b), indicating the absence of any amount effect. Similarly, no relationship of the isotopic shift between throughfall and stemflow ($\Delta\delta^{18}O_{SF-TF}$) with

cumulative throughfall or stemflow was found (Figure 9c). However, there was less variability at $\Delta\delta^{18}O_{SF-TF}$ than at $\Delta\delta^{18}O_{SF-RF}$.

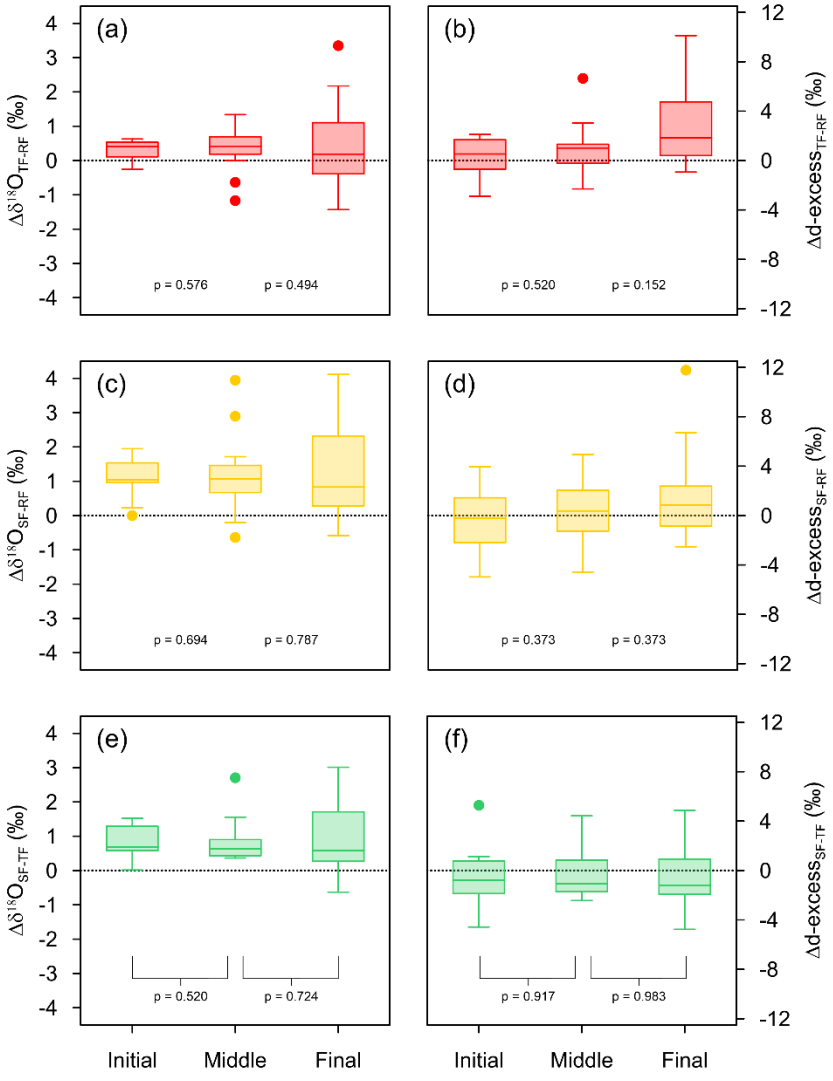

Figure 8. Boxplot of the isotopic shift between throughfall and open rainfall ($\Delta\delta^{18}O_{TF-RF}$) (a), stemflow and open rainfall ($\Delta\delta^{18}O_{SF-RF}$) (c) and stemflow and throughfall ($\Delta\delta^{18}O_{SF-TF}$) (e) and of the shift in d-excess between throughfall and open rainfall (Δd-excess$_{TF-RF}$) (b), stemflow and open rainfall (Δd-excess$_{SF-RF}$) (d) and stemflow and throughfall (Δd-excess$_{SF-TF}$) observed during the initial, middle and final stage of rainfall events.

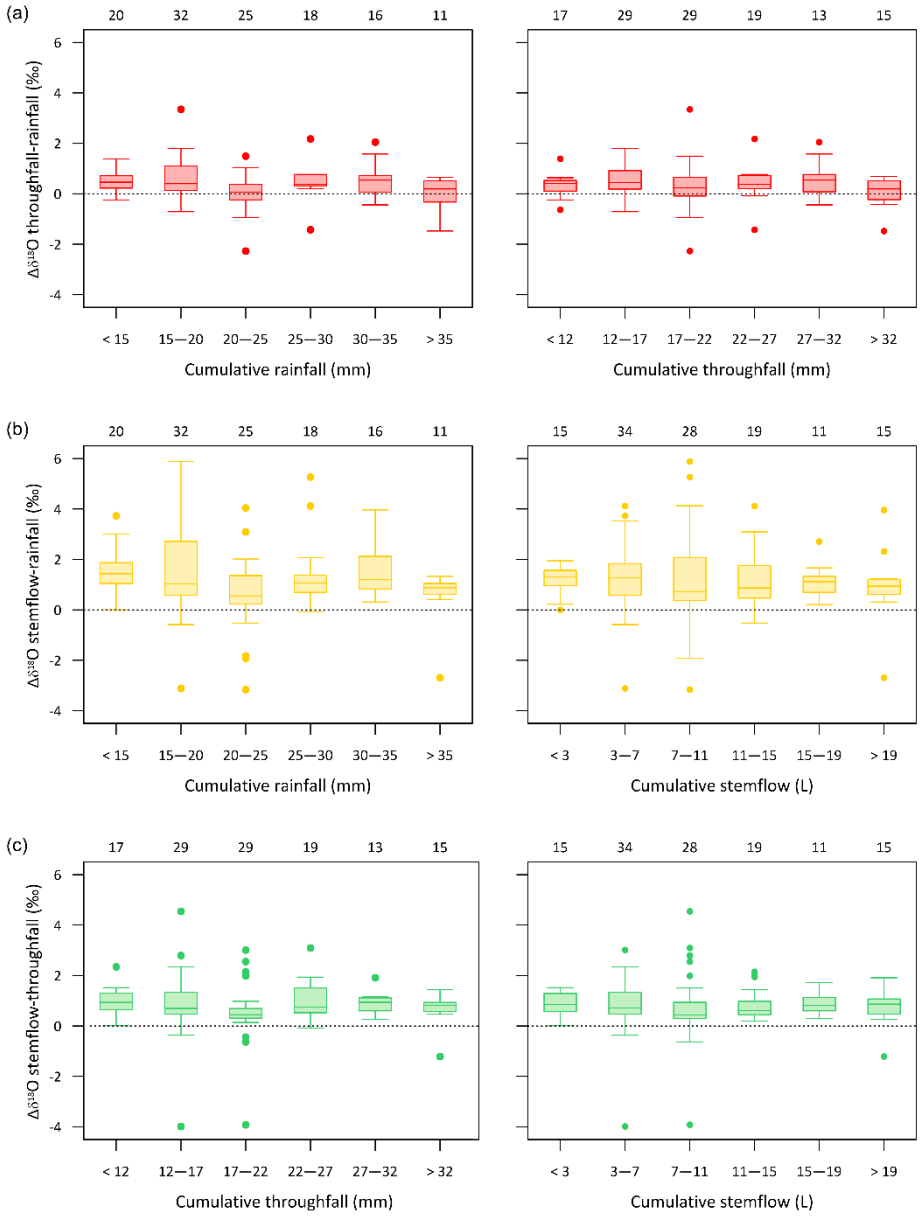

Figure 9. Boxplot of the isotopic shift between throughfall and open rainfall ($\Delta\delta^{18}O_{TF\text{-}RF}$) (a), stemflow and open rainfall ($\Delta\delta^{18}O_{SF\text{-}RF}$) (b) and stemflow and throughfall ($\Delta\delta^{18}O_{SF\text{-}TF}$) (c) for different amounts of cumulative rainfall, throughfall and/or stemflow. The number at the top of the graphs refers to the number of observations per class. Dots represent outliers.

3.3.5 Comparison of intra-storm dynamics for selected events

At the event scale, the relationship for the mean isotopic shift between throughfall and rainfall ($\Delta\delta^{18}O_{TF-RF}$) and the deuterium excess differences (Δd-excess$_{TF-RF}$) showed (Figure 10) a weak non-significant negative correlation ($R^2 = 0.21$). A similar result was obtained for the mean isotopic shift between stemflow and rainfall ($\Delta\delta^{18}O_{SF-RF}$) and the deuterium excess differences (Δd-excess$_{SF-RF}$) ($R^2 = 0.14$).

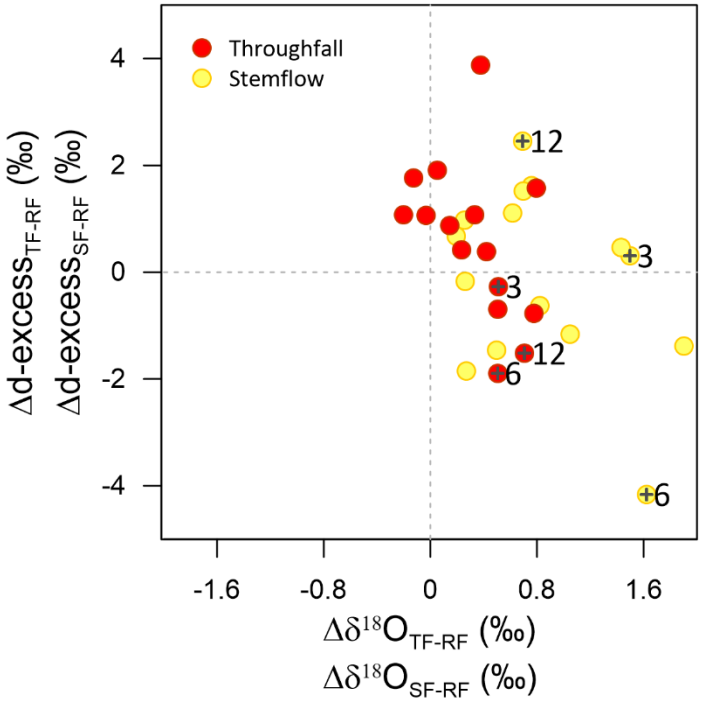

Figure 10. Relationship (event scale) of the isotopic shift between throughfall/stemflow and open rainfall ($\Delta\delta^{18}O_{TF-RF}$ or $\Delta\delta^{18}O_{SF-RF}$) and the shift in d-excess between throughfall/stemflow and open rainfall (Δd-excess$_{TF-RF}$ or Δd-excess$_{SF-RF}$). Mean $\delta^{18}O$ and d-excess for each event are weighted by the volume of each sample. Numbers 3, 6, and 12 refer to the event ID in Table S1 and to the events shown in Figure 11.

Three events in Figure 10 were selected to exemplify different intra-storm dynamics. As all the events showed a positive mean isotopic shift between stemflow and rainfall ($\Delta\delta^{18}O_{SF-RF}$), and only two events showed a slightly negative mean isotopic shift between throughfall and rainfall ($\Delta\delta^{18}O_{TF-RF}$), the three

events were selected on the basis of their observed mean d-excess differences. First, Event 6 showed the more negative Δd-excess$_{SF-RF}$ and Δd-excess$_{TF-RF}$ values; then, Event 12 showed the more positive Δd-excess$_{SF-RF}$ value, but combined with a strongly negative Δd-excess$_{TF-RF}$ value; finally, Event 3 showed Δd-excess values close to zero for both throughfall and stemflow. The meteorological and isotopic characteristics of each of these selected events are shown in Table 2.

Table 2. Meteorological characteristics of the three events analyzed at the intra-storm scale in Figures 10 and 11. RF: rainfall, TF: throughfall, SF: stemflow, D: rainfall duration, I: mean rainfall intensity, I_5: maximum 5-min rainfall intensity, I_{30}: maximum 30-min rainfall intensity, VPD: mean vapour pressure deficit, F_{int}: event intermittency fraction, N: number of sample triplets. Rainfall classes, L–H (long duration–high intensity) and L–L (long duration–low intensity), were adopted from the rainfall classification described in Pinos et al. (2020).

ID	Date (dd/mm/yyyy)	Rainfall Class	RF (mm)	TF (mm)	SF (L)	D (h)	I (mm/h)	I_5 (mm/h)	I_{30} (mm/h)	VPD (kPa)	F_{int} (%)	N	Mean weighted isotopic composition					
													RF (‰)		TF (‰)		SF (‰)	
													δ^2H	$\delta^{18}O$	δ^2H	$\delta^{18}O$	δ^2H	$\delta^{18}O$
3	01/06/2018	L–H	26.9	20.3	9.7	9.5	2.8	53.8	25.4	0.36	64	6	-45.51	-7.34	-41.71	-6.83	-33.28	-5.84
6	28/06/2018	L–H	34.3	33.6	13.0	8.8	3.9	35.1	21.8	0.13	0	8	-36.01	-6.46	-33.89	-5.96	-27.27	-4.84
12	31/01/2019	L–L	19.7	20.7	8.3	13.0	1.5	7.0	5.1	0.10	23	6	-63.08	-8.13	-58.97	-7.42	-55.12	-7.43

Stemflow was more enriched than rainfall and throughfall throughout Event 6, and throughfall was most often more enriched than rainfall (Figure 11a). The isotopic shifts between rainfall and throughfall and between rainfall and stemflow followed the same dynamic during the event and were on average about 0.30‰ for throughfall and 1.12‰ for stemflow. The maximum values of isotopic shifts were 0.72‰ for throughfall and 2.07‰ for stemflow, corresponding to the last bursts of rain during the event (between 15:50 and 17:00). The minimum values of isotopic shifts were observed at the end of the event (light rain) when throughfall was slightly depleted (−0.23‰) and stemflow slightly enriched (0.38‰). Throughout Event 6, Δd-excess$_{SF-RF}$ was almost always negative, except at the end of the event (light rain from 17:05 till the end) when it became slightly positive (average of 0.52‰).

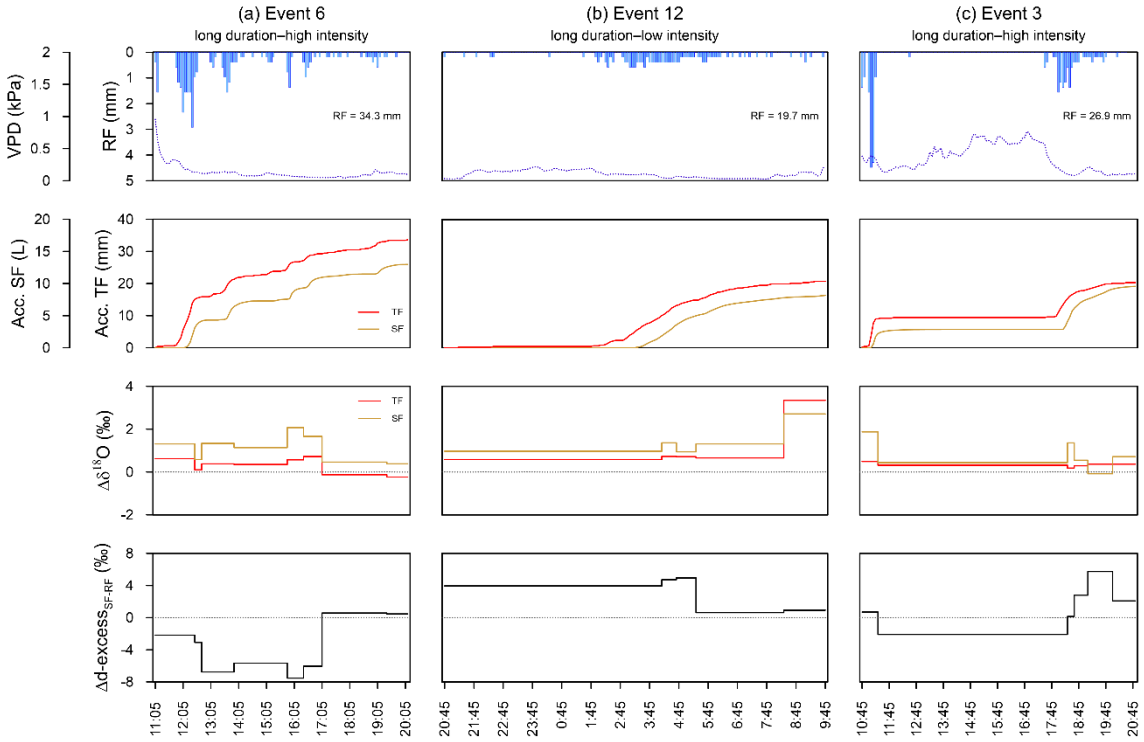

Figure 11. Comparison of the intra-storm dynamic of the three rainfall events selected in Figure 10: Event 6 (28 June 2018) (a), Event 12 (31 January 2019) (b) and Event 3 (1 June 2018) (c). From top to bottom: time series of rainfall (RF) and VPD (5-min time step) (first panel), time series of accumulated throughfall (TF) and stemflow (SF) (second panel), isotopic shift ($\Delta\delta^{18}O$) between rainfall and throughfall and between rainfall and stemflow (third panel) and deuterium excess shift (Δd-excess$_{SF-RF}$) between rainfall and stemflow (fourth panel).

For Event 12, stemflow was more enriched than rainfall and throughfall in almost all samples throughout the event, except at the end when throughfall was more enriched than stemflow (Figure 11b), and reached the maximum differences between rainfall and throughfall and between rainfall and stemflow (3.34‰ and 2.71‰, respectively). If the last interval (from 08:20 till the end) is disregarded, then the event showed similar isotopic difference values throughout the event with average throughfall and stemflow differences of 0.67‰ and 1.18‰, respectively. Δd-excess$_{SF-RF}$ was always positive and decreases at the middle of the event from 4.55‰ to 0.84‰.

For Event 3, the maximum differences between rainfall and throughfall and between rainfall and stemflow (0.49‰ and 1.87‰, respectively) were observed at the beginning of the event, which corresponds to the interval of maximum rainfall intensity (mean rainfall intensity of 23.4 mm h^{-1} between 10:45 and 11:15; Figure 11c). Throughout this event, both fluxes (throughfall and stemflow) showed different isotopic dynamics. The throughfall isotopic shift was similar throughout the event, with an average value of 0.34‰, whereas the stemflow isotopic shift varied from the beginning to the end of the event and even became slightly depleted (−0.08‰) before the end of the event (between 19:05 and 19:55). Δd-excess$_{SF-RF}$ was negative (−2.10‰) during the second sampling interval of the event (between 11:20 and 18:15) which corresponds to a period with an intermittency fraction of 87% (i.e. rainless period), and reached a maximum value of 5.75‰ during the interval with slightly depleted stemflow.

It is worth mentioning that Figure 10 shows two events with a slight negative $\Delta\delta^{18}O_{TF-RF}$. This type of events has already been observed and analysed in a previous work in our study area (see Cayuela et al., 2018).

3.4 Discussion

In this study, we develop an approach for the measurement and sampling of stemflow at high temporal resolution to overcome the lack of available knowledge on the intra-storm variability of stemflow isotopic composition. The data and results obtained in this study greatly improve understanding of throughfall and stemflow dynamics at both event and sample scale, together with their variation patterns at seasonal, event or intra-event scale.

3.4.1 Isotopic composition of throughfall and stemflow

Results at event and sample scales showed that throughfall was generally more enriched than rainfall, but depletion was also observed in a small number of events and samples. Stemflow was also always isotopically more enriched than rainfall at the event scale; and most often at the sample scale, even though there were a small number of depleted samples. These results corroborate findings in the literature, where both positive and negative event-scale isotopic differences between rainfall and throughfall and, in general, positive event-scale isotopic differences between rainfall and stemflow, have been reported.

Studies of various coniferous, deciduous species or other forests such as evergreen camphor-tree forest (*Cinnamomum camphora)* found in general greater isotopic enrichment of throughfall than of rainfall, though in some cases depletion was also observed (Saxena, 1986; Brodersen et al., 2000; Allen et al., 2014; Stockinger et al., 2017; Soulsby et al., 2017; Dai et al., 2020), whereas other studies found that mean throughfall isotopic composition was more depleted than mean rainfall isotopic composition (Siegle-Gaither, 2017; Deng et al., 2021). Similarly, studies found in general stemflow isotopic enrichment and very few cases of depletion with respect to rainfall (Brodersen et al., 2000; Allen et al., 2014; Soulsby et al., 2017); but dominant isotopic enrichment (Siegle-Gaither, 2017) and depletion (Deng et al., 2021) has also been observed. Finally, in tropical rainforest throughfall isotopic enrichment and depletion were found, and stemflow was consistently more isotopically enriched than rainfall (Leopoldo et al., 1982; Liu et al., 2008). These diverse findings support the results of Snelgrove et al. (2020) that, in a hardwood-conifer forest dominated by *Quercus rubra*, *Pinus strobus*, *Tsuga canadensis*, *Thuja occidentalis* and *Picea mariana*, throughfall and stemflow were not consistently more enriched than rainfall; and that stemflow was not more so than throughfall.

That stemflow is in general more enriched than throughfall (e.g., Cayuela et al., 2018) may be explained by differences in flow paths and residence times between stemflow and throughfall (Levia et al., 2011; Klamerus-Iwan et al., 2020). Water channeled to the bole from the canopy and flowing down has longer residence times than water stored in the leaves and branches, which favors evaporation and exchange with ambient vapour (Ikawa et al., 2011), thus contributing to increased differences in isotopic fractionation between these two fluxes.

Our results also showed that for enriched throughfall and stemflow samples d-excess differences were not always negative, indicating that processes other than evaporation were influencing throughfall and stemflow isotopic composition. However, in our study we disregarded some of the other processes that might modify throughfall and stemflow isotopic composition. For instance, the inter-event mixing of waters, that is, the mixing of rainwater with antecedent water stored in the canopy (Allen et al., 2014), should be discarded because we selected events with a previous period without rainfall of 6 h (day) or 12 h (night), which is accepted as the time needed for the canopy to dry (Llorens et al., 2014). Isotopic exchange requires relative humidity close to 100% and that rainwater and atmospheric water vapour have different

isotopic compositions (Brodersen et al., 2000). In our study we were unable to determine to what extent exchange might influence the isotopic fractionation of intercepted rainfall due to the lack of information on the isotopic composition of water vapour. However, as indicated by other authors (e.g., Ikawa et al., 2011; Cayuela et al., 2018a), the effect of isotopic exchange on throughfall and stemflow cannot be ruled out.

3.4.2 Isotopic seasonal variation patterns and meteorological characteristics

In this study, the isotopic composition of rainfall followed a seasonal pattern linked to air temperature, with higher isotopic enrichment during the growing season (summer) and lower during the dormant season (winter), which was consistent with the seasonal pattern found by Casellas et al. (2019) for the same study area. Even if our data did not show any statistical difference in TF by season, we hypothesize that less throughfall isotopic enrichment and greater stemflow isotopic enrichment than that of open rainfall was more common during the growing season (at higher temperatures) and vice versa during the dormant season (at lower temperatures). Similar results found by Cayuela et al. (2018a) for the same study plot strongly support this pattern and indicate that evaporation was not the dominant factor controlling throughfall isotopic composition. Our results are also in line with other studies that found higher throughfall enrichment during the winter season (e.g., Xu et al., 2014; Stockinger et al., 2017). These are counterintuitive findings, since one would expect more throughfall enrichment during the summer period when there is more energy available for evaporation.

Our results also showed that stemflow enrichment was greater during the growing season, reflecting a seasonal pattern linked to higher temperatures (i.e. greater evaporation). Observed stemflow enrichment during the growing season confirms earlier observations for the same study plot by Cayuela et al. (2018a) and the results obtained by Siegle-Gaither (2017), indicating that evaporation was the dominant factor controlling stemflow isotopic composition.

Isotopic variations of throughfall and stemflow samples were not related to the rainfall characteristics and meteorological variables analysed (mean rainfall intensity, maximum 5-min intensities, wind speed, sampling time, vapour pressure deficit and rain intermittency). Therefore, based on our results, it remains unclear how abiotic factors controlled isotopic changes of throughfall and stemflow. Rainfall intensity increased or reduced the residence time of water in the canopy (Keim et al., 2006; Dunkerley, 2014), which

could lead to isotopic differences between rainfall and throughfall and stemflow in both directions (enrichment or depletion). As in our study, other authors found no correlation between the throughfall isotopic shift and mean (Allen et al., 2015) or maximum rainfall intensity (Soulsby et al., 2017; Snelgrove et al., 2020), or between stemflow isotopic shift and maximum rainfall intensity (Snelgrove et al., 2020). However, no clear consensus seems to emerge on the subject, as negative correlation between throughfall isotopic shift and mean rainfall intensity was found by Dewalle and Swistock (1994) and between throughfall and stemflow isotopic shift and maximum 10-min rainfall intensity by Zhang et al. (2019).

Wind may release stored water from vegetative surfaces (leaves and small branches), reducing throughfall lag times by dripping (Nanko et al., 2006), increase stemflow by releasing water to preferential pathways along vegetative surfaces (Kuraji et al., 1997), and blow evaporated water molecules away from the canopy space, reducing partially water vapour pressure and increasing evaporation (Kucera, 1954), which might contribute to isotopic fractionation. In our study, however, no relationship of the throughfall or stemflow isotopic shift with wind speed was found. Similarly, no relationship was found between isotopic shift and vapour pressure deficit, which is often considered a good indicator of the evapotranspiration demand of the atmosphere. These results are in line with those reported by other authors (Zhang et al., 2019; Pinos et al., 2020). However, here again there is a wide variety of sometimes divergent results, as Snelgrove et al. (2020) found a relationship between throughfall and stemflow enrichment with maximum vapour pressure for pines but not for hemlock trees; and Zhang et al. (2019) found a negative relationship between vapour pressure deficit and the isotopic variations of stemflow but not of throughfall.

Finally, longer intra-event rainfall intermittency (rainless periods) could produce greater canopy evaporation by means of drying cycles (Dunkerley, 2015), leading to the greater isotopic enrichment of throughfall and stemflow. However, no relationship of the throughfall or stemflow isotopic shift with rain intermittency was found in this study, thus rainfall intermittency did not contribute to elucidate isotopic fractionation on both fluxes.

3.4.3 Variations of intra-storm isotopic composition

For all rainfall events selected in our study, rainfall $\delta^{18}O$ and d-excess decreased progressively towards the final stage of the event, indicating a Rayleigh-type rainout process (Dansgaard, 1964). As expected,

throughfall and stemflow followed this rainfall pattern, being more enriched at the initial stage and decreasing during the course of the events (Figure S4). The slightly greater isotopic shift between rainfall and throughfall observed at the initial stage, although not statistically significant, may be related to the evaporation process, since this stage coincided with higher vapour pressure deficit and a greater contribution of splash throughfall, which could promote higher splash droplet evaporation (Ikawa et al., 2011; Cayuela et al., 2018a; Tao et al., 2017; Pinos et al., 2020). Towards the end of the rainfall event, the saturation of the canopy reduced lag times and increased the contribution of canopy drip, resulting in less throughfall isotopic fractionation, as already established by Pinos et al. (2020).

Our results suggest that evaporation is the main governing factor of the isotopic shift between rainfall and stemflow throughout the events because of the predominant enrichment, but might be greater at the initial stage of a rainfall event. At this stage, since main branches and bole are dry, the time lapse needed to exceed the bark water storage capacity required to generate stemflow is longer. This promotes long stemflow residence time, which means more time for water to evaporate and, in consequence, to be enriched. This behavior is in line with Snelgrove et al. (2020), who stated that isotopic enrichment of both fluxes (throughfall and stemflow) with higher atmospheric vapour pressure deficit may reflect the potential for evaporative fractionation as a result of retention and detention of water moving through the canopy of rough-barked trees. After this stage, selective water retention, intra-event mixing of waters and to a lesser extent evaporation, individually or combined, are expected to influence temporal stemflow isotopic composition towards the end of the rainfall event (Ikawa et al., 2011; Tao et al., 2017).

Furthermore, in this study Δd-excess$_{TF-RF}$ and Δd-excess$_{SF-RF}$ increased progressively towards the end of the events, whereas Δd-excess$_{SF-TF}$ decreased slightly. As mentioned above, this is because the sub-cloud evaporation effect and a typical decrease in precipitation amount and raindrop size at the end of the rainfall event lead to the depletion of heavy isotopes in precipitation and lower d-excess (e.g., Li et al., 2021). However, the canopy selection effect may explain the higher Δd-excess$_{TF-RF}$ and Δd-excess$_{SF-RF}$ at the end of the events. The retention in the canopy of the final rainfall volume, which usually had low d-excess values, would imply that throughfall and stemflow measured at the end of the event corresponded to a lag of rainfall with higher d-excess from earlier time intervals (Cayuela et al., 2018a). Thus, fractionation caused by selection seems to be more important at the end of the event. The fact that stemflow experiences

greater evaporation than throughfall is also well supported by our results because the isotopic shift between throughfall and stemflow samples indicated, in general, enrichment with negative d-excess differences.

Our results at the intra-storm scale indicate no direct relationship between the isotopic differences ($\Delta\delta^{18}O_{TF-RF}$, $\Delta\delta^{18}O_{SF-RF}$, $\Delta\delta^{18}O_{SF-TF}$) and increased cumulative rainfall, throughfall or stemflow. These results reflect our earlier results (Pinos et al., 2020), which showed no correlation between $\Delta\delta^{18}O_{TF-RF}$ and cumulative rainfall for the same pine stand, even if isotopic shift variability was reduced when cumulative rainfall increased. In a study similar to this but at the event scale, Allen et al. (2015) did not find any relationship between the isotopic shift between rainfall and throughfall and event size; and Soulsby et al. (2017) found no statistical correlation between throughfall isotopic composition and rainfall amount. However, Kubota and Tsuboyama (2003) found that the range of $\delta^{18}O$ variations (i.e. the difference between the max and min value) in rainfall, throughfall and stemflow tended to be greater as the amounts of these fluxes increased.

3.5 Conclusion

The goal of this study was to investigate the factors affecting the isotopic fractionation of rainfall when it passes through the canopy. Our results showed that isotopic differences between rainfall and throughfall or stemflow can occur in both directions (enrichment or depletion), with enrichment being more common and stemflow being more enriched than throughfall. The differences in the routing of both fluxes could explain, to some extent, the differences between throughfall and stemflow isotopic composition. Throughfall was more isotopically enriched during the dormant season at low air temperatures, whereas stemflow was more isotopically enriched during the growing season. No relationship between the isotopic shift between rainfall and throughfall or stemflow and meteorological variables was found.

Our study at the intra-storm scale showed that the temporal dynamic of the isotopic composition of throughfall and stemflow may differ significantly from that of rainfall. It is difficult to put forward a particular reason for these differences, but it has been suggested that evaporation, canopy selection, exchange and mixing of waters or a combination of these are responsible for the fractionation that occurs at different intra-storm intervals. Our high-resolution monitoring of the isotopic composition of rainfall, throughfall and stemflow provided insights into the patterns of temporal isotopic variations of these fluxes at intra-storm scale, which can be used to improve our understanding of the effect of forest on the

hydrological cycle. In particular, the use of net precipitation isotopic signal, rather than the open rainfall signal, is highly recommended when studying water age in the vadose zone and vegetation water uptake. Further research should seek to assess the spatial isotopic differences of throughfall and stemflow at high sampling resolution for a higher number of trees and/or for different tree species. In addition, the sampling of the isotopic signature of canopy vapour could ultimately help to identify whether or not isotope exchange affects the throughfall and stemflow isotopic shift.

Appendices

Appendix A: Studies of the isotopic composition of stemflow

Table A1. List of the studies that have reported the isotopic composition of stemflow across the globe. Studies were hand-retrieved by using the Google Scholar search engine. Almost all the studies listed in the table are in English except Leopoldo et al. (1982) in Portuguese and Tao et al. (2017) in Chinese. We are therefore aware that the current list is likely to be incomplete, as any other studies in languages other than English are not included.

Source	Location	Forest type	Sampling resolution	Number of stemflow sampled events
Leopoldo et al. (1982)	NW Brasil	Tropical rainforest	Weekly	27
Kendall (1993)	SE USA	Deciduous and coniferous	Event	3
Brodersen et al. (2000)	S Germany	Deciduous and coniferous	Weekly	8
Kubota and Tsuboyama (2003)	E Japan	Coniferous	Intra-event	4
Liu et al. (2008)	SE China	Tropical rainforest	Event	17
Ikawa et al. (2011)	S Japan	Coniferous	Intra-event	1
Schmid et al. (2011)	NW Costa Rica	Tropical cloud rainforest	Daily	21
Allen et al. (2014)	NW USA	Coniferous	Event	8
DuMont (2014)	NW Costa Rica	Tropical rainforest	Daily	3
Strauch et al. (2014)	S Oman	Deciduous	Daily	5
Siegle-Gaither (2017)	SE USA	Deciduous	Event	14
Soulsby et al. (2017)	NE Scotland	Coniferous and shrub vegetation	Unset (ranged from 4 to 14 days)	12
Tao et al. (2017)	N China	Deciduous	Intra-event	2
Cayuela et al. (2018a)	NE Spain	Deciduous and coniferous	Event	22
Zhang et al. (2019)	NW China	Shrub vegetation	Event	11
Snelgrove et al. (2020)	NE Canada	Coniferous	Weekly	21
Deng et al. (2021)	SE China	Deciduous and shrub vegetation	Event	23
This study	NE Spain	Coniferous	Intra-event	21

Appendix B: Limitations of the sampling method

a) Sampling capacity

With our set-up, and for the tree monitored in our study, the sampling capacity of the stemflow automatic sampler (48 L) was exceeded for two rainfall events greater than 60 mm (according to the polynomial regression calculated to calibrate the relationship between rainfall and stemflow; Figure S2). Using the same set-up, a second division of the stemflow before entering the sampler can be added in order to sample stemflow for events with greater amount of rainfall (or trees producing more stemflow). With such modification, the collected stemflow volume would correspond to a quarter of the volume recorded by the tipping bucket.

In addition, occasionally (27% of stemflow samples) high stemflow intensities may have delivered more than 1 L of stemflow to the sampler during sampling interval, causing the sample bottle to overflow slightly, which leads to an unquantifiable uncertainty of the isotopy of the sample. Of the overflowed samples, 45% corresponded to samples from the two events that exceeded the sampling capacity, i.e. rainfall greater than 60 mm (Events 09 and 21; Table S1).

b) Sampling interval

In our study, the sampling of rainfall and throughfall (every 5 mm of rain) was not synchronized in time with the sampling of stemflow (which depended on the volume of stemflow). To overcome this problem, a volume-weighted isotopic mean was determined for rainfall and throughfall for each stemflow sampling interval. However, ultimately, the isotopic composition variability of the three fluxes will be affected by the sampling interval (Allen et al., 2017). This means that capturing the isotopic variability of rainfall and throughfall and stemflow for a synchronized time interval remains a challenge.

c) Representativity

Our study, limited to two contiguous trees, represented a strong monitoring and sampling challenge (3 automatic tipping buckets and 3 automatic samplers) with critical (and time-consuming) maintenance. However, we hope, as stated in our conclusions, that new studies will emerge to compare tree species and sample a larger number of trees.

3.6 References

Allen, S. T., Aubrey, D. P., Bader, M. Y., Coenders-Gerrits, M., Friesen, J., Gutmann, E. D., Guillemette, F., Jiménez-Rodríguez, C., Keim, R. F., Klamerus-Iwan, A., Mendieta-Leiva, G., Porada, P., Qualls, R. G., Schilperoort, B., Stubbins, A., & Van Stan, J. T. (2020). Key questions on the evaporation and transport of intercepted precipitation. In: Van Stan J. T., Gutmann E., Friesen J. (eds) Precipitation Partitioning by Vegetation (pp. 269-280). Springer, Cham. https://doi.org/10.1007/978-3-030-29702-2_16

Allen, S. T., Brooks, J. R., Keim, R. F., Bond, B. J., & McDonnell, J. J. (2014). The role of pre-event canopy storage in throughfall and stemflow by using isotopic tracers. *Ecohydrology*, *7*(2), 858-868. https://doi.org/10.1002/eco.1408

Allen, S. T., Keim, R. F., & McDonnell, J. J. (2015). Spatial patterns of throughfall isotopic composition at the event and seasonal timescales. *Journal of Hydrology*, *522*, 58-66. https://doi.org/10.1016/j.jhydrol.2014.12.029

Allen, S. T., Keim, R. F., Barnard, H. R., McDonnell, J. J., & Renée Brooks, J. (2017). The role of stable isotopes in understanding rainfall interception processes: a review. *Wiley Interdisciplinary Reviews: Water*, *4*(1), e1187. https://doi.org/10.1002/wat2.1187

Brodersen, C., Pohl, S., Lindenlaub, M., Leibundgut, C., & Wilpert, K. V. (2000). Influence of vegetation structure on isotope content of throughfall and soil water. *Hydrological Processes*, *14*(8), 1439-1448. https://doi.org/10.1002/1099-1085(20000615)14:8<1439::AID-HYP985>3.0.CO;2-3

Carlyle-Moses, D. E., Iida, S., Germer, S., Llorens, P., Michalzik, B., Nanko, K., Tischer, A., & Levia, D. F. (2018). Expressing stemflow commensurate with its ecohydrological importance. *Advances in Water Resources*, *121*, 472-479. https://doi.org/10.1016/j.advwatres.2018.08.015

Casellas, E., Latron, J., Cayuela, C., Bech, J., Udina, M., Sola, Y., Lee, K.-O., & Llorens, P. (2019). Moisture origin and characteristics of the isotopic signature of rainfall in a Mediterranean mountain catchment (Vallcebre, eastern Pyrenees). *Journal of Hydrology*, *575*, 767-779. https://doi.org/10.1016/j.jhydrol.2019.05.060

Cayuela, C., Llorens, P., Sánchez-Costa, E., & Latron, J. (2018a). Modification of the isotopic composition of rainfall by throughfall and stemflow: The case of Scots pine and downy oak forests under Mediterranean conditions. *Ecohydrology*, *11*(8), e2025. https://doi.org/10.1002/eco.2025

Cayuela, C., Llorens, P., Sánchez-Costa, E., Levia, D. F., & Latron, J. (2018b). Effect of biotic and abiotic factors on inter-and intra-event variability in stemflow rates in oak and pine stands in a Mediterranean mountain area. *Journal of Hydrology*, *560*, 396-406. ttps://doi.org/10.1016/j.jhydrol.2018.03.050

Crabtree, R. W., & Trudgill, S. T. (1985). Hillslope hydrochemistry and stream response on a wooded, permeable bedrock: the role of stemflow. *Journal of Hydrology*, *80*(1-2), 161-178. https://doi.org/10.1016/0022-1694(85)90079-4

Dai, J., Zhang, X., Luo, Z., Wang, R., He, X., & Guan, H. (2020). Spatial Variation and Stable Isotopic Characteristic of Throughfall Under *Cinnamomum camphora* Woods in Changsha. *Journal of Soil and Water Conservation*, *34*(3), 291-298. https://doi.org/10.13870/j.cnki.stbcxb.2020.03.043

Dansgaard, W. (1964). Stable isotopes in precipitation. *Tellus*, *16*(4), 436-468. https://doi.org/10.3402/tellusa.v16i4.8993

Deng, Y., Ke, J., Wu, S., Wu, H., & Zhu, A. (2021). Examining the role of throughfall and stemflow on epikarst water recharges using deuterium excess data. *Carbonates Evaporites*, *36*, 42. https://doi.org/10.1007/s13146-021-00712-x

Dewalle, D. R., & Swistock, B. R. (1994). Differences in oxygen-18 content of throughfall and rainfall in hardwood and coniferous forests. *Hydrological Processes*, *8*(1), 75-82. https://doi.org/10.1002/hyp.3360080106

DuMont, A. L. (2014). Hillslope Hydrological Processes in a Costa Rican Rainforest: Water Supply Partitioning Using Isotope Tracers. Master's thesis, Texas A&M University, USA. http://hdl.handle.net/1969.1/152744

Dunkerley, D. (2014). Stemflow production and intrastorm rainfall intensity variation: an experimental analysis using laboratory rainfall simulation. *Earth Surface Processes and Landforms*, *39*(13), 1741-1752. https://doi.org/10.1002/esp.3555

Dunkerley, D. (2015). Intra-event intermittency of rainfall: An analysis of the metrics of rain and no-rain periods. *Hydrological Processes*, *29*(15), 3294-3305. https://doi.org/10.1002/hyp.10454

Gat, J. R. (1996). Oxygen and hydrogen isotopes in the hydrologic cycle. *Annual Review of Earth and Planetary Sciences*, *24*(1), 225-262. https://doi.org/10.1146/annurev.earth.24.1.225

Green, M. B., Laursen, B. K., Campbell, J. L., McGuire, K. J., & Kelsey, E. P. (2015). Stable water isotopes suggest sub-canopy water recycling in a northern forested catchment. *Hydrological Processes*, *29*(25), 5193-5202. https://doi.org/10.1002/hyp.10706

Iida, S., Shimizu, T., Shinohara, Y., Takeuchi, S., & Kumagai, T. (2020). The necessity of sensor calibration for the precise measurement of water fluxes in forest ecosystems. In D. F. Levia, D. E. Carlyle-Moses, S. Iida, B. Michalzik, K. Nanko, & A. Tischer (Eds.), Forest-water interactions (pp. 29-54). Cham: Springer. https://doi.org/10.1007/978-3-030-26086-6_2

Ikawa, R., Shimada, J., & Shimizu, T. (2009). Development of automatic rainwater sampling system with precise time resolution. *Journal of Japanese Association of Hydrological Sciences*, *38*(3), 111-116. https://doi.org/10.4145/jahs.38.111

Ikawa, R., Yamamoto, T., Shimada, J., & Shimizu, T. (2011). Temporal variations of isotopic compositions in gross rainfall, throughfall, and stemflow under a Japanese cedar forest during a typhoon event. *Hydrological Research Letters*, *5*, 32-36. https://doi.org/10.3178/hrl.5.32

Keim, R. F., Skaugset, A. E., & Weiler, M. (2006). Storage of water on vegetation under simulated rainfall of varying intensity. *Advances in Water Resources*, *29*(7), 974-986. https://doi.org/10.1016/j.advwatres.2005.07.017

Kendall, C. (1993). Impact of isotopic heterogeneity in shallow systems on modeling of stormflow generation. Doctoral thesis, University of Maryland, USA. https://doi.org/10.13016/M2NS0M05B

Kennedy, V. C., Zellweger, G. W., & Avanzino, R. J. (1979). Variation of rain chemistry during storms at two sites in northern California. *Water Resources Research*, *15*(3), 687-702. https://doi.org/10.1029/WR015i003p00687

Klamerus-Iwan, A., Link, T.E., Keim, R.F., Van Stan, J.T. (2020). Storage and Routing of Precipitation Through Canopies. In: Van Stan, J., Gutmann, E., Friesen, J. (eds) Precipitation Partitioning by Vegetation - A Global Synthesis (pp. 17-34). Springer, Cham. https://doi.org/10.1007/978-3-030-29702-2_2

Klaus, J., & McDonnell, J. J. (2013). Hydrograph separation using stable isotopes: Review and evaluation. *Journal of Hydrology*, *505*, 47-64. https://doi.org/10.1016/j.jhydrol.2013.09.006

Kubota, T., & Tsuboyama, Y. (2003). Intra-and inter-storm oxygen-18 and deuterium variations of rain, throughfall, and stemflow, and two-component hydrograph separation in a small forested catchment in Japan. *Journal of Forest Research*, *8*(3), 179-190. https://doi.org/10.1007/s10310-002-0024-9

Kucera, C. L. (1954). Some relationships of evaporation rate to vapor pressure deficit and low wind velocity. *Ecology*, *35*(1), 71-75. https://doi.org/10.2307/1931406

Kuraji, K., Tanaka, N., Shiraki, K., Karakama, I., & Ohta, T. (1997). Effects of windspeed on stemflow volume in a mature Cryptomeria japonica and Chamaecyparis obtusa stand. *Journal of the Japanese Forestry Society*, *79*(4), 215-221. https://doi.org/10.11519/jjfs1953.79.4_215

Leopoldo, P. R., Matsui, E., Salati, E., Franken, W., & Ribeiro, M. D. N. G. (1982). Composição isotópica da água de chuva e da água do solo em floresta amazônica do tipo terra firme, região de Manaus. *Acta Amazonica*, *12*, 7-13. https://doi.org/10.1590/1809-43921982123S007

Levia, D. F., Keim, R. F., Carlyle-Moses, D. E., & Frost, E. E. (2011). Throughfall and Stemflow in Wooded Ecosystems. In: Levia D., Carlyle-Moses D., Tanaka T. (eds) Forest Hydrology and Biogeochemistry. Ecological Studies (Analysis and Synthesis), vol 216. (pp. 425-443), Springer, Dordrecht. https://doi.org/10.1007/978-94-007-1363-5_21

Li, X., Tang, C., & Cui, J. (2021). Intra-Event Isotopic Changes in Water Vapor and Precipitation in South China. *Water*, *13*(7), 940. https://doi.org/10.3390/w13070940

Liu, W. J., Liu, W. Y., Li, J. T., Wu, Z. W., & Li, H. M. (2008). Isotope variations of throughfall, stemflow and soil water in a tropical rain forest and a rubber plantation in Xishuangbanna, SW China. *Hydrology Research*, *39*(5-6), 437-449. https://doi.org/10.2166/nh.2008.110

Llorens, P., Domingo, F., Garcia-Estringana, P., Muzylo, A., & Gallart, F. (2014). Canopy wetness patterns in a Mediterranean deciduous stand. *Journal of Hydrology*, *512*, 254-262. https://doi.org/10.1016/j.jhydrol.2014.03.007

Llorens, P., Gallart, F., Cayuela, C., Roig-Planasdemunt, M., Casellas, E., Molina, A. J., … & Latron, J. (2018). What have we learnt about Mediterranean catchment hydrology? 30 years observing hydrological processes in the Vallcebre research catchments. *Geographical Research Letters*, *44*. https://doi.org/10.18172/cig.3432

Nanko, K., Hotta, N., & Suzuki, M. (2006). Evaluating the influence of canopy species and meteorological factors on throughfall drop size distribution. *Journal of Hydrology*, *329*(3-4), 422-431. https://doi.org/10.1016/j.jhydrol.2006.02.036

Pinos, J., Latron, J., Levia, D. F., & Llorens, P. (2021). Drivers of the circumferential variation of stemflow inputs on the boles of Pinus sylvestris L. (Scots pine). *Ecohydrology*, *14*(8), e2348. https://doi.org/10.1002/eco.2348

Pinos, J., Latron, J., Nanko, K., Levia, D. F., & Llorens, P. (2020). Throughfall isotopic composition in relation to drop size at the intra-event scale in a Mediterranean Scots pine stand. *Hydrology and Earth System Sciences*, *24*(9), 4675-4690. https://doi.org/10.5194/hess-24-4675-2020

Saxena, R. K. (1986). Estimation of Canopy Reservoir Capacity and Oxygen-18 Fractionation in Throughfall in a Pine Forest. *Hydrology Research*, *17*(4-5), 251-260. https://doi.org/10.2166/nh.1986.0017

Schmid, S., Burkard, R., Frumau, K. F. A., Tobón, C., Bruijnzeel, L. A., Siegwolf, R., & Eugster, W. (2011). Using eddy covariance and stable isotope mass balance techniques to estimate fog water contributions to a Costa Rican cloud forest during the dry season. *Hydrological Processes*, *25*(3), 429-437. https://doi.org/10.1002/hyp.7739

Siegle-Gaither, M. (2017). Using Deuterium and Oxygen-18 Stable Isotopes to Understand Mechanisms of Stemflow Generation as a Function of Tree Species and Climate. Master's thesis, Mississippi State University, USA. https://hdl.handle.net/11668/19679

Snelgrove, J. R., Buttle, J. M., & Tetzlaff, D. (2020). Importance of rainfall partitioning in a northern mixed forest canopy for soil water isotopic signatures in ecohydrological studies. *Hydrological Processes*, *34*(2), 284-302. https://doi.org/10.1002/hyp.13584

Soulsby, C., Braun, H., Sprenger, M., Weiler, M., & Tetzlaff, D. (2017). Influence of forest and shrub canopies on precipitation partitioning and isotopic signatures. *Hydrological Processes*, *31*(24), 4282-4296. https://doi.org/10.1002/hyp.11351

Stockinger, M. P., Lücke, A., Vereecken, H., & Bogena, H. R. (2017). Accounting for seasonal isotopic patterns of forest canopy intercepted precipitation in streamflow modeling. *Journal of Hydrology*, *555*, 31-40. https://doi.org/10.1016/j.jhydrol.2017.10.003

Strauch, G., Al-Mashaikhi, K. S., Bawain, A., Knöller, K., Friesen, J., & Müller, T. (2014). Stable H and O isotope variations reveal sources of recharge in Dhofar, Sultanate of Oman. *Isotopes in Environmental and Health Studies*, *50*(4), 475-490. https://doi.org/10.1080/10256016.2014.961451

Tanaka, T., Taniguchi, M., & Tsujimura, M. (1996). Significance of stemflow in groundwater recharge. 2: A cylindrical infiltration model for evaluating the stemflow contribution to groundwater recharge. *Hydrological Processes*, *10*(1), 81-88. https://doi.org/10.1002/(SICI)1099-1085(199601)10:1<81::AID-HYP302>3.0.CO;2-M

Tao Z, Si B., & Jin J. (2017). Canopy Interception Modified Intra-rainfall Isotopic and Hydrochemical Characteristics of Dwarfed Jujube Tree. *Journal of Soil and Water Conservation*, *31*(5), 189-195. https://doi.org/10.13870/j.cnki.stbcxb.2017.05.030

Xu, X., Guan, H., & Deng, Z. (2014). Isotopic composition of throughfall in pine plantation and native eucalyptus forest in South Australia. *Journal of Hydrology*, *514*, 150-157. https://doi.org/10.1016/j.jhydrol.2014.03.068

Zhang, Y. F., Wang, X. P., Pan, Y. X., & Hu, R. (2019). Alteration in isotopic composition of gross rainfall as it is being partitioned into throughfall and stemflow by xerophytic shrub canopies within water-limited arid desert ecosystems. *Science of The Total Environment*, *692*, 631-639. https://doi.org/10.1016/j.scitotenv.2019.07.294

CHAPTER 4

Drivers of the circumferential variation of stemflow inputs on the boles of *Pinus sylvestris L.* (Scots pine)

Drivers of the circumferential variation of stemflow inputs on the boles of *Pinus sylvestris L.* (Scots pine)

The spatial variability of stemflow on the bole of trees has rarely been the focal point of stemflow studies, despite its potential importance for stemflow-induced changes to soils. This study helps close this data gap by supplying quantitative data on possible drivers of circumferential variation of stemflow on the boles of two *Pinus sylvestris* L. (Scots pine). Hence, the objectives of the present study were to quantify the circumferential spatial variability of stemflow on tree stems and to assess how some biotic and abiotic factors affect this variability. Continuous stemflow data observed for two trees within a mature stand of Scots pine during a 20-month period (May 2018 to December 2019) showed the existence of preferential flowpaths around the stem, with patterns of stemflow distribution differing between the two trees. Data suggest that biotic factors (trunk lean, bark morphology and tree neighborhood) have a greater influence on stemflow distribution on tree stems than abiotic factors (rainfall intensity peaks). Our comprehensive spatio-temporal fine-scale measurements strongly support prior observations of non-uniform stemflow. Further studies of stemflow distribution across tree species and aboveground vegetative surfaces are needed to improve our mechanistic understand of stemflow dynamics vis-à-vis rainfall interception processes and to gain further insight as to how the circumferential variation of stemflow on tree boles alters stemflow-soil interactions.

Original work: Pinos, J., Latron, J., Levia, D. F., & Llorens, P. (2021). Drivers of the circumferential variation of stemflow inputs on the boles of *Pinus sylvestris L.* (Scots pine). Ecohydrology, 14(8), e2348. https://doi.org/10.1002/eco.2348

4.1 Introduction

Rainwater that reaches the forest floor (also termed net precipitation) is formed by throughfall and stemflow. Stemflow is defined as the intercepted precipitation that drains from leaves and branches and is channeled to the stem, which eventually flows downward and reaches the forest floor around the stem base. This concentrated flux varies widely across vegetation types and climatic regions (Yue et al., 2021). Moreover, stemflow generation and stemflow dynamics result from a complex spatio-temporal interaction between biotic and abiotic factors (Cayuela et al., 2018; Levia et al., 2010). Stemflow flux is important in ecosystem functioning due to its ecological, hydrological and biogeochemical implications of near-trunk areas (Levia and Germer, 2015). However, in comparison with throughfall, stemflow has received less attention from the hydrologic community since it represents a smaller percentage of the incident precipitation. Nevertheless, the classical funneling ratio metric (Herwitz, 1986) or new stemflow metrics (Carlyle-Moses et al., 2018; Levia and Germer, 2015) have demonstrated that stemflow often exceeds throughfall or rainfall inputs per unit basal area and infiltration area. A deeper understanding of stemflow dynamics is therefore needed for a better conceptualization of hydrological processes that occur within forests to improve ecohydrological models.

Carlyle-Moses et al. (2020) revealed that little is known about stemflow infiltration and that stemflow infiltration areas may be highly dynamic and variable and markedly influenced by soil properties. The present study represents a step forward by analyzing the stemflow dynamics around the tree stem, which has been less studied, as a way to infer the potential heterogeneity of stemflow infiltration in soils at the tree base.

Two possible patterns of stemflow distribution may be considered: uniform and non-uniform. In the case of a uniform stemflow distribution, an equal amount of water flows down around the circumference of the tree stem without preferential flowpaths. In contrast, non-uniform stemflow involves markedly dissimilar water distribution around the tree bole due to the existence of preferential flowpaths on the stem.

Most studies have pointed toward non-uniform stemflow distributions. Gersper (1970) and Gersper and Holowaychuk (1971) pointed out that larger amounts of stemflow occurred on the angled side facing the ground of slightly inclined trees. The same pattern was found for trees growing on a hillslope, where stemflow caused asymmetric soil water saturation between downslope and upslope areas around the trees

(Gersper, 1970; Gonzalez-Ollauri et al., 2020; Herwitz, 1986; Liang, 2020). Through field observations of individual shrubs, Návar and Bryan (1990) suggested that stemflow tends to follow preferential flowpaths. Circumferential variation of stemflow was also observed for American beech trees (Levia, Van Stan, et al., 2011). Förster and Schimmack (1992) found that the variable spatial distribution of radiocesium in soils around the stems of beech trees was caused by non-uniform stemflow. More recently, Imamura et al. (2017) and Tischer et al. (2020) used a passive dye technique and observed preferential stemflow flowpaths and how these flowpaths induced spatial heterogeneity in soil chemistry and infiltration patterns around konara oak and European beech trees, respectively.

We therefore argue that it is necessary to move from indirect or qualitative observations of stemflow distribution around the stem or at the base of the tree to a more quantitative approach to impart further knowledge about stemflow heterogeneity around tree stems and under what circumstances this heterogeneity might increase or decrease. The objectives of this study, which aims to contribute a stronger basis of stemflow routing behavior in rainfall interception processes, were (1) to quantify the circumferential variability of stemflow around tree stems and (2) to assess how some biotic and abiotic factors might affect this stemflow variability. To the authors' knowledge, this is the first study that directly quantifies the stemflow distribution around tree stems at fine (5-min) temporal scale.

4.2 Materials and methods

4.2.1 Description of study area

This study was conducted in a Scots pine stand (*Pinus sylvestris* L.) located at 1200 m within the Vallcebre research catchments in Catalonia, Spain (Figure 1). The catchments are located 100 km north of Barcelona, in the south-eastern part of the Pyrenees (42°12'N and 1°49'E). The climate is humid Mediterranean with a mean annual precipitation of 867 ± 223 mm, mean annual evapotranspiration of 856 ± 69 mm and a mean annual temperature of 9.2°C (1999-2018). The main forest structure characteristics are shown in Table 1. Two representative mature trees within the stand were selected for the experiment. Trees were selected based on previous knowledge of stemflow response at the event scale (Cayuela et al., 2018). Briefly, for the same plot, Cayuela et al. (2018) found (1) an effect of tree size on FRs, that is, trees with DBH between 15 and 25 cm had higher FRs than larger trees; (2) that trees with smaller crowns produced larger stemflow volumes; and (3) a trunk lean (between 2° and 5°) favored the formation of flowpaths and, therefore,

increased FRs. Taking into account the above, the selected trees had different morphological characteristics such as height (18 vs. 21 m), stem diameter (21 vs. 28 cm), crown area (12 vs. 24 m^2) and trunk lean (0° vs. 6°) to evaluate possible biotic effects on stemflow distribution. The main structural variables of the monitored trees are shown in Table 2. The trees surrounding the experimental selected trees within a 5-m radius are shown in Figure 1. The main morphological characteristics of these surrounding trees are given in Table S1.

Table 1. Stand structure characteristics of the experimental Scots pine stand (± 1 SD).

Stand area (m^2)	900
Tree density (tree·ha^{-1})	1189
Basal area (m^2·ha^{-1})	45.1
Canopy cover (%)	69.3 ± 17.7
Diameter at breast height (cm)	19.9 ± 9.2
Height (m)	17 ± 4.4

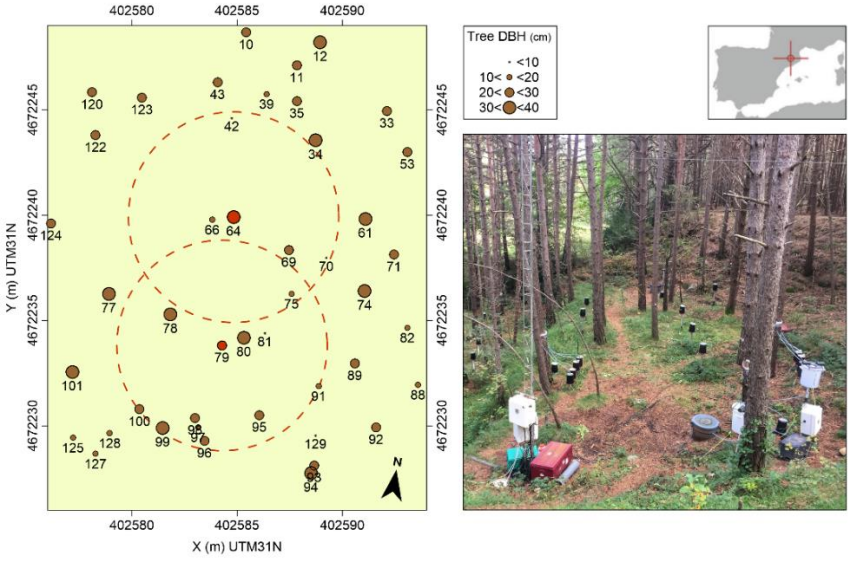

Figure 1. Location and map of the forest stand in the Vallcebre research catchments. Numbers are identifiers of trees within the forest stand (monitored trees A = 79; B = 64). Red circles represent a 5 m radius from each monitored tree.

Table 2. Biometric characteristics of the two monitored trees (adapted from Cayuela et al., 2018). DBH denotes the diameter at breast height.

Tree ID	DBH (cm)	Basal area (cm^2)	Height (m)	Crown area (m^2)	Crown volume (m^3)	Mean branch angle (º)	Mean branch diameter (cm)	Bark depth (cm)	Stem bark surface (m^2)	Bark storage capacity (mm)	Trunk lean (º)
A	20.7	336.5	21.2	11.9	118.9	29.3	2.8	2.1	7.3	0.37	0.0
B	28.0	615.8	18.3	23.8	289.1	17.7	5.6	2.9	11.0	0.58	5.7

4.2.2 Hydrometerological monitoring

Meteorological variables were measured by an automatic weather station located 2 m above the forest canopy. The station monitored air temperature and relative humidity (HMP45C, Vaisala, Vantaa, Finland), net radiation (NR Lite, Kipp & Zonen, Delft, the Netherlands), wind speed and direction (A100R, Vector Instruments, Rhyl, North Wales, UK) and recorded the data at a 5-min temporal resolution with a datalogger (Data Taker DT85, Thermo Fisher Scientific Inc., Sunbury, Victoria, Australia). Bulk rainfall was also recorded at 5-min intervals with a dynamically calibrated tipping bucket rain gauge (model AW-P, Institut Analític, Barcelona, Spain), after Iida et al. (2020), which was located at a distance of less than 100 m from the stand in an open area.

4.2.3 Stemflow monitoring – Experimental design

To determine stemflow distribution around the stem, a common stemflow collar was divided symmetrically in four sections. Each section corresponded to a cardinal direction (Figure 2). The subdivided stemflow collars were adjusted and placed around the stem at breast height, and edges were sealed with silicone. Each section was connected to a pipe and this to a covered tipping bucket (Davis Rain Collector II, Davis Instruments, Hayward, CA, USA) in order to derive stemflow volumes (Figure 2). A dynamic calibration of the tipping buckets was carried out for an accurate measurement of stemflow volume (Iida et al., 2020). The stemflow data was recorded at 5-min intervals by a datalogger (Data Taker DT85, Thermo Fisher Scientific Inc., Sunbury, Victoria, Australia).

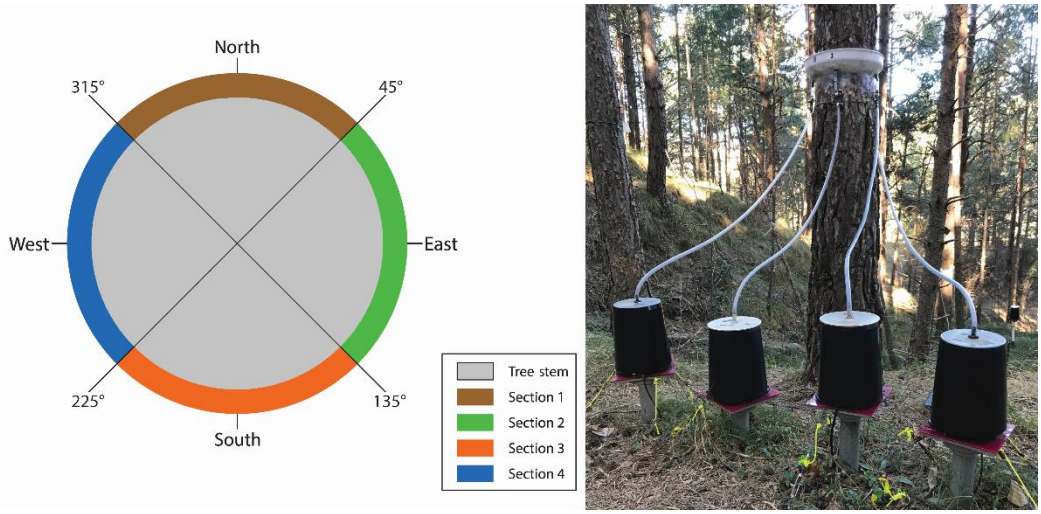

Figure 2. Setup for continuous measurement of stemflow with respect to cardinal direction. Schematic of the 4 sections collar design (left), and photograph of the experimental set-up (collar and tipping-buckets) for tree B (right).

A systematic weekly inspection of the stemflow collars was made to ensure that there were no cracks or gaps in the silicone that might allow water leaks. At this time, the various pipes and tubing were cleaned and checked to avoid connection leaks or clogs, and the tipping buckets were checked for proper function.

4.2.4 Stemflow data

Individual tree stemflow depth (SF_{depth} in mm) was calculated by divining the stemflow volume (liters) by the crown area (m^2). Following the logic of Herwitz (1986), the FR, which is the ratio of rainfall transported by stem to the tree base to the rainfall that would have reached the ground over the same area if the tree were not present, was calculated for each section as

$$FR = \frac{V}{B^* \cdot P} \quad (1)$$

where V is stemflow yield (litres), B* is the basal area associated with each of the four sections of the collar (m^2) and P is incident rainfall (mm). Since the stemflow collar of each tree was divided into four sections of equal size, the basal area corresponding to each individual section was calculated as the total basal area

divided by 4. Funneling ratios > 1 indicate the contribution of the outlying canopy to stemflow generation, that is, that canopy components other than the trunk are contributing to the concentration of rainfall as stemflow.

4.2.5 Stemflow dye experiment

To qualitatively identify the preferential stemflow flowpaths in the trees, a stemflow dye experiment was conducted for a single summer rainfall event in August 2020. Following the methods of Tischer et al. (2020), water with a high concentration (20 $g \cdot L^{-1}$) of Brilliant Blue FCF colored dye (Proquimac, Barcelona, Spain) was used to manually stain the two trees. The dye was distributed in a band (50 cm above the divided stemflow collars) around the circumference of the tree stem using a brush. Due to the nature of pine bark, a thinner brush was used to stain the bark furrows/fissures. Stemflow flowpaths were identified as those areas where the dye was removed/washed by the preferential stemflow channels, and areas that remain partially or completely covered mean that they experienced less or no stemflow.

4.2.6 Bark roughness

Bark roughness was estimated by using a simple method of sequential measurements of the bark surface above the divided stemflow collars. Every roughness measurement (defined by the distance between the trunk and the outer surface of the bark) was obtained with a Vernier caliper every 2 cm horizontally around the tree stem and every 5 cm vertically until 50 cm above the collar. Following Yarranton (1967), the circumference surrounding the outer bark represents the reference for each measurement (depth = 0); therefore, a tape nailed around the trunk was used as the external reference to measure the incisions with the caliper. All measurements were used to create a mesh which was interpolated in Surfer v.12 (Golden Software, Golden, CO, USA) to generate a 2D image that represents an estimation of bark roughness. The resulting image was subdivided for each of the four quadrants designated on each tree: north, east, south, and west.

4.2.7 Wind-driven rainfall

The protocol described in Herwitz and Slye (1995) was used for calculating wind-driven rainfall (WDR). Rainfall inclination angles were calculated at 5-min intervals using the following equations:

$$D = 2.23(0.03937P)^{0.102} \quad (2)$$

$$U_v = (3.378[\ln(D)]) + 4.213 \quad (3)$$

$$\tan(b) = \frac{W}{U_v} \quad (4)$$

where D is the raindrop diameter and P is the rainfall intensity ($mm \cdot h^{-1}$), U_v is the terminal fall velocity ($m \cdot s^{-1}$), b is the rainfall inclination angle and W is 5-min sustained wind gust ($m \cdot s^{-1}$).

Based on Herwitz and Slye (1995), an angle threshold was used to classified inclined and non-inclined rainfall. A 5-min inclination angle ≥ 19° was classified as inclined rainfall, and any 5-min inclination angle < 19° was classified as non-inclined rainfall.

4.2.8 Rainfall event selection and classification

Rainfall events were selected based on an inter-storm lapse of 6 and 12 h during the day and night respectively, to ensure dryness of the vegetative surfaces (Llorens et al., 2014). Data quality control was conducted, and events with incomplete or erroneous data were removed. Individual events were carefully scrutinized to ensure that there were (1) no errors related to the blockage of funnels/holes/tubes with pine needles or small insects, (2) no electronic failures and (3) no erroneous data due to delays in recording data during snowfall episodes (only 8% of total events). For rainfall classification, a maximum 30-min rainfall intensity threshold of 12 $mm \cdot h^{-1}$ was used to separate low- and high-intensity events, and a rainfall duration threshold of 8.5 h was used to distinguish between short-to-medium and long rainfall events. These criteria are based on the Pinos et al. (2020) rainfall event classification. However, here, we slightly widen the thresholds values (from 10 to 12 $mm \cdot h^{-1}$ and from 7 to 8.5 h) to cover the full range of events, keeping a similar number of events in the different rainfall classes. Using these two thresholds, rainfall was classified as (1) short- to medium-duration–low-intensity (SM–L) (≤ 8.5 h and ≤ 12 $mm \cdot h^{-1}$); (2) short- to medium-duration–high-intensity (SM–H) (≤ 8.5 h and > 12 $mm \cdot h^{-1}$); (3) long-duration–low-intensity (L–L) (> 8.5 h and ≤ 12 $mm \cdot h^{-1}$); and (4) long-duration–high-intensity (L–H) (> 8.5 h and > 12 $mm \cdot h^{-1}$). In addition, following Van Stan et al. (2016), intermittent events were identified using a k-means cluster analysis on three event-based statistics indicative of significant fluctuations between dry and rainy periods: (1) number

of dry periods, (2) mean duration of dry periods and (3) coefficient of variation (CV) in 5-min rainfall intensity intervals.

4.2.9 Statistical analysis

Stemflow data were not normally distributed around the circumference of the trees; therefore, the non-parametric Kruskal-Wallis test was employed to examine the overall significance of differences among the four sections. The statistical significance level was set at $p < 0.05$. If the H value from the Kruskal-Wallis test was significant, the Dunn-Bonferroni test was employed as a *post hoc* test for the pairwise comparisons to determine which groups were significantly different from each other. A two-way ANOVA was applied to examine the significance differences of bark roughness among the four sections and among trees.

4.3 Results and discussion

4.3.1 Rainfall event characteristics

Overall, for the 39 selected events (measured from May 2018 to December 2019), total rainfall was 1134 mm, with 21% of the events having rainfall smaller than 15 mm, 64% between 15 and 40 mm, and 15% with rainfall greater than 40 mm. Event rainfall ranged between 5.5 and 97.5 mm (Figure 3a), and mean rainfall intensities ranged from 0.7 to 23.4 $mm \cdot h^{-1}$ (Figure 3b). Sixty-two per cent of events had maximum 30-min rainfall intensity below 12 $mm \cdot h^{-1}$, and 44% had a duration of less than 8.5 h. According to duration and intensity, 8 rainfall events corresponded to SM–H class, 7 to L–H, 15 to L–L and 9 to SM–L. Using the k-means cluster analysis, seven events with a higher number of dry periods (from 31 to 79), mean dry period duration between 0.20 and 0.53 h, and relatively elevated CV in 5-min rainfall intensity (1.13-2.26) were classified as intermittent events (Table S2). Mean event VPD ranged from 0.02 to 0.35 kPa (Figure 3e). Mean wind speed ranged from 0.3 to 2.3 $m \cdot s^{-1}$ (Figure 3f), with 64% of events showing mean wind speed slower or equal to 1 $m \cdot s^{-1}$. Dominant wind direction oscillated between west-southwest and south (Figure 3g and Table S2). WDR inclined from the vertical was not relevant (Figure 3h), with 44% of events showing zero WDR, 38% with WDR between 0% and 10%, and 18% with WDR between 10% to 37%. Rainfall characteristics, stemflow production, wind and dry periods metrics of the selected events are shown in Table S2.

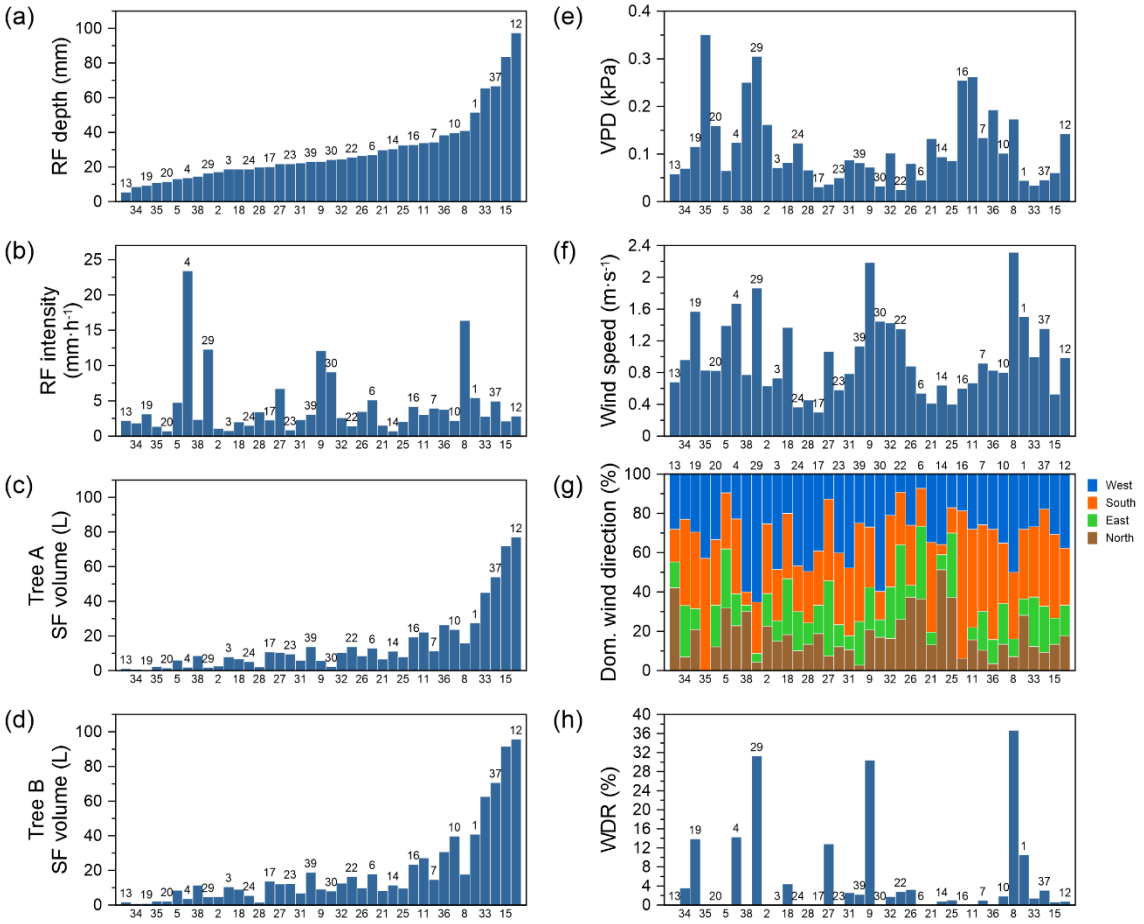

Figure 3. Meteorological characteristics of the 39 events recorded during the study period ranked according to their rainfall depth. The figure shows (a) rainfall depth, (b) rainfall mean intensity, (c) stemflow volume for tree A, (d) and B, (e) vapour pressure deficit, (f) mean wind speed, (g) dominant wind direction, and (h) wind-driven rainfall. Label numbers correspond to each event ID shown in Table S2.

4.3.2 Circumferential variation of stemflow on the pine tree boles

The total stemflow volume measured from both pine trees amounted to 571.8 L (tree A) and 749.4 L (tree B) during the observation period (Table S2), with mean values of 14.7 L (tree A) and 19.2 L (tree B) and coefficients of variation greater than unity (~122%). Stemflow depth for tree A represented between 0.4%

and 7.2% (mean = 3.3%, SD = 1.9) of the incident precipitation, while that for tree B varied between 0.3% and 4.6% (mean = 2.2%, SD = 1.2). Event stemflow volume generated by tree A ranged between 0.5 and 77 L and for tree B between 0.7 to 96 L (Figures 3c,d). The efficiency with which tree canopies converted incident rainfall into stemflow was analyzed via FR for each section. The FR for tree A ranged from 1.7 to 25.6, while for tree B ranged from 1.3 to 17.8, with no values <1. The FR for tree A were on average 1.4 times higher than those of tree B. These results reflect those of Cayuela et al. (2018) who found for the same pine stand that FRs were greater for trees with DBH less than 25 cm. The sectional FR for tree A ranged from 0.9 to 39.4 (northern), 0.2 to 11.4 (eastern), 3 to 33.1 (southern) and 1.9 to 23.5 (western), while the sectional FR for tree B ranged from 0.4 to 20 (northern), 0.3 to 17.4 (eastern), 0.8 to 11.2 (southern) and 2.1 to 30.6 (western), demonstrating that even for a single tree, stemflow channeling efficiency can be highly variable among sections. The average FR of the northern section of tree A was similar to the average of southern section, but 2.8 and 1.3 times higher than the average of the eastern and western sections, respectively. The average FR of the western section in tree B was 2.4, 1.8 and 2.8 times higher than the average of the northern, eastern and southern sections, respectively. Values <1 were never observed for the southern and western sections of tree A and the western section of tree B. Moreover, FR values <1 were seldom observed in the remaining sections ranging from a minimum of 1 to maximum of 6 observations. Thus, the FR results indicated that localized stemflow inputs considerably increase the amount of rainwater delivered to the forest floor around the tree base relative to the same area of ground outside of the forest canopy.

The two tested trees in this study showed marked individual differences in stemflow production among sections, which were strongly related to the total tree stemflow production and bulk rainfall. Overall, stemflow volume significantly increased in all sections of both trees with total stemflow volume (Figure 4a) and rainfall amount (Figure 4b), following a positive linear relationship. Not surprisingly, larger rainfall amounts generated greater stemflow volumes for all sections of both trees. The linear increase of stemflow volume with bulk rainfall was consistent with findings reported in other stemflow studies (e.g., André et al., 2008; Reynolds and Henderson, 1967). The intersection of the regression line with the *x* axis corresponds to the minimal rainfall amount needed for stemflow generation. Rainfall thresholds for stemflow occurrence in the sections of both trees ranged from 10 to 14 mm according to the linear regression functions (Figure 4b). This result is comparable with the rainfall threshold 9.3 mm for cypress trees found by Koichiro et al. (2001) and with the rainfall thresholds of 6 to 10.9 mm for leaved and leafless

seasons of an oak forest (André et al., 2008), but remarkably higher than those found by Carlyle-Moses and Schooling (2015) for a variety of isolated deciduous trees (rainfall < 3 mm). The relationship between bulk rainfall and the FR for the sections of both pine trees was logarithmic (Figure 4c), in accordance with reported results by Su et al. (2016) for various tree species. Funneling ratios were highly variable among sections (Figure 4c) and tended to increase with incident rainfall (Cayuela et al., 2018) up to a rainfall amount of ~ 40 mm, above which the FR increased only very slowly with increasing rainfall. Beyond this rain threshold (~ 40 mm), the FR can be considered relatively constant, that is, for double amount of rain (mm) we have approximately double of stemflow (L). As suggested by Carlyle-Moses and Price (2006), the FR increases until a rainfall threshold is reached. There were no clear relationship between stemflow FRs and rainfall intensity (data not shown).

From Figure 4a for tree A, significant differences in stemflow volumes among sections revealed a consistent pattern where the northern section produced the highest stemflow volume (33% of the total tree stemflow on average for all the events) followed by southern section (31%). The western section produced less stemflow than the aforementioned sections (24%) and the eastern section produced the lowest stemflow volume (12%). Tree B showed a different pattern than tree A. The western section produced the highest stemflow volume (42%), followed by the eastern section (23%), northern section (19%) and southern section (16%).

Percentages of stemflow contribution for each section were globally stable for events above a stemflow volume threshold. However, for events with less stemflow, a much higher variability was observed among percentages of stemflow contribution for each section. For tree A, the contribution from the northern section decreased (from 33% to 27%) for events with less than 5 L of stemflow, whereas the contribution from the southern section increased (from 31% to 37%). For tree B, below a 10-L stemflow threshold, the contribution from the northern section decreased (from 19% to 13%), whereas the contribution from the western section increased (from 42% to 46%) (Figure S1).

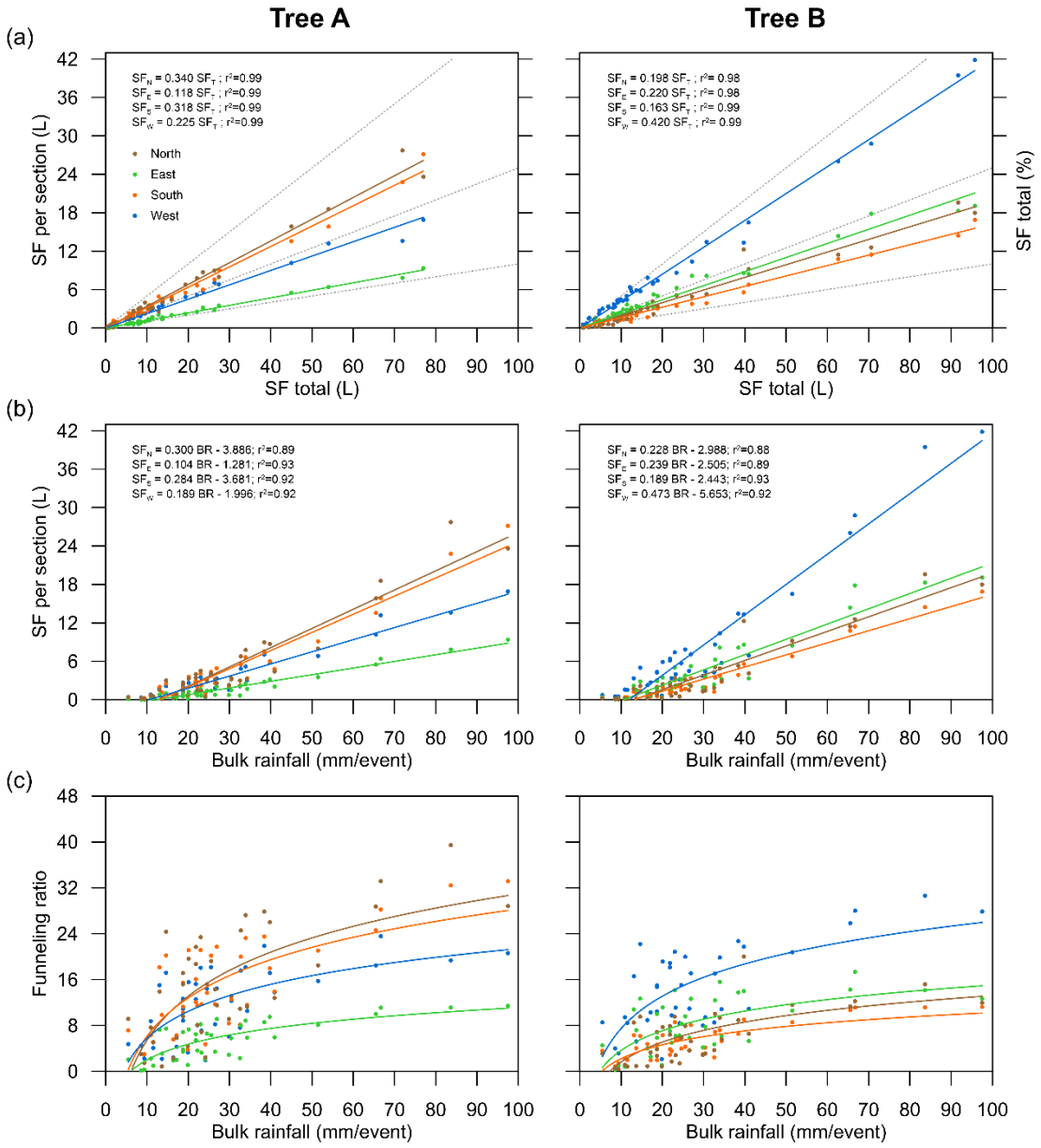

Figure 4. Event-scale relationship for tree A (left) and B (right) between (a) stemflow volume per section (litres) and tree total stemflow volume (litres), (b) stemflow volume per section (litres) and bulk rainfall (mm), and (c) funneling ratio per section and bulk rainfall (mm). Gray dotted lines in graph (a) correspond to 10%, 25% and 50% of total stemflow (right y-axis).

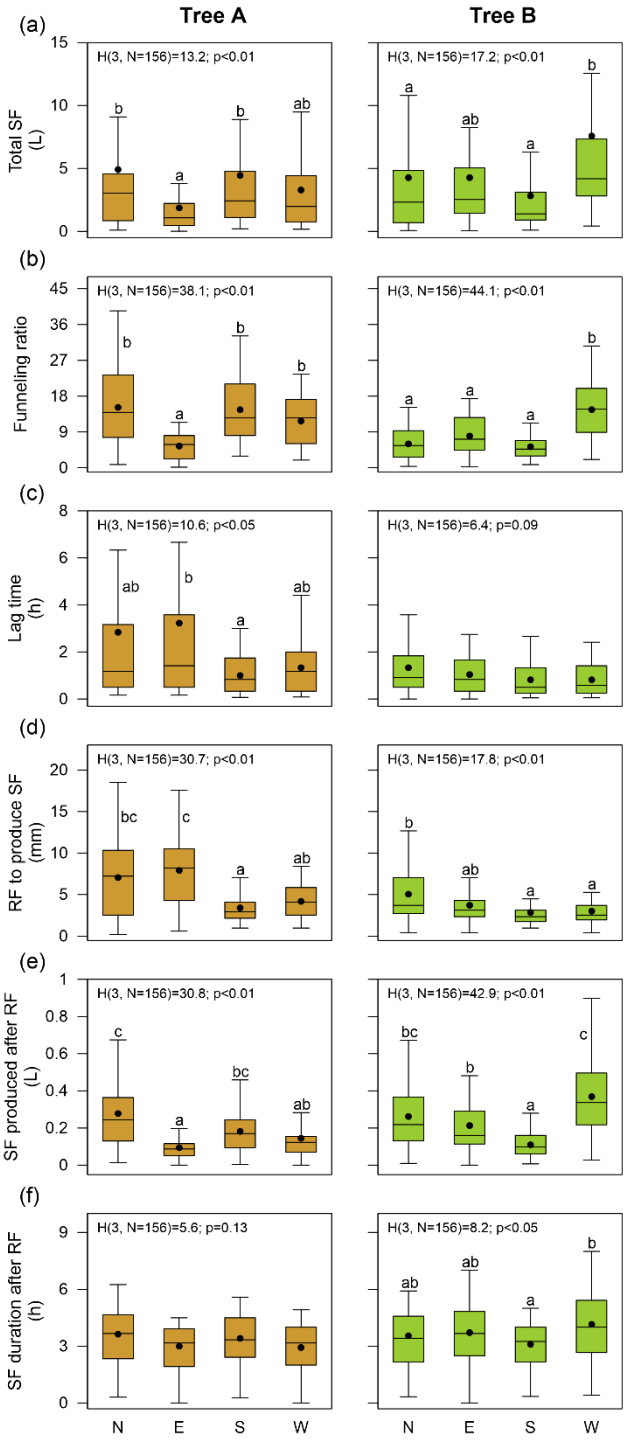

Figure 5. Box plots of (a) total stemflow, (b) funneling ratios, (c) lag time between the beginning of rainfall and the beginning of stemflow, (d) amount of rainfall required to produce stemflow, (e) stemflow duration after rainfall ended, and (f) volume of stemflow produced once rainfall ended per each section (N, E, S, W) of the stemflow collar for tree A (left) and B (right). Each box plot shows the median (center line), the interquartile range (25 to 75%) (box), the lower and upper quartile range (0-25% and 75-100%) multiple to a factor 1.5 (whiskers), and the mean (black dot). The letters indicate differences at $p < 0.05$ (tested using Kruskal-Wallis and Dunn-Bonferroni post hoc). Kruskal-Wallis statistics are shown within each graph.

Figure 5a shows that the eastern section (tree A) and southern section (tree B) generated less stemflow, matching with the lower FRs (Figure 5b). Significant differences in FRs for the eastern section (lower stemflow volume in tree A) and western section (higher stemflow volume in tree B) were found in comparison to the other sections (Figure 5b). In tree A, the northern and eastern sections needed longer lag times (> 2 h) and higher bulk rainfall volumes (> 5 mm) to produce stemflow in comparison to the southern and western sections (< 2 h and < 5 mm). In tree B, no significant differences were found in lag times among sections (~ 1 h), but the northern and eastern sections required slightly higher bulk rainfall volumes to produce stemflow (Figures 5c,d). For tree B, the amount of rainfall needed to generate stemflow in all sections was less than 5 mm. Similar values were reported by Cayuela et al. (2018) for the same stand (seven studied trees), with mean lag times of 1 h and 4 mm of mean rainfall amount needed to generate total tree stemflow. It should be noted that smaller bulk rainfall volumes were necessary for producing stemflow in the southern and western sections of both trees indicating that initial stemflow was preferentially diverted to these sections. The northern section (tree A) and western section (tree B) produced significantly higher stemflow volumes once rainfall ceased (Figure 5e), indicating that these sections remained wet longer and divert more stemflow, after the rainfall, compared to the other sections. No significant differences were found for the duration of stemflow once rainfall ceased in tree A, while tree B presented marked differences between the southern section and western section (Figure 5f).

4.3.3 The role of abiotic and biotic factors on stemflow distribution

4.3.3.1 Abiotic factors

As aforementioned stemflow showed a positive linear relationship with rainfall amount (Figure 4a). However, no direct relationship between stemflow produced by section with meteorological variables (mean rainfall intensity, wind speed, vapor pressure deficit and WDR) was found for either of the trees (Figure S2). Stemflow volume produced by each section showed a weak but positive linear relationship with wind run (Figure S2e) with coefficients of determination (R^2) ranging from 0.43 to 0.48 in both trees.

Moreover, percentages of stemflow per section did not show any clear patterns when ranked by increasing the meteorological variables values, including rainfall amount (Figure 6a), mean rainfall intensity (Figure 6b), mean wind speed (Figure 6c) and WDR (Figure 6d). These results indicate that, even if meteorological variables have been found to be relevant for total stemflow production in our forest plot (Cayuela et al.,

2018) and also in other areas and for other species (e.g., Tanaka et al., 2017; Van Stan et al., 2014), they had no or minimal influence on the heterogeneity of stemflow distribution around the tree stem for the two trees examined in this study.

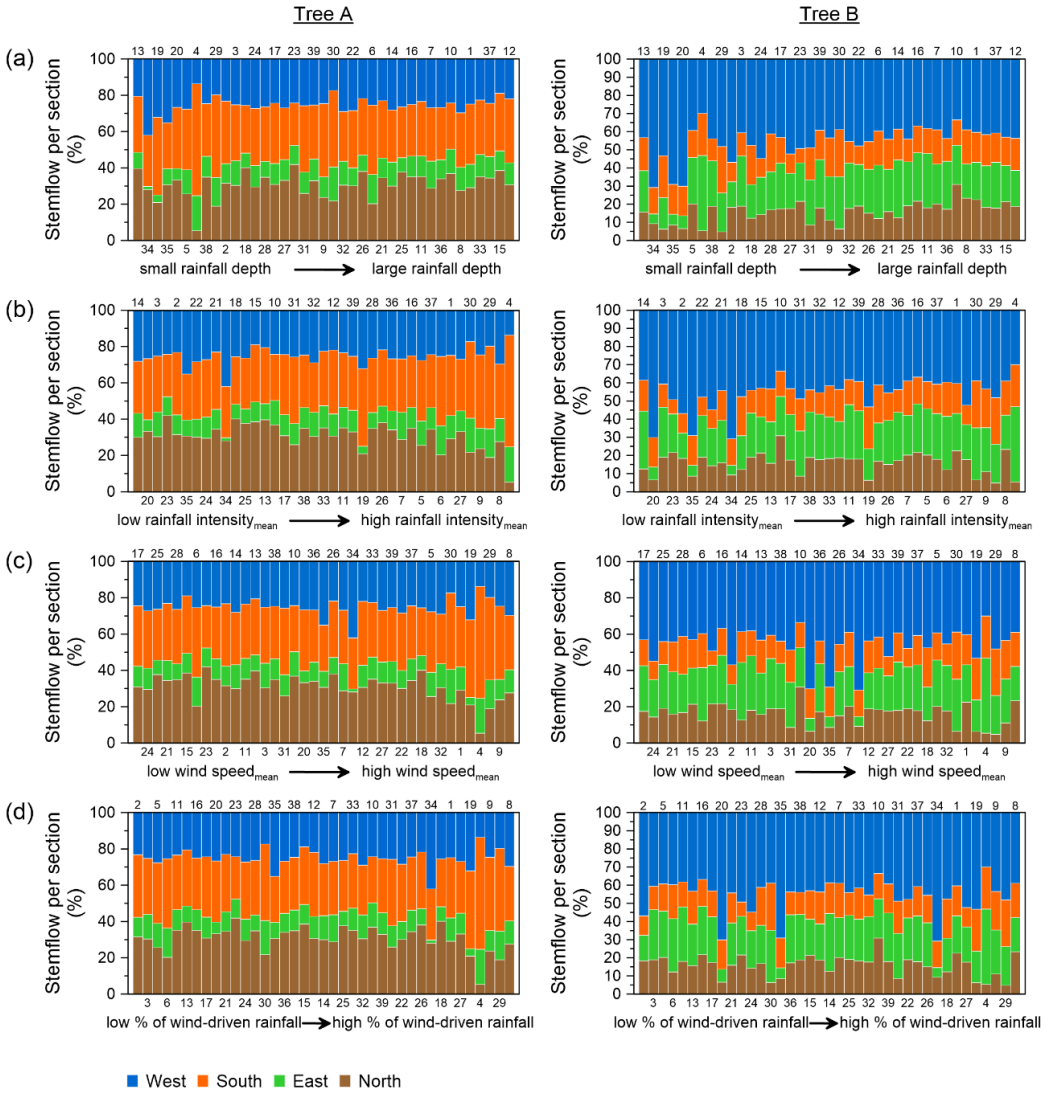

Figure 6. Percentage of total event stemflow generated per each section (N, E, S, W) of the stemflow collar for tree A (left) and B (right) for the 39 measured events. Events are ranked from smallest to largest: (a) rainfall depth, (b) mean rainfall intensity, (c) mean wind speed, and (d) percentage of wind-driven rainfall.

The relationships between stemflow per section and mean rainfall intensity is shown on Figure 6b (%) and Figure S2a (L). As found by Su et al. (2016) and Yang et al. (2008), no clear relationship between mean rainfall intensity and stemflow was identified at the event scale. In the literature there is indeed no consensus about the relationship between stemflow volume and various measures of rainfall intensity, and positive, negative or no relationships have been reported (see Dunkerley, 2014). However, at the intra-event scale, some sections could divert greater amounts of stemflow with increasing rainfall intensity, that is, with rainfall intensity peaks (see section 3.4).

Contrary to shrubs, where higher wind speeds were found to displace water flowpath (Návar and Bryan, 1990), we found no relationship between sectional stemflow and wind speed (Figure 6c and S2b). Cayuela et al. (2018) observed, however, that higher wind speeds decreased total tree stemflow volume in the study plot.

Vapor pressure deficit can reduce total stemflow production through enhanced trunk evaporation (Van Stan et al., 2014). However, since VPD exerts a more homogenous influence in the environment, all stemflow sections probably experienced a similar degree of evaporation in the interior of the forest stand. Hence, we found that stemflow heterogeneity was not correlated with VPD (Figure S2c).

Finally, following Van Stan et al. (2011) results showing that wind-driven rainfall can exert influence in total stemflow production, we explored the possibility of the influence of WDR on stemflow heterogeneity among sections. The hypothesis was that angled precipitation of WDR would cause one side of the tree to possibly intercept more rainfall and likely generate more stemflow in relation to the other sides of the tree. However, in our study, WDR percentages were relatively low and almost no WDR effect on stemflow distribution around tree stem was found (Figure 3h and S2d). Even when ranked by increasing WDR, no clear pattern was found between sectional stemflow percentage and WDR (Figure 6d). One possible explanation is that WDR effect on stemflow distribution is probably more likely to occur in forests with a more pronounced three-dimensional (3-D) canopy structure (i.e., some tropical forests) or more open forests with low tree densities, or for isolated trees, where more of the tree crown is exposed to WDR that can preferentially wet exposed surfaces and generate stemflow more quickly (Levia, Keim, et al., 2011). The high stand density of 1189 trees ha^{-1} and the overlapping crowns of the trees examined may explain the lack of relationship in our particular case (see section 3.3.2).

4.3.3.2 Biotic factors

As depicted in Figure 7, bark roughness within each section of both trees shows high heterogeneity across the measured band; however, no marked differences among sections were found. Tree B showed a greater and deeper presence of furrows in comparison to tree A. Bark roughness reached a maximum distance from the reference level of 1.0 cm for tree A and 1.7 cm for tree B. Measurements showed that the number of furrows with depth between 0 and 0.1 cm represented 40.5% (tree A) and 39.8% (tree B). Furrows 0.1 to 0.5 cm deep accounted for 45.0% and 25.4%, and those deeper than 0.5 cm 14.5% and 34.5% for tree A and B, respectively. Two-way ANOVA showed a statistically significant difference in bark roughness between both trees ($f(1) = 41.87$, $p < 0.001$), but no differences by section for either tree ($f(1) = 1.52$, $p = 0.22$). Mean bark roughness values for each section of both trees are given in Table S3. Overall, since roughness is similar among sections for a given tree, these results indicated that bark roughness (measured in the 50 cm above the stemflow collars) has no clear influence over the directional heterogeneity of the stemflow distribution for the studied trees. Even though bark roughness values did not vary by section for either given tree, it is worth noting that the bark morphology (i.e., its geometric configuration) between trees A and B may have partly accounted for some of the observed differences in sectional stemflow yield (Fig. 5a). In particular, Figure 7 shows that the furrows of tree B, especially in the western section, are better networked and connected with more pronounced furrow-ridge patterning (i.e., less platy) than those of tree A, which likely accounts for the larger stemflow yields in the western section of tree B. Conversely, the southern section of tree B has the lowest stemflow yield and appears to be the most platy section of tree B (Figure 8).

To visualize stemflow preferential pathways for one rainfall event, a dye experiment was conducted. On 27 August 2020 just after colored dye staining (see section 2.5) pictures of the four sections for both trees were taken. The trunk area was vertically separated into four sectors by strings matching the four cardinal directions (Figure 8). The pictures were taken using a cellphone with a dual-lens camera system of 12MP (iPhone 11, Apple Inc., CA, USA) and corrected for perspective in Adobe Photoshop CS5 v.12. On 2 September, new pictures were taken after the occurrence of two rainfall events during the elapsed time (6 days). The two rainfall events had the following characteristics: one large, intense event on 28 August (rainfall amount 49 mm; mean rainfall intensity 5.6 $mm \cdot h^{-1}$; maximum 30-min rainfall intensity 29.6 $mm \cdot h^{-1}$; duration 8.8 h) and one short, light rainfall event on 29 August (rainfall amount 5 mm). Figure 8 shows that dye was primarily washed off by stemflow in the furrows of the bark in each of the four sections

of both trees, indicating that stemflow was mainly routed to the ground within the furrows of the bark (both tangential and radial). In contrast, in the external bark regions (i.e., bark ridges and plates), where bark roughness was lower (~40% of the measured points in both trees), the bark remained completely stained. Since the external bark was not flushed, it confirms stemflow was mostly confined to the bark furrows that functioned as stemflow micro-channels (Tucker et al., 2020).

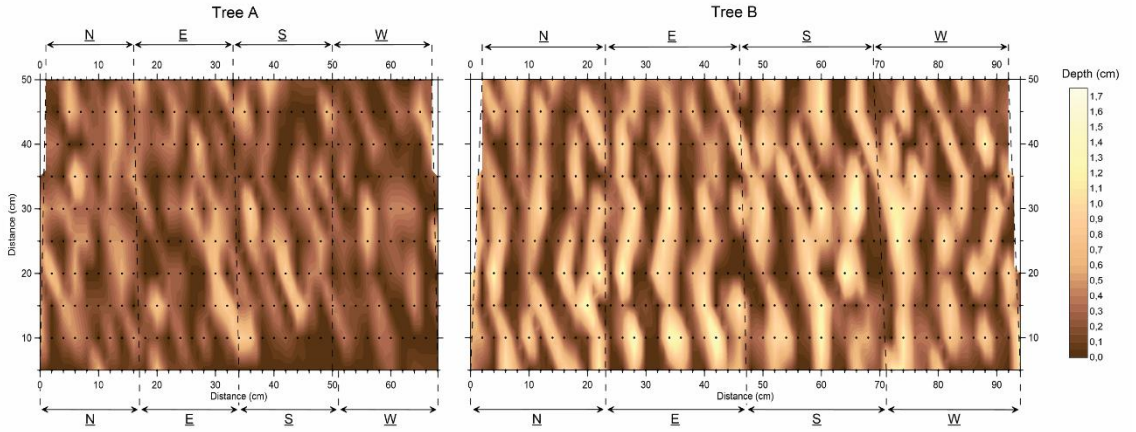

Figure 7. Distribution of bark roughness (i.e., depth from outer surface of the bark, in cm) around the stems at 50 cm above the stemflow collars for tree A and B. Black dots represented actual measurements used for interpolation. N, E, S, W refers to the cardinal directions of the four collar sections monitored for each tree.

Although no quantitative relationship between sectional stemflow volume and decolouration patterns was identified with this experiment, the different bark morphologies of the various sections are evident (Figure 8), possibly accounting for differences in stemflow yield (as pointed out for the southern section of tree B above). Unfortunately, the quantification of discoloured areas was not possible due the nature of furrows in pine bark in comparison to beech or maple observed in other studies (see fig. 2 of Tischer et al., 2020). Trunk lean can influence stemflow yields (e.g., Levia et al., 2015). Trunk lean was measured as the maximum angle from the vertical in any direction, where 0° represents a trunk without lean. Tree A had no trunk lean (0º) whereas tree B had a trunk lean around 6° with a northwest orientation (332°). For tree B, stemflow was most likely diverted in a preferential direction because of trunk lean, which could partly explain the higher stemflow production of the western section in this tree (42%). Trunk lean was also attributed to the preferential flow of stemflow on the trunk of konara oak in Japan (Imamura et al., 2017).

With respect to branches, Herwitz (1987) found that steeper branch inclination angles amplified the stemflow funneling effect. Similar findings were reported for stemflow volumes and FRs for a laurel forest in the Canary Islands, whereby interspecific differences in stemflow production were partly attributed to branch angles, the size of leaves and bark texture (Aboal et al., 1999). Thus, branch angles and trunk lean can both alter stemflow yields. Although differences in sectional stemflow yields may be more pronounced for a tree with some trunk lean, preferential flowpaths may be found even without any trunk lean. In the case of a straight pine tree trunk (tree A), bark furrows as well as natural trunk deformations (e.g., nodules) and branches, will affect stemflow routing, creating irregular stemflow paths and causing a non-uniform distribution around the tree stem.

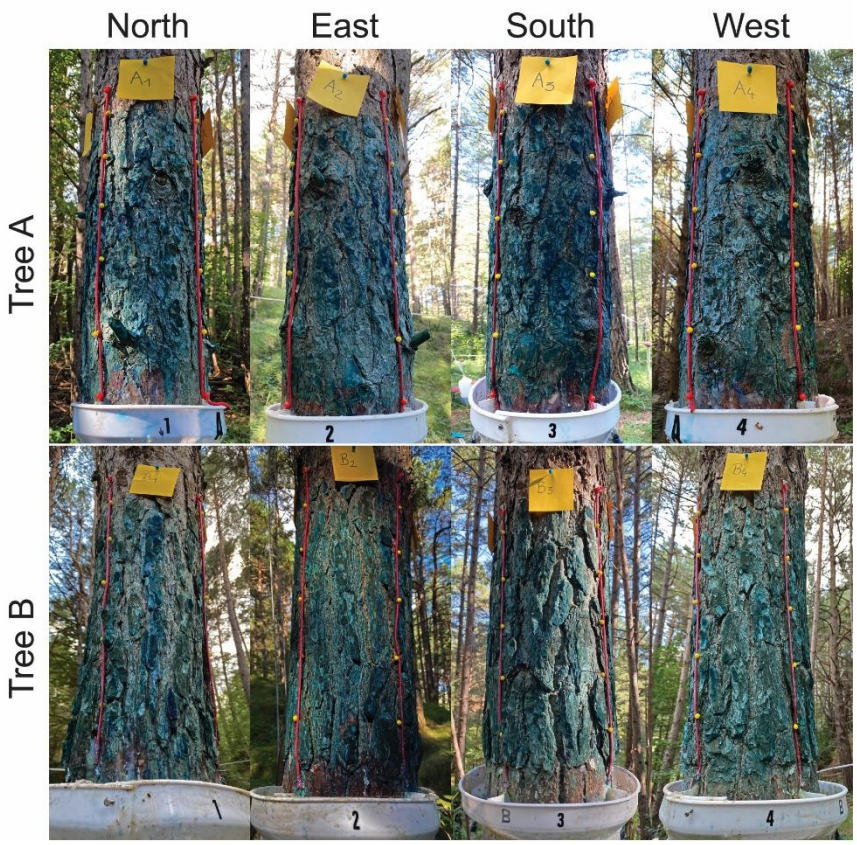

FIGURE 8. Photographs showing the four collar sections monitored for each tree after the first rainfall event (49 mm) following Brilliant Blue dye bark staining. Washed-out areas revealed that bark fissures micro-channels act as preferential stemflow pathways around tree stems.

Furthermore, Metzger et al. (2019) showed that neighborhood effect can influence the stemflow production at individual and subplot scale. Trees not dominated by neighbors with larger crowns and smoother bark were found to produce the most stemflow in a laurel forest (Aboal et al., 1999). Effective rainfall-intercepting crown areas, defined as the proportion of crown area which is not overshadowed by canopies of neighboring trees (Herwitz and Slye, 1995), could play a role in the stemflow generation by section of individual trees. Nevertheless, no clear relationship was found between sectional stemflow yield and its respective effective crown area (see Figure S3). It should be noted that circular canopies based on the mean crown radius have been assumed in Figure S3 for purposes of simplification. Despite the unclear relationship some insights are suggested. For tree A, even if 11 trees are located within a 5 m radius, the nearest tree (#80 at 1.1 m, Figure 1) likely played a key role for stemflow heterogeneity. In comparison with tree A, tree #80 has greater DBH (30.2 vs. 20.7 cm), similar height (20.4 vs. 21.2 m) and larger crown area (21.2 vs. 11.9 m^2). This tree is indeed situated in the east-northeast direction and, despite the fact that its crown area does not overlap tree A's crown, the crown space is shared between both trees (defined here as the shared crown area; Figure S3), corresponding with the eastern section that produced the lower stemflow amount. Therefore, we hypothesize that tree #80 (located within the eastern canopy area of Tree A) with a denser crown intercepted large amounts of rainwater, reducing stemflow in the east-northeast direction for tree A. Thus, even though large shared crown areas were also found in the northern, western, and southern sections, the trunk of tree #80 is further away than these sections, which suggests that in these directions this tree has a less dense canopy and therefore less interception. Tree B, has 5 trees within a 5m radius. The nearest tree #66 located at 1 m (Figure 1) has a smaller DBH (18.1 vs. 28.0 cm), lower height (16.4 vs. 18.3 m) and much smaller crown area (9.0 vs. 23.8 m^2) in comparison with tree B. As a result of its smaller size and crown area, it seems that tree #66 did not exert any influence on tree B stemflow patterns. Similarly, the overshadowed areas, which were much smaller compared to tree A, do not explain the dynamics of the stemflow per section in tree B.

4.3.4 Circumferential variation of stemflow during particular rainfall events

To gain some insights about the dynamic of stemflow distribution around the stem at the intra-event scale, stemflow dynamics among sections within particular rainfall events was investigated at 5-min intervals. One event, representative of for each one of the four rainfall classes (Figure S4), was selected.

For event 34, representative of short- to medium-duration–low-intensity event (SM–L, Figure 9a), a delay of ~ 1 hour from the beginning of the rainfall event was found before stemflow was observed for both trees. For tree A, most of stemflow during this SM–L event was diverted to the western section after ~ 2.5 h, contrary to the general trend where the northern section was the main contributor. Northern and southern sections produced similar stemflow amounts, but the southern section had a faster stemflow response. Stemflow was essentially zero for the eastern section. For tree B, the western section produced notably more stemflow than the other sections showing a marked difference around 3 h after the onset of the rainfall event. The remaining sections produced similar stemflow amounts. All sections had similar stemflow response times.

For event 27, representative of short- to medium-duration–high-intensity event (SM–H, Figure 9b), stemflow response times were much faster than for SM–L events, with response times of 10 min for tree A and 5 min for tree B. For tree A, the western and southern sections produced higher stemflow peaks than the eastern and northern sections during the first rain shower. During the second rainfall peak (time = 1 h) the northern section rapidly diverted more stemflow exceeding the other sections. The eastern section produced the lowest stemflow throughout the event. For tree B, the western section produced markedly higher stemflow from the beginning of the event. The marked stemflow peaks produced by the western section corresponded to the rainfall peaks, indicating that the tree bark was most probably saturated, producing almost immediate stemflow response. At t = 1 h, the eastern and northern sections produced similar stemflow amounts, higher than the southern section.

For event 03, representative of long-duration–low-intensity events (L–L, Figure 10a), tree A the northern and southern sections produced similar total stemflow volumes; however, the southern section showed a faster response and produced more stemflow during rainfall peaks. The western section and especially the eastern section produced lower stemflow volumes. For tree B, stemflow volume generated by the different sections followed the general trend depicted in Figure 5a. Until t = 4 h, tree B produced almost equal amounts of accumulated stemflow for sections with higher stemflow (western and eastern sections) and those with lower stemflow (northern and southern sections). After the third rainfall shower (time = ~ 4 h till the end), the western section produced more stemflow than the eastern section. Similarly, the northern section produced more stemflow than the southern section.

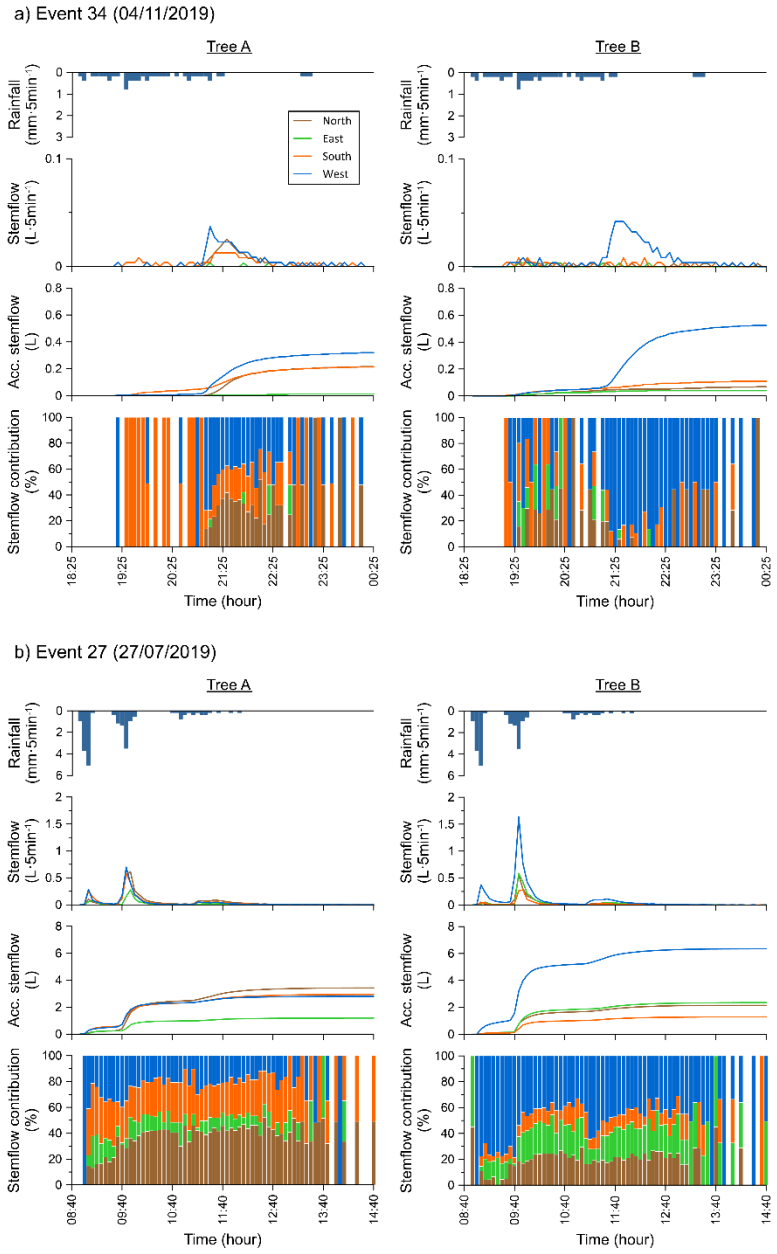

Figure 9. 5-min time step dynamics of rainfall, stemflow, accumulated stemflow and percentage of total event stemflow generated per each section (N, E, S, W) of the stemflow collar for tree A (left) and B (right) during: a) short-to-medium duration–low intensity event (SM–L), and b) short-to-medium duration–high intensity event (SM–H).

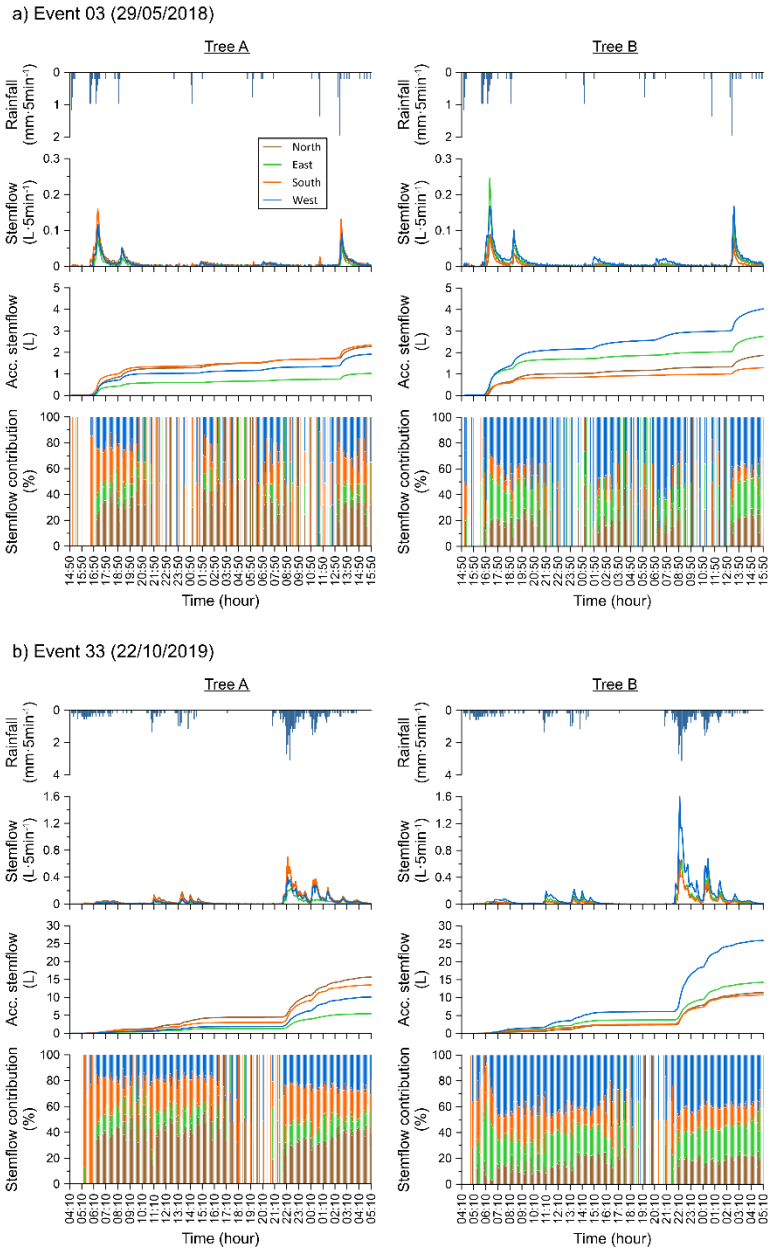

Figure 10. 5-min time step dynamics of rainfall, stemflow, accumulated stemflow and percentage of total event stemflow generated per each section (N, E, S, W) of the stemflow collar for tree A (left) and B (right) during: a) long duration–low intensity event (L–L), and b) long duration–high intensity and intermittent event (L–H).

For event 33, representative of long-duration–high-intensity and intermittent events (L–H, Figure 10b), the response time to generate stemflow was about 1 h for both trees. For tree A, stemflow volume generated by each section followed the general trend depicted in Figure 5a, with the northern section producing the highest stemflow volume followed by the southern section, which had the faster response time and mainly dominated the first hour interval (from t = 1 to 2 h). The western section ranked third and the eastern section produced the lowest total stemflow volume. In tree B, the western section produced the higher stemflow and reached the maximum difference with the other sections at t = 16 h during the more intense rainfall peak, indicating that after a heavy rain shower, tree B diverted a significant amount of stemflow to this section. The northern and southern sections produced almost the same total stemflow volume during the event.

The intra-event analyses of stemflow dynamics showed that absolute stemflow heterogeneities tended to be larger during high intensity rainfall peaks. In contrast, relative stemflow heterogeneities were especially important at the beginning of rainfall events, but relative stemflow contributions remained globally constant all along the event independently of rainfall intensity. It must be noticed that even in high-intensity rainfall peaks, a uniform stemflow generation by the sections in both trees was never attained.

4.3.5 Ecohydrological implications of stemflow distribution

Our results showed that the distribution of stemflow around the stem is clearly heterogeneous in the monitored trees. This heterogeneity will most often determine the pattern of water and solutes inputs in space (hot spots) and/or time (hot moments) in soil at the bases of trees. Therefore, the spatio-temporal heterogeneity of stemflow distribution around the stem has some important implications in hydrological and biogeochemical studies. In our view, among these implications, the most relevant are as follows:

1) Heterogenous stemflow water inputs could result in differential rates of biogeochemical reactivity in near-stem soils. Therefore, soil chemistry may vary between high- and low-stemflow areas near the base of a tree. This variability should be taken into account to get a representative sample of soil chemistry around the entire tree base (Gersper and Holowaychuk, 1971; Imamura et al., 2017).
2) Because of the preferential flowpaths of stemflow, these localized points of intense stemflow, under certain conditions, might trigger erosion processes such as those observed by Dunkerley (2020) and Keen et al. (2010), particularly for inclined trees or trees growing on sloping ground.

Therefore, stemflow distribution must be considered when forestation (i.e., afforestation and reforestation) projects are done for soil recovery purposes.

3) The preferential flowpaths of stemflow on the tree trunk corresponds to stemflow infiltration patterns on the forest floor for some species (i.e., European beech) but not others (i.e., sycamore maple) (Tischer et al., 2020). Further work is needed to determine whether bole shape and stemflow non-uniformity affect stemflow infiltration patterns (and areas) for a range of woody species.
4) Several stemflow infiltration models (e.g., Chang and Matzner, 2000; Hildebrandt and Eltahir, 2007; Sansoulet et al., 2008; Tanaka et al., 1996), which assumed a uniform circular stemflow distribution, are always (as often acknowledged by their authors) simplifications of reality. How these models cope with a more heterogeneous stemflow distribution, as the one described in this study, has yet to be investigated.
5) Disregarding near-stem throughfall, non-uniform stemflow will increase concentrated infiltration points in soil around the stem base and likely will induce preferential stemflow-root-channelization processes (called double-funneling) and macropore bypass (Johnson and Lehmann, 2006). Consequently, the infiltration can rapidly reach deeper soil layers. Therefore: (1) a better understanding of soil water storage for root water uptake will depend, in part, on the heterogeneity of stemflow distribution (Liang, 2020), and (2) stemflow funneling as an important input for groundwater recharge, since stemflow funneling along lateral roots have the potential to contribute to groundwater recharge and stormwater run-off (Tanaka, 2011). Thus, a correct understanding of the preferential infiltration stemflow-induced points will help to more precisely estimate flow amounts and rates that contribute to groundwater recharge.
6) The likely deeper infiltration of stemflow in the soil as result of stemflow heterogeneity around the stem, together with double-funneling phenomena, make proper water age estimates more complex in the vadose zone. Indeed, stemflow water routing within the soil matrix transporting young water to the deeper soil layers coupled with relocation of older water due to the hydraulic lift phenomenon from deep to shallow soil layers (Sprenger et al., 2019) greatly increase the potential heterogeneity of water age distribution within the soil. Therefore, tracing stemflow water and its heterogeneity could help to unravel (at least to some extent) water ages in the vadose zone.

While this study documented a non-uniform stemflow distribution, it is important to note that a more uniform distribution of stemflow can be observed at times for other trees species. Anecdotally, completely

wetted stems that can produce stemflow around the whole tree can sometimes be observed for long-lasting rain events that soak the stem, especially for isolated trees during large magnitude rains associated with hurricanes and extratropical storms. This is more likely for smaller and smoother-barked trees with steeper branching angles. While lower magnitude events would experience the channelization of stemflow along preferred flowpaths until the storage demands of other parts of the trunk area satisfied and produce stemflow, larger events that mostly soak the trees and mostly fill canopy, bark and stem storage capacities are more likely to have a more uniform circumferential stemflow distribution. In addition, in humid environments, fog may help to trigger a more uniform distribution of stemflow by previously saturating the tree canopy and stem before a rainfall event begins (Figueira et al., 2013).

4.3.6 Limitations and future research opportunities

Although our study was limited to two trees, which largely prohibits generalization beyond our particular study site, our detailed monitoring of sectional stemflow has provided insights on the circumferential variation of stemflow that can be used to generate clearer hypotheses related to stemflow distribution around the stem that may lead to heterogeneous inputs at the tree base. When studying the circumferential variability of stemflow, one needs to be cognizant of climatic factors, seasonality, site specific stand characteristics (e.g., stand density and 3-D geometry of the tree neighborhood), and the structural characteristics of the specific trees (e.g., trunk lean, branching patterns and crown shape) and their bark morphology. This is because all of the above can influence stemflow patterning on tree stems, and the extent to which any of these factors predominate will be partly a function of their mutual interactions at a given site.

There are many pressing research priorities for future work related with stemflow heterogeneity. First, new studies are needed to compare tree species using a higher number of tree samples. Measurements of stemflow volumes on different sides of individual trees, in combination with solute or isotopic concentrations in soil around the tree base, will be needed to support the transport and fate of non-uniform stemflow inputs. It also appears necessary to direct future research towards the determination of possible relationships between the stemflow distribution and the biotic or abiotic factors; this could help to better define the factors that govern infiltration patterns in a simpler way in order to develop stemflow infiltration models. For example, future work needs to quantify crown asymmetries among neighborhood trees in an effort to better understand the role of effective crown areas on stemflow generation. This could be done for

example using LiDAR to precisely map the 3-D geometry of the tree neighborhood. Also, the influence of wind on the circumferential variation of stemflow remains as an interesting topic that need to be addressed, especially for isolated trees. Finally, more experiments simulating natural stemflow together with artificial tracers are needed to improve our understanding of the dynamics of stemflow water infiltration and movement into forest soils.

4.4 Conclusions

In this study we assessed the circumferential variation of stemflow at the individual tree scale. Non-uniform distribution of stemflow was observed for the two monitored trees. The circumferential variability of stemflow among sections of each tree was attributed to a complex interaction of biotic and abiotic factors. For the two trees examined, our results suggest that stemflow flowpaths were partly controlled by tree structural characteristics (trunk lean and bark morphology) and tree neighborhood. Furthermore, temporal variations in rainfall intensity at intra-event scale seemed to influence the magnitudes of the stemflow heterogeneities. The results of this work fill a knowledge gap in the understanding of stemflow distribution, particularly for rough-barked trees. The existence of preferential stemflow flowpaths has potentially strong implications for ecohydrologists studying hydrological balance, groundwater recharge, soil moisture, solute and nutrients fluxes. Taking into account the stemflow distribution around the stem opens new perspectives for future research and discussion around the validity of current infiltration models in forested areas.

4.5 References

Aboal, J. R., Morales, D., Hernández, M., & Jiménez, M. S. (1999). The measurement and modelling of the variation of stemflow in a laurel forest in Tenerife, Canary Islands. *Journal of Hydrology*, *221*, 161-175. https://doi.org/10.1016/S0022-1694(99)00086-4

André, F., Jonard, M., & Ponette, Q. (2008). Influence of species and rain event characteristics on stemflow volume in a temperate mixed oak-beech stand. *Hydrological Processes*, *22*, 4455-4466. https://doi.org/10.1002/hyp.7048

Carlyle-Moses, D. E., & Price, A. G. (2006). Growing-season stemflow production within a deciduous forest of southern Ontario. *Hydrological Processes*, *20*, 3651-3663. https://doi.org/10.1002/hyp.6380

Carlyle-Moses, D. E., & Schooling, J. T. (2015). Tree traits and meteorological factors influencing the initiation and rate of stemflow from isolated deciduous trees. *Hydrological Processes*, *29*, 4083-4099. https://doi.org/10.1002/hyp.10519

Carlyle-Moses, D. E., Iida, S., Germer, S., Llorens, P., Michalzik, B., Nanko, K., Tischer, A., & Levia, D. F. (2018). Expressing stemflow commensurate with its ecohydrological importance. *Advances in Water Resources*, *121*, 472-479. https://doi.org/10.1016/j.advwatres.2018.08.015

Carlyle-Moses, D. E., Iida, S., Germer, S., Llorens, P., Michalzik, B., Nanko, K., Tanaka, T., Tischer, A., & Levia, D. F. (2020). Commentary: What We Know About Stemflow's Infiltration Area. *Frontiers in Forests and Global Change*, *3*, 577247. https://doi.org/10.3389/ffgc.2020.577247

Cayuela, C., Llorens, P., Sánchez-Costa, E., Levia, D. F., & Latron, J. (2018). Effect of biotic and abiotic factors on inter-and intra-event variability in stemflow rates in oak and pine stands in a Mediterranean mountain area. *Journal of Hydrology*, *560*, 396-406. https://doi.org/10.1016/j.jhydrol.2018.03.050

Chang, S. C., & Matzner, E. (2000). The effect of beech stemflow on spatial patterns of soil solution chemistry and seepage fluxes in a mixed beech/oak stand. *Hydrological Processes*, *14*, 135-144. https://doi.org/10.1002/(SICI)1099-1085(200001)14:1<135::AID-HYP915>3.0.CO;2-R

Dunkerley, D. (2014). Stemflow production and intrastorm rainfall intensity variation: an experimental analysis using laboratory rainfall simulation. *Earth Surface Processes and Landforms*, *39*, 1741-1752. https://doi.org/10.1002/esp.3555

Dunkerley, D. (2020). A review of the effects of throughfall and stemflow on soil properties and soil erosion. In J. T. Van Stan, E. Gutmann, & J. Friesen, (Eds.), *Precipitation Partitioning by Vegetation* (pp. 183-214). Springer, Cham. https://doi.org/10.1007/978-3-030-29702-2_12

Figueira, C., de Sequeira, M. M., Vasconcelos, R., & Prada, S. (2013). Cloud water interception in the temperate laurel forest of Madeira Island. *Hydrological Sciences Journal*, *58*, 152-161. https://doi.org/10.1080/02626667.2012.742952

Förster, H., & Schimmack, W. (1992). Influence of the stemflow on the depth distribution of radiocesium in the soil under a beech stand. *Naturwissenschaften*, *79*, 23-24. https://doi.org/10.1007/BF01132274

Gersper, P. L. (1970). Effect of American Beech Trees on the Gamma Radioactivity of Soils. *Soil Science Society of America Journal*, *34*, 318-323. https://doi.org/10.2136/sssaj1970.03615995003400020038x

Gersper, P. L., & Holowaychuk, N. (1971). Some effects of stem flow from forest canopy trees on chemical properties of soils. *Ecology*, *52*, 691-702. https://doi.org/10.2307/1934160

Gonzalez-Ollauri, A., Stokes, A., & Mickovski, S. B. (2020). A novel framework to study the effect of tree architectural traits on stemflow yield and its consequences for soil-water dynamics. *Journal of Hydrology*, *582*, 124448. https://doi.org/10.1016/j.jhydrol.2019.124448

Herwitz, S. R. (1986). Infiltration-excess caused by stemflow in a cyclone-prone tropical rainforest. *Earth Surface Processes and Landforms*, *11*, 401-412. https://doi.org/10.1002/esp.3290110406

Herwitz, S. R. (1987). Raindrop impact and water flow on the vegetative surfaces of trees and the effects on stemflow and throughfall generation. *Earth Surface Processes and Landforms*, *12*, 425-432. https://doi.org/10.1002/esp.3290120408

Herwitz, S. R., & Slye, R. E. (1995). Three-dimensional modeling of canopy tree interception of wind-driven rainfall. *Journal of Hydrology*, *168*, 205-226. https://doi.org/10.1016/0022-1694(94)02643-P

Hildebrandt, A., & Eltahir, E. A. (2007). Ecohydrology of a seasonal cloud forest in Dhofar: 2. Role of clouds, soil type, and rooting depth in tree-grass competition. *Water Resources Research*, *43*, W11411. https://doi.org/10.1029/2006WR005262

Iida, S., Shimizu, T., Shinohara, Y., Takeuchi, S., & Kumagai, T. (2020). The Necessity of Sensor Calibration for the Precise Measurement of Water Fluxes in Forest Ecosystems. In D. F. Levia, D. E. Carlyle-Moses, S. Iida, B. Michalzik, K. Nanko, & A. Tischer (Eds.), *Forest-Water Interactions* (pp. 29-54). Springer, Cham. https://doi.org/10.1007/978-3-030-26086-6_2

Imamura, N., Levia, D. F., Toriyama, J., Kobayashi, M., & Nanko, K. (2017). Stemflow-induced spatial heterogeneity of radiocesium concentrations and stocks in the soil of a broadleaved deciduous forest. *Science of The Total Environment*, *599*, 1013-1021. https://doi.org/10.1016/j.scitotenv.2017.05.017

Johnson, M. S., & Lehmann, J. (2006). Double-funneling of trees: stemflow and root-induced preferential flow. *Écoscience*, *13*, 324-333. https://doi.org/10.2980/i1195-6860-13-3-324.1

Keen, B., Cox, J., Morris, S., & Dalby, T. (2010). Stemflow runoff contributes to soil erosion at the base of macadamia trees. In: Proceedings of the 19th World Congress of Soil Science - Soil Solutions for a Changing World. 1-6 August 2010, Brisbane, Australia, pp. 240-243.

Koichiro, K., Yuri, T., Nobuaki, T., & Isamu, K. (2001). Generation of stemflow volume and chemistry in a mature Japanese cypress forest. *Hydrological Processes*, *15*, 1967-1978. https://doi.org/10.1002/hyp.250

Levia, D. F., & Germer, S. (2015). A review of stemflow generation dynamics and stemflow-environment interactions in forests and shrublands. *Reviews of Geophysics*, *53*, 673-714. https://doi.org/10.1002/2015RG000479

Levia, D. F., Keim, R. F., Carlyle-Moses, D. E., & Frost, E. E. (2011). Throughfall and stemflow in wooded ecosystems. In D. F. Levia, D. Carlyle-Moses, & T. Tanaka (Eds.), *Forest Hydrology and Biogeochemistry* (pp. 425-443). Springer, Dordrecht. https://doi.org/10.1007/978-94-007-1363-5_21

Levia, D. F., Michalzik, B., Näthe, K., Bischoff, S., Richter, S., & Legates, D. R. (2015). Differential stemflow yield from European beech saplings: the role of individual canopy structure metrics. *Hydrological Processes*, *29*, 43-51. https://doi.org/10.1002/hyp.10124

Levia, D. F., Van Stan, J. T., Mage, S. M., & Kelley-Hauske, P. W. (2010). Temporal variability of stemflow volume in a beech-yellow poplar forest in relation to tree species and size. *Journal of Hydrology*, *380*, 112-120. https://doi.org/10.1016/j.jhydrol.2009.10.028

Levia, D. F., Van Stan, J. T., Siegert, C. M., Inamdar, S. P., Mitchell, M. J., Mage, S. M., & McHale, P. J. (2011). Atmospheric deposition and corresponding variability of stemflow chemistry across temporal scales in a mid-Atlantic broadleaved deciduous forest. *Atmospheric Environment*, *45*, 3046-3054. https://doi.org/10.1016/j.atmosenv.2011.03.022

Liang, W. L. (2020). Effects of Stemflow on Soil Water Dynamics in Forest Stands. In D. F. Levia, D. E. Carlyle-Moses, S. Iida, B. Michalzik, K. Nanko, & A. Tischer (Eds.), *Forest-Water Interactions* (pp. 349-370). Springer, Cham. https://doi.org/10.1007/978-3-030-26086-6_15

Llorens, P., Domingo, F., Garcia-Estringana, P., Muzylo, A., & Gallart, F. (2014). Canopy wetness patterns in a Mediterranean deciduous stand. *Journal of Hydrology*, *512*, 254-262. https://doi.org/10.1016/j.jhydrol.2014.03.007

Metzger, J. C., Schumacher, J., Lange, M., & Hildebrandt, A. (2019). Neighbourhood and stand structure affect stemflow generation in a heterogeneous deciduous temperate forest. *Hydrology and Earth System Sciences*, *23*, 4433-4452. https://doi.org/10.5194/hess-23-4433-2019

Návar, J., & Bryan, R. (1990). Interception loss and rainfall redistribution by three semi-arid growing shrubs in northeastern Mexico. *Journal of Hydrology*, *115*, 51-63. https://doi.org/10.1016/0022-1694(90)90197-6

Pinos, J., Latron, J., Nanko, K., Levia, D. F., & Llorens, P. (2020). Throughfall isotopic composition in relation to drop size at the intra-event scale in a Mediterranean Scots pine stand. *Hydrology and Earth System Scienc*es, *24*, 4675-4690. https://doi.org/10.5194/hess-24-4675-2020

Reynolds, E. R. C., & Henderson, C. S. (1967). Rainfall Interception by Beech, Larch and Norway Spruce. *Forestry*, *40*, 165-184. https://doi.org/10.1093/forestry/40.2.165

Sansoulet, J., Cabidoche, Y. M., Cattan, P., Ruy, S., & Šimůnek, J. (2008). Spatially distributed water fluxes in an Andisol under banana plants: Experiments and three-dimensional modeling. *Vadose Zone Journal*, *7*, 819-829. https://doi.org/10.2136/vzj2007.0073

Sprenger, M., Stumpp, C., Weiler, M., Aeschbach, W., Allen, S. T., Benettin, P., Dubbert, M., Hartmann, A., Hrachowitz, M., Kirchner, J. W., McDonnell, J. J., Orlowski, N., Penna, D., Pfahl, S., Rinderer, M., Rodriguez, N., Schmidt, M., & Werner, C. (2019). The demographics of water: A review of water ages in the critical zone. *Reviews of Geophysics*, *57*, 800-834. https://doi.org/10.1029/2018RG000633

Su, L., Xu, W., Zhao, C., Xie, Z., & Ju, H. (2016). Inter-and intra-specific variation in stemflow for evergreen species and deciduous tree species in a subtropical forest. *Journal of Hydrology*, *537*, 1-9. https://doi.org/10.1016/j.jhydrol.2016.03.028

Tanaka, N., Levia, D., Igarashi, Y., Yoshifuji, N., Tanaka, K., Tantasirin, C., Nanko, K., Suzuki, M., & Kumagai, T. O. (2017). What factors are most influential in governing stemflow production from plantation-grown teak trees?. *Journal of Hydrology*, *544*, 10-20. https://doi.org/10.1016/j.jhydrol.2016.11.010

Tanaka, T. (2011). Effects of the canopy hydrologic flux on groundwater. In D. F. Levia, D. Carlyle-Moses, & T. Tanaka (Eds.), *Forest Hydrology and Biogeochemistry* (pp. 499-518). Springer, Dordrecht. https://doi.org/10.1007/978-94-007-1363-5_25

Tanaka, T., Taniguchi, M., & Tsujimura, M. (1996). Significance of stemflow in groundwater recharge. 2: A cylindrical infiltration model for evaluating the stemflow contribution to groundwater recharge. *Hydrological Processes*, *10*, 81-88. https://doi.org/10.1002/(SICI)1099-1085(199601)10:1<81::AID-HYP302>3.0.CO;2-M

Tischer, A., Michalzik, B., & Lotze, R. (2020). Nonuniform but highly preferential stemflow routing along bark surfaces and actual smaller infiltration areas than previously assumed: A case study on European beech (*Fagus sylvatica* L.) and sycamore maple (*Acer pseudoplatanus* L.). *Ecohydrology*, *13*, e2230. https://doi.org/10.1002/eco.2230

Tucker, A., Levia, D. F., Katul, G. G., Nanko, K., & Rossi, L. F. (2020). A network model for stemflow solute transport. *Applied Mathematical Modelling*, *88*, 266-282. https://doi.org/10.1016/j.apm.2020.06.047

Van Stan, J. T., Lewis, E. S., Hildebrandt, A., Rebmann, C., & Friesen, J. (2016). Impact of interacting bark structure and rainfall conditions on stemflow variability in a temperate beech-oak forest, central Germany. *Hydrological Sciences Journal*, *61*, 2071-2083. https://doi.org/10.1080/02626667.2015.1083104

Van Stan, J. T., Siegert, C. M., Levia, D. F., & Scheick, C. E. (2011). Effects of wind-driven rainfall on stemflow generation between codominant tree species with differing crown characteristics. *Agricultural and Forest Meteorology*, *151*, 1277-1286. https://doi.org/10.1016/j.agrformet.2011.05.008

Van Stan, J. T., Van Stan, J. H., & Levia, D. F. (2014). Meteorological influences on stemflow generation across diameter size classes of two morphologically distinct deciduous species. *International Journal of Biometeorology*, *58*, 2059-2069. https://doi.org/10.1007/s00484-014-0807-7

Yang, Z., Li, X., Liu, L., Wu, J., Hasi, E., & Sun, Y. (2008). Characteristics of stemflow for sand-fixed shrubs in Mu Us sandy land, Northwest China. *Chinese Science Bulletin*, *53*, 2207-2214. https://doi.org/10.1007/s11434-008-0165-0

Yarranton, G. A. (1967). An instrument for measuring the microrelief of bark. *Canadian Journal of Botany*, 45, 1173-1178. https://doi.org/10.1139/b67-125

Yue, K., De Frenne, P., Fornara, D. A., Van Meerbeek, K., Li, W., Peng, X., Ni, X., Peng, Y., Wu, F., Yang, Y., & Peñuelas, J. (2021). Global patterns and drivers of rainfall partitioning by trees and shrubs. *Global Change Biology*, *27*, 3350-3357. https://doi.org/10.1111/gcb.15644

CHAPTER 5

Routing stemflow water through the soil: a dual labelling approach with artificial tracers

Routing stemflow water through the soil: a dual labelling approach with artificial tracers

Few studies have explored the stemflow double-funnelling phenomenon, although subsurface flow along roots and macropores plays a significant role in determining hydrological responses in forested catchments. In this study, a stemflow experiment on *Pinus sylvestris L.* (Scots pine) used artificial tracers to view and quantify the preferential flow of stemflow water after infiltration into the soil. Forty-one litres of water labelled with enriched deuterium and Brilliant Blue FCF were applied at a flow rate of 7 L h^{-1} to the stem of a pine tree, which corresponds to stemflow caused by about 50 mm rainfall. TDR probes were distributed around the tree trunk and in depth profiles to measure high-resolution volumetric water content. One day after the stemflow discharge, soil pits were dug in the different cardinal directions and at varying distances from the tree. Photographs were taken for imaging analysis to quantify preferential flow metrics. Soil samples were taken from the different profiles to analyse dye concentrations and isotopic compositions. We found that stemflow infiltrated through an annulus-shaped area around the tree base. We observed a heterogenous spatiotemporal soil moisture response to stemflow and the occurrence of shallow perched water tables around the tree trunk. Dye staining demonstrated that stemflow infiltrated primarily along the surface of coarse roots and also through macropores. The dye coverage was less extensive close to the soil surface and increased with depth and with proximity to the tree trunk. Lateral flow was also observed, mainly in the shallow soil layers. A set of metrics demonstrated the prevalence of preferential flow. Deuterium and Brilliant Blue FCF concentrations correlated with each other significantly. The concentrations decreased at increasing distance from the tree trunk, indicating dilution and mixing with residual soil water. Macropores, coarse roots (living or decayed) and perched water tables produced a complex network regulating the preferential flow. Our results suggest that stemflow heavily affects soil moisture distribution, and thus also groundwater recharge and surface runoff. Our study provides insights into the physical processes controlling stemflow belowground funnelling and improves our understanding of forest-water interactions.

Original work: Pinos, J., Flury, M., Latron, J., & Llorens, P. (2022). Routing stemflow water through the soil: a dual labelling approach with artificial tracers. Hydrology and Earth System Sciences Discussions [preprint]. https://doi.org/10.5194/hess-2022-382

5.1 Introduction

Stemflow is the proportion of rain intercepted by the tree canopy that is channelled towards the bole and eventually flows downward and infiltrates into the forest floor around the stem base. Stemflow contributes higher amounts of water and solutes in near-stem soils than the throughfall contribution in the rest of the forest (Carlyle-Moses et al., 2018). Stemflow varies widely across vegetation types and climatic regions (Levia and Frost, 2003; Llorens and Domingo, 2007; Yue et al., 2021). Recent research has unveiled biotic and abiotic factors that regulate stemflow production before it is funnelled belowground (Levia and Germer, 2015; Cayuela et al., 2018; Zhang et al., 2021). Although stemflow is not a major proportion of the overall catchment water balance, it can saturate near-stem soil and may enhance overland, preferential or subsurface flow, contribute to soil water replenishment and groundwater recharge, produce soil erosion (Levia and Germer, 2015), transport chemical, particulate and biological materials (Van Stan et al., 2021), and influence root water uptake (Hildebrandt, 2020). Due to its importance in soil hydrology, biogeochemistry and ecohydrology, stemflow has become an active topic of research in recent years (see Levia et al., 2011; Van Stan et al., 2020).

A key topic in stemflow research is root-induced bypass flow, introduced by Johnson and Lehmann (2006) as the “double-funnelling of trees”. This term refers to the process whereby a first aboveground funnelling occurs when rainfall turns into stemflow, followed by a second belowground funnelling in which stemflow is led into the soil along tree roots and macropores through an unsaturated soil matrix.

While the concept of the double-funnelling phenomenon is well known, clarification of the underlying mechanisms is more challenging. Several experimental techniques, both invasive and non-invasive ones, have been used to study the double-funnelling processes of trees. The most common approaches are the monitoring of water fluxes by soil moisture sensors, the viewing of preferential flow paths by dye tracers, or a combination of the two (Liang et al., 2011; Schwärzel et al., 2012; Spencer and van Meerveld, 2016; Gonzalez-Ollauri et al., 2020; Tischer et al., 2020). Recently, non-invasive geophysical techniques such as ground-penetrating radar (GPR) and electrical resistivity tomography (ERT) have also been used to study double-funnelling processes (Guo et al., 2020; Di Prima et al., 2022). The majority of these stemflow funnelling studies, of various deciduous and evergreen trees, found that stemflow infiltration leads to

vertical and/or horizontal preferential flow along the surface of coarse roots, although matrix stemflow infiltration has been reported as well (Gonzalez-Ollauri et al., 2020).

Despite their potential for the study of water movement in the vadose zone, geophysical techniques often cannot resolve flow pathways at small-scale resolution, which limits their usefulness in stemflow infiltration research (Fan et al., 2020). On the other hand, dye tracing for staining flow pathways has become an established way to show preferential flow in soils (Flury & Wai, 2003). The results obtained from staining experiments clearly illustrate at high spatial resolution the complicated patterns of water movement (Ghodrati and Jury, 1990; Flury et al., 1994; Weiler and Flühler, 2004). However, the disadvantage of staining is that it is a destructive technique that provides only one-off results. Besides, as dyes are adsorbed to some extent by the soil matrix (e.g., Brilliant Blue FCF; Ketelsen and Meyer-Windel, 1999; German-Heins and Flury, 2000), there is a certain degree of underestimation of the flow paths. Therefore, new approaches are needed to unravel the patterns of stemflow belowground funnelling. Stable isotopes, such as deuterium (^{2}H), have been widely use in hydrology as conservative tracers (Kendall and McDonnell, 1998). In combination with dye tracers, they could be a powerful tool for unravelling stemflow double-funnelling phenomena.

In this study, we developed an approach to characterize the double-funnelling process by using high-resolution hydrometric monitoring and dual-tracer labelling (^{2}H and dye). The main goals of our study were to assess stemflow infiltration quantitatively by means of dye concentrations, isotopic compositions and hydrometric data (soil water content), and to view the spatial distribution of preferential flow pathways by dye staining. The experiment was conducted in a Mediterranean ecosystem with pine forest cover, which had not been extensively investigated for stemflow double funnelling. This study is a contribution towards the mechanistic understanding of water infiltration patterns and water-root interactions in forested catchments.

5.2 Material and methods

5.2.1 Study site

The research was conducted at the Vallcebre research catchments in Catalonia, Spain, established as hydrological and ecohydrological research sites in 1988 (Llorens et al., 2018). The catchments are located

100 km north of Barcelona, in the south-eastern part of the Pyrenees (42°12'N and 1°49'E). Their humid Mediterranean climate is characterized by a mean annual air temperature of 9.2°C and a mean annual precipitation of 856 mm (for the period 1999-2018). Precipitation is seasonal throughout the year, with spring and autumn the wettest seasons and summer and winter the driest. Nevertheless, summer convective storms also provide significant precipitation. Reference evapotranspiration shows a seasonal pattern with maximum values in summer of up to 6.9 mm d^{-1} and a mean annual rate of 823 mm. In the study area, soils developed over the mudstone lithology have a silty loam and silty clay loam texture and are characterized by a rapid decrease in their hydraulic conductivity at depth (Rubio et al., 2008).

Nowadays, Scots pine forests (*Pinus sylvestris* L.), which arose through afforestation of old agricultural terraces, are the main land cover of the catchment, but small fragments of original oak forests (*Quercus pubescens Willd.*) are also found (Poyatos et al., 2003). An experimental Scots pine forest stand (named Cal Rotes) was delineated within the Can Vila catchment to investigate forest-water interactions. The stand density and basal area is 1,189 trees ha^{-1} and 45.1 m^2 ha^{-1}, respectively. One representative mature pine tree (with a diameter at breast height of 27.3 cm and a basal area of 585.3 cm^2), which had been previously instrumented for stemflow measurement during a 6-month period (Cayuela et al., 2018), was selected for our stemflow double-funnelling experiment.

5.2.2 Artificial stemflow experiment set-up

To simulate stemflow (Figure 1), the approach of Llorens et al. (2022) was adopted in this study. A flexible PVC plastic tube (internal diameter = 10 mm) was placed around the experimental tree at breast height (1.3 m). As the trunks of pine trees are very rough, the outer bark of the tree was removed to assist the assembly of the tube. The plastic tube was perforated on the inside with 2-mm holes every 4-5 cm, such that the holes were in contact with the trunk surface. To ensure uniform wetting of the stem and to prevent splashing of water, cloths were placed between the bole and the tube. The tube was connected by a Y-shaped tubing connector to a water tank. A stopcock was installed upstream of the Y-shaped tubing connector to regulate and control the flow rate. The stopcock was set to achieve a flow rate of about 7 L h^{-1}.

Our system was designed to discharge water from a tank which was located 9 m above and ~35 m away from the trunk, creating a gravity-fed water system. Volumetric soil water-content (SWC, cm^3 cm^{-3} or %) was monitored by sixteen 30 cm-long TDR probes (CS615 probes, Campbell Scientific, Logan, UT, USA).

The probes were placed vertically in two circular rings, 10 and 30 cm from the trunk every 45°, i.e., facing the cardinal and inter-cardinal directions (Figure 1). When a physical obstacle was encountered (e.g., coarse roots or rocks) that did not allow the installation of the probe, the probe was placed as close as possible. The TDR probes were measured every 20 s and averaged at 1 min intervals by a datalogger (Data Taker DT85, Thermo Fisher Scientific Inc., Waltham, MA, USA). They were previously calibrated with long-term manual TDR measurements performed with a Tektronix 1502-C cable tester (Tektronix Inc., Beaverton, OR, USA) at the study plot. In addition, in each main cardinal direction (N, S, E, W), SWC was monitored by 4 TDR probes (CS605 probes, Campbell Scientific, Logan, UT, USA) installed vertically at depths of 0-10 cm, 0-20 cm, 30-40 cm and 30-60 cm (Figure 1). These probes were measured manually every 30 min with a Tektronix 1502-C cable tester.

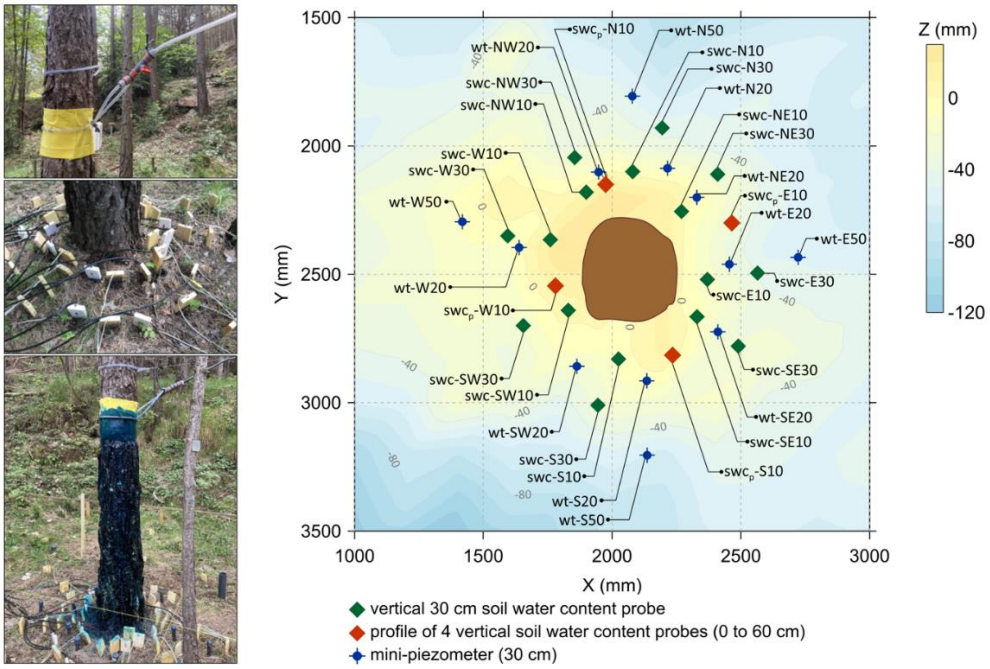

Figure 1. Tracer experiment set-up. Pictures of the artificial stemflow set-up and soil instrumentation before and after (last picture) the tracer experiment. Top view of the experimental area showing microtopography and location of instruments around the selected tree. swc = vertical 30 cm soil water content probe; swc_p = profile of 4 vertical soil water content probes; wt = mini-piezometer (30 cm deep); N = North, E = East, S = South, W = West. The number on the label of each location refers to the distance (cm) from the tree trunk.

Two piezometers were placed at 1.7 and 2.0-m depth at 1.6 m from the tree bole in opposite directions (northwest and southeast, respectively), to sample groundwater. Water levels were measured every 20 minutes with dataloggers (Micro-Diver, Van Essen Instruments, Delft, South Holland, Netherlands). Finally, twelve 30-cm deep mini-piezometers were placed at different distances (between 20 and 50 cm from the bole of the tree) in the cardinal and intercardinal directions to sample the soil water in the shallow layer (Figure 1). When a physical obstacle was encountered, the mini-piezometer was placed as close as possible. Water level was measured about every 30 min and water samples were collected for all the piezometers at one-hour intervals throughout the experiment.

Using the tree location as the centre point, a level mesh (4.8 m x 4.8 m with a grid size of 0.2 m) was placed above the ground. As depicted in Figure 1, the mesh was used as a coordinate system to georeference the installed instruments and to characterize the local topography around the tree. Depth to the ground (z) at every mesh intersection was measured, using the mesh level as the reference plane. All z values were corrected to represent the surrounding topography in relation to the tree base (z = 0) and a digital elevation model (0.2 m resolution) was interpolated from these data, with the tree base as the reference elevation (Surfer v.18, Golden Software, Golden, CO, USA).

Unlike what was done in other stemflow infiltration studies (e.g., Schwärzel et al., 2012; Llorens et al., 2022), forest litter (4.7 ± 2.4 cm thick according to Molina et al., 2019) was not removed from the forest floor around the tree bole before the experiment. This was in order to simulate as closely as possible stemflow infiltration under natural conditions, because pine litter (with considerable amounts of resins, waxes and aromatic oils) can induce various degrees of water repellence (Iovino et al., 2018), which may affect stemflow infiltration.

The stemflow experiment was conducted on 26 May 2021 when the soil had a moderate moisture condition (mean prior volumetric soil water content of 32%). During the previous 20 days, only 15 mm of rain was recorded, of which 6.4 mm occurred on 22 May. We applied 41 L of stemflow water labelled with enriched deuterium and Brilliant Blue FCF dye at a flow rate of 7 L h^{-1}. This amount of stemflow corresponds to that commonly generated by a 50-mm rainfall event for this particular tree. Enriched deuterium (99.96% fractional D abundance; Eurisotop, Cambridge Isotope Laboratories, Saint-Aubin, France) was mixed with the water to obtain a deuterium isotopic composition of ~500 ‰. To calculate the amount of enriched

deuterium to be applied, we used the "D-enriched water" Excel spreadsheet by Prof. Alex Sessions of the Division of Geological and Planetary Sciences, Caltech (http://web.gps.caltech.edu/~als/resources). To validate the amount of enriched deuterium added, preliminary mixing tests were performed and a sample of the final mixture was sent for isotopic analysis. Brilliant Blue FCF (Proquimac, Barcelona, Spain) was selected as the dye tracer because of its favourable physicochemical and toxicological characteristics (Flury and Flühler, 1995). The dye shows a Langmuir-type of sorption behaviour in soil (German-Heins and Flury, 2000). Thus, the higher the concentration, the less relative sorption is expected, as sorption sites become saturated with the dye tracer. In our experiment, a Brilliant Blue FCF concentration of 5 g L^{-1} was used.

5.2.3 Stemflow infiltration area

Just after the experiment was finished, litter was carefully removed from the surrounding area of the tree base and the stemflow infiltration area (m^2) was determined, following Llorens et al. (2022), by placing a plastic mesh over the soil surface, counting the total number of grid areas covering dye-stained soil and multiplying by the grid-square area (1.27 cm^2 grid $square^{-1}$).

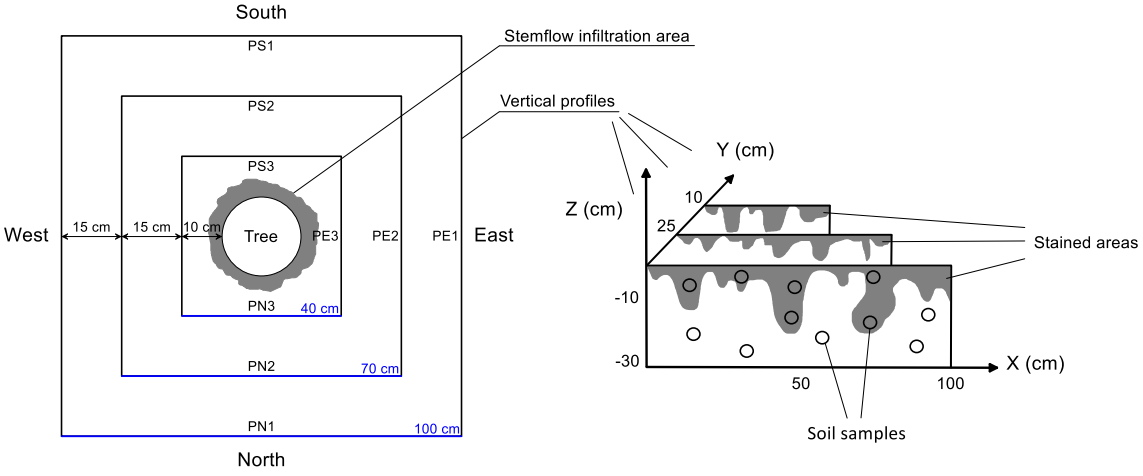

Figure 2. Top and vertical view of the different profiles excavated and the sampling.

5.2.4 Plot excavation and soil sampling

One day after the dual-labelled water application, we opened four vertical trenches (30 cm deep and 100 cm wide) in the four cardinal directions at 40 cm distance from the tree bole. Later, two more cross-sections were opened closer to the tree, at a distance of 25 cm and 10 cm in each direction (Figure 2). In total, 12

soil profiles were excavated and photographed throughout the day. The face of each profile was levelled by a steel scraper knife to minimize shadows caused by its unevenness and roughness. For each of the 12 soil profiles, dye-stained (blue) and non-stained areas were sampled with steel cylinders (100 cm^3) to measure dye concentration and isotopic composition. In total, 63 samples were collected and their location georeferenced. Immediately after the samples were taken, they were covered with plastic film and placed into coolers to maintain soil moisture and prevent evaporation, and then transported to the laboratory.

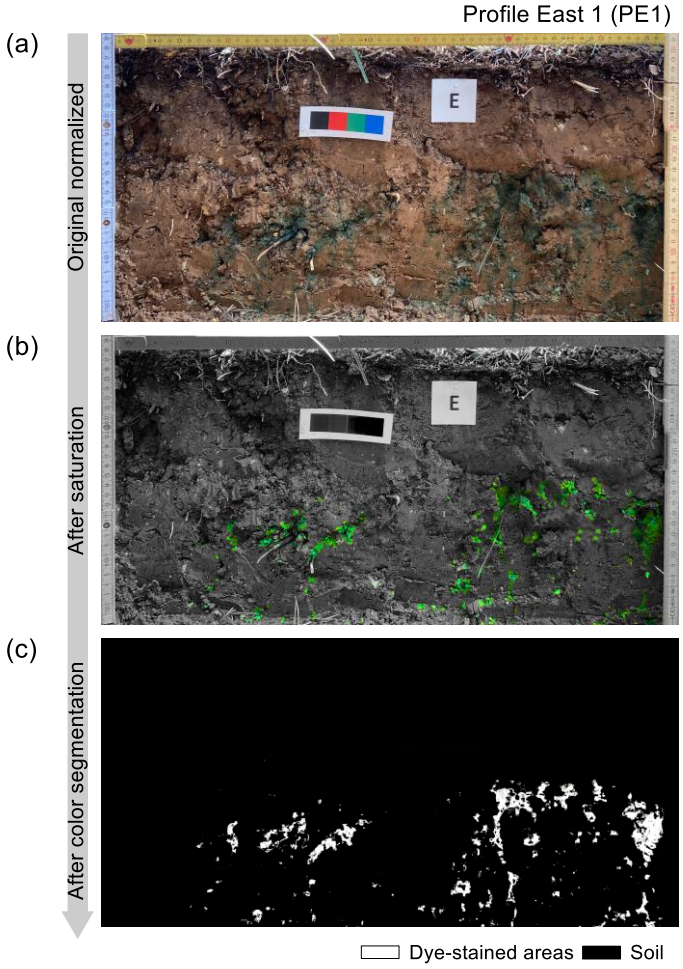

Figure 3. Image analysis procedure of soil profile photographs. (a) Geometric correction, recalibration of colours and illumination, (b) Colour saturation adjustment and (c) Colour segmentation by using a supervised classification.

5.2.5 Image analysis and preferential flow indices

Because photographs were taken at varying times during the day, with different illumination (shadows vs sunlight), they showed different tints, which made it challenging to analyse colour distribution automatically. Therefore, we used a primary colour scale as a reference to recalibrate the colours and illumination in each photograph (Figure 3a). Then, the saturation of the blue stains was maximized to make it easier to distinguish dye intensities (Figure 3b). The photographs were digitized and edited for geometric correction, contrast and brightness, using Adobe Photoshop 21.2.12 (Adobe Inc., San José, CA, USA).

These corrected images were then used to classify dye-stained and non-stained areas with the maximum-likelihood supervised classification tool in ArcGIS 10.4.1 (Environmental Systems Research Institute Inc., Redlands, CA, USA) (Figure 3c). Identifiable dye-stained and non-stained areas of interest were manually digitized for each image and used as a training set for the classification tool. Unwanted objects were manually masked out to prevent potential inaccuracies in the classification process.

Six preferential flow indices were then derived from the digitized images. These indices were calculated as follows:

Dye coverage (DC, %) (Flury et al., 1994) is the proportion of the dye-stained area to the total area. It was calculated in 10-mm depth increments (dye coverage profile) and for the entire profile (total dye coverage). Total dye coverage is lower when there is a higher degree of preferential flow.

Uniform infiltration depth (UniFr, cm) (Van Schaik, 2009) is the depth at which the dye coverage decreases below 80%. High values indicate a uniform infiltration process, whereas low values indicate preferential flow.

Preferential flow fraction (PF_{fr}, %) (Van Schaik, 2009), defined as the fraction of the total infiltration that flows through preferential flow paths, is calculated as:

$$PF_{fr} = 100 \cdot \left(1 - \frac{UniFr \cdot WP}{TSA}\right) \quad (1)$$

where *WP* is the width of the profile (cm), and *TSA* is the total stained area (cm^2).

Length index (LI, unitless) (Bargués-Tobella et al., 2014) is the sum of the absolute differences between the dye coverage (DC, %) of two consecutive depth intervals *i* and *i*+1 in a vertical profile of *n* intervals:

$$LI = \sum_{i=1}^{n-1} |DC_{i+1} - DC_i| \quad (2)$$

This index is related to the degree of heterogeneity of the dye infiltration pattern, with higher *LI* values indicating greater preferential flow.

Peak index (PI, unitless) (Bargués-Tobella et al., 2014) is the number of times that the vertical line defined by the total dye coverage intersects the dye coverage profile. This parameter is also related to the heterogeneity of the stained patterns, with high values of the parameter indicating a high degree of preferential flow.

Mass fractal dimension (D_s, unitless) (Hatano and Booltink, 1992; Hatano et al., 1992) is related to the basic shape of an object (staining patterns), for example a dot, line or plane. D_s can be derived by fractioning a stained profile into squares (pixels) of side *r* (the smallest value of *r* corresponding to the width of an original pixel), and then counting the number of partially stained squares, *N(r)*. Repetition of this process with increasing *r* values gives a series of *N(r)* values. Double logarithmic plots of *N(r)* against *r* show a linear correlation from which D_s is calculated from the slope, as follows:

$$\log N(r) = -D_s \cdot \log r + c \quad (3)$$

where *c* is a constant. D_s is calculated in the range of 0 to 2. D_s = 0 when the stained pattern is a dot pattern, D_s = 1 when it is a line pattern (long and slender) and D_s = 2 when it is the dimension of a completely filled area.

5.2.6 Dye concentration analysis

A similar dye extraction procedure to that of Forrer et al. (2000) was followed. An aliquot of 1 g was taken from the centre of each soil core on the side corresponding to the soil profile in the photographs. Then, this aliquot was mixed with 5 mL of deionized water, shaken overhead for 3 h, and centrifuged for 30 min at 3,000 rpm (ROTINA 420, Hettich, Kirchlengern, North Rhine-Westphalia, Germany). The concentration of Brilliant Blue FCF of the supernatant was measured by spectrophotometry at a wavelength of 630 nm, based on a previously established calibration curve relating absorbance (A) to dye concentration (C_d; mg

L^{-1}) (C_d = 6.83 A; R^2 = 0.99). Because we did not determine the dry mass of the soil cores, the dye concentration in the soil was then expressed as mass of dye per mass of wet soil (C; mg kg^{-1} of wet soil).

5.2.7 Isotopic analysis

A sufficient aliquot to fill a test tube (20 mL) was taken from the internal side of each of the 63 core samples. These samples were sent to the Scientific and Technical Services of the University of Lleida for isotopic analysis. Water from the soil samples was extracted by cryogenic extraction and the stable water isotopes ($\delta^{18}O$ and $\delta^{2}H$, ‰) were determined by cavity ring-down spectroscopy (Picarro L2120-i analyser, Picarro Inc., Santa Clara, CA, USA). The equipment had an accuracy of <0.1 ‰ for $\delta^{18}O$ and <0.4 ‰ for $\delta^{2}H$, based on the repetition of four reference samples provided by the International Atomic Energy Agency (IAEA). All isotopic data were expressed in terms of δ values and calculated as follows:

$$\delta = \left(\frac{R_{sample}}{R_{VSMOW}} - 1\right) \cdot 1000\ ‰ \qquad (4)$$

where *VSMOW* is Vienna Standard Mean Ocean Water, and *R* is the isotope ratio ($^{18}O/^{16}O$ or $^{2}H/^{1}H$).

5.2.8 Soil characteristics

To characterize the soil at the experimental site, six vertical 30-cm depth profiles were dug on the area where the monitored tree is located. A depth of 30 cm was the maximum because no relevant changes in soil physical properties had been observed in similar forest stands in the same study area beyond that depth (Rubio et al., 2008). Tree roots encountered during excavation were cut and removed. Soil cores were taken with steel cylinders (100 cm^3) in 5-cm depth intervals from the soil surface down to 30 cm, to determine volumetric soil water content (VWC, $cm^3\ cm^{-3}$), bulk density (BD, g cm^{-3}), soil texture, organic matter content (OM, %) and porosity (ε, %). Once taken, samples were immediately covered with plastic film and placed inside coolers to maintain sample moisture. Volumetric soil water content and bulk density were determined for each core and the latter was used to calculate porosity, assuming a particle density of 2.65 g cm^{-3} (Hao et al., 2007). Soil organic matter content was determined by loss-on-ignition following Wang et al. (2012).

For soil texture analysis the protocol described in Faé et al. (2019) was used. The dry soil cores were disaggregated and then a representative, well-mixed 50 g aliquot was collected from each sample. Gravel (diameter > 2 mm) was removed by sieving. Then organic matter was removed by use of 15% hydrogen peroxide and clay aggregates were dispersed with sodium hexametaphosphate. The soil was then sieved

through a 50-µm mesh to separate sand-sized particles (0.05 to ⩽ 2 mm). Four subsamples were taken from the < 50 µm suspension and analysed by laser diffraction (Mastersizer 2000, Malvern Panalytical Ltd., Malvern, Worcestershire, UK). Prior to the analysis, the samples were sonicated for 30 s and instrument parameters were set to refracting index 1.52, absorption 0.1, stirrer speed 750 rpm, pump speed 1,750 rpm and analysis time 30 s. Finally, the clay and silt fractions determined by the instrument were averaged after obvious outliers were discarded. The soil texture (sand, silt and clay fractions) and bulk density were then used to calculate saturated hydraulic conductivity by the Rosetta v.3 pedotransfer functions model (Zhang and Schaap, 2017).

In addition, to determine the isotopic composition of the soil profile before the experiment (see Section 2.7), disturbed soil samples were taken in each intercardinal direction from the experimental tree, at a distance of 3 m from the stem. Samples were taken at the following depth increments: 0-5, 5-10, 10-20, 20-30, 40-50, 90-100 cm.

5.3 Results and discussion

5.3.1 Soil characteristics

Data obtained from the 30-cm depth profiles were pooled (n=6) to characterize the physical properties of the soil at the forest stand. Similarly, the isotopic composition values of the four soil cores were also pooled. Figure 4 shows the average and standard deviation of the soil properties. Soil texture was classified as silt loam according to the USDA classification. Bulk density increased from about 1 g cm^{-3} at the topsoil to 1.6 g cm^{-3} at 30-cm depth. Similar bulk density values were observed by Rubio et al. (2008) in the same study area at 50-cm depth. As bulk density values > 1.6 g cm^{-3} affect root growth in silt loam soils (Zisa et al., 1980), we did not expect root growth or development to be restricted. The increase in bulk density corresponded to a decrease in saturated hydraulic conductivity, porosity and organic matter content with depth. Soil porosity decreased by about 24% from topsoil to subsoil, whereas water content at field capacity declined by only about 2%. The high organic matter content in the topsoil (16%) is due to high amounts of litter on the forest floor, as found by Molina et al. (2019). The δ^2H decrease (from -48‰ in the topsoil to -55‰ at 100-cm depth) is due to evaporation, which was also observed by Sprenger et al. (2019) in the same forest stand.

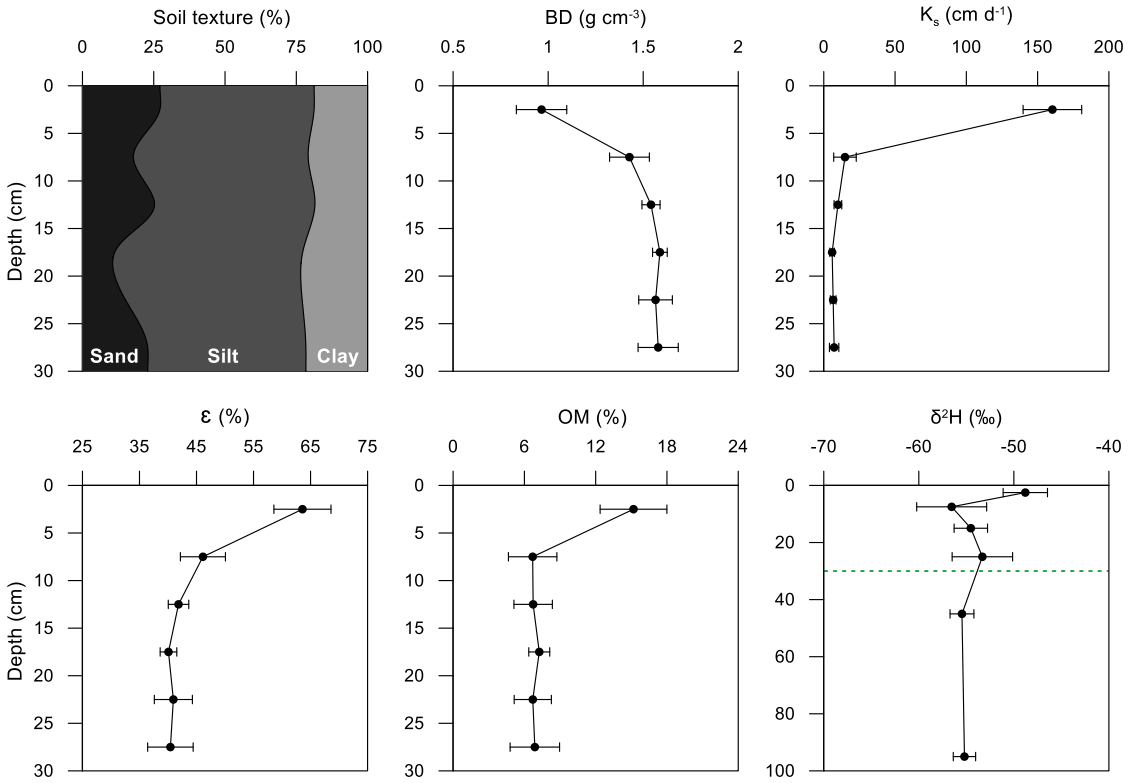

Figure 4. Soil physical properties at the pine forest stand. BD = bulk density, K_s = saturated hydraulic conductivity, ε = porosity, OM = organic matter content, δ^2H = deuterium isotopic composition of soil water. Note the different scales of the depth axes for the isotopic composition (the green dotted line is the 30-cm depth). Data represent means and standard deviations (n = 6 for physical properties and n = 4 for isotopic composition).

5.3.2 Stemflow infiltration area

There are few studies that have used dye tracers to calculate the stemflow infiltration area (see Carlyle-Moses et al., 2020). In our experiment, stemflow infiltrated into the soil in an annular shape around the base of the tree trunk. The area of the annular shape was 0.14 m^2, which is smaller than the infiltration area of 0.245 m^2 reported by Schwärzel et al. (2012). However, the other stemflow infiltration areas reported are usually much smaller (e.g., Carlyle-Moses et al., 2018; Tischer et al., 2020; Llorens et al., 2022). In pine forests there is usually a thick litter layer that repels water (Iovino et al., 2018) and causes the stemflow infiltration area to expand beyond the immediate vicinity of the tree trunk.

5.3.3 Soil water content dynamics

The spatial distribution of the soil water content around the tree before stemflow initiation was highly heterogeneous, and remained so during the stemflow experiment (Figure 5). The detailed temporal dynamics of the SWC measured with the different TDR probes is shown in Figure S1. Heterogeneous volumetric SWC around a tree, induced by stemflow, was also observed by others (Liang et al., 2011; Tischer et al., 2020). Table 1 shows the pre- and post-stemflow SWC (0 min and 510 min), the maximum SWC peak and the time elapsed until its occurrence for each of the TDR probes.

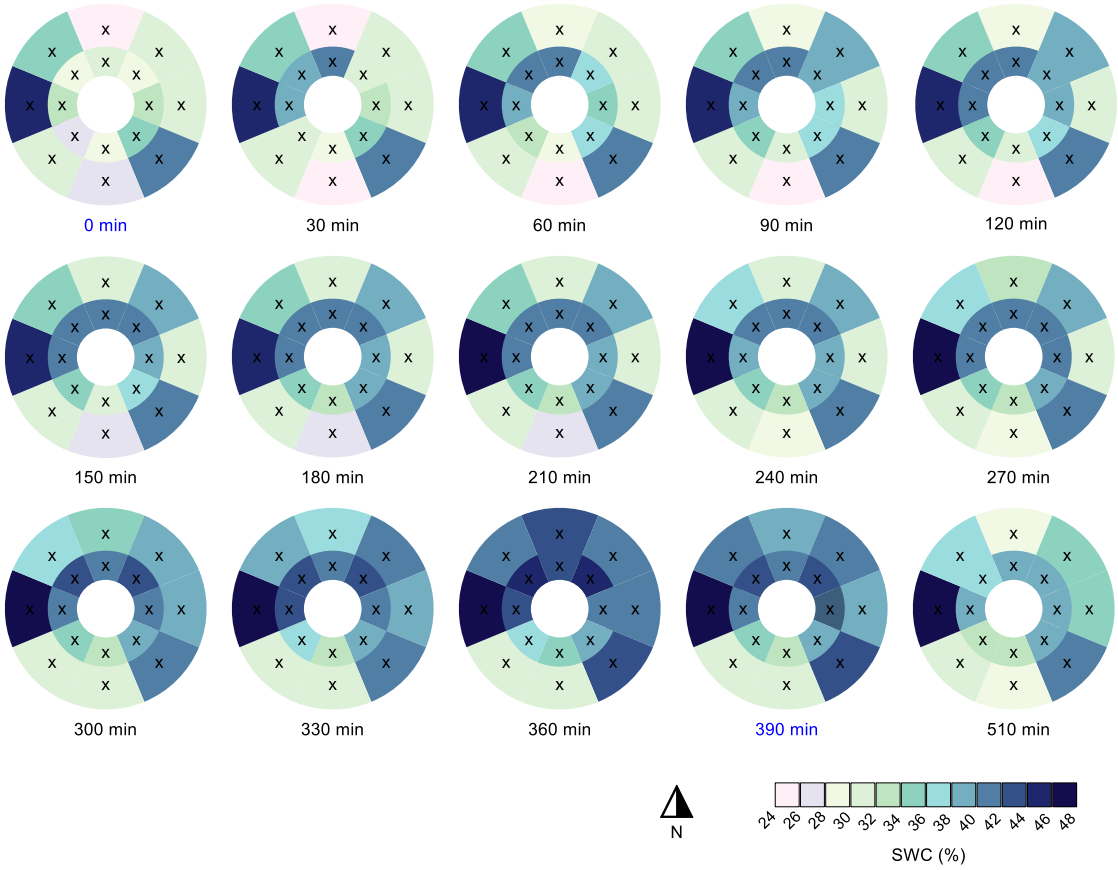

Figure 5. Time series of spatial patterns of volumetric soil water content (SWC) during the experiment. Artificial stemflow was initiated at t = 0 min and stopped after around t = 390 min (highlighted in blue). Cross marks denote TDR sensors (approximate location) and the white circle represents the tree trunk.

Table 1. Soil water content measured with TDR probes in different directions around the tree trunk. Pre-stemflow corresponds to t = 0 min and post-stemflow to t = 510 min. Peak SWC is the maximum during the experiment.

Distance/cardinal direction	TDR probe ID	Pre-stemflow SWC (%)	Post-stemflow SWC (%)	Peak SWC (%)	Maximum difference in SWC (%)	Time until peak in SWC (min)
10 cm distance						
north	swc-N10	32	38	42	11	361
northeast	swc-NE10	29	39	45	16	363
east	swc-E10	33	38	41	9	367
southeast	swc-SE10	35	39	40	5	362
south	swc-S10	29	33	34	5	363
southwest	swc-SW10	28	34	37	9	366
west	swc-W10	33	39	44	11	362
northwest	swc-NW10	29	38	44	15	360
30 cm distance						
north	swc-N30	24	30	43	19	363
northeast	swc-NE30	31	35	42	11	366
east	swc-E30	31	34	41	10	365
southeast	swc-SE30	41	42	42	†	†
south	swc-S30	26	29	32	5	369
southwest	swc-SW30	30	31	31	†	†
west	swc-W30	46	46	46	†	†
northwest	swc-NW30	35	38	42	7	381

† Denotes no real peak was observed.

Pre-stemflow SWC showed near-saturated conditions for the southeast and west directions at 30 cm distance from the trunk (Figure 5, Figure S1, Table 1). These near-saturated conditions explain the lack of response of these TDR probes during the stemflow experiment. The other TDR sensors, however, responded to the stemflow, as shown by the increase in SWC over time (Figure 5, Figure S1). As expected, faster response was observed in the TDR probes closer to the trunk: at 10 cm rather than 30 cm (Figure S1). Nevertheless, the maximum difference in SWC (i.e., difference between the max SWC and the pre-stemflow SWC) was similar at both distances (Table 1). The post-stemflow SWC (~2 h after the end of the

experiment) showed a small decrease in soil moisture from peak values, indicating that soil water was gradually percolating to deeper soil horizons while the upper horizon remained at field capacity (Figure S1).

Figure 5 shows that stemflow water was mostly directed to the west-north-east, whereas southwest-south received less. The northeast and northwest locations at 10 cm distance showed the greatest increases in SWC (15 and 16%), while SWC in the southeast and south only increased by 5%. At 30 cm distance, SWC to the north increased by 19%, whereas TDR probes to the southwest and west showed no change in SWC (Figure 5, Figure S1, Table 1). In all those TDR probes that responded to stemflow, the maximum SWC was reached close to the end of the experiment (i.e., around 6 h after initiation of the stemflow).

Our results show that stemflow affects SWC in topsoil even at a distance of 30 cm from the trunk. This finding differs from that of Tischer et al. (2020), who suggested that topsoil water content at a distance of 20 cm from the trunk of a European beech and sycamore maple was mainly driven by throughfall rather than stemflow. On the other hand, Metzger et al. (2017) found that SWC during rainfall events was lower in the immediate vicinity of tree stems than in distal areas due to macropore flow enhancing drainage near the tree trunk. These dissimilarities may be because our study excluded the throughfall contribution and examined only and exclusively stemflow infiltration dynamics. Our study found that, in the absence of throughfall, the SWC responded similarly to stemflow at 10 and 30 cm from the trunk, indicating that lateral flow was occurring even in the shallow soil layers. We found that stemflow was preferentially funnelled belowground through coarse roots (see next section). Thus, lateral stemflow redistribution within the soil was driven by the root architecture of Scots pines, which develops both horizontal (growing in shallow soil layers) and vertical (growing down to deep soil layers) coarse roots, together with their corresponding fine roots (Figure S2).

The dynamics of SWC at different depths also revealed marked differences between the cardinal directions (Figure 6). In general, SWC is greater at depth and surface probes show a more pronounced response to stemflow. However, there may be some bypass flow inducing the faster response of deeper probes (Figure 6b, c, d). For instance, in the south profile the TDR probe at 30-40 cm reacted to the stemflow more quickly than the other probes did.

SWC heterogeneity around the tree during the stemflow experiment can be attributed to four factors: (1) preferential flow of stemflow on the trunk itself (as shown in Pinos et al., 2021), (2) preferential flow of stemflow infiltrating into the soil due to the presence of coarse roots that redistribute water flow both vertically and horizontally (Schwärzel et al., 2012), (3) the temporary presence of local perched water tables, and (4) heterogeneous soil structure (Metzger et al., 2017).

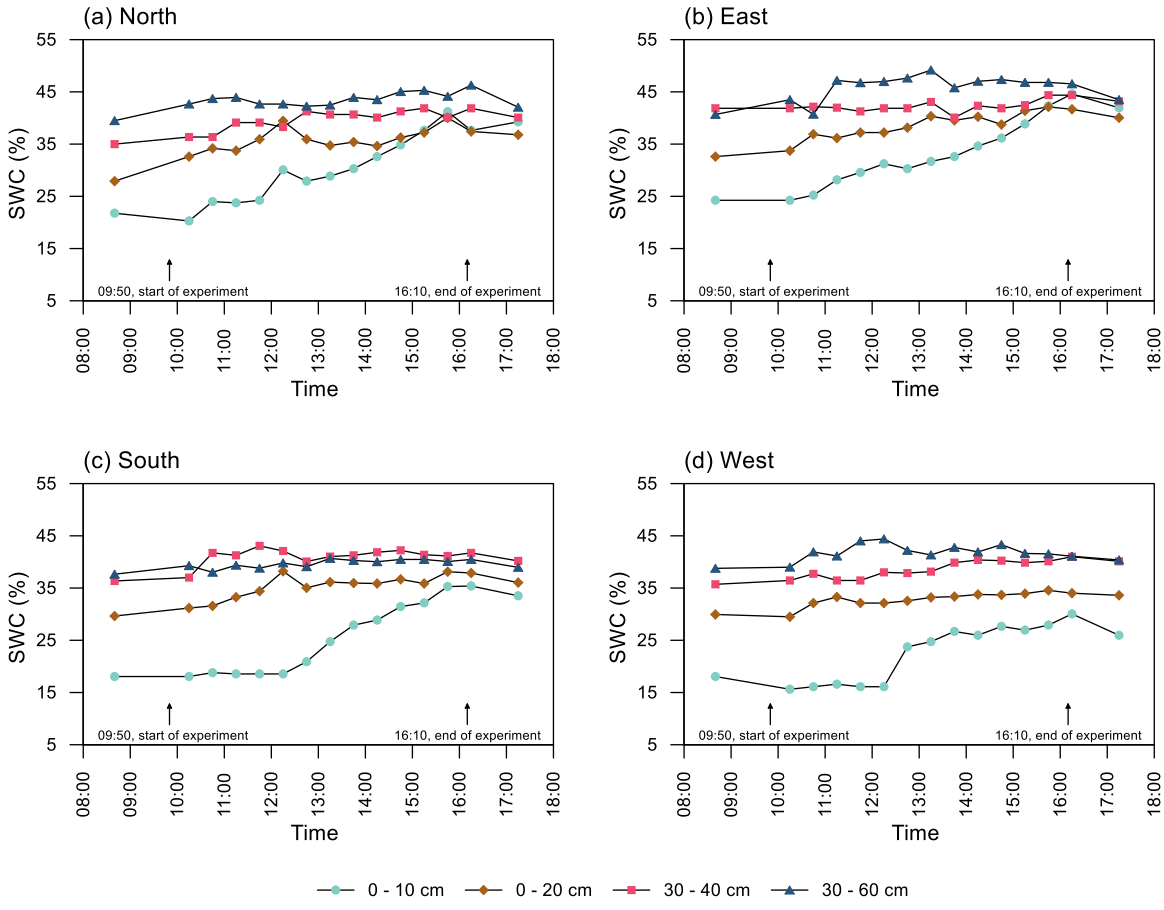

Figure 6. Temporal evolution of volumetric soil water content (SWC) in depth profiles of each cardinal direction during the stemflow experiment.

5.3.4 Water table dynamics

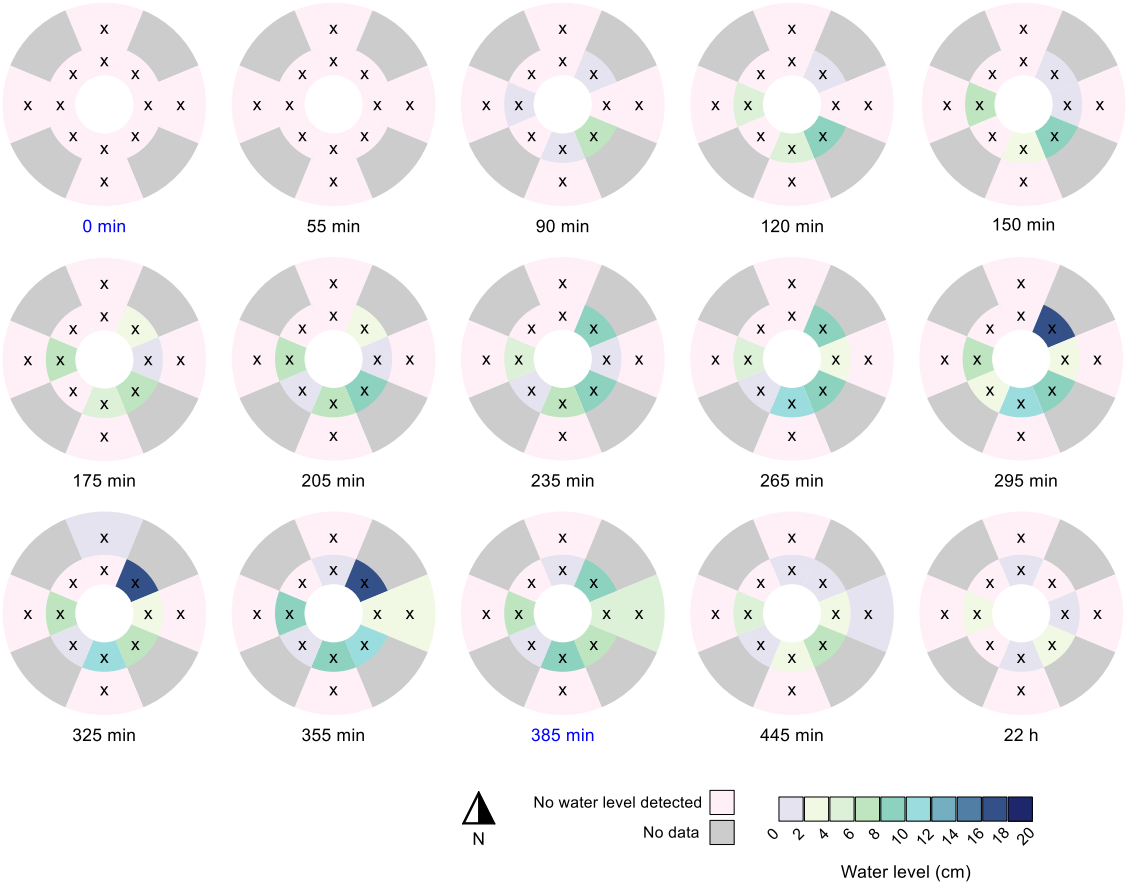

Figure 7. Time series of spatial patterns of water level in the 12 mini-piezometers during the experiment. Light pink areas indicate that no water level was detected in the 30-cm deep mini-piezometer, while grey areas indicate zones that were not monitored. Artificial stemflow was initiated at t = 0 min and stopped after around t = 385 min (highlighted in blue). Cross marks denote mini-piezometers (approximate location) and the white circle represents the tree trunk.

Water levels monitored by the mini-piezometers indicated the presence of temporary perched water tables around the tree trunk during the stemflow experiment (Figure 7). Even near-saturated locations (TDR probes swc-SE30 and swc-W30) received stemflow water, as indicated by the occurrence of blue water in nearby mini-piezometers wt-SE20 and wt-W20, respectively (Figure S3). However, no SWC response to

stemflow was observed at these locations because the soil was already saturated. Although some of the mini-piezometers were close to TDR probes, the relationship between them showed some inconsistencies. For example, no water was observed in mini-piezometer wt-NW20, located between TDR probes swc-NW10 and swc-NW30, which showed maximum SWC changes of 15% and 7%, respectively. Nor was any water found in mini-piezometer wt-N20 situated close to TDR probes swc-N10 and swc-N30, which showed maximum SWC changes of 11% and 19%, respectively (Table 1). On the contrary, increasing water levels were observed at mini-piezometer wt-S20, which was located near TDR probes swc-S10 and swc-S30, which both had a maximum SWC change of only 5%. However, simultaneous increases in water levels and SWC were observed for mini-piezometers wt-NE20 and wt-E20 (to a lesser extent) and TDR probe swc-NE10 and swc-E10, which were close to each other. Mini-piezometers wt-N50, wt-S50 and wt-W50, which were located more than 30 cm from the trunk (Figure 1), did not register any increase in water level. However, mini-piezometer wt-E50 had a minor increase in water level. Moreover, the groundwater table itself, monitored with northwest and southeast piezometers (1.7 and 2.0 m deep, respectively) at 1.6 m distance from the tree trunk, did not provide any evidence of change in groundwater levels (Figure S4). Taken together, piezometer and SWC measurements demonstrated the great temporal and spatial heterogeneity of the soil-water dynamics of stemflow infiltration.

5.3.5 Image analysis of stemflow stain patterns and preferential flow paths

Figure 8 shows the dye coverage for the soil profiles for the different cardinal directions around the tree trunk. Every cardinal direction shows the same overall trend of greater dye coverage with increasing proximity to the tree trunk. The distribution of our dye patterns differs from those observed in previous studies of trees at hillslopes (Schwärzel et al., 2012; Spencer and van Meerveld, 2016), in which dye coverage was found to be lower at the upslope than downslope profiles and a clear downward movement of the dye was seen at increasing distance from the tree. We observed the greatest dye coverage in the immediate vicinity of the tree (at 10-cm distance), which suggests that the majority of the stemflow infiltration water was directed vertically. These differences may be related to the fact that our experimental tree is located on a rather flat area with a slope close to zero.

The metrics to characterize the different dye patterns indicate the prevalence of preferential flow (Figure 8, inserts). The maximum dye coverage observed was less than 30%, highlighting that water flowed through only a small portion of the soil matrix. The metrics of uniform infiltration depth and the preferential flow

fraction indicated the absence of matrix flow (UniFr = 0 cm) and the dominance of preferential flow (PF_{fr} = 100%). The length index (LI) increased with proximity to the trunk and indicated greater irregularity in the dye patterns and hence increased preferential flow. Similarly, the peak flow metric (PI) showed irregular stained profiles. However, lower values were observed at 10 cm distance, indicating a less irregular stained pattern. The fractal dimension (D_s) of the stained patterns ranged from 1.79 to 1.96, indicating that the preferential flow pattern occurred in extensive areas (Hatano and Booltink, 1992).

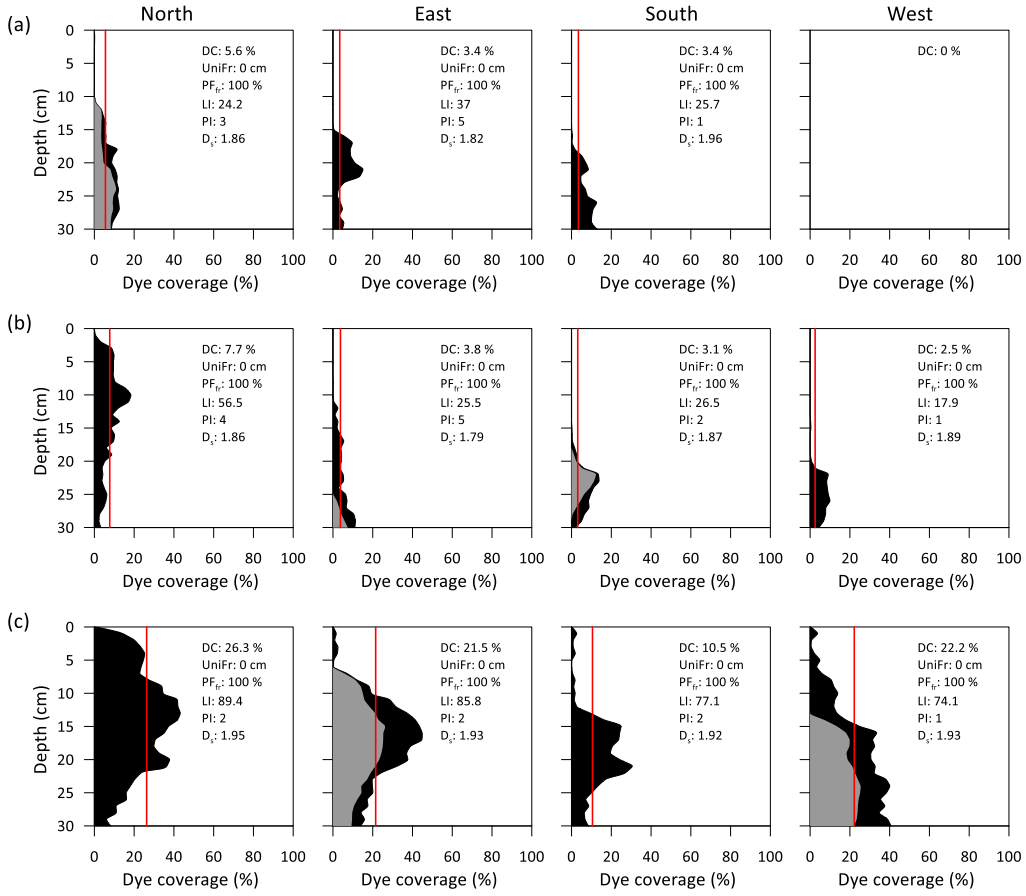

Figure 8. Dye coverage (black = soil-stained areas; grey = root-stained areas) of the different soil profiles at a distance of (a) 40 cm, (b) 25 cm and (c) 10 cm from the tree trunk. Root-stained areas refer to the area occupied by stained roots in line with the soil profile. Parameters to quantify the degree of preferential flow are shown within each graph (DC = dye coverage (%), also shown as red line; UniFr = uniform infiltration depth (cm); PF_{fr} = preferential flow fraction (%); LI = length index; PI = peak index; D_s= fractal dimension).

A substantial fraction of bypass and lateral flow occurred along the surface of coarse roots. Living roots can impede flow locally and change the flow towards soil around the root that is non-compacted and highly conductive. In some of the soil profiles, stained roots contributed larger areas to the dye patterns than stained soil (Figure 8a north, 8b south, 8c east and west). This pronounced stemflow belowground funnelling along coarse roots is shown in Figure 9. The same phenomenon was observed in several field studies using dye tracers (e.g., Liang et al., 2011; Schwärzel et al., 2012; Spencer and van Meerveld, 2016; Gonzalez-Ollauri et al., 2020; Tischer et al., 2020) and geophysical techniques (Guo et al., 2020). The dye coverage in our profiles often showed less coverage in the shallow soil layers (0-15 cm) than at greater depth (Figure 8). This indicates enhanced bypass flow in the shallow soil layers and increasing dye-matrix interaction in deeper layers. Increased dye-matrix interaction occurs when macropore channels become discontinuous and roots branch out more. This aspect was described by Van Stiphout (1987) as "Internal Catchment". Moreover, the soil matrix between macropores must be saturated before water can flow to the next macropore. Although few small stones were found during the excavation, these may influence preferential flow. We observed that some macropores were intersected by stones and extended dye coverage was found around these stones.

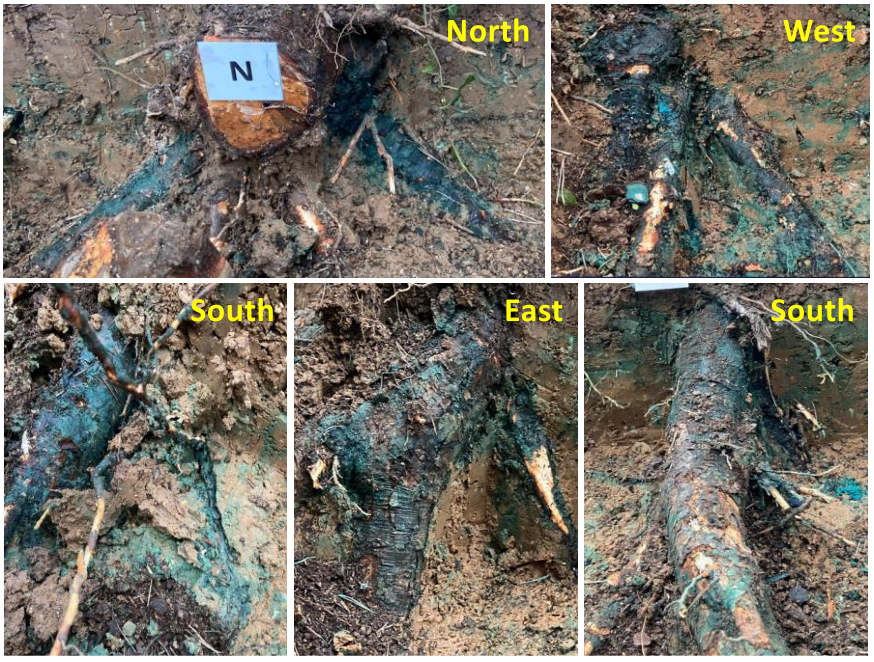

Figure 9. Examples of stained roots observed during excavation of the soil profiles around the tree trunk, illustrating the preferential belowground funnelling of stemflow along coarse roots.

It should be noted that stemflow belowground funnelling could behave differently with other tree species and their associated root-soil systems. For example, Luo et al. (2019) found with dual-tracer experiments that the degree of preferential flow was greater in coniferous than deciduous forest soil and that roots enhanced preferential flow, showing the important role of tree species and forest composition on preferential flows in forest ecosystems.

5.3.6 Dye and deuterium concentrations in soil samples

As expected, the concentrations of both tracers in the preferential flow paths (i.e., the stained areas) were significantly higher than in the surrounding soil matrix (i.e., the non-stained areas). In general, the concentrations of Brilliant Blue FCF and of the deuterium isotopic composition in the soil samples decreased with distance from the tree (R^2 = 0.49 for both tracers; Figure 10). Moreover, the maximum concentrations of both tracers in the different consecutive profiles also decreased with increasing distance from the trunk (Table S1). The Brilliant Blue FCF concentrations and deuterium isotopic compositions ranged from 0 to 473 mg kg^{-1} soil and from −56.5‰ to 277.1‰, respectively. For both tracers, the concentrations found in soil were considerably smaller than the original concentration of the labelled stemflow water, with the maximum measured in soil samples representing 9.5% and 55.4% of their original concentrations for Brilliant Blue FCF and deuterium, respectively. This can be explained by (1) sorption of Brilliant Blue FCF on the trunk bark and soil surfaces and (2) dilution of the stemflow water by residual soil water.

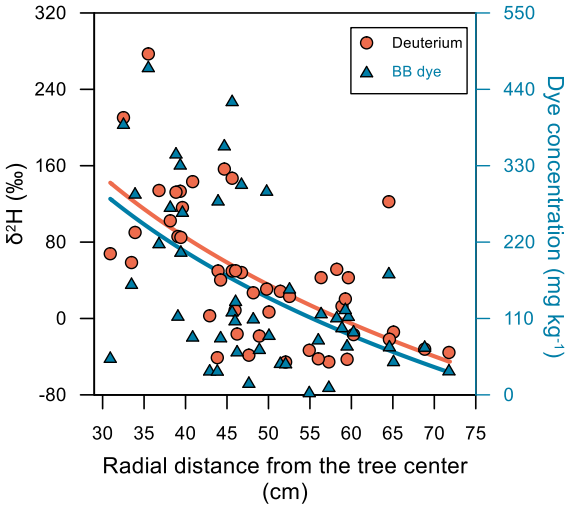

Figure 10. Relationships between travel distance (three-dimensional coordinate system) with deuterium isotopic composition and Brilliant Blue FCF dye concentration for the 63 soil samples. Solid lines indicate logarithmic fits.

Both tracers correlated significantly ($p < 0.01$; $R^2 = 0.78$; Figure S5): there was no evidence that deuterium moved deeper or farther through the soil than the dye tracer. This suggests that the two tracers could be used indifferently to delineate preferential flow pathways. It is known that Brilliant Blue FCF sorbs to soil surfaces and is therefore retarded to some extent (Flury & Flühler, 1995), but the close correlation of Brilliant Blue FCF with deuterium in our study shows that the stemflow water was mainly moving along preferential flow pathways with minimal interactions with adsorbing surfaces.

The water samples taken from the mini-piezometer revealed that the temporary perched water tables have a similar Brilliant Blue FCF concentration as the original stemflow water of ~5 g L^{-1} (Table S2). This corroborates the prevalence of preferential flow of the stemflow water once it infiltrates into the soil. However, deeper groundwater (> 1 m depth) did not show the presence of dye or deuterium enrichment, indicating that stemflow water did not penetrate deep into the subsoil.

5.4 Conclusions

Stemflow infiltration occurred in an annulus-shaped area in the vicinity of the trunk and was characterized by high spatio-temporal variability. In some locations, perched water tables developed at shallow depths. Dye patterns and isotopic composition demonstrated qualitatively and quantitatively the dominance of preferential flow in the soil. The double-funnelling phenomenon was clearly shown by the infiltration of stemflow into the soil along the surface of coarse roots and macropore channels. The root architecture was the main driver for stemflow water redistribution both horizontally and vertically in the soil matrix, followed by bypass flow along the macropore network.

The dual tracer approach (Brilliant Blue FCF dye and deuterium) together with *in situ* sensing of soil moisture delineates and quantifies stemflow belowground funnelling very well. Brilliant Blue FCF is an excellent dye tracer to stain and measure preferential flow pathways. The concentration (5 g L^{-1}) used ensured correctly that mobility would not be limited (despite its possible sorption by trunk bark and soil surfaces) by the local conditions of the present study (i.e., rough bark and silt loam soils). On the other hand, deuterium is a conservative tracer, but the preferential flow paths can be identified with extensive soil sampling and analyses.

We can infer from our dye tracing analysis of a single tree that stemflow double funnelling is a dominant hydrological feature in Mediterranean forest catchments. Stemflow infiltration can also contribute to the groundwater recharge by bypass flow, although we did not directly observe this phenomenon in our study. Although our approach allowed us to investigate the isolated effect of stemflow on infiltration and soil moisture, we must highlight that other dynamics can be expected when the effect of throughfall is not excluded (as it was in our study), leading probably to a more homogeneous distribution of SWC around the trunk. Further studies are needed to replicate our approach with more trees and species with different root architecture and under different prior soil moisture conditions. Simultaneous throughfall tracing (using additional tracers) should also be included. In addition, the belowground transport and fate of solutes (e.g., pollutants) contained in stemflow water is a related hot topic that also requires future research.

5.5 References

Bargués Tobella, A., Reese, H., Almaw, A., Bayala, J., Malmer, A., Laudon, H., and Ilstedt, U.: The effect of trees on preferential flow and soil infiltrability in an agroforestry parkland in semiarid Burkina Faso, Water Resources Research, 50, 3342-3354, https://doi.org/10.1002/2013WR015197, 2014.

Carlyle-Moses, D. E., Iida, S., Germer, S., Llorens, P., Michalzik, B., Nanko, K., Tischer, A., and Levia, D. F.: Expressing stemflow commensurate with its ecohydrological importance, Advances in Water Resources, 121, 472-479, https://doi.org/10.1016/j.advwatres.2018.08.015, 2018.

Carlyle-Moses, D. E., Iida, S., Germer, S., Llorens, P., Michalzik, B., Nanko, K., Tanaka, T., Tischer, A., and Levia, D. F.: Commentary: What we know about stemflow's infiltration area, Frontiers in Forests and Global Change, 3, 577247, https://doi.org/10.3389/ffgc.2020.577247, 2020.

Cayuela, C., Llorens, P., Sánchez-Costa, E., Levia, D. F., and Latron, J.: Effect of biotic and abiotic factors on inter-and intra-event variability in stemflow rates in oak and pine stands in a Mediterranean mountain area, Journal of Hydrology, 560, 396-406, https://doi.org/10.1016/j.jhydrol.2018.03.050, 2018.

Di Prima, S., Giannini, V., Roder, L. R., Giadrossich, F., Lassabatere, L., Stewart, R. D., Abou Najm, M. R., Longo, V., Campus, S., Winiarski, T., Angulo-Jaramillo, R., del Campo, A., Capello, G., Biddoccu, M., Roggero P. P., and Pirastru, M.: Coupling time-lapse ground penetrating radar surveys and infiltration experiments to characterize two types of non-uniform flow, Science of the Total Environment, 806, 150410, https://doi.org/10.1016/j.scitotenv.2021.150410, 2022.

Faé, G. S., Montes, F., Bazilevskaya, E., Añó, R. M., and Kemanian, A. R.: Making soil particle size analysis by laser diffraction compatible with standard soil texture determination methods, Soil Science Society of America Journal, 83, 1244-1252, https://doi.org/10.2136/sssaj2018.10.0385, 2019.

Fan, B., Liu, X., Zhu, Q., Qin, G., Li, J., Lin, H., and Guo, L.: Exploring the interplay between infiltration dynamics and Critical Zone structures with multiscale geophysical imaging: A review, Geoderma, 374, 114431, https://doi.org/10.1016/j.geoderma.2020.114431, 2020.

Flury, M. and Flühler, H.: Tracer characteristics of brilliant blue FCF, Soil Science Society of America Journal, 59, 22-27, https://doi.org/10.2136/sssaj1995.03615995005900010003x, 1995.

Flury, M. and Wai, N. N.: Dyes as tracers for vadose zone hydrology, Rev. Geophys., 41, 1002, https://doi.org/10.1029/2001RG000109, 2003.

Flury, M., Flühler, H., Jury, W. A., and Leuenberger, J.: Susceptibility of soils to preferential flow of water: A field study, Water Resources Research, 30, 1945-1954, https://doi.org/10.1029/94WR00871, 1994.

Forrer, I., Papritz, A., Kasteel, R., Flühler, H., and Luca, D.: Quantifying dye tracers in soil profiles by image processing, European Journal of Soil Science, 51, 313-322, https://doi.org/10.1046/j.1365-2389.2000.00315.x, 2000.

German-Heins, J. and Flury, M.: Sorption of Brilliant Blue FCF in soils as affected by pH and ionic strength, Geoderma, 97, 87-101, https://doi.org/10.1016/S0016-7061(00)00027-6, 2000.

Ghodrati, M. and Jury, W. A.: A field study using dyes to characterize preferential flow of water, Soil Science Society of America Journal, 54, 1558-1563, https://doi.org/10.2136/sssaj1990.03615995005400060008x, 1990.

Gonzalez-Ollauri, A., Stokes, A., and Mickovski, S. B.: A novel framework to study the effect of tree architectural traits on stemflow yield and its consequences for soil-water dynamics, Journal of Hydrology, 582, 124448, https://doi.org/10.1016/j.jhydrol.2019.124448, 2020.

Guo, L., Mount, G. J., Hudson, S., Lin, H., and Levia, D.: Pairing geophysical techniques improves understanding of the near-surface Critical Zone: Visualization of preferential routing of stemflow along coarse roots, Geoderma, 357, 113953, https://doi.org/10.1016/j.geoderma.2019.113953, 2020.

Hao, X., Ball, B. C., Culley, J. L. B., Carter, M. R., and Parkin, G. W.: Soil density and porosity, in: Soil Sampling and Methods of Analysis, Earth Sciences, Environment & Agriculture, edited by: Carter, M. R. and Gregorich, E. G., CRC Press, Boca Raton, FL, USA, 743-759, https://doi.org/10.1201/9781420005271, 2007.

Hatano, R. and Booltink, H. W. G.: Using fractal dimensions of stained flow patterns in a clay soil to predict bypass flow, Journal of Hydrology, 135, 121-131, https://doi.org/10.1016/0022-1694(92)90084-9, 1992.

Hatano, R., Kawamura, N., Ikeda, J., and Sakuma, T.: Evaluation of the effect of morphological features of flow paths on solute transport by using fractal dimensions of methylene blue staining pattern, Geoderma, 53, 31-44, https://doi.org/10.1016/0016-7061(92)90019-4, 1992.

Hildebrandt, A.: Root-Water Relations and Interactions in Mixed Forest Settings, in: Forest-Water Interactions, Ecological Studies (Analysis and Synthesis), edited by: Levia, D. F., Carlyle-Moses, D. E.,

Iida, S., Michalzik, B., Nanko, K., and Tischer, A., Springer, Cham, Zug, Switzerland, 319-348, https://doi.org/10.1007/978-3-030-26086-6_14, 2020.

Iovino, M., Pekárová, P., Hallett, P. D., Pekár, J., Lichner, Ľ., Mataix-Solera, J., Alagna, V., Walsh, R., Raffan, A., Schacht, K., and Rodný, M.: Extent and persistence of soil water repellency induced by pines in different geographic regions, Journal of Hydrology and Hydromechanics, 66, 360-368, https://doi.org/10.2478/johh-2018-0024, 2018.

Johnson, M. S. and Lehmann, J.: Double-funneling of trees: stemflow and root-induced preferential flow, Écoscience, 13, 324-333, https://doi.org/10.2980/i1195-6860-13-3-324.1, 2006.

Kendall, C. and McDonnell, J. J. (Eds.): Isotope Tracers in Catchment Hydrology, Elsevier, Amsterdam, Netherlands, 1998.

Ketelsen, H. and Meyer-Windel, S.: Adsorption of brilliant blue FCF by soils, Geoderma, 90, 131-145, https://doi.org/10.1016/S0016-7061(98)00119-0, 1999.

Levia, D. F. and Frost, E. E.: A review and evaluation of stemflow literature in the hydrologic and biogeochemical cycles of forested and agricultural ecosystems, Journal of Hydrology, 274, 1-29, https://doi.org/10.1016/S0022-1694(02)00399-2, 2003.

Levia, D. F. and Germer, S.: A review of stemflow generation dynamics and stemflow-environment interactions in forests and shrublands, Reviews of Geophysics, 53, 673-714, https://doi.org/10.1002/2015RG000479, 2015.

Levia, D. F., Carlyle-Moses, D., and Tanaka, T. (Eds.): Forest Hydrology and Biogeochemistry: Synthesis of Past Research and Future Directions, Springer, Dordrecht, Netherlands, https://doi.org/10.1007/978-94-007-1363-5, 2011.

Liang, W. L., Kosugi, K. I., and Mizuyama, T.: Soil water dynamics around a tree on a hillslope with or without rainwater supplied by stemflow, Water Resources Research, 47, W02541, https://doi.org/10.1029/2010WR009856, 2011.

Llorens, P. and Domingo, F.: Rainfall partitioning by vegetation under Mediterranean conditions. A review of studies in Europe, Journal of Hydrology, 335, 37-54, https://doi.org/10.1016/j.jhydrol.2006.10.032, 2007.

Llorens, P., Gallart, F., Cayuela, C., Roig-Planasdemunt, M., Casellas, E., Molina, A. J., Moreno-de las Heras, M., Bertran, G., Sánchez-Costa, E., and Latron, J.: What have we learnt about Mediterranean catchment hydrology? 30 years observing hydrological processes in the Vallcebre research catchments, Geogr. Res. Lett., 44, 475-501, https://doi.org/10.18172/cig.3432, 2018.

Llorens, P., Latron, J., Carlyle-Moses, D. E., Näthe, K., Chang, J. L., Nanko, K., Iida, S., and Levia, D. F.: Stemflow infiltration areas into forest soils around American beech (Fagus grandifolia Ehrh.) trees, Ecohydrology, 15, e2369, https://doi.org/10.1002/eco.2369, 2022.

Luo, Z., Niu, J., Zhang, L., Chen, X., Zhang, W., Xie, B., Du, J., Zhu, Z., Wu, S., and Li, X.: Roots-enhanced preferential flows in deciduous and coniferous forest soils revealed by dual-tracer experiments, Journal of Environmental Quality, 48, 136-146, https://doi.org/10.2134/jeq2018.03.0091, 2019.

Metzger, J. C., Wutzler, T., Dalla Valle, N., Filipzik, J., Grauer, C., Lehmann, R., Roggenbuck, M., Schelhorn, D., Weckmüller, J., Küsel, K., Totsche, K. U., Trumbore, S., and Hildebrandt, A.: Vegetation impacts soil water content patterns by shaping canopy water fluxes and soil properties, Hydrological Processes, 31, 3783-3795, https://doi.org/10.1002/hyp.11274, 2017.

Molina, A. J., Llorens, P., Garcia-Estringana, P., de Las Heras, M. M., Cayuela, C., Gallart, F., and Latron, J.: Contributions of throughfall, forest and soil characteristics to near-surface soil water-content variability at the plot scale in a mountainous Mediterranean area, Science of the Total Environment, 647, 1421-1432, https://doi.org/10.1016/j.scitotenv.2018.08.020, 2019.

Pinos, J., Latron, J., Levia, D. F., and Llorens, P.: Drivers of the circumferential variation of stemflow inputs on the boles of Pinus sylvestris L. (Scots pine), Ecohydrology, 14, e2348, https://doi.org/10.1002/eco.2348, 2021.

Poyatos, R., Latron, J., and Llorens, P.: Land use and land cover change after agricultural abandonment, Mountain Research and Development, 23, 362-368, https://doi.org/10.1659/0276-4741(2003)023[0362:LUALCC]2.0.CO;2, 2003.

Rubio, C. M., Llorens, P., and Gallart, F.: Uncertainty and efficiency of pedotransfer functions for estimating water retention characteristics of soils, European Journal of Soil Science, 59, 339-347, https://doi.org/10.1111/j.1365-2389.2007.01002.x, 2008.

Schwärzel, K., Ebermann, S., and Schalling, N.: Evidence of double-funneling effect of beech trees by visualization of flow pathways using dye tracer, Journal of Hydrology, 470, 184-192, https://doi.org/10.1016/j.jhydrol.2012.08.048, 2012.

Spencer, S. A. and van Meerveld, H. V.: Double funnelling in a mature coastal British Columbia forest: spatial patterns of stemflow after infiltration, Hydrological Processes, 30, 4185-4201, https://doi.org/10.1002/hyp.10936, 2016.

Sprenger, M., Llorens, P., Cayuela, C., Gallart, F., and Latron, J.: Mechanisms of consistently disjunct soil water pools over (pore) space and time, Hydrology and Earth System Sciences, 23, 2751-2762, https://doi.org/10.5194/hess-23-2751-2019, 2019.

Tischer, A., Michalzik, B., and Lotze, R.: Nonuniform but highly preferential stemflow routing along bark surfaces and actual smaller infiltration areas than previously assumed: A case study on European beech (Fagus sylvatica L.) and sycamore maple (Acer pseudoplatanus L.), Ecohydrology, 13, e2230, https://doi.org/10.1002/eco.2230, 2020.

Van Schaik, N. L. M. B.: Spatial variability of infiltration patterns related to site characteristics in a semi-arid watershed, Catena, 78, 36-47, https://doi.org/10.1016/j.catena.2009.02.017, 2009.

Van Stan, J. T., Gutmann, E., and Friesen, J. (Eds.): Precipitation Partitioning by Vegetation: A Global Synthesis, Springer, Cham, Switzerland, https://doi.org/10.1007/978-3-030-29702-2, 2020.

Van Stan, J. T., Ponette-González, A. G., Swanson, T., and Weathers, K. C.: Throughfall and stemflow are major hydrologic highways for particulate traffic through tree canopies, Frontiers in Ecology and the Environment, 19, 404-410, https://doi.org/10.1002/fee.2360, 2021.

Van Stiphout, T. P. J., Van Lanen, H. A. J., Boersma, O. H., and Bouma, J.: The effect of bypass flow and internal catchment of rain on the water regime in a clay loam grassland soil, Journal of Hydrology, 95, 1-11. https://doi.org/10.1016/0022-1694(87)90111-9, 1987.

Wang, X., Wang, J., and Zhang, J.: Comparisons of three methods for organic and inorganic carbon in calcareous soils of northwestern China, PLOS ONE, 7, e44334, https://doi.org/10.1371/journal.pone.0044334, 2012.

Weiler, M. and Flühler, H.: Inferring flow types from dye patterns in macroporous soils, Geoderma, 120, 137-153, https://doi.org/10.1016/j.geoderma.2003.08.014, 2004.

Yue, K., De Frenne, P., Fornara, D. A., Van Meerbeek, K., Li, W., Peng, X., Ni, X., Peng, Y., Wu, F., Yang, Y., and Peñuelas, J.: Global patterns and drivers of rainfall partitioning by trees and shrubs, Global Change Biology, 27, 3350-3357, https://doi.org/10.1111/gcb.15644, 2021.

Zhang, Y. and Schaap, M. G.: Weighted recalibration of the Rosetta pedotransfer model with improved estimates of hydraulic parameter distributions and summary statistics (Rosetta3), Journal of Hydrology, 547, 39-53, https://doi.org/10.1016/j.jhydrol.2017.01.004, 2017.

Zhang, Y., Wang, X., Pan, Y., Hu, R., and Chen, N.: Global quantitative synthesis of effects of biotic and abiotic factors on stemflow production in woody ecosystems, Global Ecology and Biogeography, 30, 1713-1723, https://doi.org/10.1111/geb.13322, 2021.

Zisa, R. P., Halverson, H. G., and Stout, B. B.: Establishment and early growth of conifers on compact soils in urban areas, U.S. Department of Agriculture, Forest Service, Northeastern Forest Experiment Station, Broomall, PA, USA, Res. Pap. NE-451, 8 pp., 1980.

CHAPTER 6

GENERAL DISCUSSION AND CONCLUSIONS

6.1 General discussion

Climate change projections for the Mediterranean region indicated a pronounced decrease in precipitation and increase of temperatures, but also shown an increase in the frequency and intensity of temperature and precipitation extremes (Ali et al., 2022). Such changes together with the anthropogenic disturbances over forested catchments will likely impact hydrological processes (Tague et al., 2019), such as canopy rainfall partitioning in terms of evapotranspiration and rainfall interception and redistribution with effects on local- and catchment-scale water balances (Llorens and Domingo, 2007). The expected increase of the intensity and possibly event size of less frequent precipitation will increase the volume of throughfall and stemflow delivered to the ground, playing an important role for soil water replenishment in these regions. Thus, determining the patterns and drivers of canopy rainfall partitioning by trees in Mediterranean conditions is one important step to improve our understanding at stand scale which will serve as input to develop catchment-scale models, vital for improving hydrological, land surface, and dynamic vegetation model predictions of water, nutrient, and carbon cycles under global climate change scenarios (Gutmann, 2020). The results obtained in this thesis allow to provide novel pieces of knowledge on the dynamics of rainfall partitioning fluxes and their implications in Mediterranean mountain forests.

6.1.1 Interception processes by means of stable water isotopes

In the last decades, the use of stable water isotopes in forest hydrology has led to a better conceptualization of the different phases of the spatiotemporal movement of water in the forested catchment (Dawson and Simonin, 2011; Sprenger et al., 2016). Overall, most of the studies are focused on throughfall because it is the major input of water into the soils, whereas stemflow have been much less studied (e.g., Gautam et al., 2017; Stockinger et al., 2017). However, there still some lack of understanding and uncertainties concerning to the isotopic fractionation processes that affect rainfall, individually or combined, when passing through the canopy (Allen et al., 2017). This is an important issue in isotope-based hydrology studies because the isotopic composition of throughfall and stemflow should be use instead of that of rainfall as the water input signal into a catchment with ample forest cover. This would facilitate the proper modeling of transport and fate of water at the plot or catchment scale and avoid errors and biases in the interpretation of results (Klaus and McDonnell, 2013).

In our study area, one of our key findings was that the enrichment in the throughfall isotopic composition during the onset of the rainfall events was related to the greater contribution of splash throughfall and vapour pressure deficit during the same stage. This enrichment pattern is attributed to the splash droplet evaporation theory introduced by Murakami (2006). During the rainfall interception, raindrops hit the canopy surfaces, and depending on the kinetic energy they can splash, and numerous small droplets can be produced. Evaporation occurs on the small droplet surfaces during their fall towards the ground in air and also in the intercepted drops that are temporarily retained in the canopy surface. A recent study by Murakami (2021) has provided evidence to support the splash droplet evaporation hypothesis. Therefore, it is inferred that this evaporation process causes the isotopic enrichment of throughfall. Our study is the first of its kind to evaluate the interrelationship of throughfall isotopic composition and drop size distribution.

In the same line, our study evaluates at high temporal resolution the intra-storm isotopic composition of stemflow and throughfall. For stemflow, we designed a novel approach in order to capture stemflow water samples at high resolution with sequential collectors. Results showed that the isotopic shift of stemflow and throughfall in relation to open rainfall occurred in both directions, although stemflow was consistently more enriched than throughfall which is in accordance with the existent literature in the field (Allen et al., 2017). We have also found some indications of seasonal isotopic differences where throughfall was more depleted during the higher air temperature season whereas stemflow was more enriched. We suggested that evaporation is the leading factor of fractionation of both fluxes, however, there is no single mechanism but a combination of factors (canopy selection, mixing of water, etc) that occur simultaneously during one event. This have been also concluded by other few studies in the field (Cayuela et al., 2018; Zhang et al., 2019).

Future research should be focus on the application of a denser monitoring network of throughfall drop sizes distribution measurements and throughfall isotopic composition sampling to assess spatiotemporal differences and likely correlations with tree traits in different species (e.g., canopy cover, number of branches, leafed and leafless phenophase). The design our approach to monitoring and sampling stemflow at high temporal resolution (based on volume of stemflow) could also be improved in order to capture all the isotopic variability of rainfall and throughfall and stemflow at synchronized time intervals.

6.1.2 Preferential flow paths of the stemflow

Research on stemflow during the last decades has provided relevant information and improved the current understanding of hydrological, biogeochemical, and ecological processes that stemflow can influence (Levia and Germer, 2015). It has also revealed the importance of stemflow was most often underestimated (Germer et al., 2010). Stemflow is a concentrated water flux that reach the forest floor around the stem base, with interactions occurring in both temporal "hot moments" and spatial "hot spots" (McClain et al., 2003). Stemflow commonly represent ~2% of gross rainfall, however, there are cases that reported stemflow exceedingly more than 30% (e.g., Slatyer 1965; Nulsen et al., 1986; Xu et al., 2005; Safeeq and Fares, 2014). Stemflow is able to influence various processes such as soil water replenishment (Liang, 2020), overland flow (Herwitz, 1986), soil erosion (Dunkerley, 2020), preferential flow paths in the vadose zone (Johnson and Lehmann, 2006), groundwater recharge (Taniguchi et al., 1996), biogeochemical cycles (macro and microelements; Tobón et al., 2004), transport atmospheric pollutants (Cayuela et al., 2019; Saidin et al., 2022) and tree water uptake (Aubrey, 2020).

In this work, we contributed new insights on stemflow dynamics by applying novel methodologies. First, we quantitatively and qualitatively evaluated for the first time the stemflow distribution around the stem of trees. In our monitored Scots pine trees, we found that stemflow followed preferential trajectories during its travel in the stems towards the ground, mainly controlled by the morphological characteristics of the trees. Thus, we corroborated the hypothesis of a non-uniform stemflow distribution on the boles of trees which was also observed in other studies by using dye tracers as in Imamura et al. (2017) or Tischer et al. (2020). Once infiltrated into the soil stemflow flow paths are hard to discern. Some studies have suggested that stemflow is preferential funneled belowground by coarse roots. We evaluated this phenomenon by carrying out an experiment under controlled conditions using artificial tracers. We found that stemflow, indeed followed preferential flow paths through coarse roots and macropores, that help to reach deeper soil layers. But also, we observed that stemflow was redistributed in the shallow soil layers, which is an effect of the root system architecture, as also shown by Nulsen et al. (1986) and Liang et al. (2011) that denote that stemflow can play an important role in controlling the soil moisture dynamics in the near-stem soil.

Overall, the analysis of stemflow in this dissertation provides a novel piece of knowledge on the rainfall partitioning in Mediterranean ecosystems. Future research should focus on stemflow infiltration patterns

within the soil after determining non-uniform or uniform stemflow distribution on the tree boles in different tree species. Studies integrating stemflow water isotopic signature to discern preferential plant water uptake are also needed, as tree water uptake is usually studied by comparing soil water isotopic composition vs. xylem isotopic composition, even if soil water isotopic composition could differ from that of stemflow, which is funneled belowground and redistributed in the root system space and also becomes available water for the tree.

6.2 General conclusions

The studies included in this dissertation guided us to the following conclusions.

Chapter 2

- Throughfall partition of a Scots pine consisted of average of 65% canopy drip, 19% free throughfall and 16% splash throughfall.
- Throughfall during low-intensity events gave higher canopy drip percentages and lower free throughfall than events with high intensities.
- The isotopic shift between throughfall and rainfall showed no direct relationship with meteorological variables, throughfall and rainfall amount, number of drops, drop velocities, or raindrop kinetic energy.
- The isotopic shift (enrichment) was higher at the beginning of events, when there is major contribution of splash throughfall and highest vapour pressure deficit, which implies that splash droplet evaporation occurred.

Chapter 3

- Isotopic shifts between rainfall and throughfall or stemflow can occur in both directions (enrichment or depletion).
- Stemflow was consistently more enriched than throughfall.
- Throughfall was more depleted during the spring-summer season, with higher air temperatures, whereas stemflow was more enriched.
- The isotopic shift did not show any direct relationship with either meteorological variables or the amount effect.
- Evaporation led to stemflow enrichment due to its longer residence time in the tree.

- Evaporation seems to have more influence at the initial stage of the events whereas canopy selection processes during the final stage. However, several fractionation processes can occur during the same event.

Chapter 4

- Marked individual differences in stemflow production among sections of two Scots pine trees were found. Differences were strongly related to the total tree stemflow production and bulk rainfall.
- Percentages of stemflow contribution for each section were globally stable for events above a stemflow volume threshold. For events below this threshold, a much higher variability was observed.
- Data suggest that biotic factors (trunk lean, bark morphology and tree neighbourhood) have a greater influence on stemflow distribution on tree stems than abiotic factors (rainfall intensity peaks).
- Non-uniform stemflow (or preferential stemflow flow paths) on the bole of trees has potentially strong implications in ecohydrology.

Chapter 5

- Stemflow infiltration occurred in a small annulus-shaped area in the vicinity of the trunk, and its belowground distribution introduced high spatio-temporal soil moisture variability.
- Dye coverage and the concentrations of Brilliant Blue FCF and of the deuterium isotopic composition in the soil samples decreased with travel distance from the tree.
- Bypass and lateral flow occurred along the surface of coarse roots and macropores, evidencing the double funnelling phenomenon.
- The root architecture was the main driver for stemflow water redistribution both horizontally and vertically in the soil matrix, followed by bypass flow along the macropore network.
- Dye patterns and isotopic composition qualitatively and quantitatively demonstrate the dominance of preferential flow in the soil.
- The dual tracer approach is a powerful approach to delineate and quantify stemflow belowground funnelling.

REFERENCES

Ali, E., Cramer, W., Carnicer, J., Georgopoulou, E., Hilmi, N. J. M., Le Cozannet, G., & Lionello, P. (2022). Cross-Chapter Paper 4: Mediterranean Region. In: Climate Change 2022: Impacts, Adaptation and Vulnerability. Contribution of Working Group II to the Sixth Assessment Report of the Intergovernmental Panel on Climate Change [H.-O. Pörtner, D.C. Roberts, M. Tignor, E.S. Poloczanska, K. Mintenbeck, A. Alegría, M. Craig, S. Langsdorf, S. Löschke, V. Möller, A. Okem, B. Rama (eds)]. Cambridge University Press, Cambridge, UK and New York, NY, USA, pp. 2233-2272.

Allam, A., Moussa, R., Najem, W., & Bocquillon, C. (2020). Hydrological cycle, Mediterranean basins hydrology. In: Zribi, M., Brocca, L., Tramblay, Y., Molle, F. (eds), Water Resources in the Mediterranean Region. Elsevier. https://doi.org/10.1016/B978-0-12-818086-0.00001-7

Allen, S. T., Keim, R. F., Barnard, H. R., McDonnell, J. J., & Renée Brooks, J. (2017). The role of stable isotopes in understanding rainfall interception processes: a review. Wiley Interdisciplinary Reviews: Water, 4(1), e1187. https://doi.org/10.1002/wat2.1187

Amatya, D. M., Douglas-Mankin, K. R., Williams, T. M., Skaggs, R. W., & Nettles, J. E. (2011). Advances in forest hydrology: challenges and opportunities. Transactions of the ASABE, 54(6), 2049-2056.

Andréassian, V. (2004). Waters and forests: from historical controversy to scientific debate. Journal of Hydrology, 291(1-2), 1-27. https://doi.org/10.1016/j.jhydrol.2003.12.015

Aubrey, D. P. (2020). Relevance of precipitation partitioning to the tree water and nutrient balance. In: Van Stan, J.T., Gutmann, E., Friesen, J. (eds), Precipitation partitioning by vegetation. Springer, Cham. https://doi.org/10.1007/978-3-030-29702-2_10

Bren, L. (2016). An Introduction to Forest Hydrology. In: Amatya, D., Williams, T., Bren, L., De Jong, C. (eds), Forest Hydrology: Processes, Management and Assessment. CABI.

Burt, T. P., & McDonnell, J. J. (2015). Whither field hydrology? The need for discovery science and outrageous hydrological hypotheses. Water Resources Research, 51(8), 5919-5928. https://doi.org/10.1002/2014WR016839

Cayuela, C., Levia, D. F., Latron, J., & Llorens, P. (2019). Particulate matter fluxes in a Mediterranean mountain forest: interspecific differences between throughfall and stemflow in oak and pine stands. Journal of Geophysical Research: Atmospheres, 124(9), 5106-5116. https://doi.org/10.1029/2019JD030276

Cayuela, C., Llorens, P., Sánchez-Costa, E., & Latron, J. (2018). Modification of the isotopic composition of rainfall by throughfall and stemflow: The case of Scots pine and downy oak forests under Mediterranean conditions. Ecohydrology, 11(8), e2025. https://doi.org/10.1002/eco.2025

Correia, F. N. (1999). Water resources in the Mediterranean region. Water International, 24(1), 22-30. https://doi.org/10.1080/02508069908692130

Dawson, T.E., & Simonin, K.A. (2011). The Roles of Stable Isotopes in Forest Hydrology and Biogeochemistry. In: Levia, D., Carlyle-Moses, D., Tanaka, T. (eds), Forest Hydrology and Biogeochemistry. Ecological Studies, vol 216. Springer, Dordrecht. https://doi.org/10.1007/978-94-007-1363-5_7

Dunkerley, D. (2020). A review of the effects of throughfall and stemflow on soil properties and soil erosion. In: Van Stan, J.T., Gutmann, E., Friesen, J. (eds), Precipitation partitioning by vegetation. Springer, Cham. https://doi.org/10.1007/978-3-030-29702-2_12

Gallart, F., Llorens, P., Latron, J., & Regüés, D. (2002). Hydrological processes and their seasonal controls in a small Mediterranean mountain catchment in the Pyrenees. Hydrology and Earth System Sciences, 6(3), 527-537. https://doi.org/10.5194/hess-6-527-2002

García-Ruiz, J. M., López-Moreno, J. I., Vicente-Serrano, S. M., Lasanta-Martínez, T., & Beguería, S. (2011). Mediterranean water resources in a global change scenario. Earth-Science Reviews, 105(3-4), 121-139. https://doi.org/10.1016/j.earscirev.2011.01.006

Gautam, M. K., Lee, K. S., Bong, Y. S., Song, B. Y., & Ryu, J. S. (2017). Oxygen and hydrogen isotopic characterization of rainfall and throughfall in four South Korean cool temperate forests. Hydrological Sciences Journal, 62(12), 2025-2034. https://doi.org/10.1080/02626667.2017.1358813

Germer, S., Werther, L., & Elsenbeer, H. (2010). Have we underestimated stemflow? Lessons from an open tropical rainforest. Journal of Hydrology, 395(3-4), 169-179. https://doi.org/10.1016/j.jhydrol.2010.10.022

Goldsmith, G. R. (2013). Changing directions: the atmosphere–plant–soil continuum. New Phytologist, 199(1), 4-6. https://doi.org/10.1111/nph.12332

Gutmann, E. D. (2020). Global modeling of precipitation partitioning by vegetation and their applications. In: Van Stan, J. T, Gutmann, E., Friesen, J. (eds), Precipitation partitioning by vegetation. Springer, Cham. https://doi.org/10.1007/978-3-030-29702-2_7

Hamilton, E. L., & Rowe, P. B. (1949). Rainfall interception by chaparral in California. California Department of Natural Resources, Division of Forestry. Sacramento, CA, USA, 43 p.

Herwitz, S. R. (1986). Infiltration-excess caused by stemflow in a cyclone-prone tropical rainforest. Earth Surface Processes and Landforms, 11(4), 401-412. https://doi.org/10.1002/esp.3290110406

Horton, R. E. (1919). Rainfall interception. Monthly Weather Review, 47(9), 603-623. https://doi.org/10.1175/1520-0493(1919)47<603:RI>2.0.CO;2

Imamura, N., Levia, D. F., Toriyama, J., Kobayashi, M., & Nanko, K. (2017). Stemflow-induced spatial heterogeneity of radiocesium concentrations and stocks in the soil of a broadleaved deciduous

forest. Science of the Total Environment, 599, 1013-1021. https://doi.org/10.1016/j.scitotenv.2017.05.017

Johnson, M. S., & Lehmann, J. (2006). Double-funneling of trees: stemflow and root-induced preferential flow. Ecoscience, 13(3), 324-333. https://doi.org/10.2980/i1195-6860-13-3-324.1

Klaus, J., & McDonnell, J. J. (2013). Hydrograph separation using stable isotopes: review and evaluation. Journal of Hydrology, 505, 47-64. https://doi.org/10.1016/j.jhydrol.2013.09.006

Kofroňová, J., Šípek, V., Hnilica, J., Vlček, L., & Tesař, M. (2021). Canopy interception estimates in a Norway spruce forest and their importance for hydrological modelling. Hydrological Sciences Journal, 66(7), 1233-1247. https://doi.org/10.1080/02626667.2021.1922691

Lana-Renault, N., Morán-Tejeda, E., Morena de las Heras, M., Lorenzo-Lacruz, J., & López-Moreno, N. (2020). Land-use change and impacts. In: Zribi, M., Brocca, L., Tramblay, Y., Molle, F. (eds), Water Resources in the Mediterranean Region. Elsevier. https://doi.org/10.1016/B978-0-12-818086-0.00010-8

Latron, J., Llorens, P., & Gallart, F. (2009). The hydrology of Mediterranean mountain areas. Geography Compass, 3(6), 2045-2064. https://doi.org/10.1111/j.1749-8198.2009.00287.x

Latron, J., Soler, M., Llorens, P., & Gallart, F. (2008). Spatial and temporal variability of the hydrological response in a small Mediterranean research catchment (Vallcebre, Eastern Pyrenees). Hydrological Processes, 22(6), 775-787. https://doi.org/10.1002/hyp.6648

Levia, D. F., & Germer, S. (2015). A review of stemflow generation dynamics and stemflow-environment interactions in forests and shrublands. Reviews of Geophysics, 53(3), 673-714. https://doi.org/10.1002/2015RG000479

Levia, D.F., Keim, R.F., Carlyle-Moses, D.E., & Frost, E.E. (2011a). Throughfall and Stemflow in Wooded Ecosystems. In: Levia, D.F., Carlyle-Moses, D., Tanaka, T. (eds), Forest Hydrology and

Biogeochemistry. Ecological Studies, vol 216. Springer, Dordrecht. https://doi.org/10.1007/978-94-007-1363-5_21

Levia, D.F., Carlyle-Moses, D.E., & Tanaka, T. (2011b). Reflections on the State of Forest Hydrology and Biogeochemistry. In: Levia, D., Carlyle-Moses, D., Tanaka, T. (eds), Forest Hydrology and Biogeochemistry. Ecological Studies, vol 216. Springer, Dordrecht. https://doi.org/10.1007/978-94-007-1363-5_36

Liang, W. L. (2020). Effects of stemflow on soil water dynamics in forest stands. In: Levia, D.F., Carlyle-Moses, D.E., Iida, S., Michalzik, B., Nanko, K., & Tischer, A. (eds), Forest-Water Interactions. Springer, Cham. https://doi.org/10.1007/978-3-030-26086-6_15

Liang, W. L., Kosugi, K. I., & Mizuyama, T. (2011). Soil water dynamics around a tree on a hillslope with or without rainwater supplied by stemflow. Water Resources Research, 47(2). https://doi.org/10.1029/2010WR009856

Llorens, P., & Domingo, F. (2007). Rainfall partitioning by vegetation under Mediterranean conditions. A review of studies in Europe. Journal of Hydrology, 335(1-2), 37-54. https://doi.org/10.1016/j.jhydrol.2006.10.032

Llorens, P., Gallart, F., Cayuela, C., Roig-Planasdemunt, M., Casellas, E., Molina, A. J., Molina, A. J., Bertran, G., Sánchez-Costa, E., & Latron, J. (2018). What have we learnt about Mediterranean catchment hydrology? 30 years observing hydrological processes in the Vallcebre research catchments. Geographical Research Letters, (44), 475-502. http://doi.org/10.18172/cig.3432

McClain, M. E., Boyer, E. W., Dent, C. L., Gergel, S. E., Grimm, N. B., Groffman, P. M., Hart, S. C., Harvey, J. W., Johnston, C. A., Mayorga, E., McDowell, W. H., & Pinay, G. (2003). Biogeochemical hot spots and hot moments at the interface of terrestrial and aquatic ecosystems. Ecosystems, 301-312. http://www.jstor.org/stable/3659030

McGuire, K.J., & Likens, G.E. (2011). Historical Roots of Forest Hydrology and Biogeochemistry. In: Levia, D., Carlyle-Moses, D., Tanaka, T. (eds), Forest Hydrology and Biogeochemistry. Ecological Studies, vol 216. Springer, Dordrecht. https://doi.org/10.1007/978-94-007-1363-5_1

Moore, G., McGuire, K., Troch, P., & Barron-Gafford, G. (2015). Ecohydrology and the Critical Zone: Processes and patterns across scales. In: Giardino, J.R., Houser, C. (eds), Developments in Earth Surface Processes, vol. 19, Elsevier. https://doi.org/10.1016/B978-0-444-63369-9.00008-2

Murakami, S. (2006). A proposal for a new forest canopy interception mechanism: splash droplet evaporation. Journal of Hydrology, 319(1-4), 72-82. https://doi.org/10.1016/j.jhydrol.2005.07.002

Murakami, S. (2021). Water and energy balance of canopy interception as evidence of splash droplet evaporation hypothesis. Hydrological Sciences Journal, 66(7), 1248-1264. https://doi.org/10.1080/02626667.2021.1924378

Nanko, K., Hotta, N., & Suzuki, M. (2006). Evaluating the influence of canopy species and meteorological factors on throughfall drop size distribution. Journal of Hydrology, 329(3-4), 422-431. https://doi.org/10.1016/j.jhydrol.2006.02.036

Nulsen, R. A., Bligh, K. J., Baxter, I. N., Solin, E. J., & Imrie, D. H. (1986). The fate of rainfall in a mallee and heath vegetated catchment in southern Western Australia. Australian Journal of Ecology, 11(4), 361-371. https://doi.org/10.1111/j.1442-9993.1986.tb01406.x

Poyatos, R., Latron, J., & Llorens, P. (2003). Land use and land cover change after agricultural abandonment. Mountain Research and Development, 23(4), 362-368. https://doi.org/10.1659/0276-4741(2003)023[0362:LUALCC]2.0.CO;2

Robinson, M., & Ward, R. C. (2017). Hydrology: Principles and Processes. IWA Publishing, London, UK.

Rubio, C. M., Llorens, P., & Gallart, F. (2008). Uncertainty and efficiency of pedotransfer functions for estimating water retention characteristics of soils. European Journal of Soil Science, 59(2), 339-347. https://doi.org/10.1111/j.1365-2389.2007.01002.x

Safeeq, M., & Fares, A. (2014). Interception losses in three non-native Hawaiian forest stands. Hydrological Processes, 28(2), 237-254. https://doi.org/10.1002/hyp.9557

Saidin, Z. H., Levia, D. F., Kato, H., Kurihara, M., Hudson, J. E., Nanko, K., & Onda, Y. (2022). Vertical distribution and transport of radiocesium via branchflow and stemflow through the canopy of cedar and oak stands in the aftermath of the Fukushima Daiichi Nuclear Power Plant accident. Science of The Total Environment, 818, 151698. https://doi.org/10.1016/j.scitotenv.2021.151698

Slatyer R. O. (1965). Measurements of precipitation interception by an arid zone plant community (*Acacia aneura* F. Muell.). Proceedings of the Montpellier Symposium N. 25, Arid Zone Research – Methodology of Plant Eco-Physiology, pp. 181-92. United Nations Educational, Scientific and Cultural Organization. Paris, France.

Sprenger, M., Leistert, H., Gimbel, K., & Weiler, M. (2016). Illuminating hydrological processes at the soil-vegetation-atmosphere interface with water stable isotopes. Reviews of Geophysics, 54(3), 674-704. https://doi.org/10.1002/2015RG000515

Stockinger, M. P., Lücke, A., Vereecken, H., & Bogena, H. R. (2017). Accounting for seasonal isotopic patterns of forest canopy intercepted precipitation in streamflow modeling. Journal of Hydrology, 555, 31-40. https://doi.org/10.1016/j.jhydrol.2017.10.003

Tague, C. L., Moritz, M., & Hanan, E. (2019). The changing water cycle: The eco-hydrologic impacts of forest density reduction in Mediterranean (seasonally dry) regions. Wiley Interdisciplinary Reviews: Water, 6(4), e1350. https://doi.org/10.1002/wat2.1350

Taniguchi, M., Tsujimura, M., & Tanaka, T. (1996). Significance of stemflow in groundwater recharge. 1: Evaluation of the stemflow contribution to recharge using a mass balance approach. Hydrological Processes, 10(1), 71-80. https://doi.org/10.1002/(SICI)1099-1085(199601)10:1<71::AID-HYP301>3.0.CO;2-Q

Tischer, A., Michalzik, B., & Lotze, R. (2020). Nonuniform but highly preferential stemflow routing along bark surfaces and actual smaller infiltration areas than previously assumed: A case study on European beech (Fagus sylvatica L.) and sycamore maple (Acer pseudoplatanus L.). Ecohydrology, 13(6), e2230. https://doi.org/10.1002/eco.2230

Tobón, C., Sevink, J., & Verstraten, J. M. (2004). Solute fluxes in throughfall and stemflow in four forest ecosystems in northwest Amazonia. Biogeochemistry, 70(1), 1-25. https://doi.org/10.1023/B:BIOG.0000049334.10381.f8

Van Stan, J. T., & Friesen, J. (2020). Precipitation partitioning, or to the surface and back again: historical overview of the first process in the terrestrial hydrologic pathway. In: Van Stan, J.T., Gutmann, E., Friesen, J. (eds), Precipitation partitioning by vegetation. Springer, Cham. https://doi.org/10.1007/978-3-030-29702-2_1

Van Stan, J. T., Ponette-González, A. G., Swanson, T., & Weathers, K. C. (2021). Throughfall and stemflow are major hydrologic highways for particulate traffic through tree canopies. Frontiers in Ecology and the Environment, 19(7), 404-410. https://doi.org/10.1002/fee.2360

Xu, X., Wang, Q., & Hirata, E. (2005). Precipitation partitioning and related nutrient fluxes in a subtropical forest in Okinawa, Japan. Annals of Forest Science, 62(3), 245-252. https://doi.org/10.1051/forest:2005016

Yue, K., De Frenne, P., Fornara, D. A., Van Meerbeek, K., Li, W., Peng, X., Ni, X., Peng, Y., Wu, F., Yang, Y., & Peñuelas, J. (2021). Global patterns and drivers of rainfall partitioning by trees and shrubs. Global Change Biology, 27(14), 3350-3357. https://doi.org/10.1111/gcb.15644

Zhang, Y. F., Wang, X. P., Pan, Y. X., & Hu, R. (2019). Alteration in isotopic composition of gross rainfall as it is being partitioned into throughfall and stemflow by xerophytic shrub canopies within water-limited arid desert ecosystems. Science of The Total Environment, 692, 631-639. https://doi.org/10.1016/j.scitotenv.2019.07.294

SUPPLEMENTARY DATA

SUPPORTING INFORMATION CHAPTER 2

Table S1. Meteorological characteristics and isotopic composition of open rainfall and throughfall for the 21 events during the study period, May 2018 to July 2019.

Date	Rainfall class	Rainfall (mm)	Throughfall (mm)	Rainfall duration (h)	Max 30-min rainfall intensity (mm h^{-1})	Samples	Mean weighed rainfall $\delta^{18}O$ (‰) (mean ± SD)	Mean weighed throughfall $\delta^{18}O$ (‰) (mean ± SD)
12 May 2018	L-H	52.5	48.3	9.8	19.9	10	-4.95 ± 0.17	-4.67 ± 0.17
19 May 2018	S-L	12.5	10.7	6.6	7.8	3	-5.26 ± 0.59	-5.31 ± 0.88
28 May 2018	L-L	37.4	33.2	50.8	6.2	7	-6.18 ± 0.21	-6.08 ± 0.28
1 June 2018	L-H	26.9	20.3	9.8	25.4	5	-7.34 ± 0.72	-6.83 ± 0.47
6 June 2018	S-H	26.9	25.7	5.8	18.3	5	-8.55 ± 0.41	-8.34 ± 0.67
10 June 2018	S-L	7.8	5.4	3.0	5.9	2	-6.84 ± 3.82	-5.34 ± 1.66
23 June 2018	S-H	20.5	18.6	3.3	38.2	4	-3.67 ± 0.34	-3.51 ± 0.44
28 June 2018	L-H	34.3	33.6	9.2	21.8	7	-6.46 ± 0.28	-5.96 ± 0.32
11 July 2018	S-H	12.5	8.6	2.8	16.4	2	-6.37 ± 2.79	-6.41 ± 2.63
9 August 2018	L-H	39.4	37.6	20.6	11.7	7	-4.06 ± 0.20	-4.08 ± 0.29
12 August 2018	S-H	16.8	14.0	5.4	19.9	4	-4.76 ± 0.75	-4.71 ± 0.92
23 August 2018	S-L	6.0	3.8	3.3	8.2	2	-3.98 ± 1.01	-4.50 ± 0.81
3 September 2018	S-H	32.8	28.6	3.1	17.6	6	-4.19 ± 0.34	-4.07 ± 0.27
9 October 2018	L-L	34.3	31.1	13.2	8.6	7	-11.75 ± 0.29	-11.41 ± 0.47
2 April 2019	L-L	13.5	12.5	23.6	2.7	3	-5.98 ± 0.41	-5.60 ± 0.57
1 May 2019	L-L	27.9	23.8	43.8	5.1	6	-5.29 ± 0.37	-4.52 ± 0.34
20 May 2019	S-L	8.8	6.9	7.0	5.1	2	-6.43 ± 0.03	-6.16 ± 1.17
24 May 2019	L-L	18.7	16.9	12.7	5.1	4	-4.59 ± 0.41	-3.86 ± 0.42
11 June 2019	L-L	32.6	33.0	16.2	5.9	7	-7.61 ± 0.12	-7.11 ± 0.21
14 July 2019	S-L	7.6	5.6	1.8	9.4	2	-3.12 ± 0.68	-2.46 ± 0.29
17 July 2019	S-H	13.3	9.4	1.7	15.2	3	-5.86 ± 1.32	-4.83 ± 0.79

Table S2. Average percentage of throughfall types for each of the rainfall classes. SP: splash throughfall, FR: free throughfall, and DR: canopy drip.

Rainfall class	SP (%)	FR (%)	DR (%)
L-H	16.9	21.3	61.8
S-L	14.3	16.4	69.3
S-H	19.0	25.0	56.4
L-L	14.6	13.5	72.0

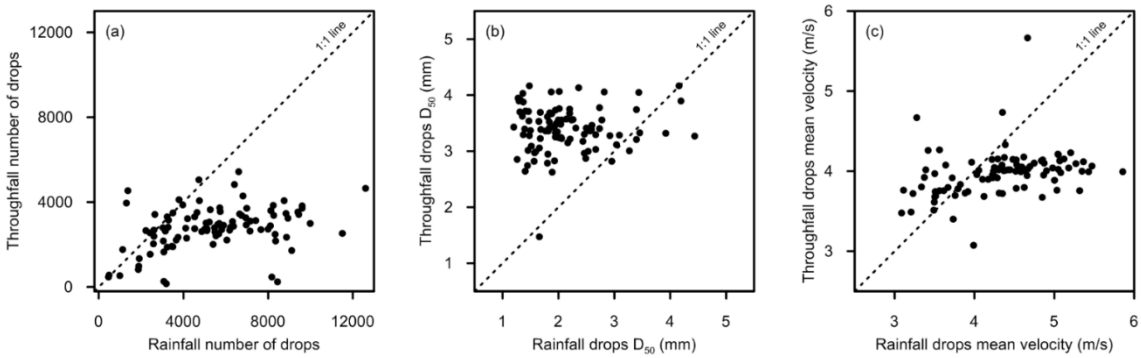

Figure S1. Relationship between open rainfall and throughfall for: (a) number of drops, (b) median volume drop diameter (D_{50}) and (c) drops' mean velocity.

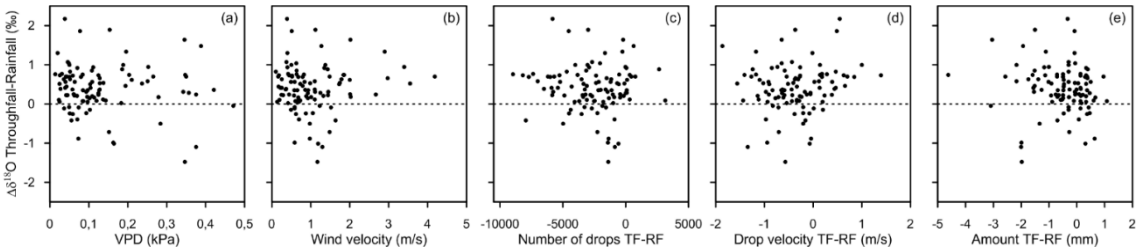

Figure S2. Isotopic shift variability ($\delta^{18}O_{TF\text{-}RF}$) *versus*: (a) vapor pressure deficit, (b) mean wind velocity, (c) differences in number of drops, (d) differences in mean drop velocity and (e) differences in amount per sample.

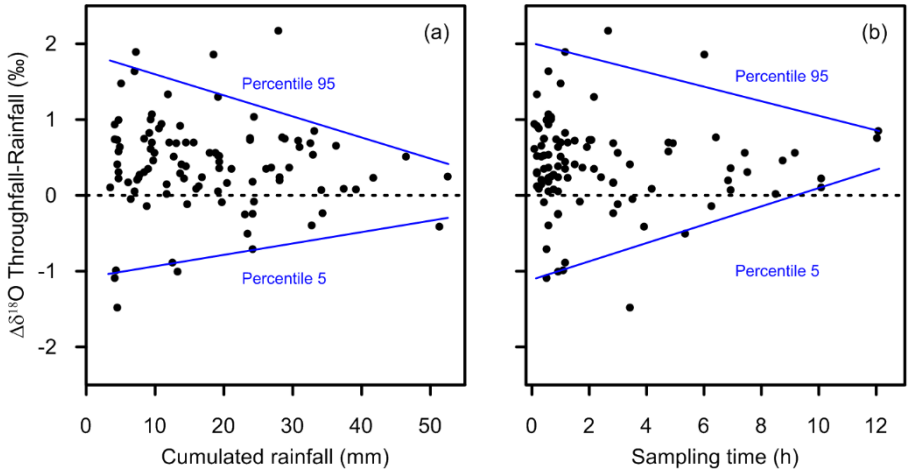

Figure S3. Isotopic shift variability ($\delta^{18}O_{TF\text{-}RF}$) *versus*: (a) cumulative rainfall throughout the rainfall event and (b) sampling time (i.e. time each 5 mm sample took to be filled).

SUPPORTING INFORMATION CHAPTER 3

Table S1. Meteorological characteristics and isotopic composition of open rainfall, throughfall and stemflow for the 21 events during the study period (May 2018 to December 2019). A total of 178 triplets of samples (i.e., rainfall, throughfall and stemflow samples for the same time interval) were collected. In addition, 5 delayed stemflow samples corresponding to the stemflow produced once rainfall and throughfall ended for some events were also collected († in the column "number of triplets of samples"). In the same column, ‡ indicated the events where the 24 samples capacity was exceeded.

ID	Date (dd/mm/yyyy)	Rainfall (mm)	Throughfall (mm)	Stemflow (L)	Rainfall duration (h)	Mean rainfall intensity (mm/h)	Number of triplets of samples	Mean weighed rainfall (‰)		Mean weighed throughfall (‰)		Mean weighed stemflow (‰)	
								$\delta^{2}H$	$\delta^{18}O$	$\delta^{2}H$	$\delta^{18}O$	$\delta^{2}H$	$\delta^{18}O$
1	12/05/2018	51.5	47.9	26.3	9.5	5.4	14†	-28.24	-4.88	-25.95	-4.64	-27.94	-4.61
2	29/05/2018	18.7	15.9	4.9	24.8	0.8	4	-28.98	-5.16	-26.94	-5.01	-23.06	-4.34
3	01/06/2018	26.9	20.3	9.7	9.5	2.8	6	-45.51	-7.34	-41.71	-6.83	-33.28	-5.84
4	06/06/2018	26.9	25.7	16.5	5.3	5.1	9	-61.28	-8.49	-58.94	-8.44	-55.25	-7.87
5	23/06/2018	20.5	18.6	3.6	1.2	17.7	2	-14.71	-3.67	-13.48	-3.51	-12.13	-3.12
6	28/06/2018	34.3	33.6	13.0	8.8	3.9	8	-36.01	-6.46	-33.89	-5.96	-27.27	-4.84
7	09/08/2018	39.4	37.6	28.7	16.5	2.4	13†	-20.04	-4.05	-19.25	-4.09	-17.04	-3.80
8	09/10/2018	34.3	31.1	23.3	12.5	2.7	13	-82.49	-11.74	-78.77	-11.41	-74.83	-10.99
9	30/10/2018	83.7	82.3	81.0	39.5	2.1	24‡	-82.89	-13.10	-82.43	-12.91	-82.25	-12.76
10	05/11/2018	32.8	30.5	20.6	7.8	4.2	11†	-36.89	-6.69	-33.15	-6.27	-29.82	-6.00
11	08/11/2018	20.3	19.9	11.2	9.7	2.1	7	-55.82	-8.54	-48.93	-8.16	-43.98	-7.11
12	31/01/2019	19.7	20.7	8.3	13.0	1.5	6	-63.08	-8.13	-58.97	-7.42	-55.12	-7.43
13	01/05/2019	27.9	23.8	12.2	43.3	0.6	8†	-26.27	-5.29	-20.86	-4.52	-23.78	-4.80

Table S1. Continued

ID	Date (dd/mm/yyyy)	Rainfall (mm)	Throughfall (mm)	Stemflow (L)	Rainfall duration (h)	Mean rainfall intensity (mm/h)	Number of triplets of samples	Mean weighed rainfall (‰)		Mean weighed throughfall (‰)		Mean weighed stemflow (‰)	
								δ^2H	$\delta^{18}O$	δ^2H	$\delta^{18}O$	δ^2H	$\delta^{18}O$
14	20/05/2019	8.8	7.1	1.0	7.1	1.2	2	-44.98	-6.43	-41.46	-6.16	-18.35	-3.51
15	24/05/2019	19.7	17.6	6.1	22.2	0.9	5	-24.34	-4.79	-16.45	-4.00	-10.58	-2.89
16	11/06/2019	32.6	33.0	16.7	16.0	2.0	10[†]	-48.72	-7.61	-45.39	-7.11	-41.52	-6.56
17	17/07/2019	13.3	9.4	2.9	1.5	8.8	2	-35.21	-5.86	-27.42	-4.83	-31.39	-5.39
18	29/08/2019	17.6	13.0	4.9	4.1	4.3	3	-22.94	-4.13	-22.17	-4.26	-20.73	-3.94
19	10/09/2019	14.4	10.2	1.8	8.0	1.8	2	-40.74	-7.19	-37.07	-6.75	-28.66	-5.42
20	18/09/2019	24.4	19.9	11.3	2.7	9.0	5	-44.40	-7.11	-44.95	-7.31	-42.51	-6.85
21	19/12/2019	66.7	63.5	68.1	13.5	4.9	24[‡]	-66.99	-9.35	-61.10	-8.94	-60.49	-8.52

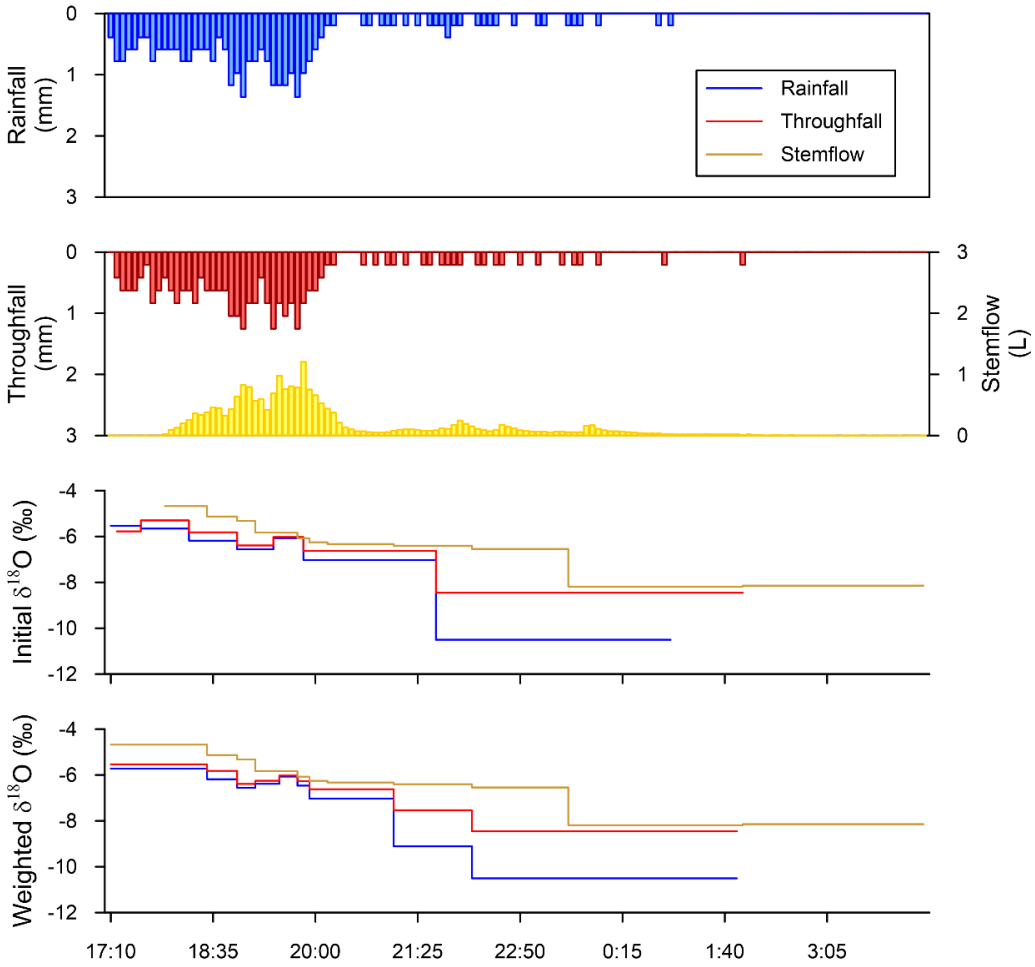

Figure S1. Representation of the methodology used to pair volume-weighted mean isotopic composition of rainfall and throughfall with stemflow time intervals (Event 1). A delayed stemflow sample corresponding to the stemflow produced once rainfall ended was also collected for this event.

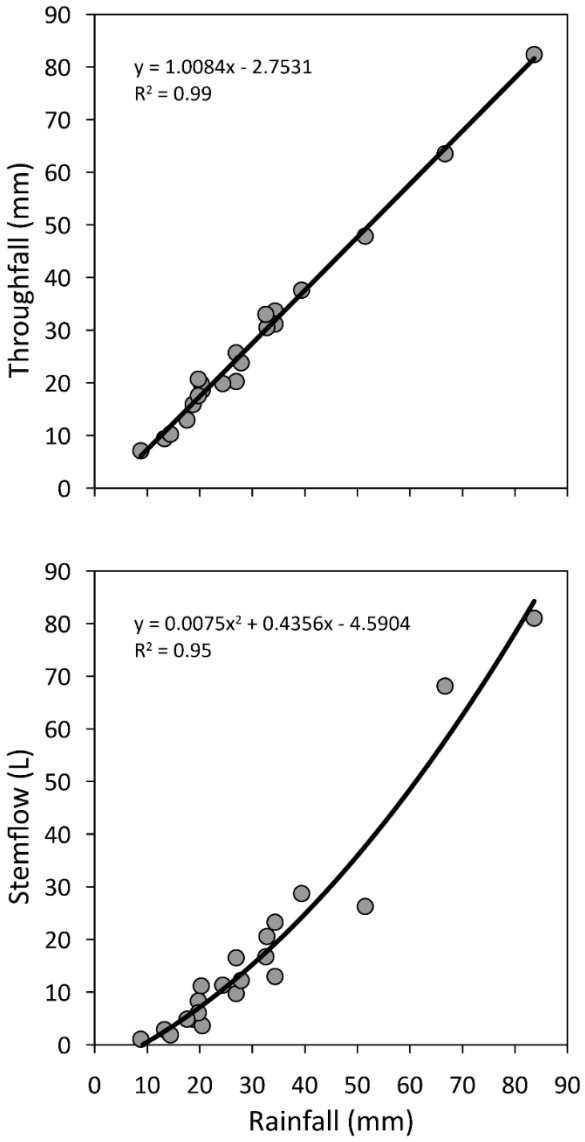

Figure S2. Relationships between rainfall, and throughfall and stemflow fluxes for the 21 events measured in this study in the Scots pine forest stand.

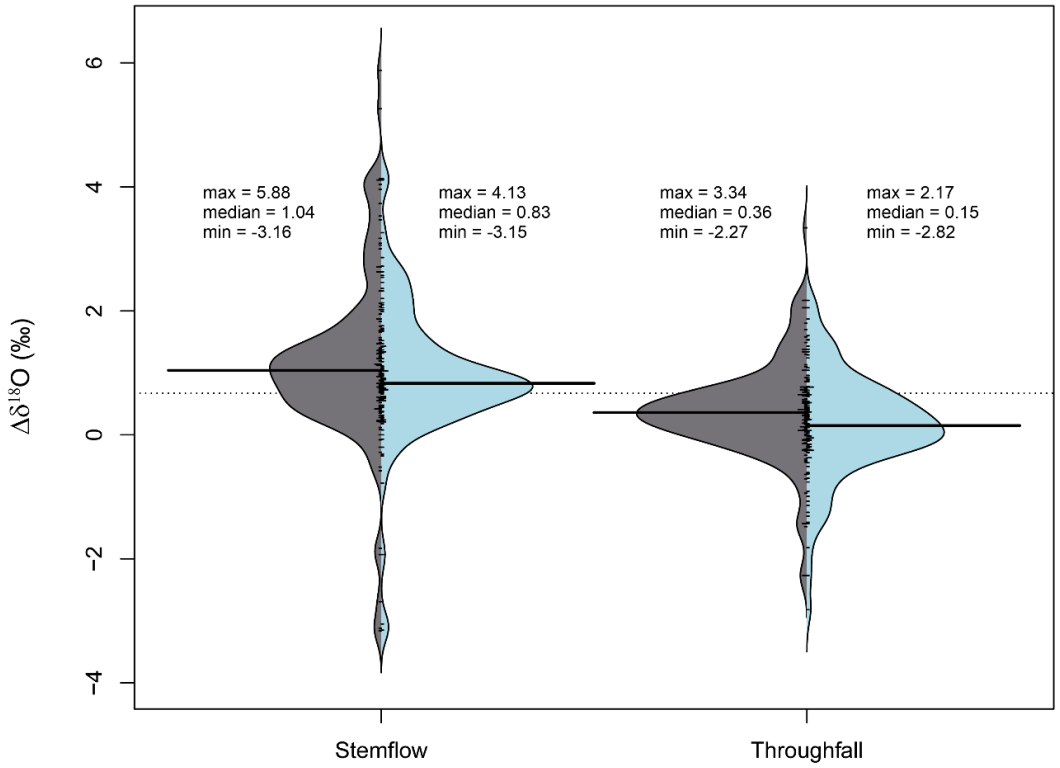

Figure S3. Comparison of isotopic shift between stemflow/throughfall with respect to rainfall in the corresponding (grey) and previous (light blue) time interval. Each violin plot indicates the distribution, median (horizontal line), individual observations (small lines), and maximum and minimum values (violin limits).

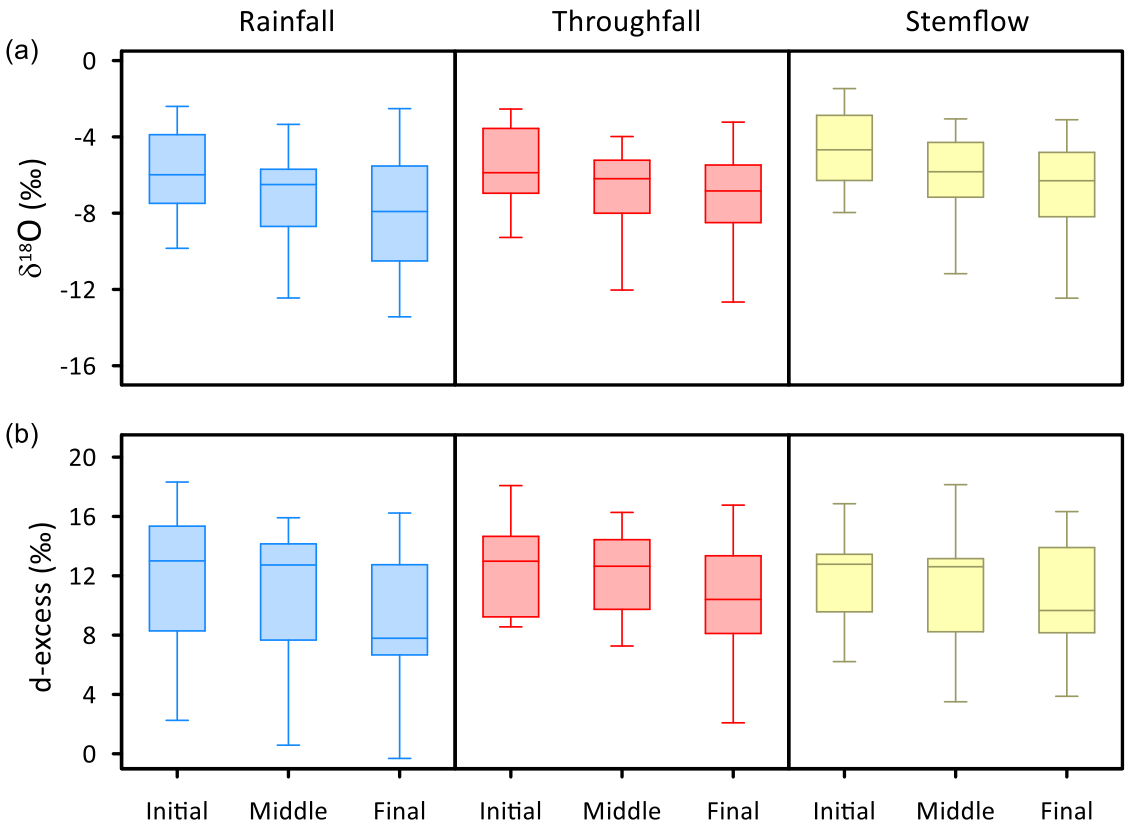

Figure S4. Boxplots of the intra-storm dynamics of 15 rainfall events (≥ 3 stemflow samples) at the study pine stand. (a) rainfall, throughfall and stemflow $\delta^{18}O$, and (b) rainfall, throughfall and stemflow d-excess. Sequential boxplots represent a different phase (initial, middle, and final) of the event. Box-Whisker plot indicates median (center line), the interquartile range (25 to 75 %) (box) and the lower and upper quartile range (0-25 % and 75-100 %) multiple to a factor 1.5 (whiskers).

SUPPORTING INFORMATION CHAPTER 4

Table S1. Morphological characteristics of surrounding trees within a radius of 5 m from the monitored trees (A and B).

Tree ID	DBH (cm)	Height (m)	Crown depth (m)	Mean crown radius (m)	Crown area (m^2)	Distance (m)
Tree A						
75	19.4	16.8	5.4	1.8	10.0	4.1
78	38.2	22.5	10.6	3.2	32.8	2.8
80	30.2	20.4	8.4	2.6	21.2	1.1
81	5.7	10.0	1.6	0.8	3.0	2.1
91	15.9	15.5	4.5	1.5	7.5	5.0
95	23.9	18.4	6.7	2.1	14.1	3.8
96	25.1	18.8	7.0	2.2	15.4	4.6
97	18.1	16.4	5.1	1.7	9.0	4.0
98	20.4	17.2	5.7	1.9	10.8	3.6
99	35.3	21.8	9.8	3.0	28.3	4.8
100	28.0	19.7	7.8	2.4	18.6	4.9
Tree B						
42	8.7	11.9	2.5	1.0	3.9	4.7
66	18.1	16.4	5.1	1.7	9.0	1.0
69	29.9	20.3	8.3	2.6	20.9	3.0
70	8.6	11.9	2.4	1.0	3.8	4.8
75	19.4	16.8	5.4	1.8	10.0	4.6

Table S2. Meteorological characteristics of the 39 rainfall events considered in the study. Percentage of wind-driven rainfall during an event was calculated from all 5-min observations during the event. Mean wind direction and its standard deviation were calculated based on the vector decomposition for wind direction data protocol described in Van Stan et al. (2011). Events determined as 'intermittent' based on the K-means cluster analysis are indicated with an asterisk (*) in Rainfall Class column. SD = standard deviation; CV = coefficient of variation.

Rainfall event	ID	Rainfall amount (mm)	Rainfall duration (h)	Mean rainfall intensity (mm/h)	Rainfall class	Mean wind speed ± SD (m/s)	Mean wind direction (SD) (°)	Wind-driven rainfall (%)	Stemflow volume *tree A* (L)	Stemflow volume *tree B* (L)	CV intensity (mm/5min)	Number of dry periods	Mean dry period (h)
12 May 2018	1	51.5	9.5	5.4	L-H	1.5 ± 1.3	325.6 (41.3)	10.5	27.4	40.9	1.43	16	0.21
28 May 2018	2	17.2	15.6	1.1	L-L	0.6 ± 0.5	169.3 (49.6)	0	2.6	4.8	2.63	26	0.43
29 May 2018	3	18.7	24.8	0.8	L-L	0.7 ± 0.4	228.2 (40.7)	0	7.9	10.4	3.49	23	0.93
01 June 2018 (1)	4	13.7	0.6	23.4	SM-H	1.7 ± 0.9	234.4 (29.1)	14.3	1.8	3.7	0.89	1	0.08
01 June 2018 (2)	5	13.1	2.8	4.8	SM-H	1.4 ± 0.6	213.3 (47.1)	0	6.0	8.5	1.10	3	0.19
06 June 2018	6	26.9	5.3	5.1	SM-H	0.5 ± 0.5	114.6 (39.9)	0	12.8	17.8	1.40	8	0.17
28 June 2018	7	34.3	8.8	3.9	L-H	0.9 ± 0.5	196.9 (41.2)	1.0	11.3	14.7	1.63	19	0.21
09 July 2018	8	41.0	2.5	16.4	SM-H	2.3 ± 1.0	287.3 (36.5)	36.7	16.0	17.7	1.50	3	0.33
24 July 2018	9	23.2	1.9	12.1	SM-H	2.2 ± 0.9	248.8 (47.2)	30.4	5.6	9.1	1.05	2	0.17
16 August 2018	10	39.8	18.1	2.2	L-H	0.8 ± 0.8	204.4 (41.8)	1.8	23.6	39.7	2.74	10	1.25
09 October 2018	11	33.9	11.2	3.0	L-L	0.7 ± 0.4	249.9 (43.9)	0	22.1	27.2	1.15	8	0.64
13 October 2018	12	97.5	34.6	2.8	L-H*	1.0 ± 0.7	154.7 (44.1)	0.7	77.0	95.8	2.26	41	0.53
18 October 2018	13	5.5	2.5	2.2	SM-L	0.7 ± 0.4	237.1 (52.1)	0	1.1	1.7	0.89	7	0.12
26 October 2018	14	30.4	42.3	0.7	L-L*	0.6 ± 0.7	254.2 (45.8)	0.8	11.2	11.4	1.71	79	0.39
30 October 2018	15	83.7	39.5	2.1	L-L*	0.5 ± 0.5	249.0 (45.2)	0.6	71.9	91.7	1.29	57	0.34
05 November 2018	16	32.8	7.8	4.2	SM-L	0.6 ± 0.5	146.0 (48.5)	0	19.3	23.4	1.06	12	0.21
08 November 2018	17	20.1	8.9	2.3	L-L	0.3 ± 0.4	222.8 (42.0)	0	10.7	13.7	1.15	19	0.18
01 February 2019	18	18.7	9.4	2.0	L-L	1.4 ± 0.8	234.0 (46.1)	4.4	6.7	9.1	1.07	18	0.24
06 March 2019	19	9.4	3.0	3.1	SM-L	1.6 ± 1.0	178.4 (61.0)	13.9	0.5	0.9	0.78	1	0.67
02 April 2019	20	11.5	15.8	0.7	L-L	0.8 ± 0.7	217.0 (45.3)	0	1.5	2.1	1.88	24	0.48
05 April 2019	21	29.8	19.7	1.5	L-H	0.4 ± 0.5	275.5 (46.8)	0	6.6	8.3	1.86	21	0.59
24 April 2019	22	25.5	17.8	1.4	L-L	1.4 ± 0.6	157.4 (45.9)	2.8	13.7	16.4	1.36	23	0.43
02 May 2019	23	21.8	25.9	0.8	L-L*	0.6 ± 0.5	101.1 (37.9)	0	9.5	12.4	2.14	43	0.45

24 May 2019	24	18.7	12.5	1.5	L-L*	0.4 ± 0.4	287.0 (33.3)	0	5.1	5.5	1.13	31	0.20
11 June 2019	25	32.6	16.0	2.0	L-L*	0.4 ± 0.4	67.0 (40.8)	1.0	7.9	9.7	1.15	35	0.20
09 July 2019	26	26.5	7.7	3.5	SM-L	0.9 ± 0.7	225.5 (39.7)	3.3	8.4	9.8	1.21	10	0.33
27 July 2019	27	21.8	3.3	6.7	SM-H	1.1 ± 1.1	326.8 (45.7)	12.8	10.4	12.2	1.98	5	0.27
20 August 2019	28	19.9	5.8	3.4	SM-L	0.5 ± 0.4	42.9 (46.6)	0	2.1	1.6	1.26	11	0.17
29August 2019	29	16.4	1.3	12.3	SM-H	1.9 ± 1.1	207.7 (37.8)	31.3	1.7	4.7	1.03	1	0.17
18 September 2019	30	24.2	2.7	9.1	SM-H	1.4 ± 0.6	217.7 (38.1)	0	2.3	8.1	1.30	3	0.39
14 October 2019	31	22.2	9.7	2.3	L-H	0.8 ± 0.5	191.7 (49.7)	2.6	5.8	6.9	2.21	11	0.58
20 October 2019	32	24.6	9.5	2.6	L-L	1.4 ± 0.5	198.6 (51.3)	1.8	10.3	12.5	1.66	15	0.37
22 October 2019	33	65.5	23.7	2.8	L-H*	1.0 ± 0.7	216.8 (48.9)	1.4	45.0	62.6	1.75	34	0.36
04 November 2019	34	8.6	4.7	1.8	SM-L	1.0 ± 0.7	239.2 (45.9)	3.6	0.8	0.7	1.05	6	0.32
14 November 2019	35	10.9	8.0	1.4	SM-L	0.8 ± 0.5	253.5 (38.7)	0	2.3	2.3	0.98	21	0.17
22 November 2019	36	38.4	10.3	3.7	L-L	0.8 ± 0.5	177.4 (47.4)	0	26.4	30.7	0.81	16	0.13
19 December 2019	37	66.7	13.5	4.9	L-L	1.4 ± 0.6	173.0 (47.1)	3.1	54.0	70.6	0.66	15	0.16
20 December 2019	38	14.6	6.3	2.3	SM-L	0.8 ± 0.4	204.5 (44.6)	0	8.6	11.4	0.79	11	0.16
21 December 2019	39	23.0	7.5	3.1	SM-L	1.1 ± 0.5	246.9 (46.3)	2.2	13.7	18.8	1.34	6	0.58

Table S3. Average values of bark roughness for the 4 sections (N, E, S, W) of the monitored trees (A and B). CV = coefficient of variation.

	Tree A		Tree B	
	Average bark roughness (cm)	CV	Average bark roughness (cm)	CV
Section North	0.29	0.83	0.40	1.02
Section East	0.26	0.95	0.44	1.03
Section South	0.26	1.10	0.44	1.02
Section West	0.19	1.07	0.40	1.02

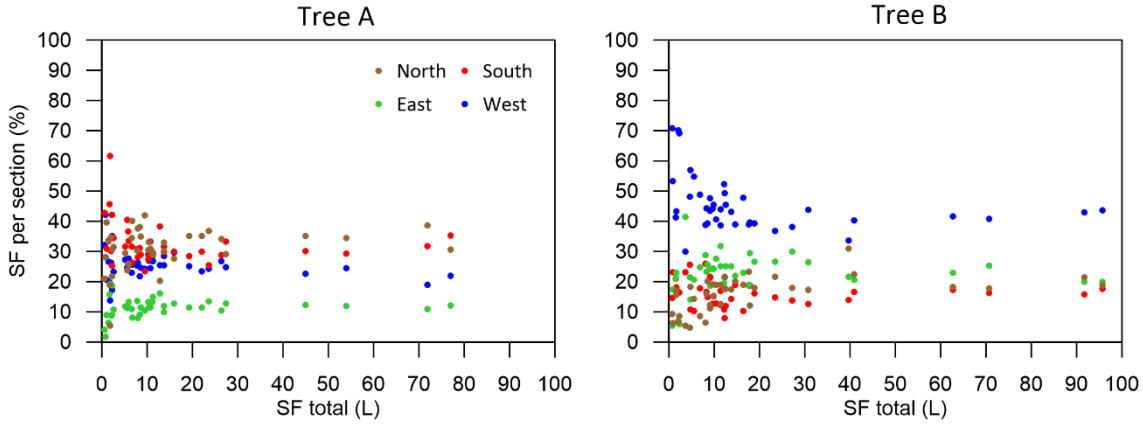

Figure S1. Event-scale relationship between the percentage of stemflow volume per section (N, E, S, W) and the total stemflow for tree A (left) and B (right).

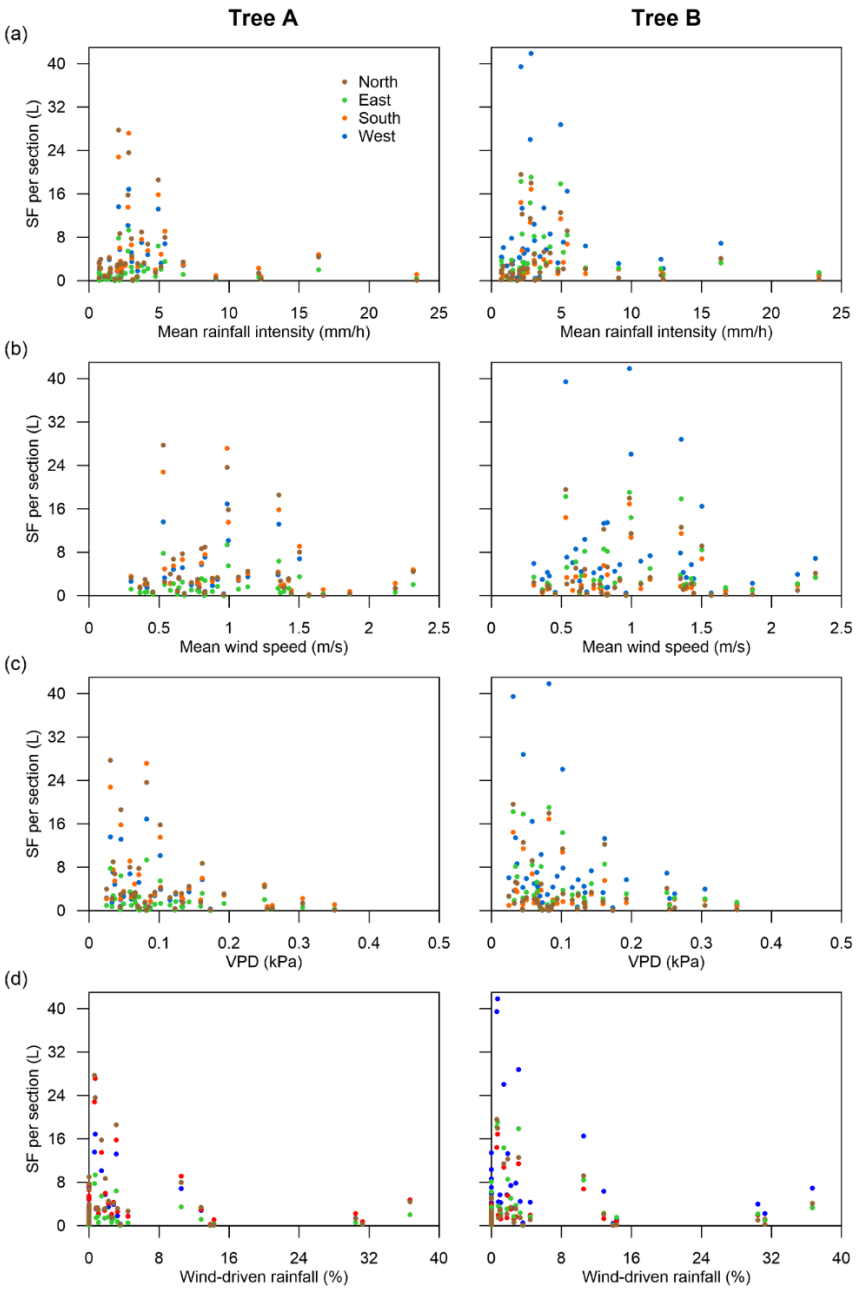

Figure S2. Event-scale relationship between the stemflow volume per section (N, E, S, W) and (a) mean rainfall intensity, (b) mean wind speed, (c) vapour pressure deficit, and (d) wind-driven rainfall for tree A (left) and B (right).

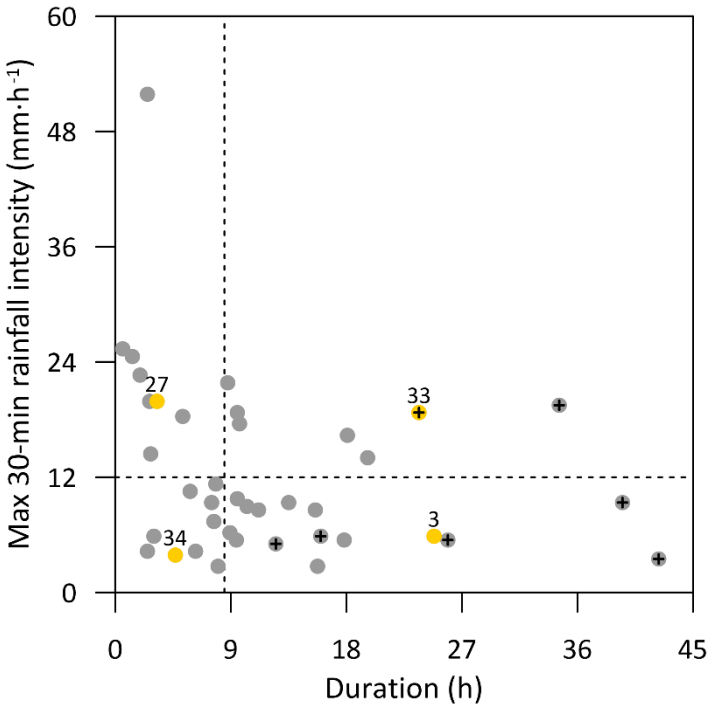

Figure S3. Rainfall classes defined for the analysis, based on max 30-min rainfall intensity and rainfall duration. Yellow dots represent the events selected in Figure 9 and 10 and the cross symbols indicate the events classified as intermittent.

SUPPORTING INFORMATION CHAPTER 5

Table S1. Maximum concentrations of Brilliant Blue FCF and deuterium isotopic compositions in soil profiles for the different cardinal directions and distances from the trunk.

Profile	Distance from the tree trunk (cm)	*n*	Brilliant Blue FCF	Deuterium
			Max.	
			mg kg^{-1} soil	‰
PN1	40	8	92.33	−14.27
PN2	25	6	176.04	122.30
PN3	10	6	472.96	277.14
PE1	40	6	124.52	51.47
PE2	25	5	280.89	102.32
PE3	10	4	348.63	132.27
PS1	40	6	114.65	42.69
PS2	25	6	154.11	23.09
PS3	10	6	332.68	134.06
PW1	40	2	0	−51.53
PW2	25	4	360.28	156.49
PW3	10	4	391.26	210.35

n indicates the number of samples.

Table S2. Brilliant Blue FCF dye concentration of the water samples taken from the mini-piezometers (wt) during the stemflow experiment.

Time	NW20	N50	N20	NE20	E20	E50	SE20	S20	S50	SW20	W20	W50
	Brilliant Blue FCF dye concentration (g L^{-1})											
10:45	†	†	†	†	†	†	†	†	†	†	†	†
11:50	†	†	†	‡	†	†	4.96	‡	†	†	‡	†
12:45	†	†	†	‡	‡	†	4.74	4.59	†	†	5.40	†
13:45	†	†	†	5.34	‡	†	5.11	4.86	†	‡	5.80	†
14:45	†	†	†	5.89	‡	†	5.52	5.31	†	‡	5.77	†
15:45	†	†	‡	6.31	‡	‡	5.97	5.60	†	‡	5.89	†

† Denotes that no water was recorded and ‡ that the level was not sufficient for a sample to be taken.

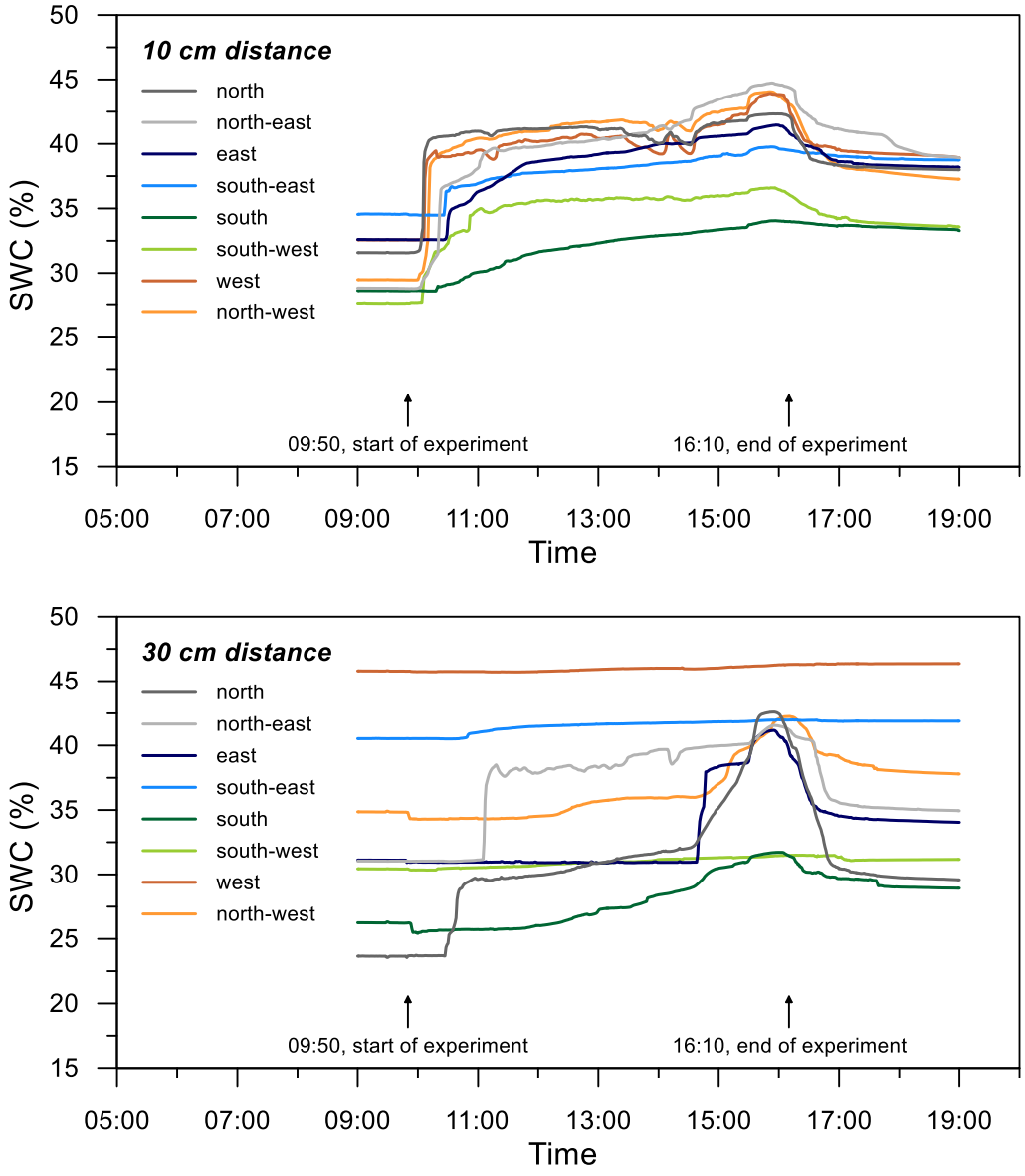

Figure S1. Temporal evolution of volumetric soil water content (SWC) at 1-min resolution derived from TDR sensors along the four cardinal and the four intercardinal directions at 10 cm distance to the trunk (top) and 30 cm distance (bottom).

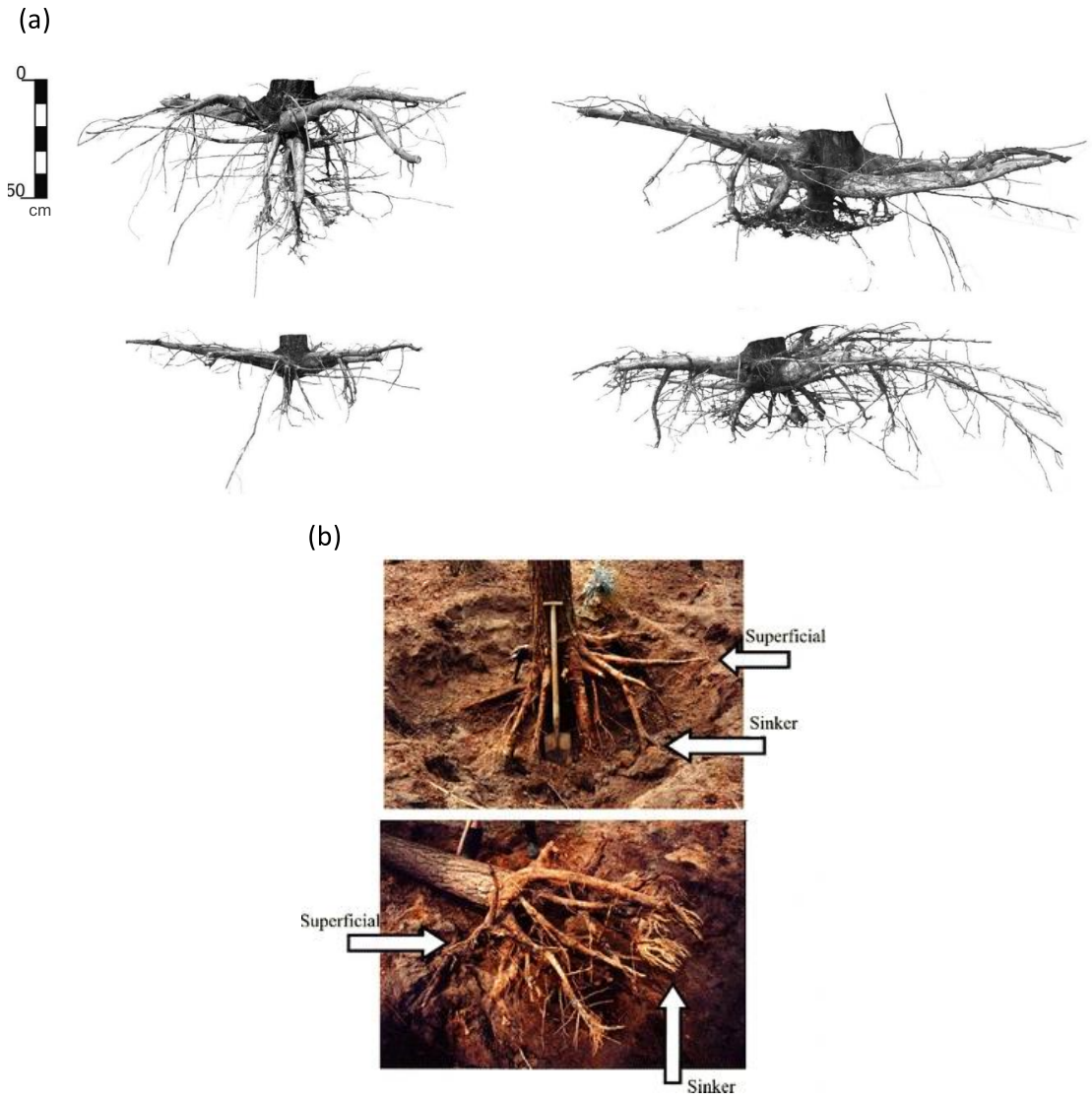

Figure S2. Examples of Scots pine root system architecture. Source (a) Pietrzykowski et al. (2017), *Forest Research Papers*, 78, 323–331. https://doi.org/10.1515/frp-2017-0036; and (b) Čermák et al. (2008), *Plant and Soil*, 305(1), 61-75. https://doi.org/10.1007/s11104-007-9433-z. Figures are reproduced based on open access Creative Commons Attribution License.

Figure S3. Dye colored water observed at mini-piezometer wt-W20, located next to the west TDR probe (30 cm distance from tree trunk; swc-W30).

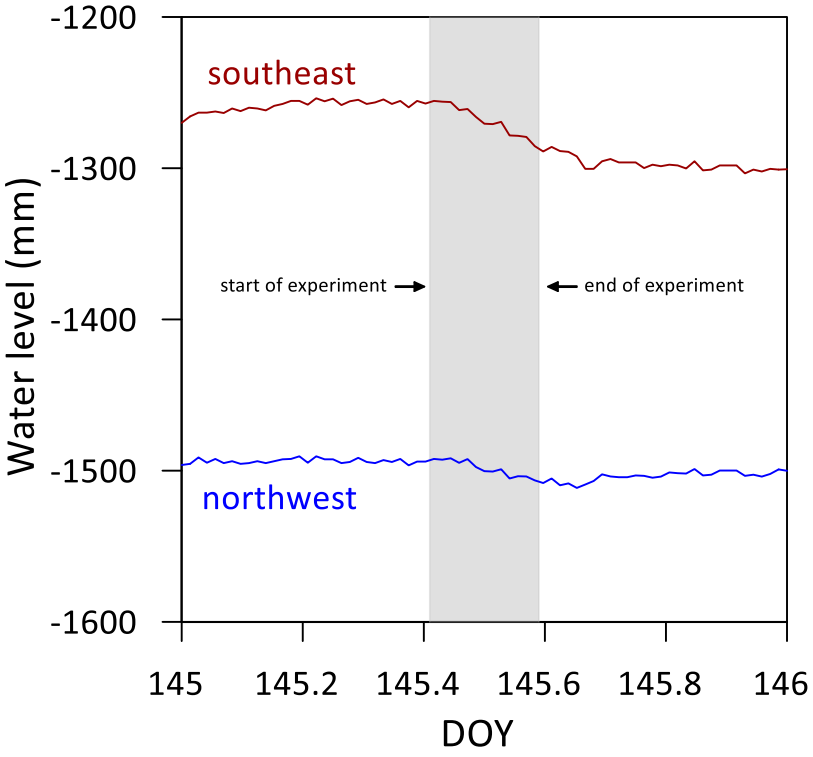

Figure S4. Dynamics of groundwater table at 20 min resolution in the southeast and northwest deep piezometers. Gray area indicates the time period of the stemflow experiment. DOY = day of the year.

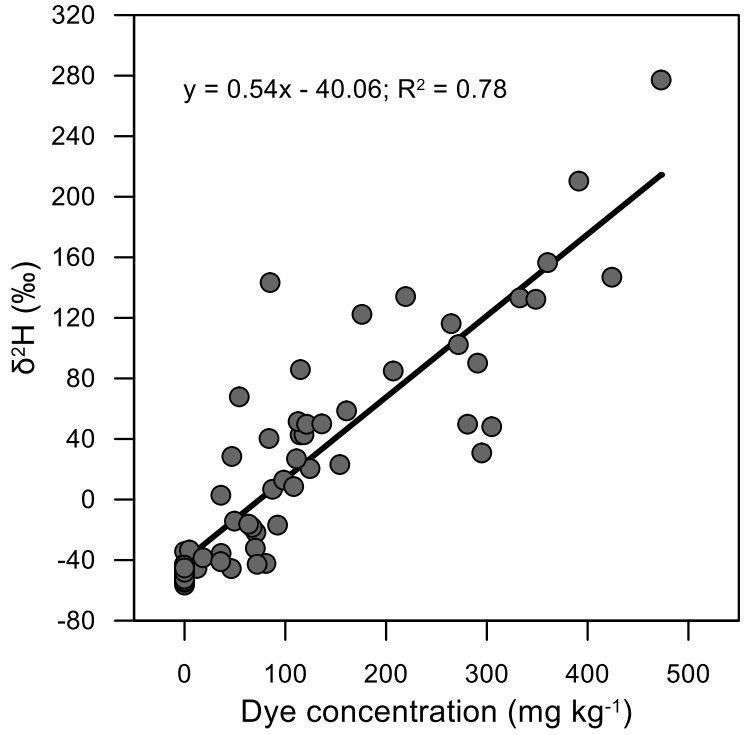

Figure S5. Relationship between deuterium isotopic composition and Brilliant Blue FCF dye concentration for the 63 soil samples taken from the 12 profiles excavated after the stemflow experiment.